2010

Developmental Expression of Calcium Buffering Proteins in Central Auditory Pathways of Normal Hearing and Congenitally Deaf Mice

Adam S. Deardorff
Wright State University, deardorff.2@wright.edu

DEVELEPMENTAL EXPRESSION OF CALCIUM BUFFERING PROTEINS IN CENTRAL AUDITORY PATHWAYS OF NORMAL HEARING AND CONGENITALLY DEAF MICE

A thesis submitted in partial fulfillment
of the requirements for the degree of
Master of Science

By

ADAM S. DEARDORFF
B.A. Environmental Science, Zoology
Miami University, 2003

2010
Wright State University

WRIGHT STATE UNIVERSITY

SCHOOL OF GRADUATE STUDIES

May 20, 2010

I HEREBY RECOMMEND THAT THE THESIS PREPARED UNDER MY SUPERVISION BY Adam S Deardorff ENTITLED Developmental Expression of Calcium Buffering Proteins in the Central Auditory Pathways of Normal Hearing and Congenitally Deaf Mice BE ACCEPTED IN PARTIAL FULFUILLMENT OF THE REQUIREMENTS FOR THE DEGREE OF Master of Science.

Robert E.W. Fyffe, Ph.D.
Thesis Director

Timothy C. Cope, Ph.D.
Department Chair, NCBP

Committee on
Final Examination

Robert E.W. Fyffe, Ph.D.

John C. Pearson, Ph.D.

Larry J. Ream, Ph.D

John A. Bantle, Ph.D.
Vice President, Research and Graduate Studies;
Interim Dean, School of Graduate Studies

ABSTRACT

Deardorff, Adam S., M.S. Anatomy, Department of Neuroscience, Cell Biology, and Physiology, Wright State University, 2010. Developmental Expression of Calcium Buffering Proteins in Normal Hearing and Congenitally Mice.

These experiments analyze differences in synaptic development in central auditory pathways between normal hearing (CBA/J) and congenitally deaf (*dn/dn*) mice, which provide valuable insight into central synaptic plasticity corresponding to human congenital deafness. Immunofluorescent analysis of the developmental expression of the calcium buffering proteins calretinin, calbindin d-28k, and parvalbumin at various postnatal time points was performed to assess the effects of altered neural activity on the level and/or pattern of protein expression within these nuclei. Results indicate that the pattern of calbindin and parvalbumin is unaffected by congenital deafness in *dn/dn* mice. However, the pattern of calretinin expression in the MNTB during development of *dn/dn* mice differed significantly from that of CBA/J mice, indicating that calcium buffering may be impaired in these synapses without appropriate afferent stimulation.

TABLE OF CONTENTS

LIST OF FIGURES

Page

ACKNOWLEDGEMENT

This thesis would not have been possible were it not for my advisor and mentor, Dr. Robert EW Fyffe, whose unending patience, support, and guidance has been invaluable in my educational and professional development. To him I owe my deepest gratitude.

I am profoundly thankful to have met and worked with Dr. Larry J. Ream. Nothing I have accomplished as a graduate student would have been possible without him.

To Dr. John C. Pearson, who not only taught me neuroscience, but also the art of teaching it, I am heartily grateful.

I am forever indebted to my many colleagues. To Shannon Romer, Mellissa Bautista, Roger Fecher, Robert Tracy, Valerie Seimbab, Courtney Smith, Kathleen Friedman, and Amber McCurdy: thank you for your friendship and thank you for teaching me everything there is to know about working in a lab. To Dan Miska, it has been one of my great privileges and honors to teach along side you.

Finally, I would like to thank Beth Harper. Without her, I could not be.

For my mom and dad...

I. INTRODUCTION

The ability to extract biologically relevant information from environmental sound is a critical adaptation. It is the basis of conspecific communication and provides a three-dimensional representation of space in which individuals can detect and respond appropriately to danger, hunt and capture prey, and navigate their environment successfully. Despite numerous advances in research, information regarding central auditory processes necessary to filter relevant information from broadband environmental noise is still fragmentary. However, because cochlear information must be faithfully propagated through several synapses before the binaural comparisons underlying sound localization occur, it can be said with certainty that such ability requires an auditory system in which both central and peripheral structures are specialized to maintain a high frequency and fidelity of neuronal firing and synaptic transmission.

Because the external ear has no mechanism to encode the azimuthal source of incoming sound waves, central auditory nuclei are specialized to extract such information from precisely timed binaural cues. The medial nucleus of the trapezoid body (MNTB) and anteroventral cochlear nucleus (AVCN) are key brainstem relays involved in sound localization. The primary excitatory (glutamatergic) input to the bushy cells of the AVCN is formed by specialized endbulb of Held synapses, which arise from axons of ipsilateral spiral ganglion cells. The glutamatergic globular bushy cells of the AVCN, in turn, send axonal projections to the glycinergic principal cells of the contralateral MNTB to form

the calyx of Held synapse. This part of the circuit forms a sign-inverting relay in which the excitatory drive of the cochlear nucleus is converted to contralateral inhibition, the main targets of which are the medial and lateral superior olivary nuclei (MSO and LSO), which also receive glutamatergic input from bushy cells of the ipsi- and contralateral cochlear nuclei (Figure 1).

Binaural comparisons in the LSO and MSO are considered to be the foundation of sound localization (Smith et al 1993). These nuclei extract, from precisely timed MNTB and AVCN synaptic input, interaural timing and intensity differences (ITD and IID) small enough to encode the location of a sound to within a single degree.

The synapses within the AVCN and MNTB are of particular interest because in addition to their critical importance in sound localization, several common features have made them useful for studying central synaptic transmission. For most central neurons, the small size of synaptic terminals and widespread distribution of synaptic contacts over an extensive dendritic tree greatly complicates combined structure – function studies. Within the MNTB, however, the large size of the calyx of Held terminal allows it to be visualized and simultaneous pre- and postsynaptic patch clamp recordings obtained (Forsythe, 1994; Borst and Sakmann, 1995) (Figure 2). Additionally, the majority of excitatory and inhibitory synaptic contacts are located on the round to oval shaped principal cell somata, a feature which facilitates the observation of immunolabelled cytoplasmic and membrane proteins and effectively eliminates electronic complications in postsynaptic electrophysiological recordings created

by dendritic filtering. Similar advantages pertain to endbulb of Held synapses within the AVCN. When physiological recordings from these synapses are studied with anatomical data taken via immunohistochemistry and electron microscopy, researchers gain insight into direct structure – function relationships underlying chemical synaptic response properties.

A variety of mechanisms underlie AVCN and MNTB synaptic response properties and discharge capabilities in accordance with a tonotopic map present throughout the auditory system (Figure 3). One such mechanism is likely to be intracellular calcium buffering. Calcium buffering proteins such as parvalbumin, calretinin, and calbindin can be found throughout the central nervous system. They reduce intracellular calcium levels on the order of milliseconds and, when present at high concentration, can buffer incoming calcium before the ions reach their intracellular target. Such mechanisms are important pre- and post-synaptically to modulate neurotransmitter release and high frequency firing.

Erwin Neher (1998) posed two questions regarding our understanding presynaptic function. The first regarded mechanisms of vesicle pool dynamics. Can we associate the changes seen in certain forms of presynaptic plasticity with mechanisms of calcium coupled vesicle release or replenishment of the readily releasable vesicle pool? The second regarded the calcium signal itself. How high must local [Ca^{2+}] rise in order to release a vesicle and what are the functional consequences of local [Ca^{2+}] gradients at the active zone, in terms of short- and long-term plasticity? He concludes that "we will probably not have reliable

answers to these questions unless we know more about calcium buffers in the nerve terminal."

We have previously shown differences in the physiological properties of brainstem auditory neurons between normal hearing and congenitally deaf mice that could be related to altered calcium buffering (Oleskevich and Walmsley, 2002). The aim of the present study is to determine the developmental distribution of parvalbumin, calretinin, and calbindin within the AVCN and MNTB of normal hearing mice (CBA/J). We will also determine, using a congenitally deaf (*dn/dn*) mouse model that lacks spontaneous and sound evoked auditory nerve activity throughout development, if altered neural activity causes changes in the expression of these proteins, thereby elucidating which processes regulating synaptic firing properties are activity dependent and activity independent.

We have also shown that a differential expression of ion channels along the medial - lateral tonotopic gradient of the MNTB exists in normal hearing CBA/J mice, but is disrupted in congenitally deaf *dn/dn* mice (Leao et. al., 2006). In the current study we will determine the proportion of calyces / principal cells expressing calcium binding proteins in medial, intermediate, and lateral regions of the MNTB. By examining the expression of calcium binding proteins with regard to the tonotopic gradient, we hope to further implicate structural factors relating differences in firing frequencies between neurons of the same type as well as further elucidate which processes regulating synaptic firing properties are activity dependent and activity independent.

II. SPECIFIC AIMS

Hypothesis: due to a lack of spontaneous and acoustically evoked afferent activity in the cochlear nerve, patterns of CBP expression are altered in the MNTB and AVCN of *dn/dn* mice compared to CBA/J mice.

Aim: Determine and compare the pre- and postsynaptic developmental distribution of the calcium binding proteins parvalbumin, calbindin, and calretinin in the calyx of Held – principal cell synapses of the medial nucleus of the trapezoid body and endbulb of Held – globular bushy cell synapse of the anteroventral cochlear nucleus in normal hearing (CBA/J) and congenitally deaf (*dn/dn*) mice.

III. BACKGROUND & SIGNIFICANCE

Hearing Impairment

Historically, the visual system has dominated the field of sensorineural research. However, the societal impact and potential for treatment of hearing impairment has recently brought auditory research to the forefront of neurobiology (Hudspeth, A.J. 1997). An increase in global population and longer life expectancies has brought the number of people worldwide suffering from moderate to profound hearing loss in both ears to 278 million individuals, approximately 80% of whom are living in low- and middle- income countries (WHO, 2006). Hearing loss has a greater economic impact and afflicts twice as many people as blindness and four times as many people as epilepsy, multiple sclerosis, spinal injury, stroke, Huntington's disease, and Parkinson's disease combined (CDC, 2009).

Nearly 30 million Americans (one in every ten) suffer from varying degrees of deafness, costing the nation over $56 billion annually (CDC, 2009). It is the number one birth defect in America, 20 times more prevalent than Phenylketonuria (PKU) and afflicting 3 in every 1000 newborns (CDC, 2009). For those affected by hearing loss during infancy, the services, special education, and adaptive needs will cost about $1,020,000 throughout the individual's lifetime (Grosse, 2001). For this reason, the strain of hearing loss weighs disproportionately on the poor. Without intervention, these children experience marked delay in the development of speech and language comprehension, as well

as cognitive skills, resulting in slow learning, difficulty progressing in school, and social stigmatization / isolation. Upon reaching adulthood, these effects translate into difficulty obtaining and keeping employment, greatly reducing chances to escape poverty.

The Joint Committee on Infant Hearing (2000) recommends that all infants be screened for hearing loss by one month of age, have a diagnostic follow-up by three months, and receive appropriate intervention services by 6 months of age. However, current hearing loss screening protocol mandates such measures be taken only in cases exhibiting predetermined risk factors, a protocol which only identifies 10-20% of afflicted infants (Elssmann, S.F., et al., 1987; Grosse, S., et al., 2001). Screening methods include two electrophysiological procedures that can be performed painlessly while the newborn sleeps. Auditory brainstem responses (ABR) are measured by placing sensors on the infant's head that record brainwave activity in response to sound introduced through tiny earphones to the baby. Otoacoustic emissions (OAE) are faint sounds produced by most normal inner ears. During testing, a tiny flexible plug, through which sound is projected, is inserted into the infant's ear. A microphone within the plug records otoacoustic emissions that the normal ear produces in response to incoming sound. These tests are painless, take about five minutes, and can be performed at a cost of about $25 - $60, a cost which is one tenth that of the mandatory screening of newborns for PKU (Grosse, S. 2001).

The first few months of life are critical to proper maturation of developing central auditory pathways. A lack of afferent stimulation during this time can

lead to improper temporal processing of the auditory code, a condition clinically manifested as significantly delayed speech and language development. Since even mild hearing loss can interfere with language perception and education performance, failure to identify hearing impaired children within these critical months has a profound socioeconomic effect on individuals, families, communities, and countries. However, prior to 6 months of age, if identified children receive appropriate intervention they exhibit marked improvement in speech and reading comprehension, minimizing the need for special education programs and lifelong habilitation (Yoshinaga-Itano and Apuzzo 1998). For example, if a child receiving adequate treatment can be mainstreamed into regular elementary and secondary school classes, as much as $420,000 in educational costs can be saved by his or her high school graduation (Joint Committee on Infant Hearing, 2000).

Cochlear Implants

Following the reintroduction of afferent stimuli via hearing aids or cochlear implants, patients suffering from moderate to profound hearing loss in both ears still exhibit poor language perception. Knowledge of the anatomical and functional status of central auditory nuclei in the congenitally deaf and the ability of these structures to reorganize following reintroduction of afferent stimuli are important issues in the care and management of the hearing impaired.

Functional imaging and biophysical studies of patients with cochlear implants provide a unique opportunity to study the central auditory system's

response to complete auditory deprivation followed by the reintroduction of afferent stimuli (Shepherd, R. et. al., 1997). Adult cochlear implant recipients appeared less successful at perceiving different rates of auditory stimulation as well as stimulus gap detection, evidencing a poor temporal processing ability crucial to speech perception and sound localization. Additionally, in comparing subjects deafened pre- and post linguistically, the former typically showed worse speech perception than those deafened after the onset of language development. However, in both cases, the duration of deafness was strongly negatively correlated with speech perception while experience using a cochlear implant exhibited a strong positive correlation.

These results indicate that despite the decreased signal to noise ratio of artificial neural transduction devices, maturational processes underlying the precise central temporal processing of the auditory code may be inherently plastic. In other words, the reduced temporal processing ability of post linguistically deafened cochlear implant recipients may simply reflect the limitation of "unnaturally" encrypting of the acoustic waveform into neural code. However, because these patients show improvement in temporal processing ability, we are left with the conclusion that pre-existing maturational changes are altered in response to new afferent stimulation. This, in turn, raises the implication that the mature state of central pathways may only persist in the presence of normal activity, and during the period of deafness, the silent neuronal circuits pathologically revert to a previously attained or brand new immature state. For

supporting evidence to this implication, we can look to the negative correlation between the length of deafness and performance in temporal processing tasks.

Clinical studies such as this also provide evidence of the need for the identification and early treatment of congenitally deaf individuals. If cochlear implants are given at an age that is early enough for central auditory pathways to be functionally mature by the time individual starts school, he of she may avoid placement in high cost special education classrooms.

dn/dn Mouse Model

The combination of pathological auditory brainstem responses resulting in poor speech discrimination and temporal processing ability is characteristic of auditory neuropathy. It is reasonable to conclude that factors contributing to the reduced performance are related to a reduction in spiral ganglion cells and / or an incomplete maturation of central auditory structures. The improvement of cochlear implant patients in temporal discrimination and gap detection of auditory stimuli, is evidence that the reintroduction of afferent stimuli was able to partially reverse the effects of auditory deprivation on central structures, but specific cellular mechanisms are largely unknown (Hudspeth, A.J., 1997). Many of these changes can be directly observed with the use of animal models. The current study hopes to determine specific developmental changes between normal hearing and congenitally deaf animal models.

The *dn/dn* "deafness" mouse is a naturally occurring strain in which there is a heritable, recessive mutation in the TMC1 (transmembrane cochlear-

expressed gene 1) gene, resulting in the malfunction, morphological abnormality, and degeneration of cochlear hair cells and spiral ganglion neurons (Kurima, et al. 2002; Leao, et al., 2004, Youssoufian, et al., 2008). There is 95-96% homology between the human and the mouse TMC1 amino acid sequence orthologs, and the mutation which occurs in the "deafness" mouse is also naturally occurring in humans, making the *dn/dn* mouse a useful model of human congenital deafness (Kurima et. al, 2003; Youssoufian, et al., 2008).

During the first 12 days of postnatal life, *dn/dn* inner ear development appears structurally normal, save for a poorly developed space of Nuel within the organ of Corti (Steel and Bock, 1980; Webster, D.B. 1992). At P12-P14, most inner and outer hair cells are present but undergo progressive degeneration such that by P40, fewer than 15% remain, and by P50 all inner and outer hair cells have degenerated along with 75% of spiral ganglion neurons (Steel and Bock, 1980; Webster, D.B., 1985; Webster D.B., 1992). As the hair cells degenerate, other cells of the organ of Corti lose their characteristic morphological appearance, until P50, when the structure appears to consist of an undifferentiated, cuboidal epithelium sitting upon a collapsed tunnel of Corti (Webster, D.B., 1992).

Evidence indicates that congenital deafness caused by the *dn/dn* mutation does not affect central connectivity to a large degree. Physiological studies have indicated that evoked potentials in response to direct electrical stimulation of the cochlear nerve can be recorded as far rostrally as the inferior colliculus, (Bock, et al., 1982). Similarly, anatomical studies have shown that the ipsilateral projections from the anteroventral cochlear nucleus (AVCN) to the lateral

superior olive (LSO) and the contralateral projections from the AVCN to the medial nucleus of the trapezoid body (MNTB) of the *dn/dn* mouse are intact (Youssoufian, et al., 2008).

Despite the presence of hair cells, the *dn/dn* mice are profoundly deaf at birth, with no evidence for spontaneous or acoustically evoked auditory nerve activity (Bock et al., 1982; Keats and Berlin, 1999; Oleskevich, et al., 2004; Leao et al., 2004a&b; Leao. et al., 2006). At young ages, the hair cells of *dn/dn* mice display an increased electrical resistance but an identical endocochlear potential when compared to age matched controls, suggesting that the mutation has not affected the driving force for K^+ to cross the apical membrane of the hair cell (Steel and Bock, 1980). Thus, the most likely explanation for the deafness (and possibly the subsequent degeneration) is that a mutation in the transmembrane protein encoded by the TMC1 gene prevents ion channels in the apical surface of the hair cell from opening correctly (Steel and Bock, 1980; Kurima, et al., 2002).

Many mouse mutants have an apparent deficiency in the responsiveness to sound, but most of them, including *shaker-1* and *Ames waltzer*, have non-auditory related abnormalities which throw doubt on their usefulness as models for congenital deafness in man (Steel and Bock, 1980). Additionally, animal models of cochlear ablation introduce trauma into the experimental model, which itself cause changes in CNS structures independent from a mere lack of afferent stimulation. Because the *dn/dn* deafness mouse exhibits no other abnormalities, when it is bred from the CBA/J strain - which exhibits no age related hearing loss - experiments using both strains of mice are particularly powerful in their

implications into human congenital deafness (Bock, et. al, 1982; Keats and Berlin, 1999; Oleskevich, et al., 2004; Leao et al., 2004a&b; Leao. et al., 2006; Walmsley et. al., 2006).

It is important to understand the functional capabilities of auditory synapses in congenital deafness, particularly in endbulb and calyceal synapses (Ryugo, et al., 1997). These synapses are not only integral to the temporal processing of sound localization, but may also be essential to analyzing the temporal features of intraspecies vocalizations (Ryugo et al., 1997). Data which shows altered firing properties that would clearly disrupt the precision and high frequency at which these synapses can respond to and encode auditory stimuli is pertinent to reports on the success of patients with cochlear implants. By performing developmental analysis on deaf animal models, such as the present study, we can further our understanding of what factors may impede proper temporal processing and subsequent speech recognition in patients with cochlear implants. Additionally, we can learn specific time points when pre- and post-linguistically deafened patients need to receive cochlear implants in order to effectively counter any deleterious effects deafness might have on central auditory structures as well as bolster the need to liberalize requirements for pre and post natal screening for hearing impairments.

Endbulb and calyceal type synapses, which contain thousands of active zones, are the largest known synaptic endings in the central nervous system (Figure 2). Such structural characteristics are consistent with the notion that these synapses are developmentally specialized to ensure a high fidelity of synaptic

transmission in which every presynaptic event triggers a postsynaptic response, a necessary "fail safe" for neurons tightly coupled to the precisely timed auditory code (Pfeiffer, 1966). In this regard, studies on congenital deafness have implications far beyond that of the disease itself. They provide critical insight into questions concerning the general role of activity on the developmental regulation of synaptic transmission and neuronal membrane properties.

Deafness and the Endbulb of Held – Globular Bushy Cell Synapse

Experiments of this type have not only led to a deeper understanding of the central effects of congenital deafness, but have also elucidated which processes regulating synaptic firing properties and neuronal signaling capabilities are activity dependent and activity independent. Oleskevich and Walmsley (2002), showed by focally stimulating single auditory nerve fibers while taking simultaneous whole cell recordings from bushy cells of the AVCN (mean age ~P13) that the endbulb of Held – bushy cell synapse in *dn/dn* mice have altered physiological properties. Specifically, *dn/dn* bushy cells exhibit eEPSCs (evoked excitatory postsynaptic currents) that are approximately 170% larger than those in age matched CBA/J mice. Additionally, deaf mice exhibit an increase in frequency but not in amplitude of asynchronous mEPSCs (miniature excitatory postsynaptic potentials), indicating that the enhanced excitability is not due to an increase in quantal content, but an increase in transmitter release probability. Because the application of EGTA to the *dn/dn* recording preparation is able to reduce the synaptic excitability to a level equivalent with CBA/J mice, Oleskevich

and Walmsley (2002) suggest the increase in presynaptic release probability is possibly due to altered Ca^{2+} buffering. Aim 1 and 2 of the current study will provide immunohistochemical data showing the pattern of expression of calcium buffering proteins within these synapses in CBA/J and *dn/dn* mice.

It should be noted that Ryugo et al. (1997) has shown significant hypertrophy of pre- and postsynaptic densities in congenitally deaf white cats as well as a significant increase in synaptic vesicles per postsynaptic density that could be a homeostatic response to diminished transmitter release. An increase in docked or readily releasable vesicle pools in *dn/dn* mice could cause an increase in release probability similar to that observed by Oleskevich and Walmsley (2002). In this scenario, presynaptic active zones are more sensitive to Ca^{2+} influx, and the EGTA-induced decrease in excitability counters this effect. Studies are currently being performed in our lab to determine if an increase in docked or readily releasable vesicle pools in *dn/dn* mice could account for the increased excitability observed in the endbulb-bushy cell synapse.

The increase in excitability suggests a homeostatic mechanism of synaptic plasticity designed to maintain average firing rate near a desired level (Turrigiano and Nelson, 2004; Walmsley et al., 2006) in which decreased firing rate causes an increase in presynaptic release probability without affecting postsynaptic membrane properties. However, the mechanisms observed by Oleskevich and Walmsley (2002), stand in contrast to apparent homeostatic mechanisms in the primary auditory cortex of cochlear ablated gerbils, in which layer 2/3 pyramidal neurons display larger amplitude eEPSCs resulting from postsynaptic alterations.

In this study, decreased frequency and increased amplitude of mEPSCs, coupled with a depolarized postsynaptic resting membrane potential, suggest that a decrease in presynaptic release probability is compensated for by an increase in excitatory response (Kotak et al., 2005).

Anatomical studies of the endbulb of Held – bushy cell synapse have revealed several structural changes in *dn/dn* mice compared to age matched CBA/J mice. Postsynaptically, bushy cells in *dn/dn* mice exhibit similar membrane properties and morphology age controls (Walmsley et al., 2006), but a significant decrease in size (Webster, D.B., 1985). Saada et al., (1996) and Seldon & Clark (1991) made similar observations regarding soma size in the cochlear nucleus in deaf white cats and profoundly deaf humans, respectively. Presynaptically, both strains show an age related increase in the fenestration of endbulbs of Held, visible as more complex axonal endings with increased branching at older ages (Youssoufian, et al., 2008). However, the volumes of endbulbs in P20-P22 dn/dn mice were approximately 200 μm^3 less than aged matched CBA/J (Youssoufian, et al., 2008). This correlates with observations of the endbulb of Held in deaf white cats. Endbulb area is significantly smaller in deaf white cats than normal cats, presumably due to stunted arborizations of the presynaptic terminals (Ryugo, et al., 1997). Data presented in these studies, when taken with observations by Ryugo et. al (2006) that endbulbs arising from auditory nerve fibers exhibiting high spontaneous firing rates have greater aborization with more numerous synaptic specializations than those arising from low-spontaneous rate fibers, suggest that spontaneous auditory nerve activity is

directly correlated with endbulb size and morphology (Walmsley, et al., 2006; Youssoufian, et al., 2008). Studies using electron microscopy and serial reconstructions are currently being performed in our lab to determine if the altered input in *dn/dn* mice affects the size and morphology of endbulbs of Held compared to age matched CBA/J mice.

Deafness and the Calyx of Held – MNTB Principal Cell Synapse

Results of a study focusing on the synapse formed by axonal projections from the AVCN globular bushy cell, suggest that physiology at the MNTB calyx of Held – principal cell synapse is also altered in *dn/dn* mice compared to age matched CBA/J animals. However, the altered physiology is manifested not as a change in basal synaptic transmission, as it is in the endbulb – bushy cell synapse but as a radical difference in postsynaptic firing properties. Within the MNTB calyx – principal cell synapse, Oleskevich et al. (2004) found no significant differences between age matched *dn/dn* and CBA/J mice in the amplitude of eEPSCs or frequency of mEPSCs. Instead, Leao et al. (2004) showed that a substantially smaller DTX-sensitive, low threshold K^+ current, which activates near resting potential, increases the excitability of *dn/dn* principal cells. In CBA/J mice, these cells respond to suprathreshold current steps (150 pA, 800 ms) with a single short latency action potential, while larger current injections (>250 pA, 800ms) result in 2 – 5 short latency action potentials within only the first 10 ms of the current pulse (see also Brew et al., 2003). In contrast, principal cells of *dn/dn* mice reach threshold with a smaller amplitude current pulse (50 pA) and respond

to suprathreshold current injections with a train of 10 to 50 action potentials that directly varies in frequency with the amplitude of the injected current. Leao et al. (2004) suggests the depolarized resting membrane potential and repeated firing correlates with a reduction in outwardly directed, low voltage activated K^+ currents found in *dn/dn* principal cells.

The implication that low threshold K^+ currents play a role in regulating central synaptic excitability correlates well with previous research. By applying Margatoxin, a low voltage activated K^+ channel antagonist, to the calyx of Held, Ishikawa, et al., (2003) was able to reduce the amount of depolarization required for action potential generation, thereby inducing a burst of spikes in response to prolonged depolarization.

In further studies of the effects of deafness on ion channel expression Leao et al. (2005; 2006) has shown physiological evidence for tonotopic gradients of both low and high threshold K^+ currents as well as hyperpolarization-activated cation currents in the MNTB of CBA/J mice which are absent in *dn/dn* mice. Immunohistochemical data confirms the existence tonotopic gradients of $K_v1.1$, $K_v3.1$, and HCN4 channel expression in CBA/J but not *dn/dn* which could account for this finding. These results, which indicate that depolarizing activity in central neurons plays a role in regulating ion channel expression, correlate well with Leao et al. (2004) as well as with observations of tissue cultured cortical neurons by Desai et al., (1999) where a reduction in activity (by bath application of TTX) results in a down regulation of K^+ currents.

It should be noted, however, when interpreting the role of deafness on results of calyx – principal cell studies, that spontaneous auditory nerve activity is present in the ventral cochlear nucleus of deaf mice (Youssoufian, et al., 2008). This spontaneous activity could be adequate to ensure the proper connectivity and morphology (in terms of both synaptic size and degree of fenestration) of this synapse, but that acoustic evoked activity is necessary for proper regulation of neuronal membrane properties.

Sound Localization Pathways

The mouse, like all vertebrates, is capable of critically examining the auditory code to reveal where events arise in the environment and what they represent. A goal fundamental to understanding the auditory system concerns identifying the critical features of neuronal transmission necessary for the detection, localization, and interpretation of acoustic events and the manner in which these features are represented within the central nervous system.

The cochlea encrypts the auditory signal into precisely timed action potentials conveying information regarding both the frequency and intensity of a sound (see appendix 1). From the cochlea, auditory information, which is contained in both the spatial activation of auditory nerve fibers as well as their temporally precise firing patterns, is sent to the cochlear nucleus. It is the job of the cochlear nucleus, the obligate terminal for auditory nerve fibers, to begin deciphering this spatial and temporal code, rebuilding its elements into a coherent image of the outside world (Ferragamo and Oertel, 2002). Divergent central

pathways faithfully propagate this information through several synapses before extracting information regarding the location of sound from temporally precise binaural comparisons of time and intensity at the superior olivary complex (Figure 1).

Within the anteroventral cochlear nucleus, spherical and globular bushy cells of the AVCN receive from the auditory nerve large, calyceal-type glutamatergic synaptic terminals called endbulbs of Held (Oleskevich, et ala, 2004). The spherical bushy cells send bilateral glutamatergic projections the medial superior olive (MSO) (although the extent to which this occurs in mice is debated) and ipsilateral projections to the lateral superior olive (LSO). Globular bushy cells send contralateral glutamatergic projections to the principal cells of the medial nucleus of the trapezoid body (MNTB). Within the MNTB, these axonal projections give rise to a single calyceal type synaptic terminal, called the calyx of Held.

The MNTB, in turn, gives rise to inhibitory, glycinergic axons that project ipsilaterally to both the MSO and LSO (Harrison and Irving, 1964, 1965, 1966; Morest, 1968; Kuwabara and Zook, 1991; Smith, et al., 1991, 1993, 1998; Bergsman, et al., 2004). Thus, the calyx of held is sign-inverting relay, converting excitatory glutamatergic input into inhibitory glycinergic output. Neurons of the LSO, extract the azimuthal location of a sound source by comparing the intensity of precisely timed excitatory input from the ipsilateral ear with inhibitory input by way of the MNTB from the contralateral ear.

The endbulbs and calyces of Held have become the subjects of increasing scrutiny as they are specialized for the precise timing of high frequency synaptic transmission. Further, the large size of the calyx of Held has permitted researchers to simultaneously record from central presynaptic terminals and their postsynaptic targets (Forsythe, 1994; Borst, et al., 1995). To date, this has not been accomplished in the endbulb of Held due to its smaller surface area. However, that both endbulbs and calyces form large axosomatic contacts with their target cells have made them ideal models for central synaptic research.

These two calyceal type terminals share many morphologic and physiologic features (Ryugo et al., 1997, Smith, et al., 1998, Nicol & Walmsley, 2002; Taschenberger et al., 2002, Oleskevish et al., 2004). The calyx of Held is a cup like structure with finger like stalks that covers roughly 40% of the principal cell surface area (Smith, et al., 1998). Only one calyx of Held contacts each single principal cell. Although many bushy cells receive more than one endbulb of Held, these endbulbs also develop into finger-like stalks that cover a comparable percentage of the bushy cells surface area (Kuwabara, et al., 1991, Kandler & Friauf 1993; Oleskevich et al., 2004). Both endbulbs and calyces contain hundreds of active zones with clusters of spherical vesicles (Ryugo et al., 1997; Smith et al., 1998; Nicol & Walmsley 2002; Taschenberger et al., 2002, Oleskevish et al., 2004). Similar developmental changes occur at each synapse with regard to the specific complement of ion channels and AMPA receptors which allow for faithful transmission of high frequency action potential trains conveying critical information for sound localization (Oleskevish et al., 2004).

This study seeks to determine the developmental distribution of calcium buffering proteins within these synapses, as the role of calcium is critical in neuronal signaling and synaptic transmission. (For more information on the anatomy of sound localization pathways see appendix 2.)

Tonotopic Organization in the Auditory Pathway

A tonotopic organization of cells that optimally fire at different characteristic frequencies exists throughout the auditory system (Friauf & Lohmann, 1999; Leao et al., 2006). Beginning in the cochlea itself, where inner hair cells in the basal region of the cochlea are maximally stimulated by high frequency sound and those in the apical region of the cochlea respond bets to low frequency sound, this organization, this organization continues into the brainstem and extends as far rostrally as the auditory cortex. Within the MNTB, cells responding best to high frequency auditory stimulation are located medially, while those responding best to low frequency auditory stimulation are located laterally (Leao, et al., 2006) (Figure 3). While this gradient is initially established by labeled lines in which low frequency regions of the MNTB ultimately receive input from the apical portion of the cochlea (and vice versa for high frequency regions of the MNTB an the basal cochlea), distinct medio-lateral gradients of ion channels develop which provide a each calyx-principal cell pair with a particular molecular profile efficient for efficiently generating precisely timed trains of pre and postsynaptic action potentials. For example, in normal mice, low threshold $K_V1.1$ channels are preferentially located in more lateral regions of the nucleus,

while high threshold $K_V3.1$ channels and HCN4 channels are preferentially located in the medial portion of the nucleus (Leao, et al. 2006). Interestingly, these gradients are abolished in deaf animals (Leao et. al., 2006). Thus, these ion channel gradients are presumably established during postnatal development, after the onset of hearing, when calyx-principal cell synapses are driven at a particular range of frequencies. There is evidence, that ongoing nervous activity establishes the $K_V3.1$ channel gradient through differential activation of the CREB pathway, owing to varying levels of cAMP and calcium in response to stimuli of varying frequencies (Kaczmarek et al., 2005). Because cAMP and calcium levels rise as a result of repetitive stimulation, and both cAMP and calcium can lead to the phosphorylation of CREB and, the activity of the CRE-containing $K_V3.1$ promoter is enhanced by neuronal stimulation (Kaczmarek et al., 2005). Thus, the selective distribution of ion channels may allow for the efficient and faithful transmission of auditory signals.

Calcium Buffering Proteins

When a presynaptic action potential reaches a synaptic terminal, the voltage dependent Ca^{2+} current creates a large spike in $[Ca^{2+}]_i$, which triggers the fusion of presynaptic vesicles with the plasma membrane and the subsequent release of neurotransmitter into the synaptic cleft (Katz & Miledi, 1965, 1967, 1968, 1970; Felmy et al., 2003). In order to reduce aberrant transmitter release and achieve its role as a second messenger, $[Ca^{2+}]_I$ is tightly regulated in space, time, and magnitude. The spatiotemporal characteristics of short lived and highly

localized Ca^{2+} signals results from the dynamic interplay of Ca^{2+} influx/ extrusion mechanisms, intracellular sequestering mechanisms, and mobile/stationary Ca^{2+} buffering proteins (CaBP) (Faas, et al., 2007). Various Ca^{2+} extrusion and sequestering systems have evolved maintain low $[Ca^{2+}]_i$. Na+/ Ca^{2+} exchangers and Ca^{2+} ATPases (PMCA) in the plasma membrane can energetically drive Ca^{2+} out of the cell (Garcia & Strehler 1999; Carafoli et al. 2001), and Ca^{2+} pumps in the endo(sarco)plasmic reticulum (SERCA) and transporters in mitochondrial membranes can sequester Ca^{2+} in the endo(sarco)plasmic reticulum and mitochondrial matrices, respectively (Carafoli et al. 2001). Additionally, several CaBPs, including calretinin (CR), calbindin (CB) and parvalbumin (PV), are found throughout the central nervous system to help maintain tightly regulated Ca^{2+} signals (Celio, 1990; Rogers & Resibios, 1992).

CB and PV belong to the EF-hand family of CaBPs, consisting of a Ca^{2+} coordinating helix-loop-helix peptide sequence (Chard, et al., 1993). CB has six EF-hand domains, two of which are non-functional, thus binding Ca^{2+} with a stoichiometry of four (Chard, et al., 1993). PV, conversely, has only 2 high affinity Ca^{2+} binding domains. The concentrations of these proteins vary between cells, but each has been estimated to be as high as 1mM (Heizmann & Hunziker, 1991). Chard, et al., (1993) showed that CB, when introduced into DRG cells caused an 8-fold decrease in the rate of rise of $[Ca^{2+}]_I$ and altered the decay kinetics of $[Ca^{2+}]_I$ to a single slow component. PV, however, only minimally slowed the rate of rise $[Ca^{2+}]_I$ and selectively increased the fast component of the decay of $[Ca^{2+}]_I$ signal. These differing effects on $[Ca^{2+}]_I$ owes to the differential

binding kinetics between these two CaBPs. CB, which has fast kinetics, was able to bind Ca^{2+} ions fast enough to slow the rate of $[Ca^{2+}]_I$ but was quickly saturated such that the decay rate of $[Ca^{2+}]_I$ consisted of only a single slow component. However, PV, which has slow binding kinetics, could not bind Ca^{2+} ions fast enough to slow the rate of $[Ca^{2+}]_I$ but did not saturate until during the decay of the Ca^{2+} signal, thereby increasing the fast component of the decay of $[Ca^{2+}]_I$ signal until PV saturation, at which point, decay kinetics slowed.

Fewer studies exist on the Ca^{2+} buffering properties of CR, also a member of the EF-hand family of CaBPs. Its structural similarity to CB has led most researchers to believe it functions in a nearly identical manner. However, that neurons typically express one protein or the other and only occasionally express both CR and CB, indicates the possibility that differences exist in the effect each protein could have on the Ca^{2+} signal. Further, recent studies have shown that CR contains 5, not 4, functionally active Ca^{2+} binding domains, of which two pairs (sites I-II and III-IV) exhibit cooperative binding (Schwaller et al., 1997). It is unclear whether cooperative binding exists in PV or CB. This cooperative nature of Ca^{2+} binding to CR results in accelerated binding as free $[Ca^{2+}]_I$ increases from cytoplasmic resting conditions (Faas et al., 2007). As a consequence, the Ca^{2+} buffering speed of CR is largely dependent on the prevailing free $[Ca^{2+}]_I$ prior to perturbation of the Ca^{2+} signal. This could create subtle differences in the effect of Ca^{2+} signaling between CR and CB, which would account for their differential, and sometimes overlapping, expression.

Despite the abundance of research as the exact role of Ca^{2+} buffering proteins remains elusive. It is clear that they are capable of the passive modulation of synaptic activity described above, but it remains contentious whether they play an active role in Ca^{2+} mediated signal transduction. Within the calyx of Held, these Ca^{2+} buffering proteins reversibly bind Ca^{2+} ions, modulating transmitter release and Ca^{2+} -dependent forms of synaptic plasticity (Felmy & Schneggenburger, 2004). CR and CB have been shown to decrease peak $[Ca^{2+}]_I$ by biding incoming Ca^{2+} ions before they reach their intracellular target, thereby modulating transmitter release probability during basal synaptic transmission (Nagerl, et al., 2000, Felmy & Schneggenburger, 2004). Conversely, PV decreases residual $[Ca^{2+}]$ following Ca^{2+} influx, resulting in the suppression of synaptic facilitation without altering the amplitude of the Ca^{2+} current (Caillard et al., 2000). Here we compare the developmental distributions of CR, CB, and PV in the MNTB of normal hearing (CBA/J) and congenitally deaf (*dn/dn*) mice to define regions along the MNTB tonotopic axis where they may be singly or co-localized. It is hoped that the precise definition of the pattern of CaBP expression during normal development and in the absence of afferent auditory nerve activity will provide further insight into the specific function of each protein as well as what effect neuronal activity plays on their expression.

Figure 1. The auditory pathway in mammals
This is a simplified schematic diagram showing and the central projections of spiral ganglion cells, the auditory nerve fibers (AN), which form giant calyceal type excitatory synapses, the endbulbs of Held, on bushy cells in the anteroventral cochlear nucleus (AVCN). Spherical bushy cells (pink) in the AVCN make ipsilateral contacts with cells in the lateral superior olive (LSO) and bilateral contacts with cells in the medial superior olive (MSO). Globular bushy cells (blue) give rise to axons that form giant calyceal type excitatory synapses, the calyces of Held, with principal cell somata in the contralateral medial nucleus of the trapezoid body (MNTB). The principal cells in the MNTB, in turn, give rise to inhibitory axons which project to the ipsilateral MSO and ipsilateral LSO. Inhibitory glycinergic neurons and synapses are shown in red, while excitatory glutamatergic neurons and synapses are shown in black. (Reprinted, with permission, from Walmsley et al. 2006)

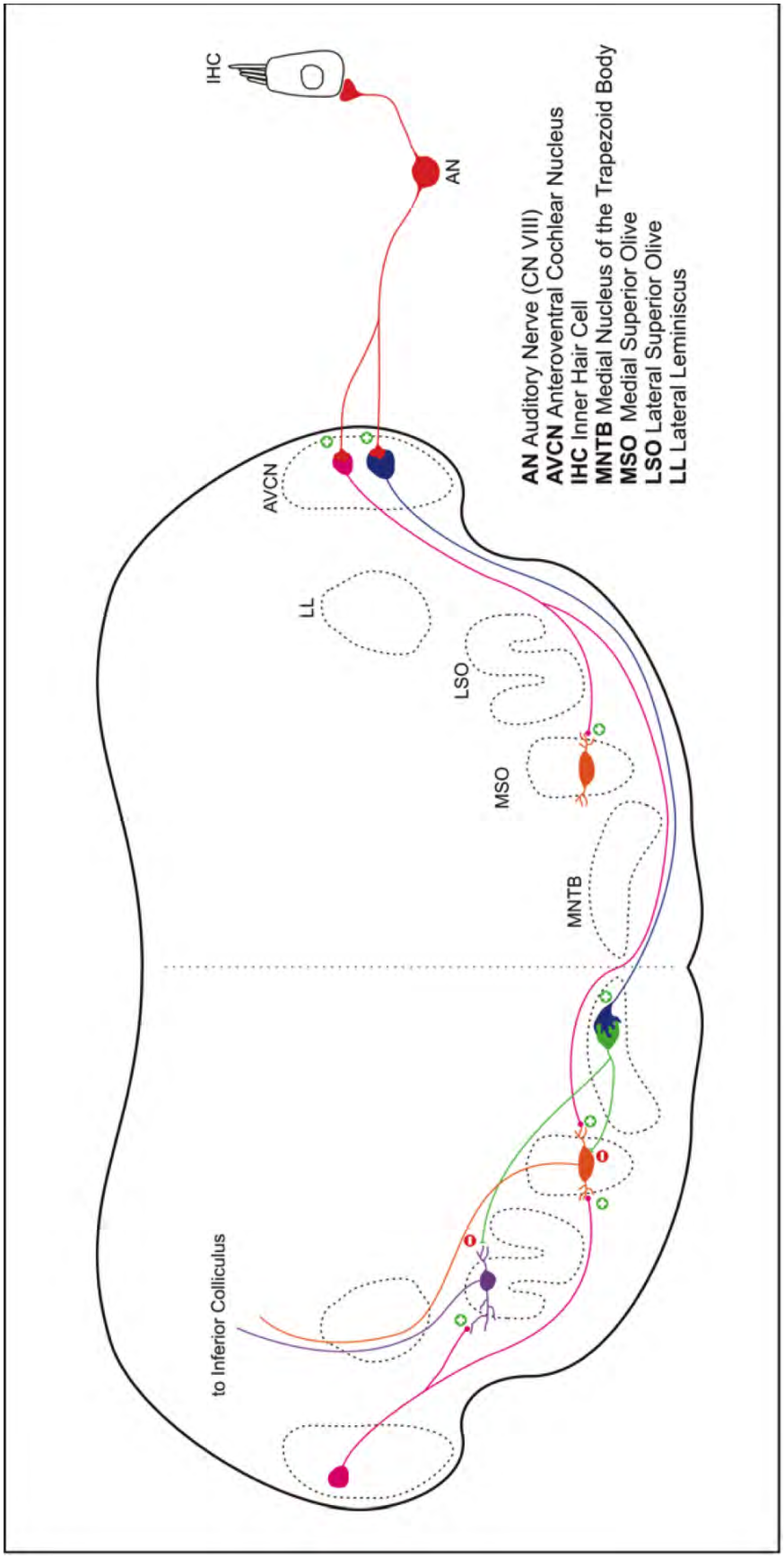
IHC
AN
AVCN
LL
LSO
MSO
MNTB
to Inferior Colliculus
AN Auditory Nerve (CN VIII)
AVCN Anteroventral Cochlear Nucleus
IHC Inner Hair Cell
MNTB Medial Nucleus of the Trapezoid Body
MSO Medial Superior Olive
LSO Lateral Superior Olive
LL Lateral Leminiscus

Figure 2. A calyceal-type terminal
This is a schematic depicting an example of a calyceal-type terminal, like those found at the Endbulb of Held synapse in the AVCN and the Calyx of Held synapse in the MNTB. (Reprinted, with permission, from Walmsley, Alvarez & Fyffe 1998).

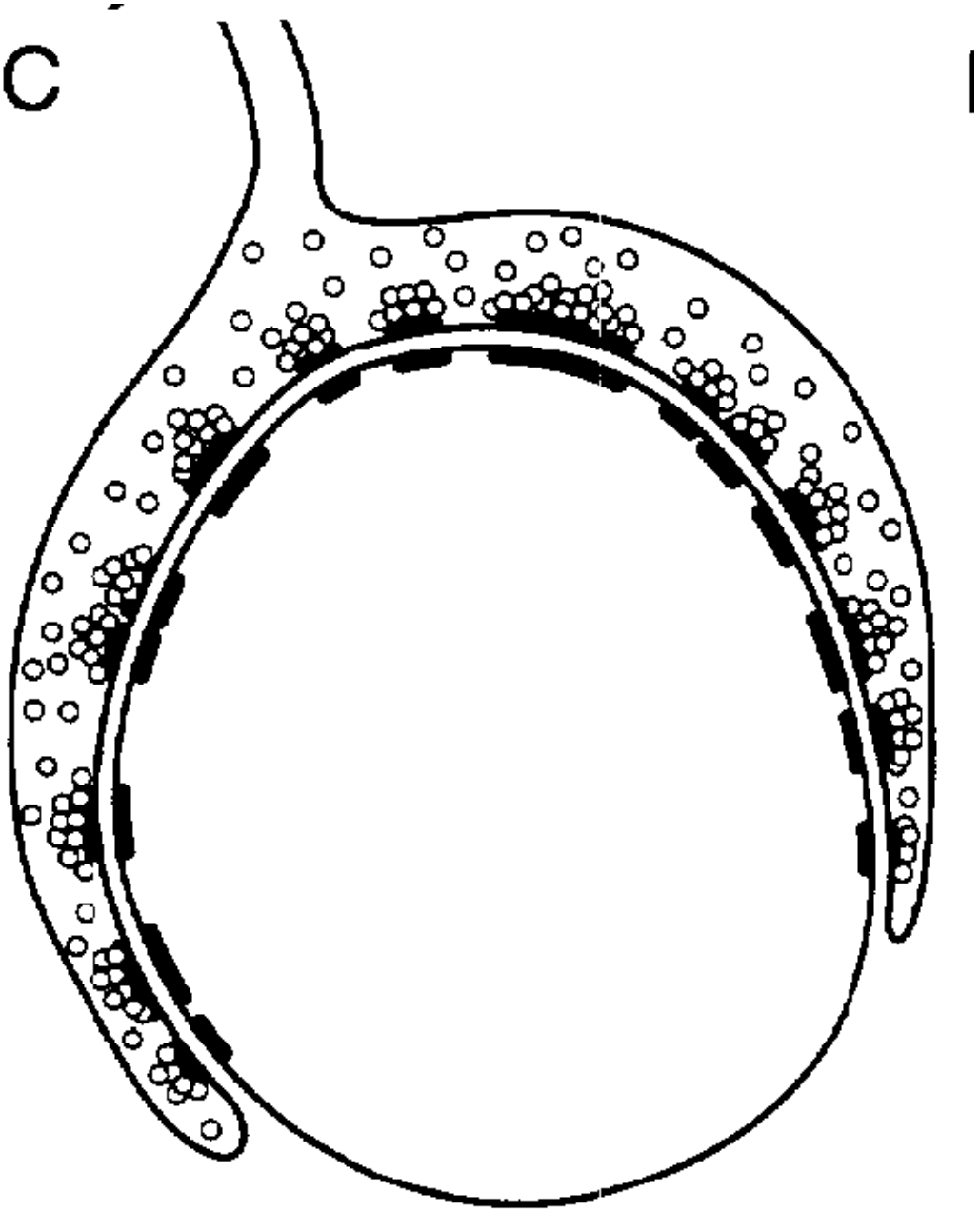
C

Figure 3. Tonotopic organization of the MNTB in normal and *dn/dn* mice
Schematics at the top of the figure represent the medio-lateral tonotopic organization of the MNTB. Schematic at left illustrates that in normal mice, medially located principal cells respond best to high frequency stimulation, and laterally-located principal cells respond best to low frequency stimulation. Below this schematic, gradients of channel expression that underlie the tonotopic organization of the MNTB in normal mice are illustrated. Kv3.1 and HC4 channels are preferentially located in medial principal cells, while Kv1.1 channels are preferentially located in lateral principal cells. Schematic at right illustrates that in *dn/dn* mice, no tonotopic organization of cells is observed. Below this schematic, the lack of gradients of channel expression in the MNTB of *dn/dn* mice is illustrated. (Reprinted, with permission, from Walmsley et al. 2006).

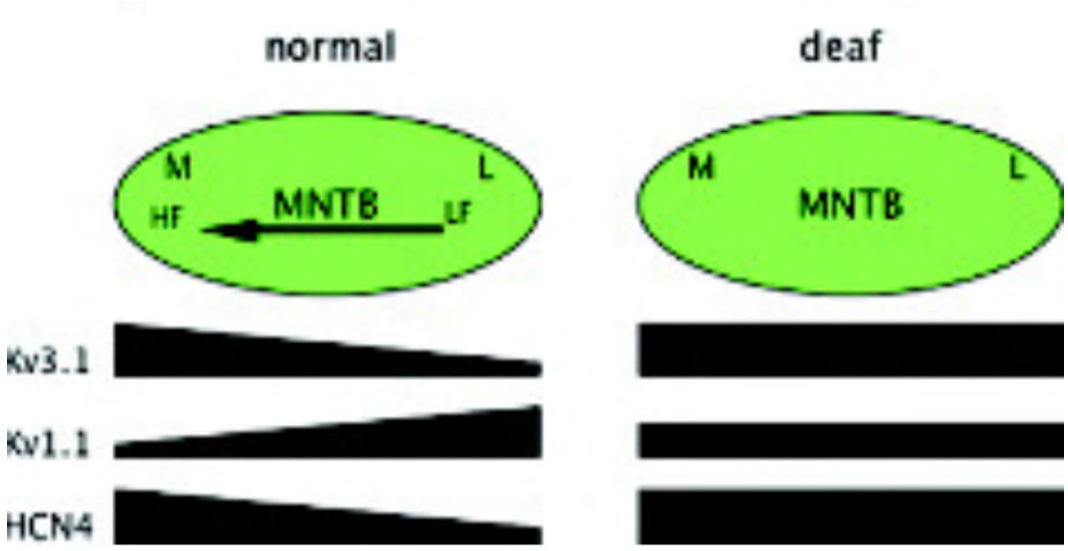
normal
deaf
M
L
HF
MNTB
LF
M
L
MNTB
Kv3.1
Kv1.1
HCN4

IV. METHODS

Tissue Processing

All animal use was in accordance with National Institute of Health guidelines and approved by Wright State University LACUC. Normal hearing CBA/J and congenitally deaf (dn/dn) mice (9 days, 13 days, and 30 days postnatal) were euthanized and perfused intracardially by fixative (4% paraformaldehyde). The 9 and 13 days postnatal time points were chosen to represent points just before and just after the opening of the ear canal in both CBA/J and *dn/dn* mice. The opening of the ear canal, occurring at 11 days postnatal (Oleskevich and Walmsley, 2002), corresponds with the onset of hearing in CBA/J mice. 30 and 49 days postnatal were chosen as time points in which the mice had advanced in development and calyces of Held reached functional development. Transverse sections (14 μm thick) were obtained at the level of MNTB/AVCN on a cyrostat (Microm HM505E). Two - four animals were analyzed per age group within control and deaf strains.

All mice were anaesthetized intraperitoneally with Nembutal (50mg/ml) at 100 mg/kg body weight and perfused via the left ventricle with cold vascular rinse (.01M phosphate buffer with 137 mM NaCl, 3.4 mM KCl, and 6.0 $NaHCO_3$ at 4^oC) followed by room temperature fixative (4% paraformaldehyde in 0.1 M phosphate buffer at pH 7.4) for 10-15 minutes. Following perfusion, brains and spinal cords were dissected out and post-fixed (4% paraformaldehyde in 0.1 M phosphate buffer at pH 7.4) at 4^oC overnight. The next day, nervous tissue was

transferred into 15% Sucrose (in 0.1 M phosphate buffer) solution at 4°C until ready for sectioning.

Immunohistochemistry

Before sectioning, the brainstem and cerebellum were isolated at the level of the pons and medulla as well as the lumbar/thoracic enlargement of the spinal cord (for spinal cord images). A Microm HM 505E cryostat (Carl Zeiss, Inc., Thornwood NY) was used for sectioning.

Tissue was submerged in cryoprotectant solution (500 ml 0.1 M phosphate buffer at pH 7.2, 300 g sucrose 10 g polyvinylpyrrolidone, 300 ml ethylene glycol, 200 ml double distilled H_2O) for 5 – 10 minutes, OCT (Tissue-Tek #4583) for 5 – 10 minutes, flash frozen on a cryostat stage in liquid nitrogen, and cooled to -25°C in the cryostat for 30+ minutes.

Transverse sections (14 μm thick) were cut from the brainstem/cerebellum at the level of the Pons and Medulla at the location of the cochlear nucleus and superior olivary complex and mounted directly onto slides. Sections were washed once for 5 minutes with 0.01 M phosphate buffered saline solution (PBS) and then twice for 10 minutes in 0.01 M phosphate buffered saline solution with 0.1 – 0.3% Triton X-100 (PBS-T). Sections were then incubated at room temperature in Normal Horse Serum (1:10 in 0.01 M PBS-T) for 1-2 hours. After removing the Normal Horse Serum, double and triple labeling was performed by incubating the sections overnight at 4°C using any combination of the following primary antibodies: mouse monoclonal anti-calretinin (1:500 in PBS-T; Zymed; San

Franciso, CA), mouse monoclonal anti-parvalbumin (1:2000 in PBS-T; Chemicon; Temecula, CA), mouse monoclonal anti-calbindin D-28k (1:1000 in PBS-T; Swant; Belllizona, Switzerland), and rabbit polyclonal anti-calbindin D-28k (1:2000 in PBS-T; Chemicon; Temecula, CA) to label calcium buffering proteins; guinea pig polyclonal anti-vesicular glutamate transporter 1 (VGlut1) (1:1000 in PBS-T; Chemicon; Temecula, CA) to label glutamatergic presynaptic terminals; and mouse monoclonal anti-gephryn 7a (1:100 in PBS-T; Boehringer Mannheim, Indianapolis, IN) and the mouse monoclonal GABAergic marker anti-Glutamic Acid Decarboxylase (GAD65) (1:200 in PBS-T; BD Pharminogen) to label inhibitory postsynaptic receptors and presynaptic terminals, respectively. Immunostaining was revealed by 3x10 minute washes in PBS-T followed by light protected incubation for 2-4 hours in CY3, CY5, and FITC conjugated secondary antibodies (1:50 - 1:200 in PBS-T; Jackson Immuno; West Grove, PA) at room temperature. Sections were then washed in 0.01 M PBS-T for 2×10 minutes and 0.01 M PBS for 2×10 minutes, allowed to air dry, and coverslipped with fluorescence mounting medium (Vectashield; Vector; Burlingame, CA). Alternatively, sections labeled for Nissl Bodies were incubated at room temperature in pre-conjugated FITC anti-Nissl (1:100 in PBS; Molecular Probes; Eugene, OR) for 30 minutes following the 2-4 hour incubation in CY3 and/or CY5 conjugated secondary antibodies. These sections were then washed and coverslipped as detailed above.

Specificity of Antibodies

Mouse anti-calretinin monoclonal antibody (Zymed, San Francisco, CA) is a mouse IgG that reacts with calretinin, a protein with a Molecular Weight (M.W.) of 29 kDa. Specificity was verified via immunoblotting followed by two-dimensional gel analysis. Endogenous expression was shown through microscopy, which is standard protocol for Zymed (personal communication). Mouse anti-parvalbumin monoclonal antibody (Chemicon, Temecula, CA) is a mouse IgG that has been shown to react with Parvalbumin (MW 12 kDa) in human, rat, bovine, porcine, feline, rabbit, canine, frog, fish and goat neural and muscular tissue. By immunoblot it recognizes a M.W. protein of 12 kDa. The antibody is directed against an epitope at the first Ca^{2+}-binding site and specifically stains the Ca^{2+}-bound form of parvalbumin. Mouse anti-calbindin D-28k monoclonal antibody (Swant, Bellinzona, Switzerland) is a mouse IgG that reacts with calbindin D-28k (MW 28 kDa) from human, monkey, rabbit, rat, mouse and chicken tissues. It does not react with other known Ca^{2+}-binding proteins, as it specifically stains the 45CA-binding spot of calbindin D-28k (MW 28 kDa, IEP 4.8) in a two-dimensional gel. In radioimmunoassay it detects calbindin D-28k with a sensitivity of 10 ng/assay and an affinity of 1.6 x 1012 L/M. Rabbit anti-calbindin D-28k polyclonal antibody (Chemicon, Temecula, CA) is an affinity purified rabbit IgG that has been shown to react with calbindin D-28k (MW 28 kDa) from human, rat, and mouse tissue. It does not cross-react with calretinin as evidenced by Western Blot and affinity preabsorbtion against calretinin. Immunoblot produces one band at 28 kDa. Mouse anti-glutamic acid decarboxylase (GAD65) monoclonal antibody (BD Pharminogen) is a mouse

IgG2a immunogen purified by affinity chromatography. That has been shown to react with GAD65 (MW 65 kDa) from human, rat, and pig nervous tissue. The specific epitope recognized by this antibody is a linear epitope localized in the last 41 amino acids of GAD65. Western blot analysis produces a single bar at 65 kDa. guinea pig anti-vesicular glutamate transporter 1 (VGLUT1) polyclonal antibody (Chemicon, Temecula, CA) reacts with VGLUT1 protein in nerve fibers and terminals (Fig. 4-5). Preabsorption of the VGLUT1 antiserum with immunogen peptide eliminates all immunostaining, thus confirming its specificity.

Cy-3-conjugated donkey anti-mouse IgG secondary antibody (Jackson, West Grove, PA) reacts with the heavy chains on mouse IgG and with the light chains common to most mouse immunoglobulins, based on immunoelectrophoresis. No antibody was detected against non-immunoglobulin serum proteins. It has been tested by ELISA and/or solid-phase adsorbed to ensure minimal cross-reaction with bovine, chicken, goat, guinea pig, Syrian hamster, horse, human, rabbit, and sheep serum proteins. FITC-conjugated donkey anti-guinea pig IgG secondary antibody (Jackson, West Grove, PA) reacts with the heavy chains on guinea pig IgG and with the light chains common to most guinea pig immunoglobulins. No antibody was detected against non-immunoglobulin serum proteins. It has been tested by ELISA and/or solid-phase adsorbed to ensure minimal cross-reaction with bovine, chicken, guinea pig, Syrian hamster, horse, human, mouse, rabbit, rat, and sheep serum proteins. Green fluorescent Nissl stain (Molecular Probes, Eugene, OR) binds to Nissl substance,

or rough endoplasmic reticulum, within the soma of a neuron. Specifically, it binds to ribosomal RNA on the surface of endoplasmic reticulum which is found in abundance in neuronal somata due to their large need for protein synthesis. The stain is essentially nonfluorescent, except when bound to DNA or RNA.

When analyzing expression of CR, CB, and PV in the MNTB, the pattern of expression of each of these proteins in the cerebellum was observed (Figure 4, 5, & 6). In the cerebellum, any Ca2+-binding protein expression should not be affected by the presence or absence of auditory nerve activity. Thus, the pattern of Ca2+-binding protein expression in the cerebellum served as a negative control, and was used to ensure that the staining conditions in the MNTB were consistent from animal to animal. In addition, a control experiment, in which the primary antibodies were omitted, was conducted to ensure that the secondary antibodies were only binding to the desired primary antibodies. The results of this experiment showed that the secondary antibodies were not binding to any other antigens.

Microscopy and Image Analysis

Sections (4-8 per stain per mouse) were imaged using a laser scanning confocal microscope (Olympus Fluoview FV-300 & FV-1000) with a 20X dry or 60x oil objective and digitally magnified 1.5-3.0X at 1024 × 768 pixel resolution. Fluorescent molecular labels were excited at laser wavelength 488nm (FITC), 568nm (CY-3), and 647nm (CY-5). Each MNTB section was digitally divided into three equal segments (medial, intermediate and lateral) and percentage of

CR/CB/PV-IR+ postsynaptic principal cells/presynaptic calyces of Held was determined per segment as well as for the entire visible cross section of the MNTB. Determining proportion of CR/CB/PV-IR+ principal cells/calyces of Held in each segment provided data used in determining any changes along the tonotopic gradient in protein expression which may occur at different time point between and within strains as well as any segment which may contain a greater proportion of cells/calyces expressing a particular protein. Images were analyzed, using Neurolucida computing software, at increasing levels of brightness and contrast to correct for faint staining**.** Statistics were calculated using Prism v.4.0, GraphPad Software, Inc.

Figure 4. Calbindin expression in the cerebellum.
Double immunofluorescence images with primary antibodies against CB (CY-3) and FITC-conjugated Nissl stain are shown in a 14μm thick section of cerebellum. CB antibodies used in this study characteristically label only Purkinje cell soma and dendrites. This is consistent with reported pattern of cerebellar CB expression. Note as mouse ages, CB immunoreactivity elucidates the development of the extensive Purkinje cell dendritic arbor as is displaces small cells from the superficial molecular layer. Scale Bar = 100μm.

P9 Wild-Type (CBA/J) Cerebellum
P13 Wild-Type (CBA/J) Cerebellum
P30 Wild-Type (CBA/J) Cerebellum
Calbindin-IR
Nissl-IR + Calbindin-IR
Nissl-IR
A
B
C
D
E
F
G
H
I

Figure 5. Calretinin expression in the cerebellum.
Double immunofluorescence images with primary antibodies against CR (CY-3) and FITC-conjugated Nissl stain are shown in a 14μm thick section of cerebellum. CR antibodies used in this study do not label Purkinje Cells. This is consistent with reported pattern of cerebellar CR expression. Note CR immunoreactivity is not apparent until P13, when it is visible in the granular layer. By P30, CR immunoreactivity can be seen in both the granular and molecular layer, but is conspicuously absent from Purkinje Cells. Scale Bar = 100μm.

P9 Wild-Type (CBA/J) Cerebellum
P13 Wild-Type (CBA/J) Cerebellum
P30 Wild-Type (CBA/J) Cerebellum
Calretinin-IR
Nissl-IR + Calretinin-IR
Nissl-IR
A
B
C
D
E
F
G
H
I

Figure 6. Parvalbumin expression in the cerebellum.
Double immunofluorescence images with primary antibodies against PV (CY-3) and FITC-conjugated Nissl stain are shown in a 14μm thick section of cerebellum. PV antibodies used in this study characteristically label only Purkinje cell soma and dendrites. This is consistent with reported pattern of cerebellar PV expression. Note as mouse ages, PV immunoreactivity elucidates the development of the extensive Purkinje cell dendritic arbor as is displaces small cells from the superficial molecular layer. Scale Bar = 100μm.

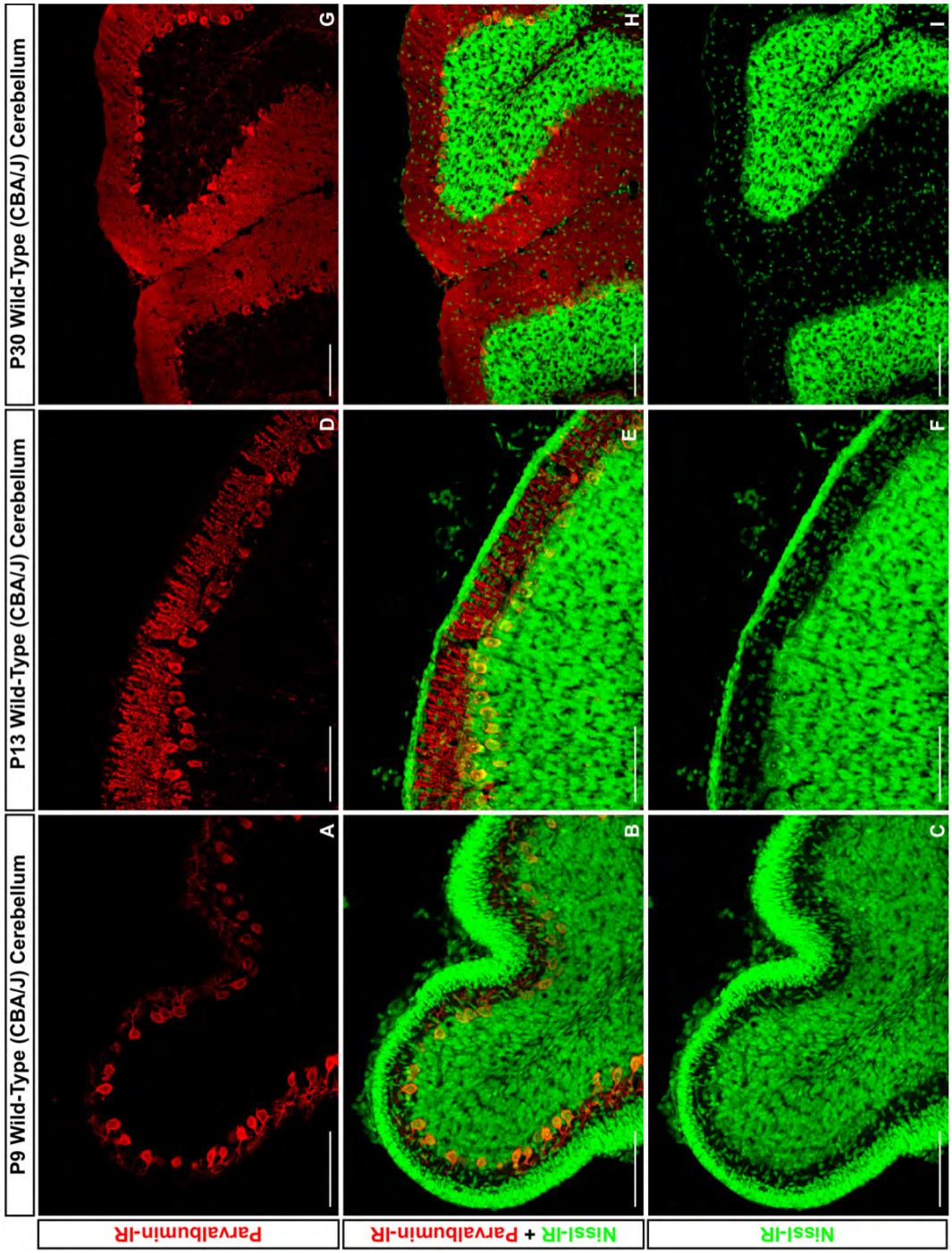
P9 Wild-Type (CBA/J) Cerebellum
P13 Wild-Type (CBA/J) Cerebellum
P30 Wild-Type (CBA/J) Cerebellum
Parvalbumin-IR
Nissl-IR + Parvalbumin-IR
Nissl-IR
A
B
C
D
E
F
G
H
I

V. RESULTS

PARVALBUMIN IN THE MNTB

Parvalbumin immunoreactivities (PV-IRs) were compared in the MNTB of normal hearing (CBA/J) and congenitally deaf (dn/dn) mice at various stages of development. A number of postnatal time points were analyzed [9 days (P9), 13 days (P13), 30 days (P30), and 49 days (P49)] to determine the normal time course of PV expression, and to analyze possible alterations resulting from the absence of spontaneous and acoustically evoked afferent activity in the cochlear nerve. The postnatal ages P9 and P13 were chosen to represent points just before and just after the opening of the ear canal in both CBA/J and *dn/dn* mice. The opening of the ear canal, occurring at 11 days postnatal (Oleskevich and Walmsley, 2002), corresponds with the onset of hearing in CBA/J mice. 30 and 49 days postnatal were chosen as time points in which the mice had advanced in development. 6–8 sections of MNTB per animal were analyzed (n = 6 – 8) from 2–4 animals per age per strain (N = 2-4). The same sections of MNTB were used to analyze calyceal and somatic PV expression in the whole MNTB as well as in subdivisions corresponding to different characteristic frequencies (broadly defined as high, medium, and low frequencies) of the tonotopic gradient. No statistical differences were found between sections from different animals of the same age and strain ($p>0.05$ One Way ANOVA). Therefore all data from sections of the same age and strain were pooled together.

In these experiments, we used vesicular glutamate transporter 1 immunoreactivity (VGluT1-IR) to visualize to presynaptic calyces of Held in the MNTB. Analysis of the MNTB in low magnification confocal images (20X, 1.5 digital zoom) using fluorescent antibodies directed against vesicular VGluT1 reveals single calyces of Held among negatively staining neuropil (Figure 7). At higher magnification (60X), individual calyces are discernable by their circular staining pattern surrounding a single, negatively stained principal cell somata. Colocalization of VGluT1 with Rab3a confirms VGluT1 immunoreactivity within the MNTB is located only within presynaptic structures (Figure 7).

Three types of neurons, distinguished by there respective morphology can be seen within the MNTB: the elongate cell, the stellate cell, and the principal cell. To be certain the presynapticVGluT1 immunoreactivity abuts principal cell somata, dual immunofluorescence for VGluT1 and Nissl in the MNTB was analyzed (Figure 1). Nissl stained cells classified as MNTB principal cells were those which displayed an oval somata that was 10-20μm in diameter across the long axis and had an eccentric nucleus (Harrison and Warr, 1962; Morest 1968a&b, 1973; Spangler et al., 1985; Smith et al., 1998) (Figure. 7). Double staining the MNTB with anti-VGluT1 and anti-Nissl confirms that presynaptic VGluT1 immunoreactivity is adjacent to principle cell somata and, presumably, corresponds to glutamatergic calyces of Held (Figure. 7).

Parvalbumin (PV) is expressed in both MNTB principal cells and calyces of Held in CBA/J and *dn/dn* mice

Confocal analysis of PV-IR in the MNTB of CBA/J and *dn/dn* mice in low magnification (20X, 1.5 zoom) and high magnification (60X, 2.0-3.0 zoom) revealed that PV is expressed in a clear majority of principal cells somata and calyces of Held throughout development, with no apparent differential expression across the tonotopic, medial – lateral axis of the MNTB. Findings were nearly identical in *dn/dn* mice.

Developmental Expression of Parvalbumin in presynaptic calyces of Held in the MNTB of normal hearing CBA/J mice and congenitally deaf (*dn/dn*) mice

Low magnification (20X, 1.5 zoom) confocal analysis of calyceal PV-IR in the MNTB of CBA/J and *dn/dn* mice was performed by counting PV+ calyces of Held through stacks of 2μm optical sections from 14μm thick coronal section of MNTB. An average of 1104 VGluT1-IR calyces of Held or principal cells were analyzed for PV expression per age group for CBA/J animals (range: 956 – 1281) and 1054 per age group for *dn/dn* animal (range 986 – 1196). No statistically significant differences in the number of VGluT1-IR calyces of Held or Nissl stained principal cells per section were found between CBA/J and *dn/dn* mice (CBA/J: 109.6 ± 8.7, *dn/dn*: 101.5 ± 6.4; mean ± SEM; $p = 0.87$ *t-test*).

Percentages of calyces of Held which were PV-IR were obtained for the whole of the MNTB. A clear majority of calyces express PV, with no significant increase in the percent of VGluT1-IR calyces of Held expressing PV at any age

points analyzed (P9: 98.4 ± 0.4%, P13: 99.4 ± 0.2%, P30 ± 99.2 ± 0.5%, P49: 99.4 ± 0.6%; mean ± SEM; p = 0.403 One Way ANOVA). *Post hoc* test indicate no significant change in calyceal PV expression between any age points analyzed (p>0.05 *post hoc* Tukey's test) (Figure 8, 10, 12). Similarly in *dn/dn* mice, PV was expressed in clear majority of VGluT1-IR calyces of Held, with no significant increase in PV expression at any age points analyzed (P9: 98.3 ± 0.3%, P13: 99.2 ± 0.2%, P30: 99.3 ± 0.3%, P49: 98.9 ± 0.5%; mean ± SEM; p = 0.289 One Way ANOVA). *Post hoc* test indicates no significant change in calyceal PV expression between any age points analyzed (p>0.05 *post hoc* Tukey's test) (Figure 9, 11, 12). When comparing wild-type to deaf, no significant differences in the percentage of calyces of Held that express PV were detected at P9 (p = 0.846 t test), P13 (p = 0.488 t test), P30 (p = 0.865 t test), and P49 (p = 0.523 t test) (Figure 12). These data suggest that PV immunoreactivity is present in nearly 100% of VGluT1-IR calyces of Held before the onset of hearing in both control and deaf mice and that, in both strains, PV expression stays constant throughout development to P49.

It should be noted that after P13, postsynaptic principal cells stained so strongly for PV it is difficult to definitely determine whether the fluorescent signal which extends into the presynaptic calyx of Held region is due to true immunopositive labeling of calyx of Held or to artifactual bleedover of fluorescence into the calyx region. However, previous studies have indicated PV as an endogenous calcium buffer in rat and mouse calyces of Held (Felmy and Schneggenburger, 2004; Muller, et al., 2007), findings which are corroborated in

the present experiments by the clear labeling of axon bundles traversing the MNTB with anti-PV antibody. Thus, in lieu of adequate data suggesting that PV immunoreactivity in the region of the calyx of Held is artifact, the present study considers such immunofluorescence to be indicative of calyceal PV expression.

In the following section, the expression of PV was separately analyzed in calyces of Held located in each of the lateral, intermediate, and medial thirds of the nucleus. These data indicate that, PV-IR calyces of Held show no preferential pattern of expression along the tonotopic gradient of the MNTB.

Expression of Parvalbumin in Calyces of Held is Homogeneous along the Tonotopic Axis During Postnatal Development in Normal Hearing (CBA/J) and Congenitally Deaf (*dn/dn*) Mice

To assess the developmental distribution of PV-IR calyces along the tonotopic axis, the same confocal images used in the previous section were analyzed. As in Aims 1&2, the MNTB in each image was subdivided into lateral, intermediate, and medial thirds. Counts of VGluT1-IR and PV-IR calyces of Held were made for each of the 3 subdivisions so that percentages of VGlut1-IR calyces that co-express PV could be obtained for each third of the nucleus.

In the lateral third of the MNTB of CBA/J mice, the frequency of VGluT1-IR calyces of Held which co-express PV did not significantly change during the first 49 days of postnatal development (P9: 98.7 ± 0.6%, P13: 99.8 ± 0.2%, P30: 99.5 ± 0.3%, P49: 99.6 ± 0.6%; mean ± SEM; $p = 0.4214$ One Way ANOVA). *Post hoc* test indicates no significant change in calyceal PV expression

between any age points analyzed (p>0.05 *post hoc* Tukey's test) (Figure 8, 10, 13). Similarly, in *dn/dn* mice, the frequency of PV expression in the lateral third of the MNTB did not significantly change in calyces of Held at any age points analyzed (P9: 98.3 ± 0.5%, P13: 99.6 ± 0.3%, P30: 99.4 ± 0.8%, P49: 99.2 ± 0.8%; mean ± SEM; p = 0.473 One Way ANOVA). *Post hoc* test indicate no significant change in calyceal PV expression between any age points analyzed (P>0.05 *post hoc* Tukey's test) (Figure 9, 11, 13).

Similar findings were detected in the intermediate and medial thirds of the MNTB in CBA/J and *dn/dn* mice. The frequency of VGluT1-IR calyces of Held which co-express PV did not significantly change during the first 49 days of postnatal development in the intermediate (P9: 97.8 ± 0.5%, P13: 99.8 ± 0.2%, P30: 99.2 ± 0.4%, P49: 99.3 ± 0.7%; mean ± SEM; p = 0.061 One Way ANOVA; p>0.05 *post hoc* Tukey's test) and medial (P9: 98.8 ± 0.5%, P13: 98.2 ± 0.8%, P30: 99.3 ± 0.5%, P49: 99.4 ± 0.8%, mean ± SEM; p = 0.588 One Way ANOVA; p<0.05 *post hoc* Tukey's test) thirds of the MNTB (Figure 8, 10, 13). Likewise, in *dn/dn* mice, the no significant differences were detected in the frequency of PV-IR calyces among VGluT1-IR calyces in the intermediate (P9: 98.5 ± 0.4%, P13: 99.5 ± 0.3%, P30: 99.5 ± 0.9%, P49: 99.7 ± 0.5%; mean ± SEM; p = 0.185 One Way ANOVA; p>0.05 *post hoc* Tukey's test) and medial (P9: 98.7 ± 0.8%, P13: 99.2 ± 0.4%, P30: 99.5 ± 0.5%, P49: 99.3 ± 0.6%; mean ± SEM; P = 0.765 One Way ANOVA; p>0.05 *post hoc* Tukey's test) (Figure 9, 11, 13).

Consequently, as there were no significant differences detected in the frequency of calyceal PV expression between age matched CBA/J and *dn/dn* mice

across the whole of the MNTB (see previous results), there were no significant differences detected in the frequency of calyceal PV expression between age matched CBA/J and *dn/dn* mice ($p<0.05$ t test). These data suggest that during development in CBA/J and *dn/dn* mice, PV is expressed in nearly 100% of calyces of Held in each third of the MNTB, and that no significant changes are detected in the proportion of VGluT1-IR calyces of Held in any region of the MNTB which would indicate a preferential pattern of calyceal PV expression along the tonotopic axis of the MNTB at any age points analyzed.

Additionally, within each strain, percentages of VGluT1-IR calyces of Held co-expressing PV in each third of the MNTB were compared against the other two MNTB subdivisions in age matched mice. At all ages analyzed, no significant differences were seen in the percentage of VGluT1-IR calyces of Held expressing PV between any region of the MNTB in CBA/J or *dn/dn* mice ($p>0.05$ One Way ANOVA, $p>0.05$ *post hoc* Tukey's test) (Figure 13). These data further suggest that, in both strains at all age points analyzed, the pattern of calyceal PV expression is homogenous throughout the medial–lateral axis of the MNTB and does not appear to be to correspond to the MNTB's tonotopic gradient of characteristic firing frequency.

Developmental Expression of Parvalbumin in principal cells of the MNTB of normal hearing CBA/J mice and congenitally deaf (*dn/dn*) mice.

The same confocal images used to analyze calyces of Held for PV expression were analyzed for somatic expression of PV in principal cells of the

MNTB. Analysis of somatic PV-IR in the MNTB of CBA/J and *dn/dn* mice was performed by counting PV+ principal cells through stacks of 2μm optical sections from 14μm thick coronal section of MNTB. When analyzing sections dual stained with anti-VGluT1 and anti-PV, somatic PV-IR qualified as a PV+ principal cell only if it met the criteria of displaying an oval shaped somata that was 10-20μm in diameter surrounded by a VGluT1-IR calyx of Held.

Percentages of principal cells which were PV-IR were obtained for the whole of the MNTB. A clear majority of principal cells express PV, with an a significant increase in the percent of principal cells expressing PV from P9 to P13, but not after P13 (P9: 93.1 ± 0.6%, P13: 97.3 ± 0.5%, P30 ± 99.3 ± 0.2%, P49: 98.8 ± 0.7%; mean ± SEM; $p>0.001$ One Way ANOVA) (Figure 8, 10, 14). *Post hoc* test indicate a significant change in somatic PV expression between P9 and all other age points analyzed ($p<0.01$ *post hoc* Tukey's test). No differences were detected between animals at P13, P30, or P49 ($p>0.05$ *post hoc* Tukey's test) (Figure 8, 10, 14). Similarly in *dn/dn* mice, PV was expressed in clear majority of principal cells at all ages analyzed, significantly increasing from P9 to P13, but not after P13 (P9: 92.8 ± 0.7%, P13: 97.0 ± 0.6%, P30: 98.7 ± 0.5%, P49: 99.1 ± 0.9%; mean ± SEM; $p<0.001$ One Way ANOVA) (Figure 9, 11, 14). *Post hoc* test indicate a significant change in somatic PV expression between P9 and all other age points analyzed ($p<0.01$ *post hoc* Tukey's test). No differences were detected between animals at P13, P30, or P49 ($p>0.05$ *post hoc* Tukey's test) (Figure 14). When comparing wild-type to deaf, no significant differences in the percentage of principal cells that express PV were detected at P9 ($p = 0.747$ t

test), P13 ($p = 0.705$ t test), P30 ($p = 0.277$ t test), and P49 ($p = 0.796$ t test). These data suggest that PV immunoreactivity is present in clear majority of principal cells before the onset of hearing in both control and deaf mice and that, in both strains, PV expression significantly increases to nearly 100% around the onset of hearing.

Expression of Parvalbumin in Principal Cell Somata is Homogenous along the Tonotopic Axis During Postnatal Development in Normal Hearing (CBA/J) and Congenitally Deaf (dn/dn) Mice

To assess the developmental distribution of PV-IR principal cells along the tonotopic axis, the same confocal images used in the previous sections were analyzed. As above, the MNTB in each image was subdivided into lateral, intermediate, and medial thirds. Counts of Nissl stained and PV-IR principal cells were for each of the three subdivisions so that percentages of principal cells that express PV could be obtained for each third of the nucleus.

In the lateral third of the MNTB of CBA/J mice, the frequency of PV-IR principal cells increased significantly from P9 to P13 (P9: 92.5 ± 0.8%, P13: 96.6 ± 0.6%, P30: 98.9 ± 0.5%, P49: 99.1 ± 0.7%; mean ± SEM; $p<0.001$ One Way ANOVA). *Post hoc* test indicate a significant change in somatic PV expression between P9 and all other age points analyzed ($p<0.01$ *post hoc* Tukey's test). No differences were detected between animals at P13, P30, or P49 ($p>0.05$ *post hoc* Tukey's test) (Figure 8, 10, 15). Similarly, in *dn/dn* mice, the frequency of PV expression in the lateral third of the MNTB increased significantly in principal

cell somata from P9 to P13 (P9: 92.1 ± 1.8%, P13: 97.3 ± 0.7%, P30: 98.3 ± 0.8%, P49: 99.4 ± 0.6%; mean ± SEM; $p<0.001$ One Way ANOVA). *Post hoc* test indicate a significant change in somatic PV expression between P9 and all other age points analyzed ($P<0.05$ *post hoc* Tukey's test). No differences were detected between animals at P13, P30, or P49 ($p>0.05$ *post hoc* Tukey's test) (Figure 9, 11, 15).

Similar findings were detected in the intermediate and medial thirds of the MNTB in CBA/J and *dn/dn* mice. In the intermediate third of CBA/J mice, the frequency of PV-IR principal cells increased from P9 to P13 (P9: 93.3 ± 1.1%, P13: 99.8 ± 0.9%, P30: 98.0 ± 0.7%, P49: 98.7 ± 1.4%; mean ± SEM; $p<0.001$ One Way ANOVA). *Post hoc* test indicate a significant change in somatic PV expression in the intermediate third of the MNTB between P9 and all other age points analyzed ($p<0.01$ *post hoc* Tukey's test). Like the lateral third, no differences were detected between animals at P13, P30, or P49 ($p>0.05$ *post hoc* Tukey's test) (Figure 8, 10, 15). In *dn/dn* mice, the frequency of CB-IR principal cells in the intermediate third of the nucleus increased from P9 to P13 (P9: 93.7 ± 0.6%, P13: 99.5 ± 1.0%, P30: 99.5 ± 0.7%, P49: 99.2 ± 0.7%; mean ± SEM; $p<0.001$ One Way ANOVA). *Post hoc* test indicate a significant change in somatic PV expression in the intermediate third of the MNTB in *dn/dn* animals between P9 and all other age points analyzed ($p<0.01$ *post hoc* Tukey's test). No differences were detected between animals at P13, P30, or P49 ($p>0.05$ *post hoc* Tukey's test) (Figure 9, 11, 15).

In the medial third of the MNTB in CBA/J mice, once again the frequency of principal cells expressing CB increased from P9 to P13, but not after P13 (P9: 93.8 ± 1.0%, P13: 98.2 ± 0.8%, P30: 99.3 ± 0.5%, P49: 99.4 ± 0.9%; mean ± SEM; $p>0.001$ One Way ANOVA). *Post hoc* test indicate a significant change in somatic PV expression in the intermediate third of the MNTB between P9 and all other age points analyzed ($p<0.01$ *post hoc* Tukey's test). No differences in the percentage of PV-IR principal cells were detected between animals at P13, P30, or P49 ($p>0.05$ *post hoc* Tukey's test) (Figure 8, 10, 15). Similarly, in *dn/dn* mice the frequency of PV-IR principal cells increased from P9 to P13 (P9: 91.9 ± 1.4%, P13: 99.2 ± 0.4%, P30: 99.5 ± 0.5%, P49: 99.4 ± 0.6%; mean ± SEM; $p>0.001$ One Way ANOVA). *Post hoc* test indicate a significant change in somatic PV expression in the medial third of the MNTB in *dn/dn* animals between P9 and all other age points analyzed ($p<0.01$ *post hoc* Tukey's test). No differences were detected between animals at P13, P30, or P49 ($p>0.05$ *post hoc* Tukey's test) (Figure 9, 11, 15).

Consequently, as there were no significant differences detected in the frequency of PV expression between age matched CBA/J and *dn/dn* mice across the whole of the MNTB (see previous results), there were no significant differences detected in the frequency of CB expression between age matched CBA/J and *dn/dn* mice ($p>0.05$ t test). These data suggest that during development in CBA/J and *dn/dn* mice, PV is expressed in nearly 100% of principal cells in each third of the MNTB, and that the significant increase detected from P9 to P13, but not after P13, in each strain (see previous results)

corresponds to increases in somatic PV expression detected each third of the MNTB. As such, there is nothing in these data which would indicate a preferential pattern of PV expression along the tonotopic axis of the MNTB at any age points analyzed

Additionally, within each strain, percentages of Nissl stained principal cells expressing PV in each third of the MNTB were compared against the other two MNTB subdivisions in age matched mice. At all ages analyzed, no significant differences were seen in the percentage of principal cells expressing PV between any region of the MNTB in CBA/J or *dn/dn* mice ($p>0.05$ One Way ANOVA, $p>0,05$ *post hoc* Tukey's test) (Figure 15). These data further suggest that, in both strains and at all age points analyzed, the pattern of somatic PV expression is homogenous throughout the medial–lateral axis of the MNTB and does not appear to be to correspond to the MNTB's tonotopic gradient of characteristic firing frequency.

Expression of Parvalbumin (PV) in the MNTB of adult Wistar Rats

The developmental expression of PV reported in this study, is similar to the expression of PV observed in experiments conducted on adult wild-type Wistar rats. Images generated during this study indicate that adult Wistar rats express PV in a clear majority of MNTB principal cells and calyces of Held (Figure 16).

VI. DISCUSSION

PARVALBUMIN IN THE MNTB

Developmental regulation of parvalbumin (PV) expression in the MNTB of normal hearing (CBA/J) mice

We investigated the cellular localization of PV in the MNTB during postnatal development of CBA/J mice. In normal hearing mice, the pattern of PV expression appears to only minimally change during development from postnatal day 9 to postnatal day 49.

At postnatal day 9, prominently stained PV-IR calyces of Held were detected surrounding weakly stained PV-IR principal cell somata. At this age, PV is expressed in an average of 98.4 ± 0.4% of calyces of Held and 93.1 ± 0.6% of principal cell somata within the MNTB of P9 CBA/J mice. No apparent gradient existed in the expression of PV in presynaptic or postsynaptic structures existed along the medial – lateral axis of the MNTB, as PV was expressed in 98.7 ± 0.6%, 97.8 ± 0.5 and 98.8 ± 0.5% of calyces of Held and 92.5 ± 0.8%, 93.3 ± 1.1% and 93.8 ± 0.5% of principal cells in the lateral, intermediate, and medial thirds of the MNTB, respectively. Principal cells classified PV (-) cannot, however, be definitively excluded from the population of principal cells which express PV, as the concentration of PV in some principal cells may simply have been too low to detect with immunofluorescence. Irrespective of this possibility, the data strongly suggest a strong homogeneity in PV immunoreactivity among MNTB principal cells and calyces of Held.

By postnatal day 13, PV expression in principal cells throughout the nucleus increased significantly to 97.3 ± 0.2%, which corresponded to increases in PV expression in principal cells located in each of the lateral (96.6 ± 0.8%), intermediate (98.0 ± 0.7%), and medial (97.4 ± 0.8%) thirds of the MNTB. No statistically significant differences in the percent of PV-IR principal cells were detected with further maturation after P13. Similarly, no significant differences were seen in calyceal PV expression after P9 (P13: 99.4 ± 0.2%, P30: 99.2 ± 0.5%, P49 ± 99.4 ± 0.6%). Throughout developmental time points studied, PV-IR calyces remained evenly distributed along the medial – lateral axis of the MNTB.

Thus throughout development, PV is expressed in a clear majority (nearly 100%) of principal cells and calyces of Held throughout the MNTB, with no apparent differential expression along its tonotopic axis. It is probable that after P9, all MNTB principal cells and calyces of Held express PV. These percentages of PV-IR calyces of Held should be interpreted with caution, however, as the simultaneous staining of principal cells and their closely opposed of calyces of Held makes it impossible to absolutely quantify the percentages of calyces that express PV versus those which only appear to express PV as a result of intense somatic staining artifactually colocalizing with VGluT1 immunoreactivity. This is consistent with other studies of PV expression in the MNTB (Felmy and Schneggenburger, 2004). That PV is expressed in calyces of Held is corroborated by the increase in PV immunoreactivity in fibers coursing through the trapezoid body and among principal cells of the MNTB as the mice age. Presumably, these PV-IR fibers give rise to the presynaptic calyces of Held.

The present study verifies the findings of Felmy and Schneggenburger (2004), which show that PV is expressed in a majority of MNTB principal cells and calyces of Held in C57/BL6 mice. Similar results were obtained in the present experiments for *dn/dn* mice.

Developmental regulation of parvalbumin (PV) expression in the MNTB of congenitally deaf (*dn/dn*) mice

No differences were detected in the developmental regulation and pattern of expression of PV in the MNTB of congenitally deaf (*dn/dn*) mice compared to age matched wild-type (CBA/J) mice. On average, P9 *dn/dn* mice express PV in 98.3 ± 0.3% of calyces of Held and 92.8 ± 0.7% of principle cells and 97.6 ± 0.6% throughout the nucleus. There was no apparent gradient in the pattern of expression across the medial – lateral axis, as PV was expressed in 98.3 ± 0.5%, 98.5 ± 0.4% and 98.7 ± 0.8% of calyces of Held and 92.1 ± 1.8%, 93.7 ± 0.6% and 91.9 ± 1.4% of principal cells in the lateral, intermediate, and medial thirds of the MNTB, respectively. Like CBA/J mice, despite the possibility that cells containing concentrations of PV too low for adequate immunofluorescence were erroneously classified as PV (-) these data indicate a strong homogeneity in PV immunoreactivity among MNTB principal cells and calyces of Held in *dn/dn* mice.

By postnatal day 13, PV expression in principal cells throughout the nucleus increased significantly to P13: 97.0 ± 0.6%, which corresponded to increases in PV expression in principal cells located in each of the lateral (98.3 ±

0.5%), intermediate (98.5 ± 0.4%), and medial (98.7 ± 0.8%) thirds of the MNTB. No statistically significant differences in the percent of PV-IR principal cells were detected with further maturation after P13. Similarly, no significant differences were seen in calyceal PV expression after P9 (P13: 99.2 ± 0.2%, P30: 99.3 ± 0.3%, P49 ± 98.9 ± 0.5%). Throughout developmental time points studied, PV-IR principal cells and calyces of Held remained evenly distributed along the medial – lateral axis of the MNTB.

Throughout development, PV is expressed in a clear majority (nearly 100%) of principal cells and calyces of Held in the MNTB, with no apparent differential expression along its tonotopic axis. Thus, the developmental pattern of PV expression among principle cells and calyces of Held in the MNTB of *dn/dn* mice shows no apparent differences to those of CBA/J mice. In neither strain was a gradient observed along the medial – lateral axis of the MNTB, although a detailed optical density analysis using DAB staining should be performed to determine if a difference in the intensity of staining exists along the tonotopic gradient in either animal as well as to determine any differences in the overall intensity of staining between animals.

An additional implication is that if both CBA/J and *dn/dn* mice exhibit PV immunoreactivity in nearly 100% of principal cells and calyces of Held throughout development, it follows that the calyceal and somatic expression of calbindin and calretinin shown in the following sections occur in calyces of Held and MNTB principal cells that also express PV.

Expression of Parvalbumin (PV) in the MNTB of adult Wistar Rats

The developmental expression of PV reported in this study, is similar to the expression of PV observed in experiments conducted on adult wild-type Wistar rats. Images generated during this study indicate that adult Wistar rats express PV in a clear majority of MNTB principal cells and calyces of Held (Figure 16).

Implications of calyceal parvalbumin (PV) on synaptic transmission in the MNTB

It is well established that loading cells with exogenous high-affinity Ca^{2+} buffers will influence the amplitude and/or decay kinetics of the spatially averaged $[Ca^{2+}]_I$ transient, depending on whether the introduced buffers have fast or slow Ca^{2+} binding kinetics (Neher and Augustine, 1992; Helmchen et al., 1997). Parvalbumin, a high affinity Ca^{2+} buffer with slow binding kinetics, has been previously shown to modulate short term plasticity at inhibitory cerebellar synapses, where paired-pulse facilitation observed in PV knockout (-/-) mice became paired-pulse depression in wild-type mice (Caillard et al, 2000). It is likely that the ability of PV to convert paired-pulse facilitation to paired-pulse depression, is related to the finding that PV, in cerebellar interneurons, accelerates the decay of $[Ca^{2+}]_I$ (Collin et al., 2005) and, in calyces of Held, accelerates the decay kinetics of paired-pulse facilitation while only marginally affecting the amplitude of $[Ca^{2+}]_I$ transient (Muller et al., 2007).

Previous observations at the calyx of Held indicate that transmitter release facilitation could not, with the postulated local Ca^{2+} signal necessary for transmitter release, be quantitatively accounted for by linear summation of the measured residual Ca^{2+} signal and that Ca^{2+} saturation could cause a supralinearity in the summation of the two Ca^{2+} signals (Felmy et al., 2003). In light of this evidence for the "Ca^{2+} buffer saturation" mechanism of transmitter facilitation, the preponderance of studies (this one included) that indicate the main endogenous Ca^{2+} buffer in presynaptic calyces of Held is PV, which has slow binding kinetics and speeds up the decay of paired-pulse facilitation, is surprising (Felmy and Scneggenburger, 2004; Muller et al., 2007). In calyces of Held, the presence of a presynaptic Ca^{2+} buffer with slow binding kinetics, together with a low endogenous Ca^{2+} buffering capacity ($\kappa_s \sim 30$) and a high Ca^{2+} extrusion rate (Helmchen et al., 2007) causes a fast decay of the spatially averaged presynaptic $[Ca^{2+}]_I$ transient, without effecting its amplitude, will limit the build up of residual Ca^{2+} during high frequency trains of action potentials (Muller et al., 2007).

A Ca^{2+} buffer which causes facilitation via the "Ca^{2+} buffer saturation mechanism" needs, therefore, to have relatively fast binding kinetics, allowing it to intercept local Ca^{2+} ions in the vicinity of readily releasable vesicular pools before the ions reach the intracellular Ca^{2+} sensor for vesicle release (Neher, 1998; Matveev et al., 2004; Muller et al., 2007). It is possible, however, an additional high affinity Ca^{2+} buffer, like calretinin, that when present in calyces of Held influences transmitter release facilitation, allowing for temporally precise, high frequency synaptic transmission (see calretinin results).

Interestingly, many neurons within the auditory brainstem, which necessarily fire repetitively at high frequencies, express PV (Celio, 1990; Lohmann and Friauf, 1996). One likely explanation for this ability is accounted for by particular complements of ion channels. For example, previous evidence indicates that fast activating K^+ channels of the K_V3 subunit family contribute to high frequency firing in mouse auditory brainstem neurons (Wang et al., 1998). The expression of parvalbumin could thus serve as one adaptive mechanism which allows such fast spiking neurons to effectively handle Ca^{2+} during high frequency trains of presynaptic action potentials.

Figure 7. VGluT1 expression in the MNTB of normal hearing (CBA/J) mice. **A-C:** VGluT1 immunofluorescence is colocalized with Rab3a immunofluorescence, indicating that VGluT1 is expressed in presynaptic nerve terminals within the MNTB. 20x. Scale bar = 100μm. **D:** 60x image of figure 6A. Single calyceal-type VGluT1 synaptic terminals are visible against negatively staining neuropil and postsynaptic cell. Scale bar = 10μM. **E&F:** VGluT1 immunofluorescence is adjacent to principal cell somata, indicating that VGLuT1 immunoreactivity corresponds to presynaptic calyx of Held nerve terminal. Scale bar = 10μm.

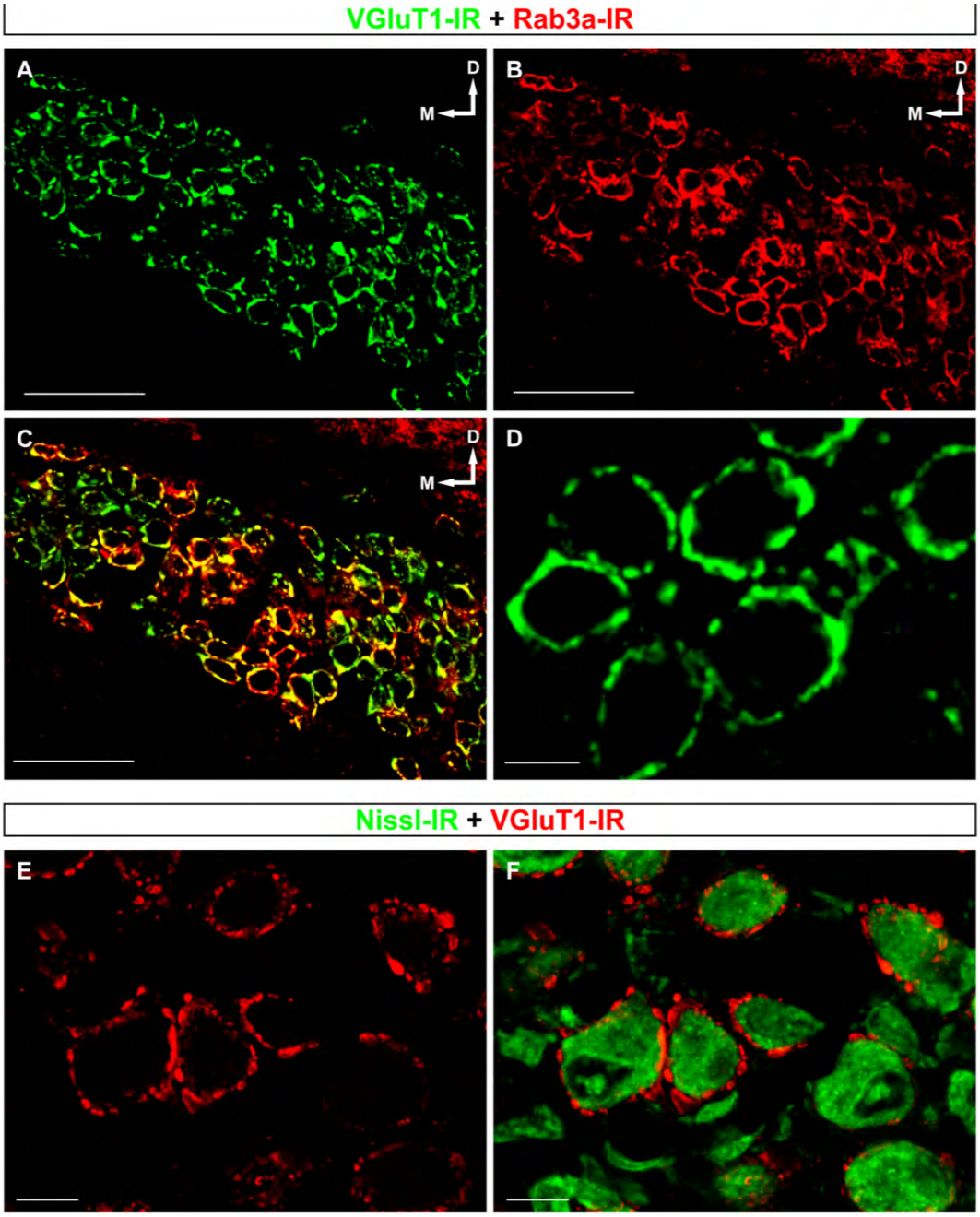
VGluT1-IR + Rab3a-IR
A
D
M
B
D
M
C
D
M
D
Nissl-IR + VGluT1-IR
E
F

Figure 8. Parvalbumin expression in the MNTB of normal hearing (CBA/J) mice at 9 days postnatal. Double immunofluorescence images with primary antibodies against Nissl (FITC) and PV (CY-3) are shown in a 14μm thick section of brainstem. PV is expressed in nearly every principal cell and calyx of Held in the MNTB. Scale Bar = 100μm.

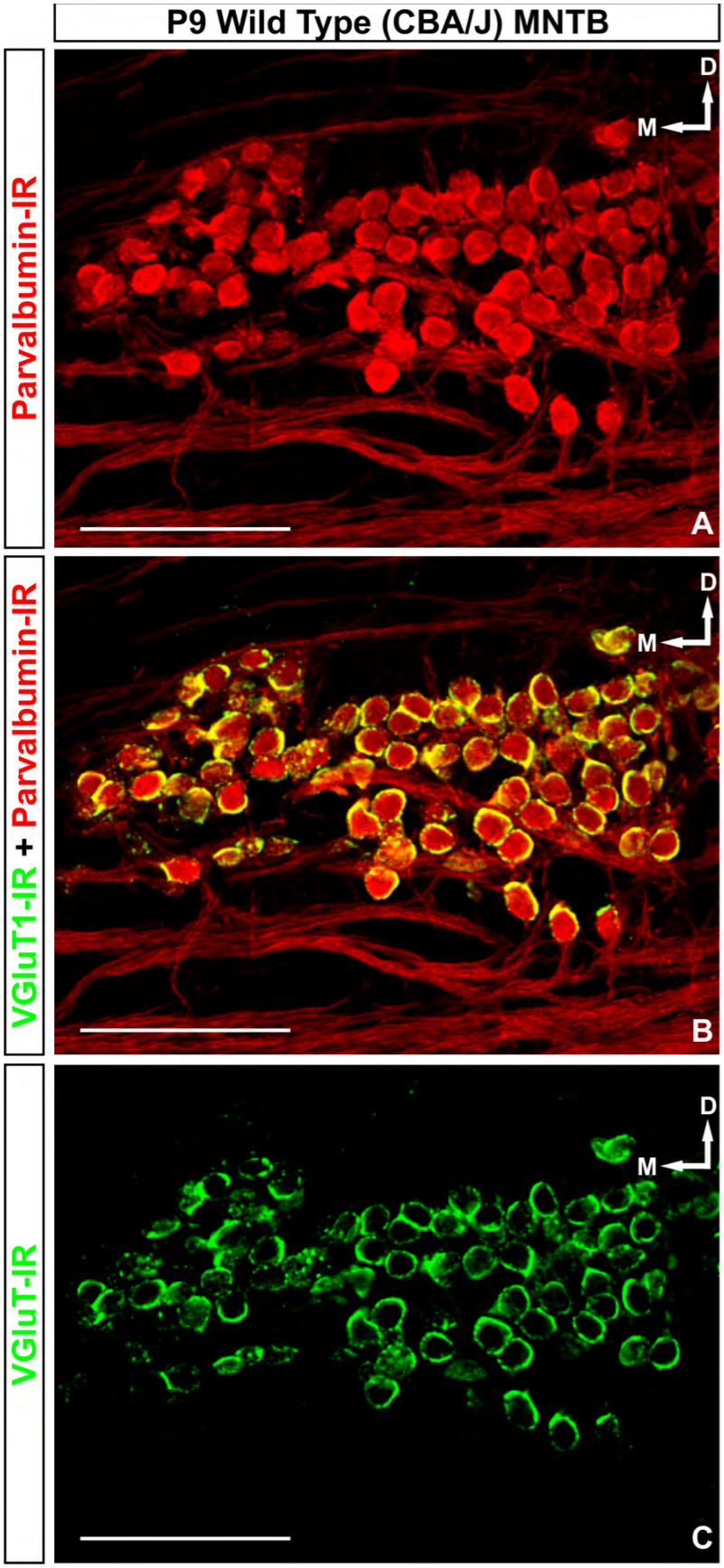
P9 Wild Type (CBA/J) MNTB
Parvalbumin-IR
VGluT1-IR + Parvalbumin-IR
VGluT-IR
D
M
A
B
C

Figure 9. Parvalbumin expression in the MNTB of congenitally deaf (*dn/dn*) mice at 9 days postnatal. Double immunofluorescence images with primary antibodies against Nissl (FITC) and PV (CY-3) are shown in a 14μm thick section of brainstem. PV is expressed in nearly every principal cell and calyx of Held in the MNTB. Scale Bar = 100μm.

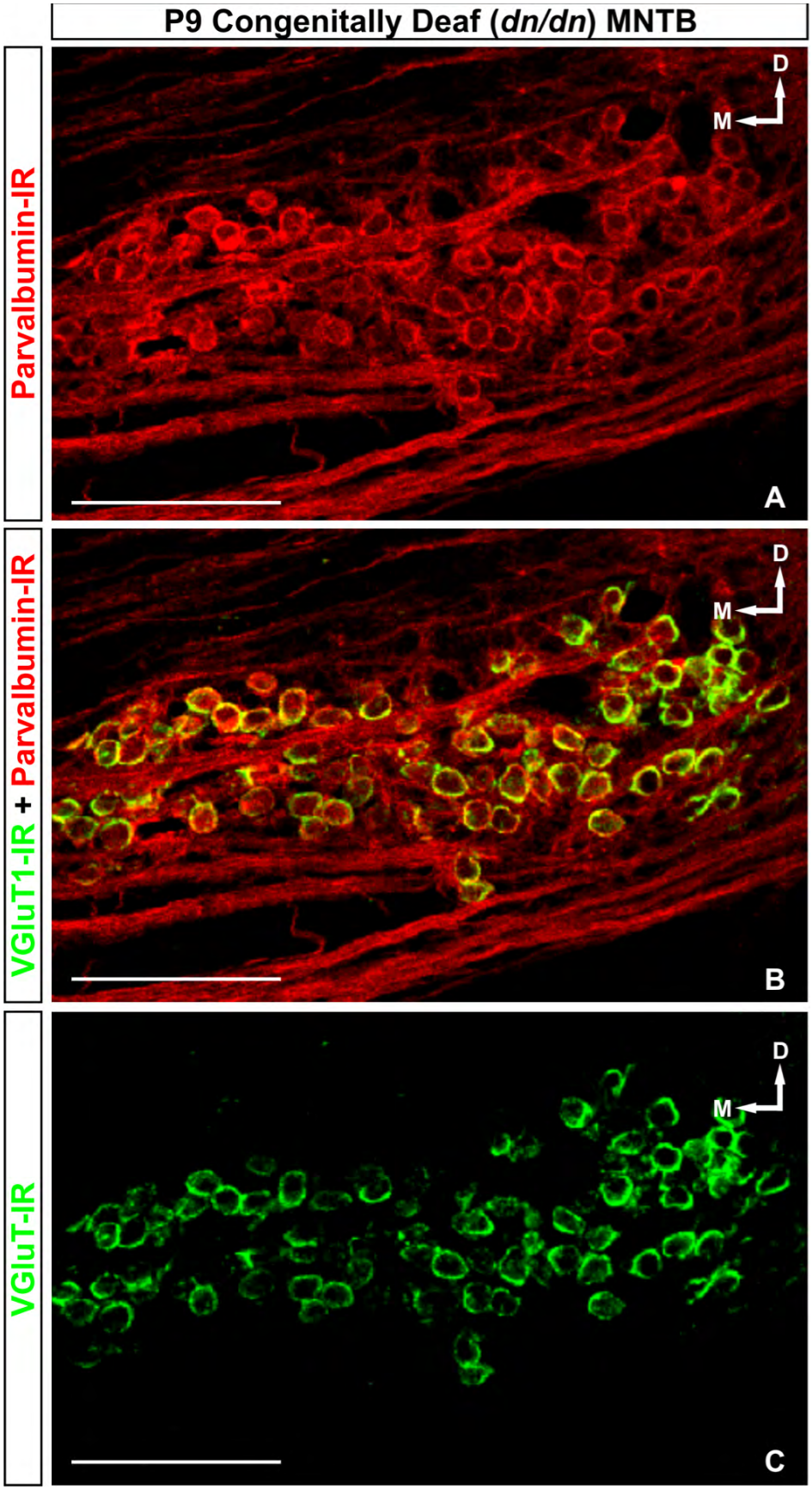
P9 Congenitally Deaf (*dn/dn*) MNTB
Parvalbumin-IR
VGluT1-IR + Parvalbumin-IR
VGluT-IR
D
M
A
B
C

Figure 10. Parvalbumin expression in the MNTB of normal hearing (CBA/J) mice at 49 days postnatal. Double immunofluorescence images with primary antibodies against Nissl (FITC) and PV (CY-3) are shown in a 14μm thick section of brainstem. PV is expressed in nearly every principal cell and calyx of Held in the MNTB. Scale Bar = 100μm.

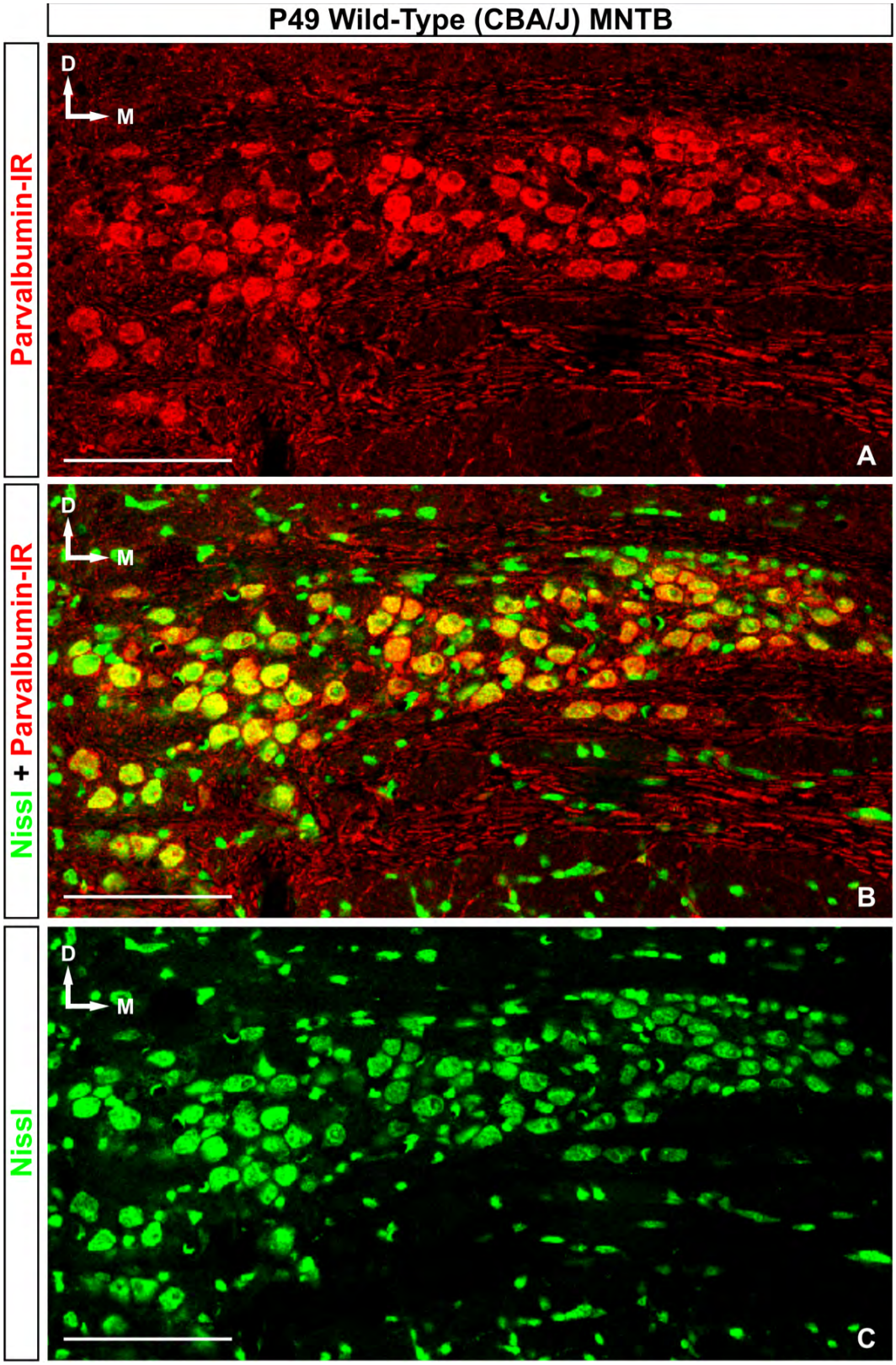
P49 Wild-Type (CBA/J) MNTB
Parvalbumin-IR
Nissl + Parvalbumin-IR
Nissl
D
M
A
B
C

Figure 11. Parvalbumin expression in the MNTB of congenitally deaf (*dn/dn*) mice at 49 days postnatal. Double immunofluorescence images with primary antibodies against Nissl (FITC) and PV (CY-3) are shown in a 14μm thick section of brainstem. PV is expressed in nearly every principal cell and calyx of Held in the MNTB. Scale Bar = 100μm.

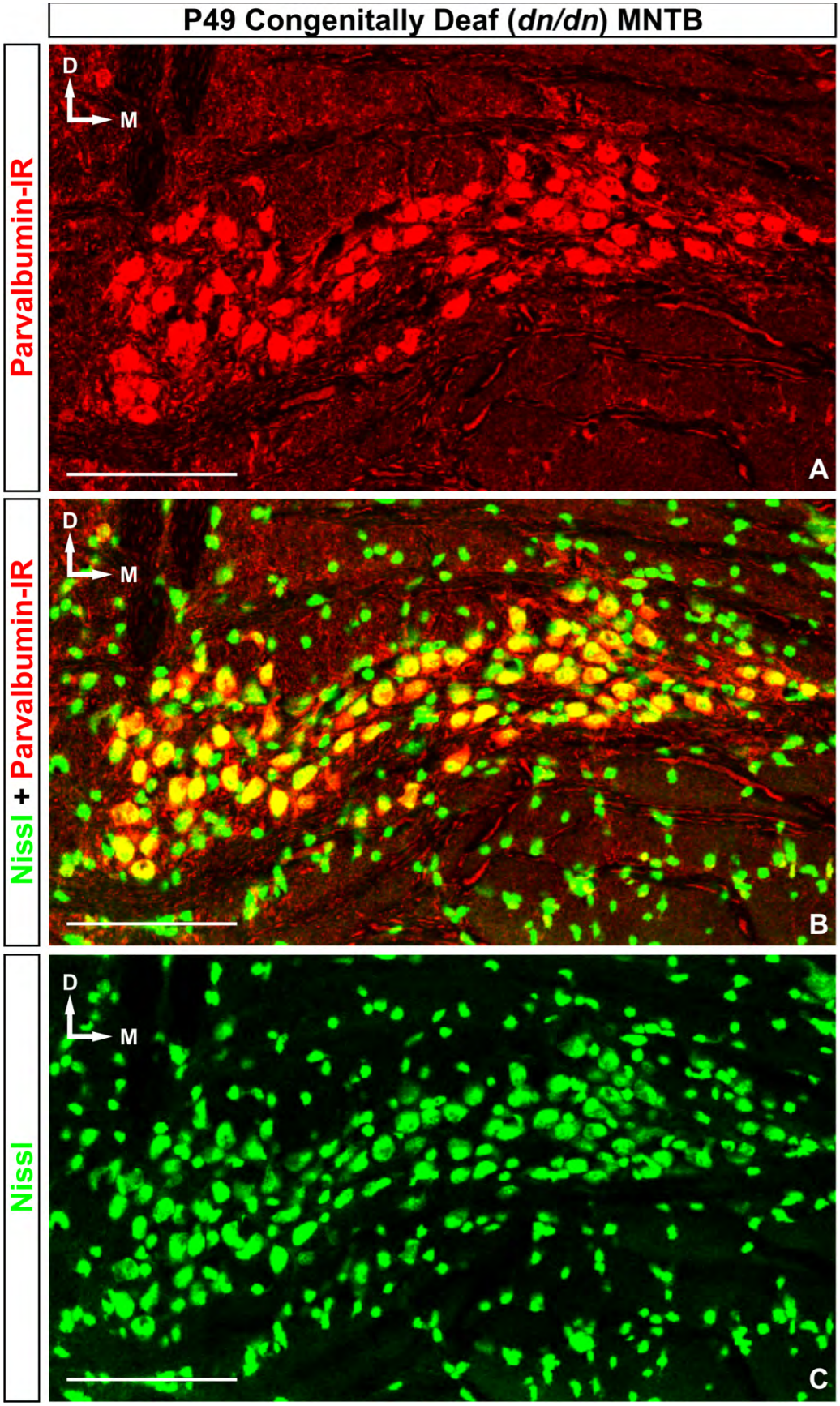
P49 Congenitally Deaf (dn/dn) MNTB
Parvalbumin-IR
Nissl + Parvalbumin-IR
Nissl
D
M
A
B
C

Figure 12. Parvalbumin expression in calyces of Held.
Top shows the percent of VGluT1-IR calyces found throughout the medial lateral axis of the MNTB which also express PV. After P9, no significant differences in the expression of CR were found in any age points analyzed in CBA/J or *dn/dn mice*. Additionally, no significant differences in VGLuT1-IR calyces expressing PV at any postnatal ages analyzed between CBA/J and *dn/dn* mice. **Bottom:** Chart of data used in graph (above).

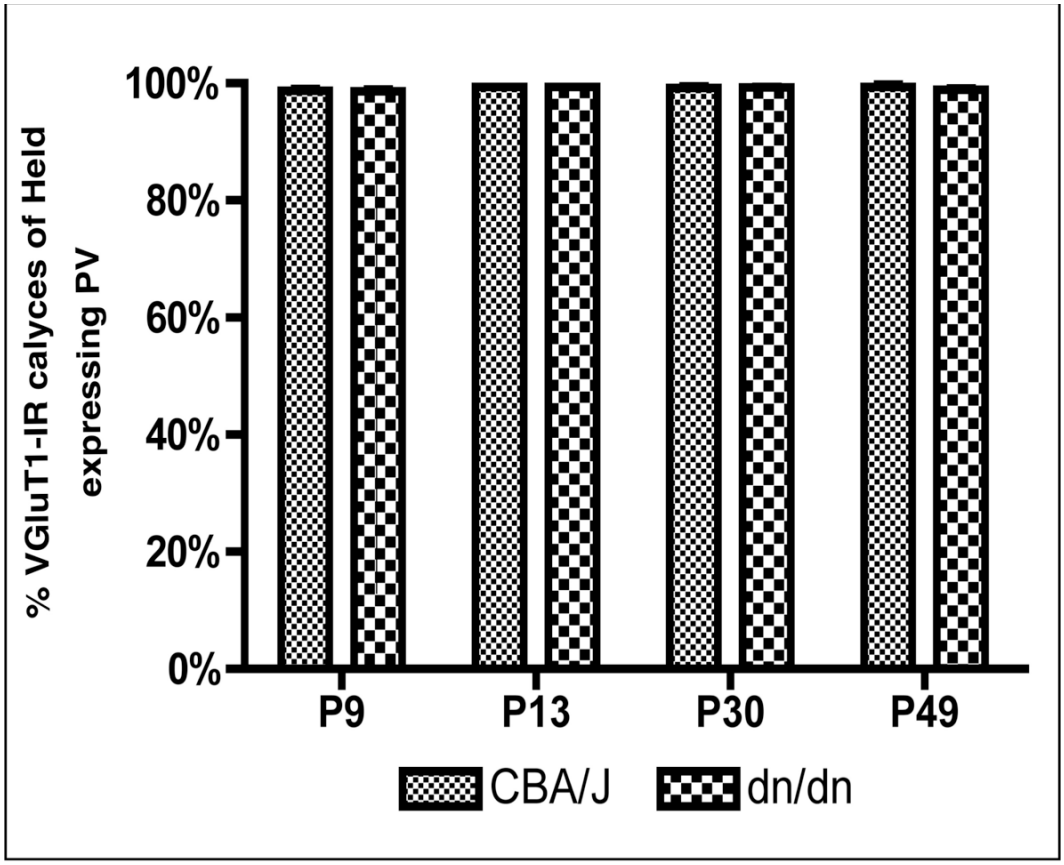

Age	% VGluT1-IR calyces of Held expressing PV*	
	CBA/J	*dn/dn*
P9	98.4 ± 0.4	98.3 ± 0.3
P13	99.4 ± 0.2	99.2 ± 0.2
P30	99.2 ± 0.5	99.3 ± 0.3
P49	99.4 ± 0.6	98.9 ± 0.5

*Mean ± SEM

Figure 13. Regional parvalbumin expression in calyces of Held.
Above: In **A & B**, the percent of principal cells located in each region of the MNTB which also express PV are shown for each age point analyzed in CBA/J and *dn/dn* mice, respectively. An average of 1104 VGluT1-IR calyces of Held or principal cells were analyzed for PV expression per age group for CBA/J animals (range: 956 – 1281) and 1054 per age group for *dn/dn* animal (range 986 – 1196). **A)** In each third of the MNTB, no significant changes in PV expression among calyces of Held was detected during development of CBA/J mice at any age point analyzed ($p>0.05$ One Way ANOVA). Further, no significant differences were detected in the percent of calyces of Held expressing PV between the lateral, intermediate, and medial thirds of the nucleus at any age point analyzed ($p>0.05$ One Way ANOVA). **B)** Like CBA/J mice, in each third of the MNTB, calyceal PV expression did not significantly change during developmental time point analyzed ($p>0.05$ One Way ANOVA). Again, no significant differences were detected in the percent of principal cells expressing PV between the lateral, intermediate, and medial thirds of the nucleus at any age point analyzed ($p>0.05$ One Way ANOVA). **Below:** Data used in compiling the above graphs.

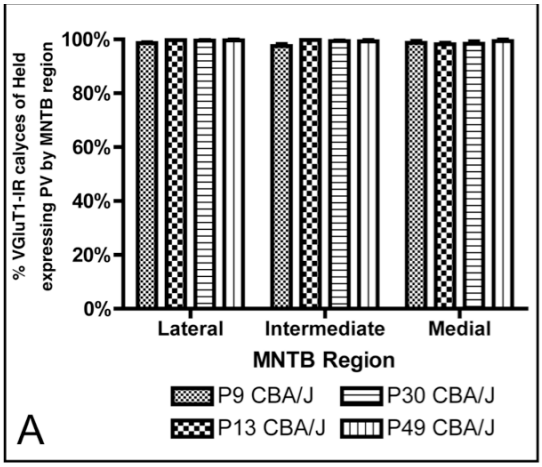

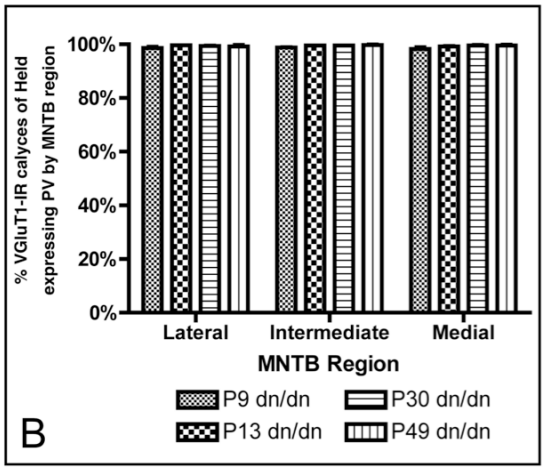

MNTB Region	Age	% VGluT1-IR calyces of Held expressing PV by region*	
		CBA/J	*dn/dn*
Lateral	P9	98.7 ± 0.6	98.3 ± 0.5
	P13	99.8 ± 0.2	99.6 ± 0.3
	P30	99.5 ± 0.3	99.4 ± 0.8
	P49	99.6 ± 0.6	99.2 ± 0.8
Intermediate	P9	97.8 ± 0.5	98.5 ± 0.4
	P13	99.8 ± 0.9	99.5 ± 1.0
	P30	99.2 ± 0,4	99.5 ± 0.7
	P49	99.3 ± 0.7	99.7 ± 0.5
Medial	P9	98.8 ± 0.5	98.7 ± 0.8
	P13	98.2 ± 0.8	99.2 ± 0.4
	P30	99.3 ± 0.5	99.5 ± 0.5
	P49	99.4 ± 0.8	99.3 ± 0.6

*Mean ± SEM

Figure 14. Parvalbumin expression in MNTB principal cells.
Top shows the percent of principal cells found throughout the medial lateral axis of the MNTB which express PV. A significant increase in the expression of PV was found in CBA/J as well as *dn/dn* mice from 9 days postnatal to 13 days postnatal. In neither strain were further developmental increases were detected after postnatal day 13. No significant differences were detected in the proportion of principal cells expressing CB between age matched CBA/J and *dn/dn* animals. Double asterisk indicates $p<0.001$. **Bottom:** Chart of data used in graph (above).

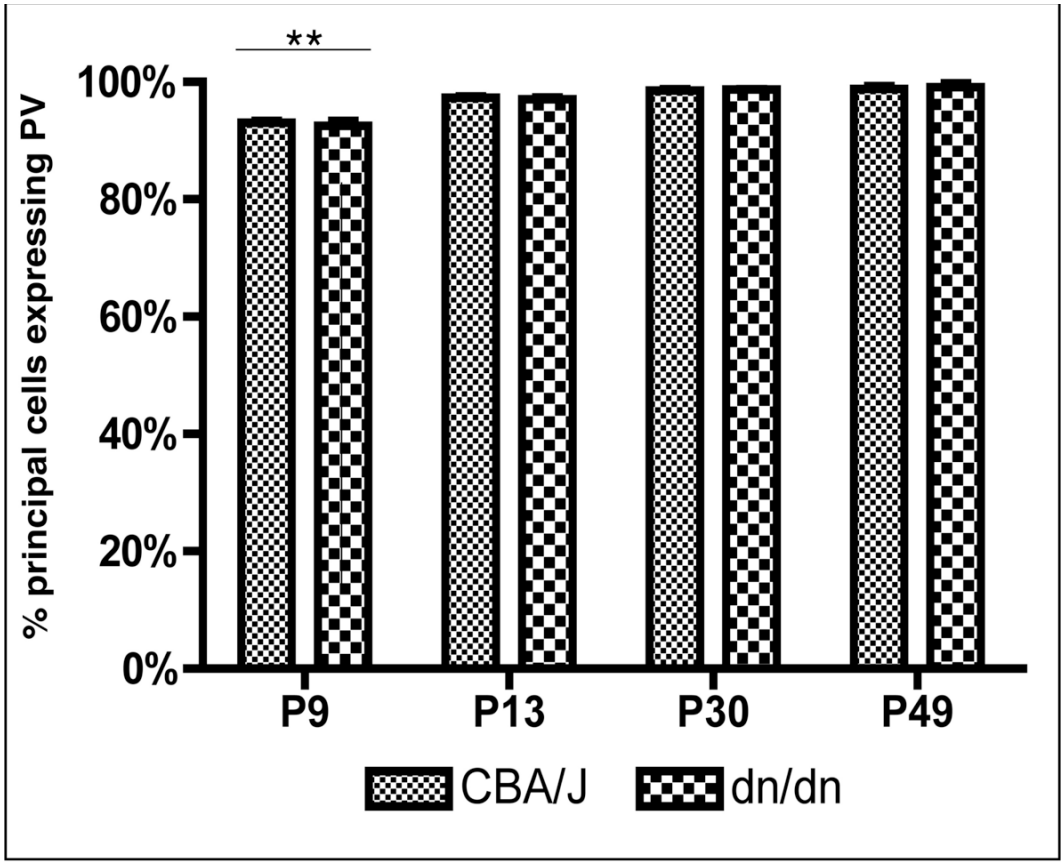

Age	% principal cells expressing PV*	
	CBA/J	*dn/dn*
P9	93.1 ± 0.6	92.8 ± 0.3
P13	97.3 ± 0.5	97.0 ± 0.6
P30	99.3 ± 0.2	98.7 ± 0.5
P49	98.8 ± 0.7	98.9 ± 0.5

*Mean ± SEM

Figure 15. Regional parvalbumin expression in MNTB principal cells.
Above: In **A & B**, the percent of principal cells located in each region of the MNTB which express PV are shown for each age point analyzed in CBA/J and *dn/dn* mice, respectively. An average of 1104 VGluT1-IR calyces of Held or principal cells were analyzed for PV expression per age group for CBA/J animals (range: 956 – 1281) and 1054 per age group for *dn/dn* animal (range 986 – 1196). **A)** In each third of the MNTB, a significant increase in PV expression among principal cells was detected during development of CBA/J mice from postnatal day 9 to postnatal day 13 (double asterisk: $p<0.001$, One Way ANOVA). However, no significant differences were detected in the percent of principal cells expressing PV between the lateral, intermediate, and medial thirds of the nucleus at any age point analyzed ($p>0.05$ One Way ANOVA). **B)** Like CBA/J mice, in each third of the MNTB, somatic PV expression increased significantly during development from postnatal day 9 to postnatal day 13 (double asterisk: $p<0.001$, One Way ANOVA). Again, no significant differences were detected in the percent of principal cells expressing PV between the lateral, intermediate, and medial thirds of the nucleus at any age point analyzed ($p>0.05$ One Way ANOVA). **Below:** Data used in compiling the above graphs.

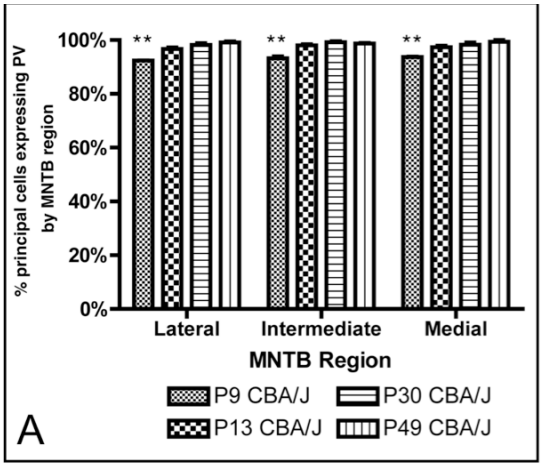

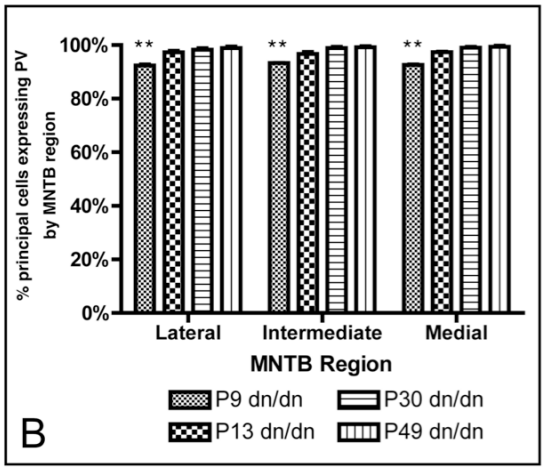

MNTB Region	Age	% principal cells expressing PV by region*	
		CBA/J	*dn/dn*
Lateral	P9	92.5 ± 0.8	92.1 ± 1.8
	P13	96.6 ± 0.8	97.3 ± 0.7
	P30	98.9 ± 0.5	98.3 ± 0.8
	P49	99.1 ± 0.7	98.9 ± 0.8
Intermediate	P9	93.3 ± 1.1	93.7 ± 0.6
	P13	98.0 ± 0.7	96.7 ± 0.8
	P30	99.3 ± 0.5	98.9 ± 0.7
	P49	98.7 ± 1.4	99.2 ± 0.7
Medial	P9	93.8 ± 1.0	91.9 ± 1.4
	P13	97.4 ± 0.8	97.3 ± 0.7
	P30	99.7 ± 0.3	99.5 ± 0.5
	P49	99.4 ± 0.9	99.4 ± 0.6

*Mean ± SEM

Figure 16. Parvalbumin expression the MNTB of normal hearing wistar rats. Double immunofluorescence images with primary antibodies against VGluT1 (FITC) and PV (CY-3) are shown in a 14μm thick section of brainstem from the level of the MNTB. **A & B:** 20X Image shown. Scale bar = 100μm. **C & D:** 60X image shows that PV immunoreactivity extends into the calyx of Held to colocalize with VGluT1 immunoreactivity. Scale bar = 10μm. D = dorsal. M = medial.

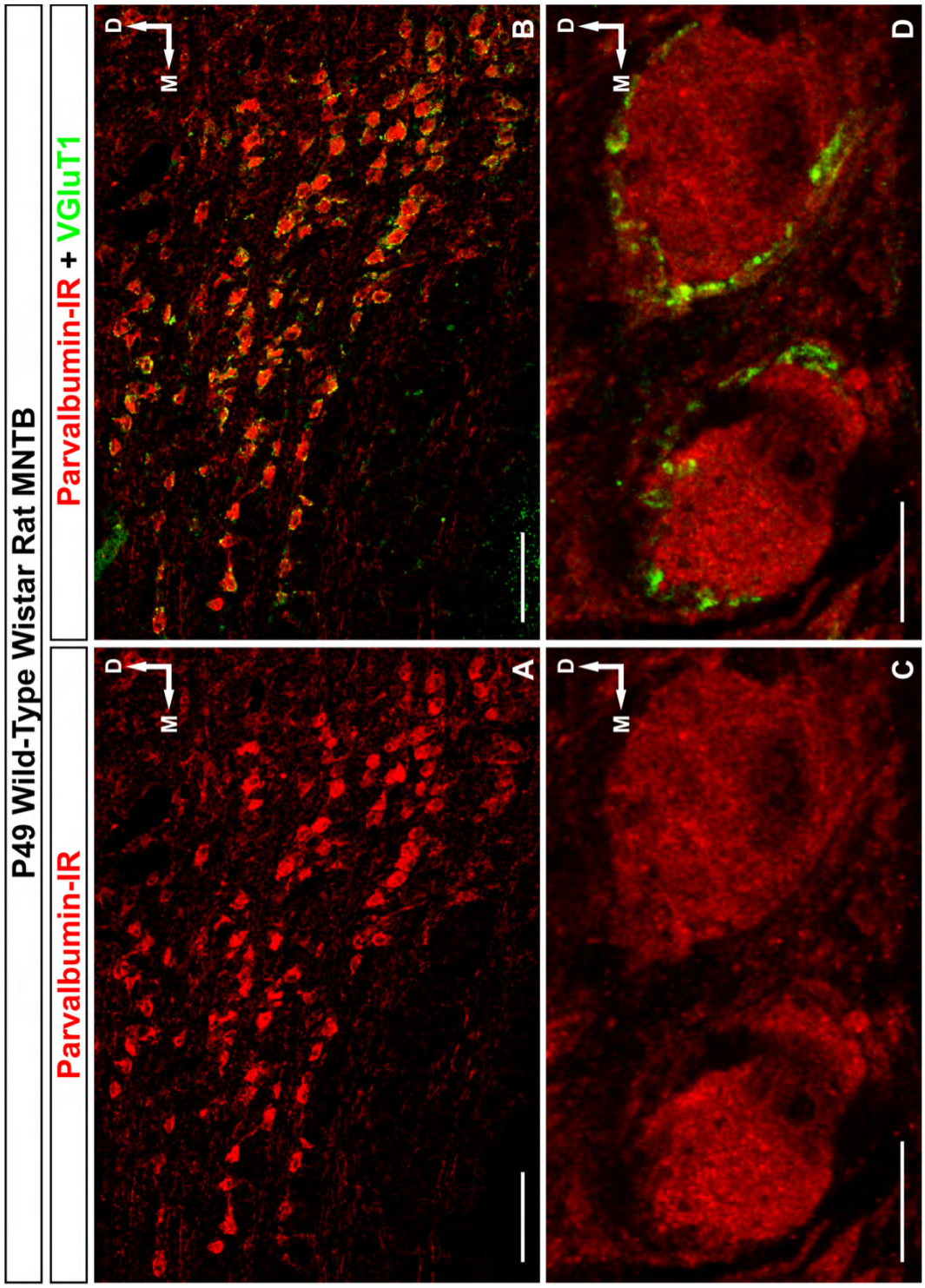
P49 Wild-Type Wistar Rat MNTB
Parvalbumin-IR
Parvalbumin-IR + VGluT1
A
B
C
D
D
M

VII. RESULTS

CALBINDIN D-28K IN THE MNTB

Calbindin D-28k immunoreactivities (CB-IRs) were compared in the MNTB of normal hearing (CBA/J) and congenitally deaf (dn/dn) mice. A number of postnatal time points were analyzed [9 days (P9), 13 days (P13), 30 days (P30), and 49 days (P49)] to obtain the normal time course of CB expression and possible alterations from its normal developmental expression in the absence of spontaneous and acoustically evoked afferent activity in the cochlear nerve. For analysis, tissue was co-labeled with VGluT1 antibodies and Nissl stain. When analyzing sections dual labeled with anit-VGluT1 and anti-CB, somatic CB-IR qualified as a CB-IR principal cell only if it met the criteria of displaying an oval somata 10-20μm in diameter across its long axis surrounded by a VGluT1-IR calyx. 6–8 sections of MNTB per animal were analyzed (n = 6 – 8) from 2–4 animals per age per strain (N = 2-4). The same sections of MNTB were used to analyze somatic CR expression in the whole MNTB as well as in subdivisions corresponding to different characteristic frequencies (broadly defined as high, medium, and low frequencies) of the tonotopic gradient No statistical differences were found between sections from different animals of the same age and strain ($p>0.05$ One Way ANOVA). Therefore all data from sections of the same age and strain were pooled together.

Calbindin D-28k (CB) is expressed in MNTB principal cells of CBA/J and *dn/dn* mice

Confocal analysis of CB-IR in the MNTB of CBA/J and *dn/dn* mice in low magnification (20X, 1.5 zoom) and high magnification (60X, 2.0-3.0 zoom) revealed that CB is expressed in a clear majority of principal cells somata and no calyces of Held throughout development (Figure 17). Findings were nearly identical in *dn/dn* mice.

Nearly every principal cell appears to be immunopositive for calbindin D-28k in CBA/J and *dn/dn* mice, with no apparent gradient in the pattern of expression across the medial – lateral axis of the MNTB. CB-IR cell processes emerging from the principle cells are discernable within and extending from the boundaries of the MNTB, as are fibers within axon bundles coursing through the trapezoid body. It appears that there is no differential expression of CB along the tonotopic axis of the MNTB.

Developmental Expression of Calbindin D-28k in principal cells of the MNTB of normal hearing (CBA/J) mice and congenitally deaf (*dn/dn*) mice

Low magnification (20X, 1.5 zoom) confocal analysis of somatic CB-IR in the MNTB of CBA/J and *dn/dn* mice was performed by counting CB+ principal cells through stacks of 2μm optical sections from 14μm thick coronal section of MNTB. An average of 1613 principal cells were analyzed for CB expression per age group for CBA/J animals (range: 1362 – 1798) and 1240 per age group for *dn/dn* animals (range: 1074 – 1502). No statistically significant

differences in the total number of principal cells in each section were found between CBA/J and *dn/dn* mice (CBA/J: 107.5 ± 15.8, *dn/dn*: 98.0 ± 9.8; mean ± SEM; p = 0.625 *t-test*).

Percentages of principal cells which were CB-IR were obtained for the whole of the MNTB. A clear majority of principal cells express CB, with an a significant increase in the percent of principal cells expressing CB from P9 to P13, but not after P13 (P9: 95.5 ± 0.3%, P13: 97.4 ± 0.4%, P30 ± 98.0 ± 0.3, P49: 97.9 ± 0.3%; mean ± SEM; p > 0.001 One Way ANOVA) (Figure 18, 20, 26). *Post hoc* test indicate a significant change in somatic CB expression between P9 and all other age points analyzed (p<0.01 *post hoc* Tukey's test). No differences were detected between animals at P13, P30, or P49 (p>0.05 *post hoc* Tukey's test) (Figure 26). Similarly in *dn/dn* mice, CB was expressed in clear majority of principal cells at all ages analyzed, significantly increasing from P9 to P13, nut not after P13 (P9: 95.4 ± 0.2%, P13: 97.3 ± 0.3%, P30: 97.7 ± 0.3%, P49: 98.3 ± 0.5%; mean ± SEM; p<0.001 One Way ANOVA) (Figure 19, 21, 22). *Post hoc* test indicate a significant change in somatic CB expression between P9 and all other age points analyzed (p<0.01 *post hoc* Tukey's test). No differences were detected between animals at P13, P30, or P49 (p>0.05 *post hoc* Tukey's test) (Figure 22). When comparing wild-type to deaf, no significant differences in the percentage of principal cells that express CB were detected at P9 (p = 0.592 t test), P13 (p = 0.878 t test), P30 (p = 0.545 t test), and P49 (p = 0.838 t test). These data suggest that CB immunoreactivity is present in nearly 100% of principal cells before the onset of hearing in both control and deaf mice and that,

in both strains, CB expression is increases slightly, albeit significantly, immediately after the onset of hearing but not after P13. No CB expression was detected in presynaptic calyces of Held at any age point analyzed in CBA/J and *dn/dn* mice.

In the following section, the expression of CB was separately analyzed in principal cells located in each of the lateral, intermediate, and medial thirds of the nucleus. These data indicate that, CB-IR principal cells show no preferential pattern of expression along the tonotopic gradient of the MNTB.

Expression of Calbindin D-28k in Principal Cell Somata is Homogenous along the Tonotopic Axis During Postnatal Development in Normal Hearing (CBA/J) and Congenitally Deaf (*dn/dn*) Mice

To assess the developmental distribution of CB-IR principal cells along the tonotopic axis, the same confocal images used in the previous sections were analyzed. As in Aim 1, the MNTB in each image was subdivided into lateral, intermediate, and medial thirds. Counts of Nissl stained and CB-IR principal cells were for each of the three subdivisions so that percentages of principal cells that express CB could be obtained for each third of the nucleus.

In the lateral third of the MNTB of CBA/J mice, the frequency of CB-IR principal cells increased significantly from P9 to P13 (P9: 96.1 ± 0.3%, P13: 98.0 ± 0.6%, P30: 97.9 ± 0.5%, P49: 98.3 ± 0.4%; mean ± SEM; $p = 0.024$ One Way ANOVA). *Post hoc* test indicate a significant change in somatic CB expression between P9 and all other age points analyzed ($p<0.01$ *post hoc* Tukey's test). No

differences were detected between animals at P13, P30, or P49 ($p>0.05$ *post hoc* Tukey's test) (Figure 18, 20, 23). Similarly, in *dn/dn* mice, the frequency of CB expression in the lateral third of the MNTB increased significantly in principal cell somata from P9 to P13 (P9: 96.0 ± 0.3%, P13: 97.6 ± 0.5%, P30: 98.1 ± 0.6%, P49: 98.3 ± 0.6%; mean ± SEM; $p = 0.012$ One Way ANOVA). *Post hoc* test indicate a significant change in somatic CB expression between P9 and all other age points analyzed ($P<0.05$ *post hoc* Tukey's test). No differences were detected between animals at P13, P30, or P49 ($p>0.05$ *post hoc* Tukey's test) (Figure 19, 21, 23).

Similar findings were detected in the intermediate and medial thirds of the MNTB in CBA/J and *dn/dn* mice. In the intermediate third of CBA/J mice, the frequency of CB-IR principal cells increased from P9 to P13 (P9: 95.1 ± 0.5%, P13: 97.4 ± 0.5%, P30: 98.0 ± 0.7%, P49: 97.8 ± 0.4%; mean ± SEM; $p<0.001$ One Way ANOVA). *Post hoc* test indicate a significant change in somatic CB expression in the intermediate third of the MNTB between P9 and all other age points analyzed ($p<0.01$ *post hoc* Tukey's test). Like the lateral third, no differences were detected between animals at P13, P30, or P49 ($p>0.05$ *post hoc* Tukey's test) (Figure 18, 20, 23). In *dn/dn* mice, the frequency of CB-IR principal cells in the intermediate third of the nucleus increased from P9 to P13 (P9: 95.3 ± 0.4%, P13: 97.9 ± 0.8%, P30: 97.8 ± 0.5%, P49: 98.1 ± 0.5%; mean ± SEM; $P = 0.004$ One Way ANOVA). *Post hoc* test indicate a significant change in somatic CB expression in the intermediate third of the MNTB in *dn/dn* animals between P9 and all other age points analyzed ($p<0.01$ *post hoc* Tukey's test). No

differences were detected between animals at P13, P30, or P49 ($p>0.05$ *post hoc* Tukey's test) (Figure 19, 21, 23).

In the medial third of the MNTB in CBA/J mice, once again the frequency of principal cells expressing CB increased from P9 to P13, but not after P13 (P9: 95.2 ± 0.6%, P13: 96.8 ± 0.8%, P30: 98.3 ± 0.5%, P49: 97.5 ± 0.6%; mean ± SEM; $p = 0.019$ One Way ANOVA). *Post hoc* test indicate a significant change in somatic CB expression in the intermediate third of the MNTB between P9 and all other age points analyzed ($p<0.01$ *post hoc* Tukey's test). No differences in the percentage of CB-IR principal cells were detected between animals at P13, P30, or P49 ($p>0.05$ *post hoc* Tukey's test) (Figure 18, 20, 23). Similarly, in *dn/dn* mice the frequency of CB-IR principal cells increased from P9 to P13 (P9: 94.4 ± 0.8%, P13: 97.2 ± 0.7%, P30: 97.4 ± 0.6%, P49: 98.4 ± 0.6%; mean ± SEM; $p = 0.001$ One Way ANOVA). *Post hoc* test indicate a significant change in somatic CB expression in the medial third of the MNTB in *dn/dn* animals between P9 and all other age points analyzed ($p<0.01$ *post hoc* Tukey's test). No differences were detected between animals at P13, P30, or P49 ($p>0.05$ *post hoc* Tukey's test) (Figure 19, 21, 23).

Consequently, as there were no significant differences detected in the frequency of CB expression between age matched CBA/J and *dn/dn* mice across the whole of the MNTB (see previous results), there were no significant differences detected in the frequency of CB expression between age matched CBA/J and *dn/dn* mice ($p>0.05$ t test). These data suggest that during development in CBA/J and *dn/dn* mice, CB is expressed in nearly 100% of

principal cells in each third of the MNTB, and that the significant increase detected from P9 to P13, but not after P13, in each strain (see previous results) corresponds to increases in somatic CB expression detected each third of the MNTB. As such, there is nothing in these data which would indicate a preferential pattern of CB expression along the tonotopic axis of the MNTB at any age points analyzed

Additionally, within each strain, percentages of Nissl stained principal cells expressing CB in each third of the MNTB were compared against the other two MNTB subdivisions in age matched mice. At all ages analyzed, no significant differences were seen in the percentage of principal cells expressing CB between any region of the MNTB in CBA/J or *dn/dn* mice ($p>0.05$ One Way ANOVA, $p>0,05$ *post hoc* Tukey's test) (Figure 23). These data further suggest that, in both strains at all age points analyzed, the pattern of somatic CB expression is homogenous throughout the medial–lateral axis of the MNTB and does not appear to be to correspond to the MNTB's tonotopic gradient of characteristic firing frequency.

Expression of Calbindin (CB) in the MNTB of adult Wistar Rats

The developmental expression of CB reported in this study, is similar to the expression of CB observed in experiments conducted on adult wild-type Wistar rats. Images generated during this study indicate that adult Wistar rats express CB in a clear majority of MNTB principal cells (Figure 24).

Calbindin D-28k (CB) labels cell processes of MNTB principal cells

Aim 2 of this study, shows that cell processes, presumably dendrites, of principal cells may be labeled by CR, if the principal cell somata from which the dendrites arises is labeled with the antibody. Similarly, cell processes from CB-IR principal cells in CBA/J mice, *dn/dn* mice, and wistar rats are also labeled by anti-CB antibodies (Figure 25). Further, it appears that these cell processes may receive both excitatory and inhibitory synaptic contacts (Figure 25). Many of these cell processes are also labeled by antibodies raised against the dendritic marker microtubule associated protein 2 (MAP2), indicating that they are likely dendrites (Figure 26). It remains unclear whether CB will additionally label principal cell axons.

In cursory series of experiments looking at principal cell dendrites, this study has shown that these dendrites may receive synaptic contacts of unspecified origins. In addition to possible VGluT1-IR presynaptic terminals, which were also shown apposed to CR-IR cell processes in Aim 2 of this study, and gephryn-IR presynaptic terminals, many of these cell processes appear to be contacted by GAD65 presynaptic terminals (Figure 27, 28). However, without electron microscopy, it can not be definitively stated whether the close proximity of presynaptic marker proteins with principal cell dendrites are, in fact, synapses. Additionally, these experiments revealed the possible presence of Kv3.4 channels on or near these dendrites (Figure 28). In several instances, Kv3.4 labeling was observed closely apposed to, but not colocalized with, GAD-65 immunoreactivity. It may be that these ion channels serve a role in transmission at these inhibitory

synapses which modulate firing capability of the principal cell. However, without ultrastructural or physiological studies, it cannot be stated whether these channels are located in presynaptic or postsynaptic structures.

VIII. DISCUSSION

CALBINDIN D-28K IN THE MNTB

Developmental regulation of calbindin D-28k (CB) expression in the MNTB of normal hearing (CBA/J) mice

We investigated the cellular localization of CB in the MNTB during postnatal development of CBA/J mice. In normal hearing mice, the pattern of CB expression appears to only minimally change during development from postnatal day 9 to postnatal day 49.

At postnatal day 9, principal cells can be differentiated with Nissl stain using previously defined morphological characteristics. At this age, CB staining is prominent in principal cell somata and, even under optimal imaging conditions, cannot be detected in VGluT1-IR calyces of Held. On average, P9 CBA/J mice express CB in 95.5 ± 0.3% of principal cells throughout the nucleus. There was no apparent change in expression across the medial-lateral axis of the MNTB, as CB was expressed in 96.1 ± 0.3%, 95.1 ± 0.5%, 95.2 ± 0.6% of principal cells in the lateral, intermediate, and medial thirds of the nucleus, respectively.

By postnatal day 13, CB expression throughout the nucleus increased significantly to 97.4 ± 0.4% of principal cells. This increase corresponded to increases in CB expression in principal cells located in each of the lateral (98.0 ± 0.6%), intermediate, (97.4 ± 0.5%), and medial (96.8 ± 0.8%) thirds of the MNTB. No statistically significant differences in the percent of CB-IR principal

were detected with further maturation after P13 (P30: 98.0 ± 0.3%, P49: 97.9 ± 0.3%).

Felmy and Schneggenburger (2004) reported that at P10 and later, but not at P6, the population of CB-expressing MNTB neurons in C57/BL6 mice is nearly identical with the neurons that receive a Rab3A (+) calyceal type synaptic ending, indicating that CB is probably expressed by all MNTB principal cells. The results of the present experiment, which indicate that the proportion of CB containing principal cells increase to nearly 100% at P13, verify the findings of Felmy and Schneggenburger. Indeed, when costained with anti-VGluT1, the population of CB-IR principal cells in CBA/J mice is nearly identical to those neurons which receive a VGluT1-IR calyx of Held synaptic terminal (Figure 17). However, fitting with the data, occasional VGluT-IR calyces of Held were detected surrounding a CB (-) principal cell (Figure 29)

That nearly 20% of cells in the MNTB are elongate and stellate cells (rat: Sommer et al., 1993) indicates a possibility that some Nissl stained cells which were CB (-) may represent a small portion of MNTB elongate and stellate cells which, due to plane of section, met morphological criteria necessary to be counted as principal cells upon Nissl stain. Such morphological similarity is more likely to have influenced counts in younger animals, as some cells may not yet have reached mature size and morphology. In this regard, the significant increase in CB-IR principal cells detected from P9 to P13 should be interpreted with a degree of caution, as it may be attributable to morphological similarity at postnatal day 9 between CB (+) principal cells and CB (-) stellate and elongate cells. Regardless,

the results of Felmy and Schneggenburger (2004), which show a similar increase in CB expression from P6 to P10, indicate that it is probably not until the onset of hearing the CB is expressed in nearly 100% of principal cells.

Thus, CB is expressed in principal cell somata throughout the MNTB, with no apparent differential expression along its tonotopic axis. Similar results were obtained during postnatal development in *dn/dn* mice.

Developmental expression of calbindin D-28k (CB) expression in the MNTB of congenitally deaf (*dn/dn*) mice

At 9 days postnatal, and throughout developmental time points studied, MNTB principle cells in *dn/dn* mice take on the characteristic morphology upon Nissl stain as those described by Morest, Osen, Harrison, and Irving (see Appendix 2). Further, no differences were detected in the developmental regulation and pattern of expression of PV in the MNTB of congenitally deaf (*dn/dn*) mice compared to age matched wild-type (CBA/J) mice. On average, P9 *dn/dn* mice express CB in 95.4 ± 0.2% of principle cells throughout the nucleus. There was no apparent gradient in the pattern of expression across the medial – lateral axis, as CB was expressed in 96.0 ± 0.3%, 95.3 ± 0.4%, and 94.4 ± 0.8% of principle cells located in the lateral, intermediate, and medial thirds of the nucleus, respectively. No staining is present in the calyx region immediately surrounding the principal cell. From P9 to P13, the percentage of CB-IR principle cell somata increased to nearly 100% (P13: 97.3 ± 0.3%) with no statistically significant differences in the percent of PV-IR principal cells were detected after

P13 (P30: 97.7 ± 0.3%, P49: 98.3 ± 0.5%). Like age matched CBA/J mice, CB-IR somata were evenly distributed along the medial – lateral axis of the MNTB at all age points studied.

By postnatal day 13, PV expression in principal cells throughout the nucleus increased significantly to P13: 97.0 ± 0.6%, which corresponded to increases in PV expression in principal cells located in each of the lateral (98.3 ± 0.5%), intermediate (98.5 ± 0.4%), and medial (98.7 ± 0.8%) thirds of the MNTB. No statistically significant differences in the percent of PV-IR principal cells were detected with further maturation after P13. Similarly, no significant differences were seen in calyceal PV expression after P9 (P13: 99.2 ± 0.2%, P30: 99.3 ± 0.3%, P49 ± 98.9 ± 0.5%). Throughout developmental time points studied, PV-IR principal cells and calyces of Held remained evenly distributed along the medial – lateral axis of the MNTB.

Thus, the pattern of CB expression in the MNTB of *dn/dn* mice shows no apparent differences from the pattern of CB expression in age matched CBA/J animals. No gradient of expression in either strain was observed along the medial – lateral tonotopic gradient of the MNTB. However, detailed optical density analysis using a DAB stain should be carried to determine a difference in the intensity of staining exists along the tonotopic gradient in either animal as well as to determine any differences in the overall intensity of staining between animals.

It should be further noted that because both CBA/J and *dn/dn* mice exhibit CB immunoreactivity in nearly 100% of principal cells throughout development, then CB is coexpressed with PV in nearly every principal cell, regardless

peripheral afferent activity. Such coexpression suggests the possibility of differential roles for each protein in postsynaptic Ca^{2+} signaling, which may arise from the relative fast Ca^{2+} binding kinetics of CB versus the relatively slow Ca^{2+} binding kinetics of PV.

Calbindin D-28k (CB) labels cell processes of MNTB principal cells

The MNTB has received considerable attention in the discipline of synaptic physiology. The large size of the primary synaptic input, the calyx of Held, and the simple round morphology of the principal cell have allowed researchers to obtain simultaneous recordings from presynaptic and postsynaptic neurons (Forsythe, 1994; Barnes-Davies and Forsythe, 1995). That, despite the one or two short dendrites exhibited by principal cells, the majority of inhibitory and excitatory presynaptic terminals contact the cell soma, have allowed for the interpretation of such recordings without additional complications of distorted synaptic responses due to dendritic filtering. In fact, principal cell dendrites are often not considered capable of performing complex computational tasks and are hence ignored, reducing these neurons, especially in modeling studies, to a simple sphere (Leao, et al., 2008). However, the presence of significant functional dendritic inputs to the principal cell has recently become a contentious issue. Furthering the debate, these dendrites may comprise up to 25% of the neuronal surface area, adding considerable capacitance to the neuron and the potential to affect postsynaptic firing capabilities (Leao, et al., 2008).

Because the neuropil in the vicinity of the MNTB is lightly stained with anti-CB antibodies, CB is a useful principal cell marker capable of labeling dendritic structures for many tens of microns. Comparing dendritic labeling with anti-CB antibodies compared to anti-MAP2 antibodies illustrates the usefulness of such a technique (Figure 26). The dendrite labeled in Figure 26D-F is lost in the neuropil when stained with anti-MAP2, but may be followed well outside the MNTB when labeled with anti-CB.

This stain can be an effective dendritic marker in mice as well as rats. Indeed, dendrites several microns in diameter can be seen emerging from principal cells in the rat and extending ventrally into the region of the trapezoid body, suggesting that principal cells may receive extensive collateral input from axons traversing the trapezoid body (Figure 25).

In a cursory inspection of principal cell dendrites in both normal hearing and congenitally deaf mice, the results of this study indicate the presence of excitatory (glutamatergic) and inhibitory (glycinergic and GABAergic) synaptic proteins in the vicinity of the principal cell dendrite. In some cases these possible contacts were observed many tens of microns away from the cell soma. While previous studies have confirmed the presence of calyceal glutamatergic synapses on the most proximal portions of dendrites (Morest, 1968b; von Gersdoff and Borst, 2002) as well as noncalyceal glutamatergic inputs to dendrites up to 20μm away from the soma (Leao et al., 2008), we are unable to confirm or deny that the synaptic proteins shown contacting principal cell dendrites in these experiments are, indeed, synapses.

In a study on the effect of dendrites on principal cell firing capabilities, Leao, et al. (2008) showed the existence of dendritic voltage gated sodium channels which could serve as an additional source of inward current for the maintenance of action potential amplitude, especially during repetitive firing in response to calyceal EPSCs. Because action potential propagation in myelinated nerve fibers depends on the amplitude the signal at the initial segment, such dendritic specializations may be critical adaptations for the high fidelity synaptic transmission. Further, Leao, et al., (2008) demonstrate that such active principal cell dendrites may amplify and delay dendritic EPSPs, which occur in response to noncalyceal synaptic inputs, with no interference in interference in action potential timing resulting from calyceal EPSPs. They postulate that this delay in dendritic action potential propagation would allow the principal cell to distinguish between calyceal and non-calyceal inputs, providing additional evidence that 1) these dendrites are capable of computational tasks and 2) principal cells may be more than simple sign inverting relays.

If these dendrites do indeed play an active role in the maintenance of high fidelity synaptic transmission across the calyx of Held synapse and provide computational ability beyond that of a simple sign inverting relay, high and low-threshold voltage-activated potassium channels may additionally contribute to the dendritic machinery necessary to perform such postsynaptic functions. In the principal cell soma as well as the calyx of Held, it has been shown that K_V1 and K_V3 potassium channels contribute differentially to high fidelity synaptic transmission at the calyx of Held. Both pre- and post-synaptically, K_V1 channels

contribute to a rapidly activating, low-voltage activated K^+ current that limits spiking in both principal cells and calyces of Held to a single action potential, thereby improving temporal precision by limiting aberrant firing, decreasing membrane time constants, and decreasing temporal summation (Brew and Forsythe, 1995; Ishakawa, et al., 2003). Conversely, K_V3 channels contribute to a rapidly activating, high-voltage activated K^+ current with slow inactivation kinetics, which rapidly repolarizes action potentials to facilitate high frequency firing (Brew & Forsythe, 1995; Ishakawa, et al., 2003).

Experiments in this study have shown the existence of Kv3.4 channels in the vicinity of principal cell dendrites. If these channels are indeed located on the dendritic plasma membrane, they may subserve a vital role in the active propagation of excitatory or inhibitory signals in the MNTB. Further studies need to be done to assess the pre- or postsynaptic distribution of these channels as well as their functional significance.

Figure 17. Calbindin D-28k is expressed in majority of MNTB principal cells. Double immunofluorescence images with primary antibodies against VGluT1-IR (FITC) and CB (CY-3) are shown in a 14μm thick section of brainstem from the level of the MNTB in P20 CBA/J mouse. CB is expressed only in principal cells and not calyces of Held. To confirm that CB is expressed in only principal cells, line profiles were taken along the vertical and horizontal dotted lines in the high magnification overlay image. High magnification scale bar = 50μm; Low magnification scale bar = 20μm.

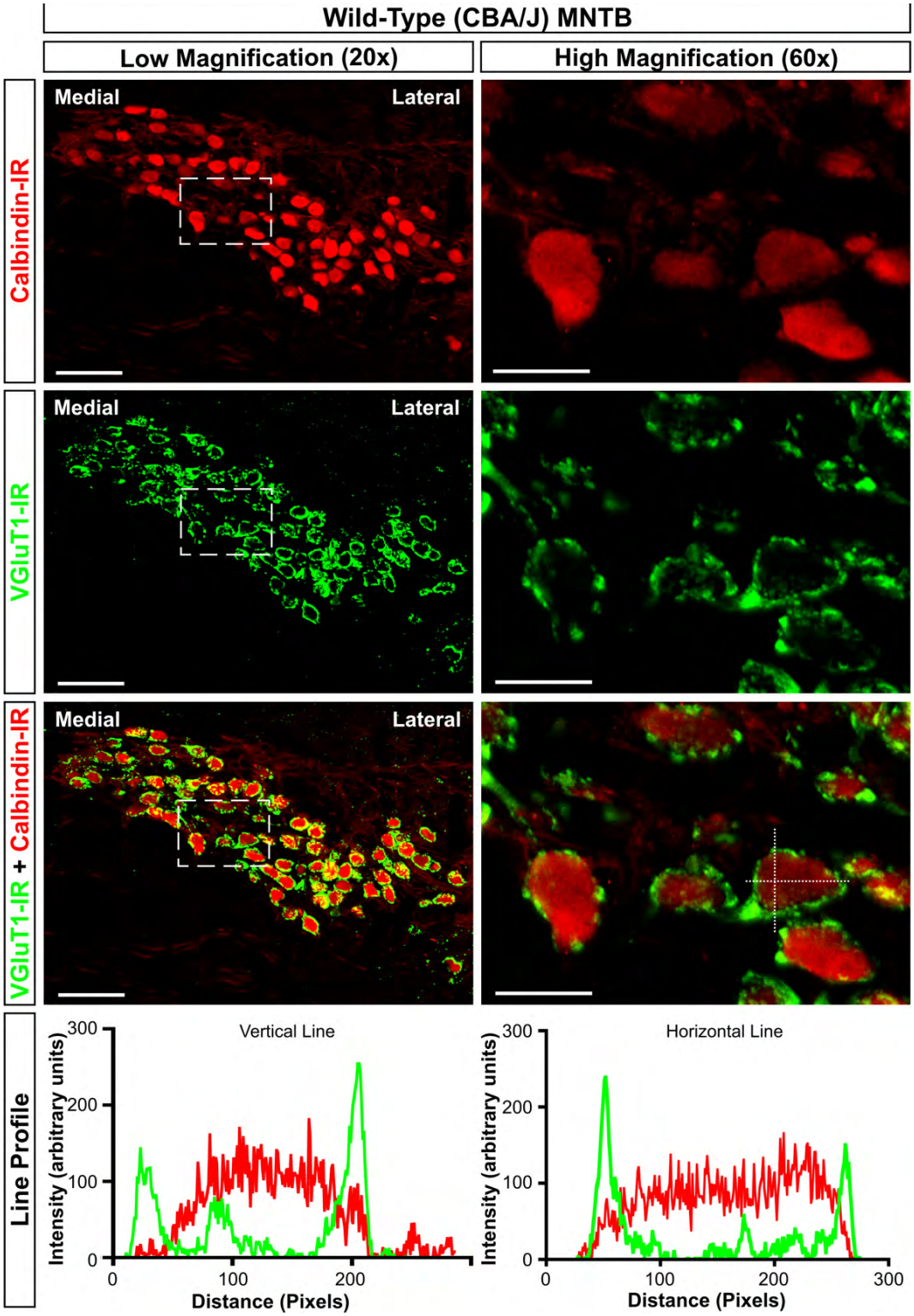
Wild-Type (CBA/J) MNTB
Low Magnification (20x)
High Magnification (60x)
Calbindin-IR
VGluT1-IR
VGluT1-IR + Calbindin-IR
Line Profile
Medial
Lateral
Vertical Line
Horizontal Line
Intensity (arbitrary units)
Distance (Pixels)
0
100
200
300

Figure 18. Calbindin D-28k expression in the MNTB of normal hearing (CBA/J) mice at 9 days postnatal. Double immunofluorescence images with primary antibodies against Nissl (FITC) and CB (CY-3) are shown in a 14μm thick section of brainstem from the level of the MNTB. CB is expressed in nearly every principal cell of the MNTB. Scale Bar = 100μm.

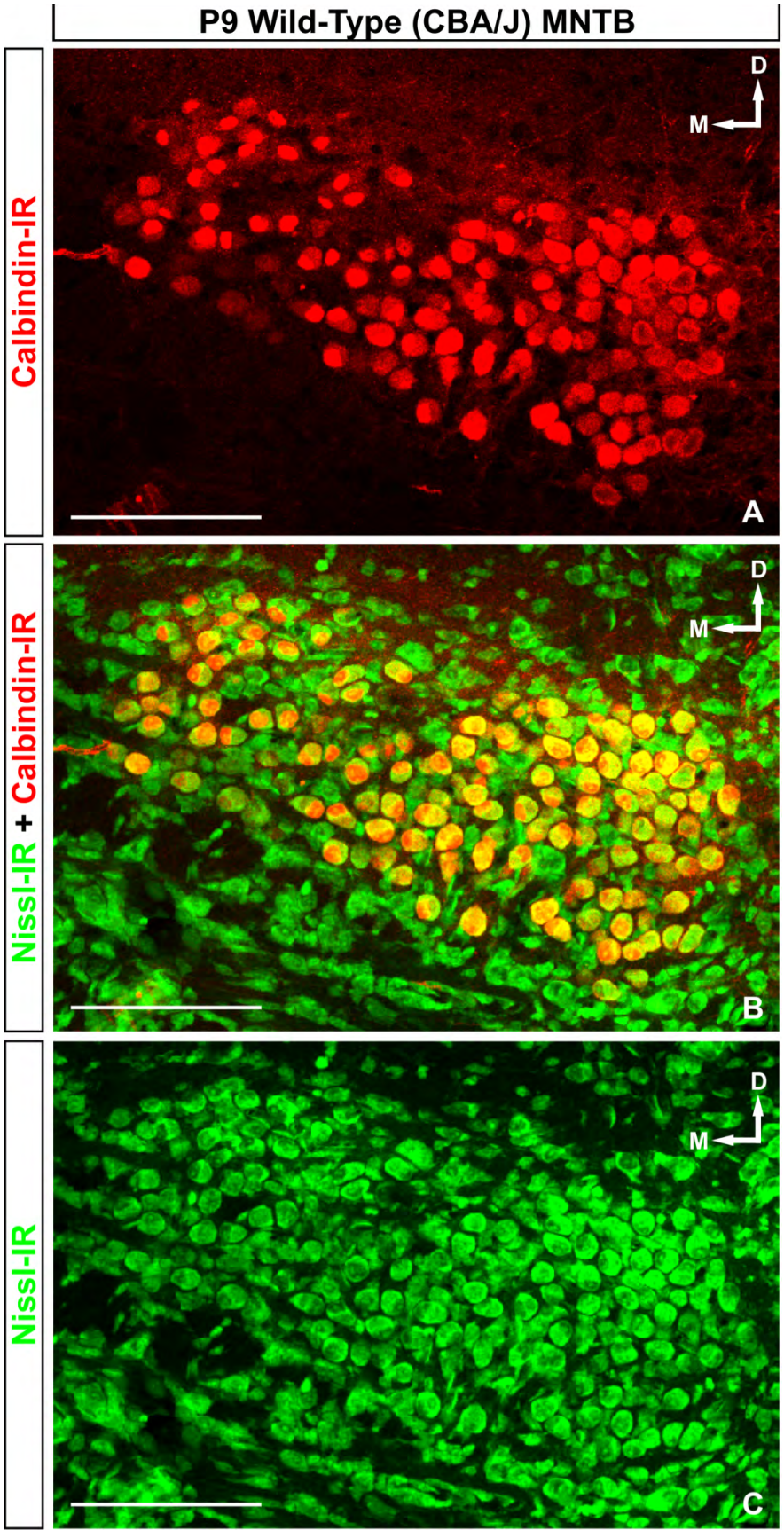
P9 Wild-Type (CBA/J) MNTB
Calbindin-IR
D
M
A
Nissl-IR + Calbindin-IR
D
M
B
Nissl-IR
D
M
C

Figure 19. Calbindin D-28k expression in the MNTB congenitally deaf (*dn/dn*) mice at 9 days postnatal. Double immunofluorescence images with primary antibodies against Nissl (FITC) and CB (CY-3) are shown in a 14μm thick section of brainstem from the level of the MNTB. CB is expressed in nearly every principal cell of the MNTB. Scale Bar = 100μm.

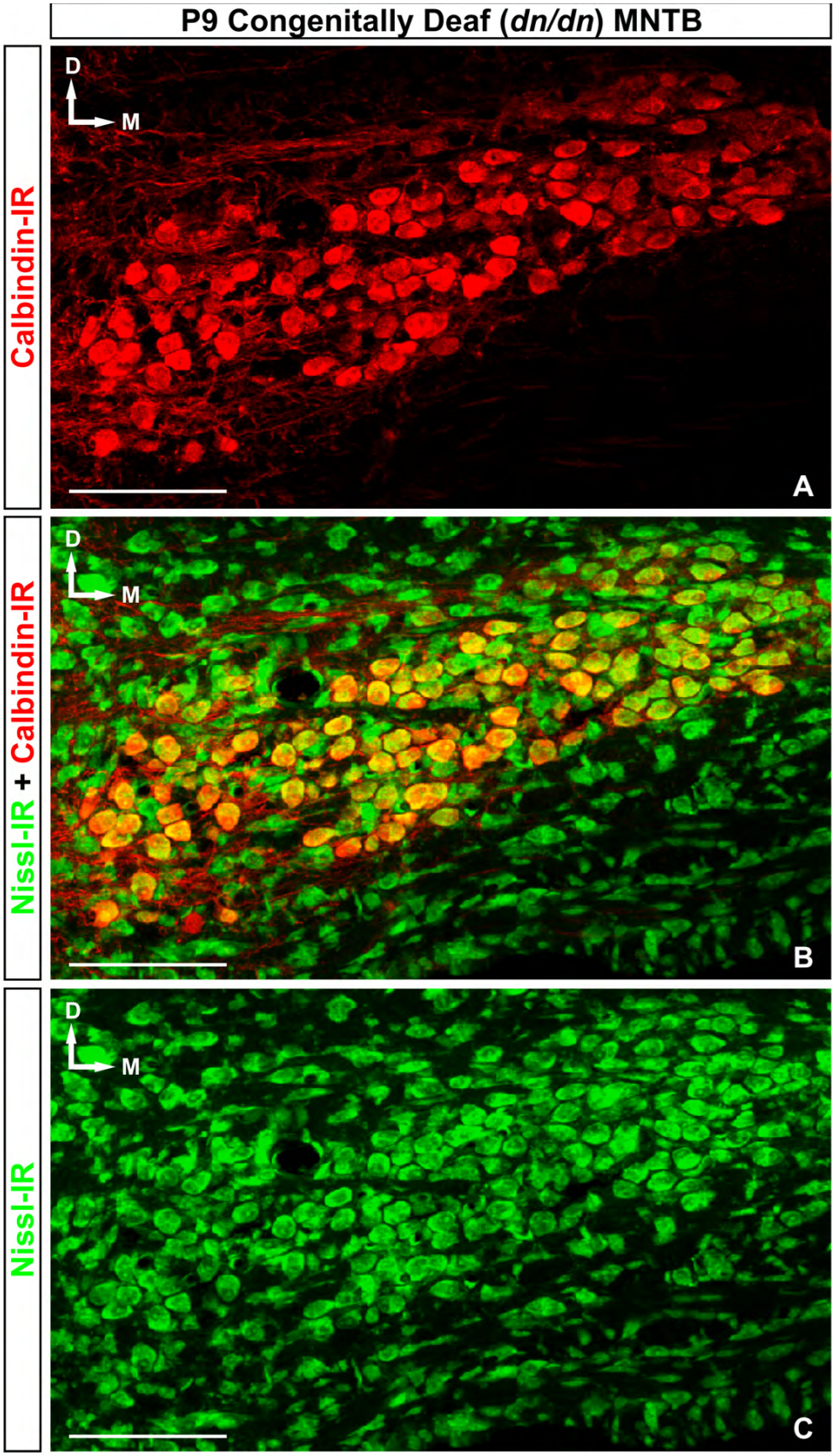
P9 Congenitally Deaf (dn/dn) MNTB
Calbindin-IR
Nissl-IR + Calbindin-IR
Nissl-IR
D
M
A
B
C

Figure 20. Calbindin D-28k expression in the MNTB normal hearing (CBA/J) mice at 49 days postnatal. Double immunofluorescence images with primary antibodies against Nissl (FITC) and CB (CY-3) are shown in a 14μm thick section of brainstem from the level of the MNTB. CB is expressed in nearly every principal cell of the MNTB. Scale Bar = 100μm.

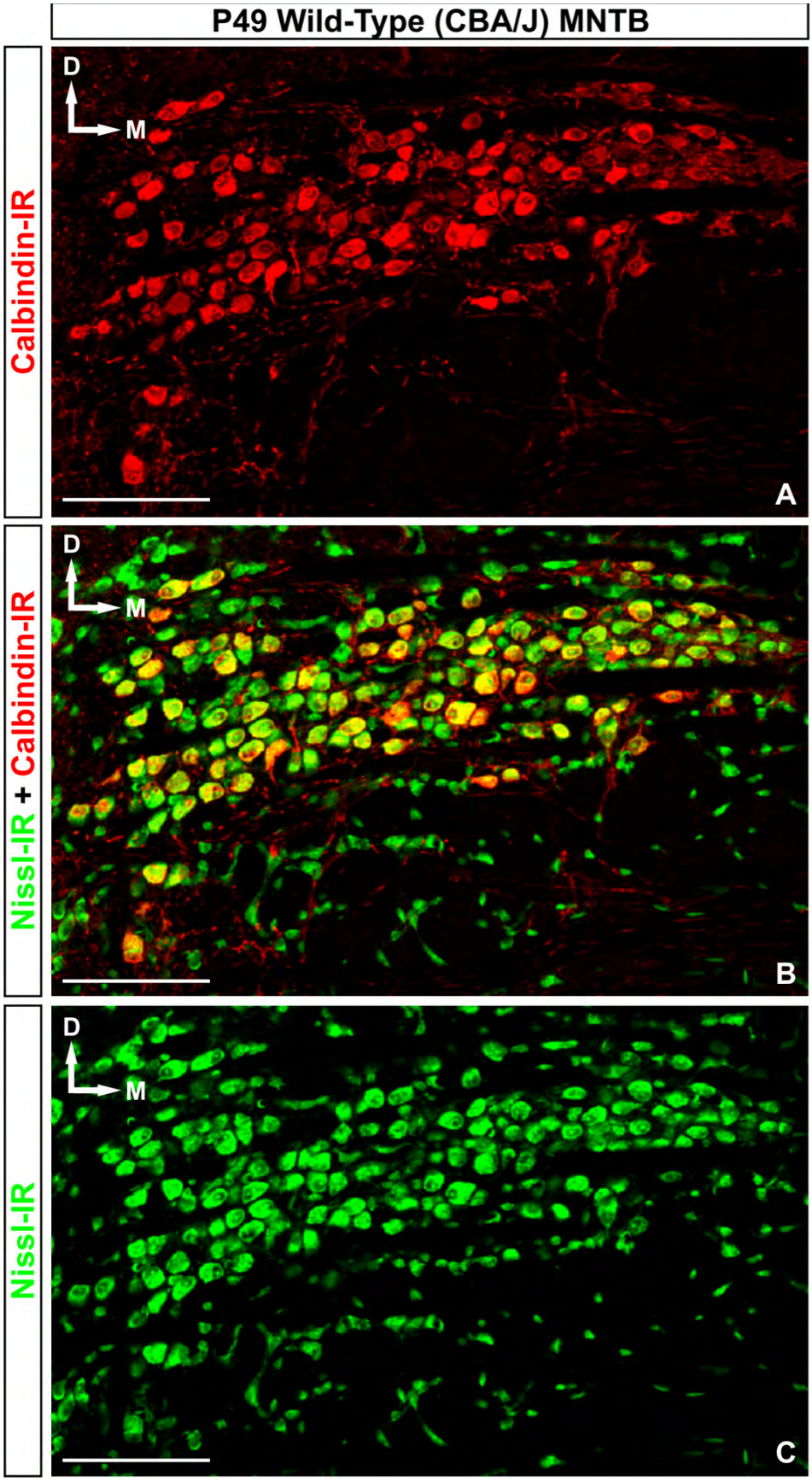
P49 Wild-Type (CBA/J) MNTB
Calbindin-IR
D
M
A
Nissl-IR + Calbindin-IR
D
M
B
Nissl-IR
D
M
C

Figure 21. Calbindin D-28k expression in the MNTB of congenitally deaf (*dn/dn*) mice at 49 days postnatal. Double immunofluorescence images with primary antibodies against Nissl (FITC) and CB (CY-3) are shown in a 14μm thick section of brainstem from the level of the MNTB in a P30 CBA/J mouse. CB is expressed in nearly every principal cell of the MNTB. Scale Bar = 100μm.

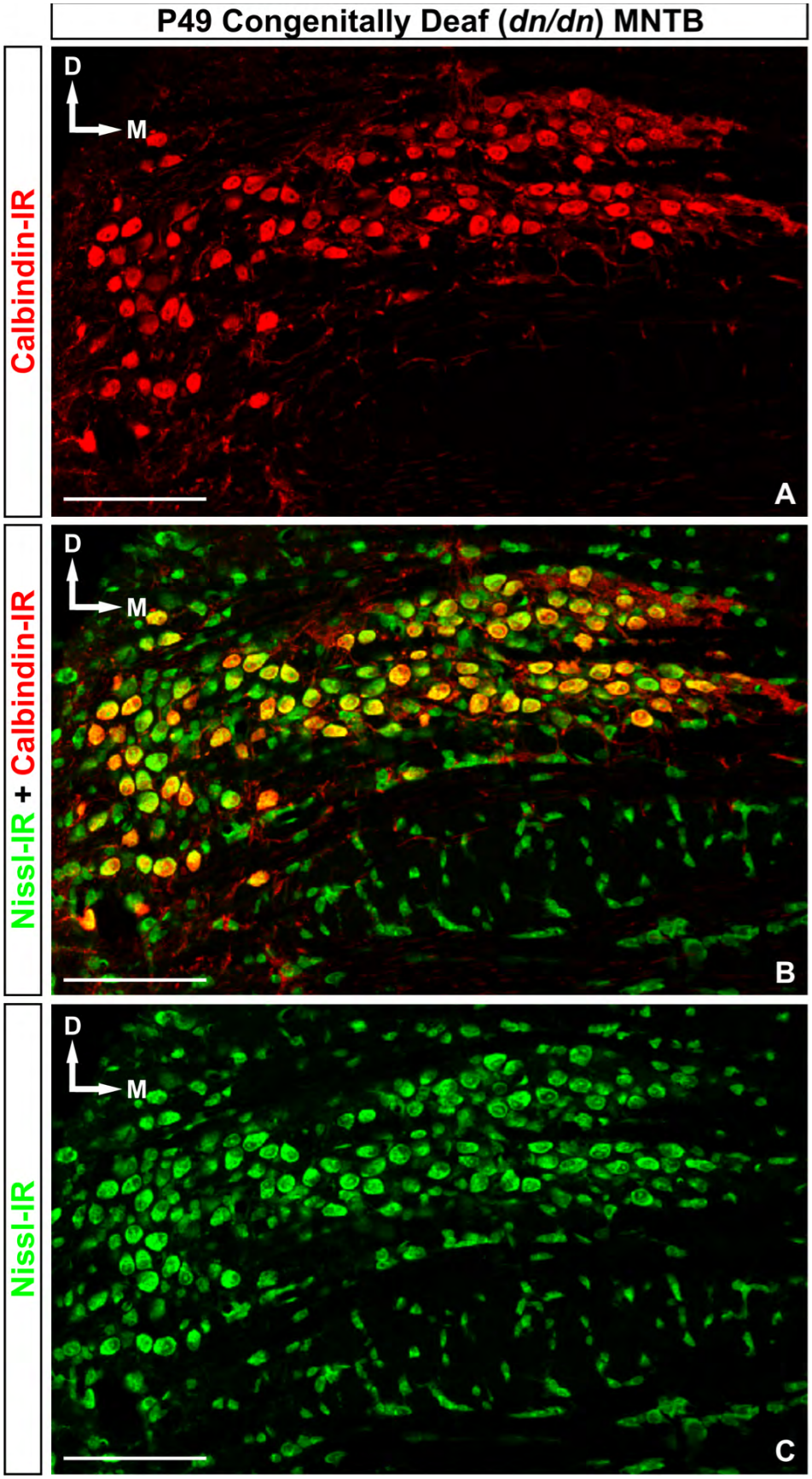
P49 Congenitally Deaf (*dn/dn*) MNTB
Calbindin-IR
D
M
A
Nissl-IR + Calbindin-IR
D
M
B
Nissl-IR
D
M
C

Figure 22: Calbindin D-28k expression in MNTB principal cells
Top shows the percent of principal cells found throughout the medial lateral axis of the MNTB which express CB. A significant increase in the expression of CB was found in CBA/J as well as *dn/dn* mice from 9 days postnatal to 13 days postnatal. In neither strain were further developmental increases were detected after postnatal day 13. No significant differences were detected in the proportion of principal cells expressing CB between age matched CBA/J and *dn/dn* animals. Double asterisk indicates $p<0.001$. **Bottom:** Chart of data used in graph (above).

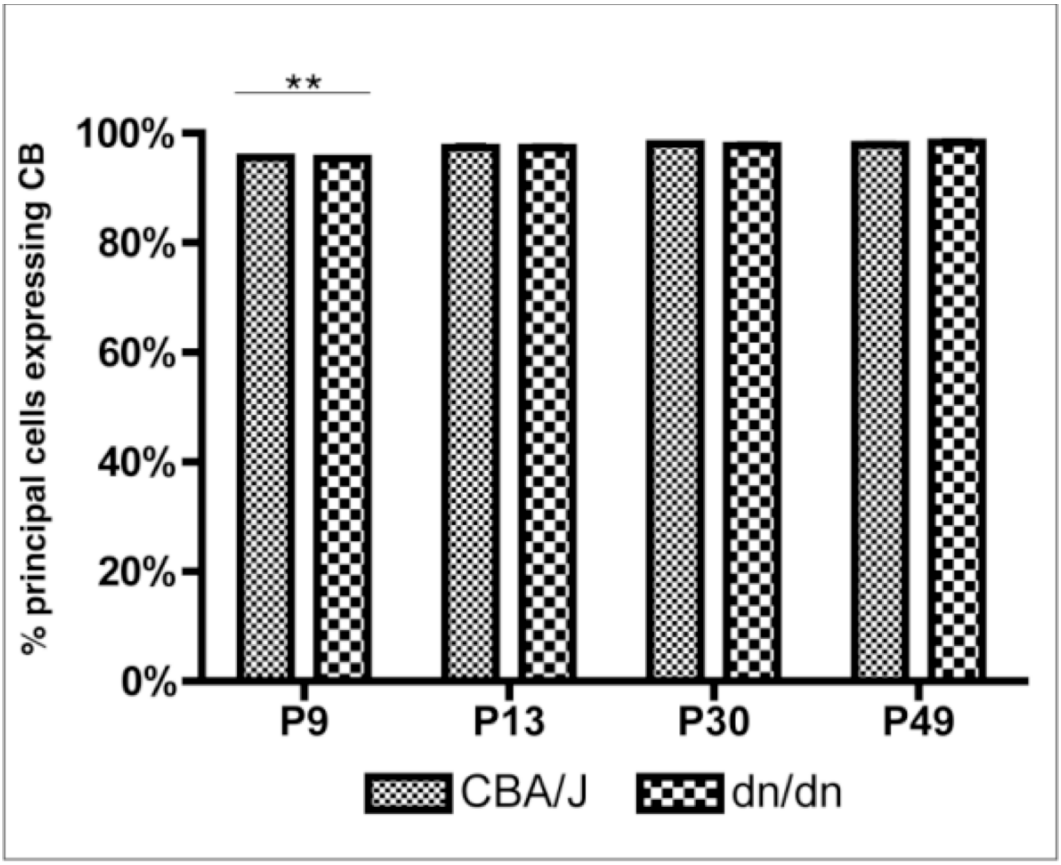

Age	% principal cells expressing CB*	
	CBA/J	dn/dn
P9	95.5 ± 0.3	95.4 ± 0.2
P13	97.4 ± 0.4	97.3 ± 0.3
P30	98.0 ± 0.3	97.7 ± 0.3
P49	97.9 ± 0.3	98.3 ± 0.5

*Mean ± SEM

Figure 23. Regional calbindin D-28k expression in MNTB principal cells.
Above: In **A & B**, the percent of principal cells located in each region of the MNTB which also express CB are shown for each age point analyzed in CBA/J and *dn/dn* mice, respectively. An average of 1613 principal cells were analyzed for CB expression per age group for CBA/J animals (range: 1362 – 1798) and 1240 per age group for *dn/dn* animals (range: 1074 – 1502). **A)** In each third of the MNTB, a significant increase in CB expression among principal cells was detected during development of CBA/J mice from postnatal day 9 to postnatal day 13 (double asterisk: $p<0.001$, One Way ANOVA). However, no significant differences were detected in the percent of principal cells expressing CB between the lateral, intermediate, and medial thirds of the nucleus at any age point analyzed ($p>0.05$ One Way ANOVA). **B)** Like CBA/J mice, in each third of the MNTB, somatic CB expression increased significantly during development from postnatal day 9 to postnatal day 13 (double asterisk: $p<0.001$, One Way ANOVA). Again, no significant differences were detected in the percent of principal cells expressing CB between the lateral, intermediate, and medial thirds of the nucleus at any age point analyzed ($p>0.05$ One Way ANOVA). **Below:** Data used in compiling the above graphs. The fist data column corresponds with graph A, the second with graph B, the third with graph C, and the fourth with graph D.

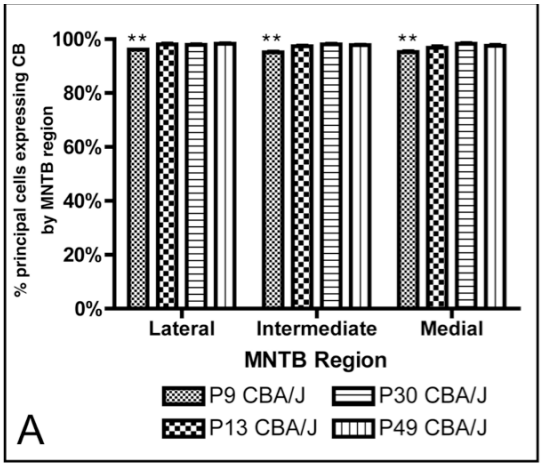

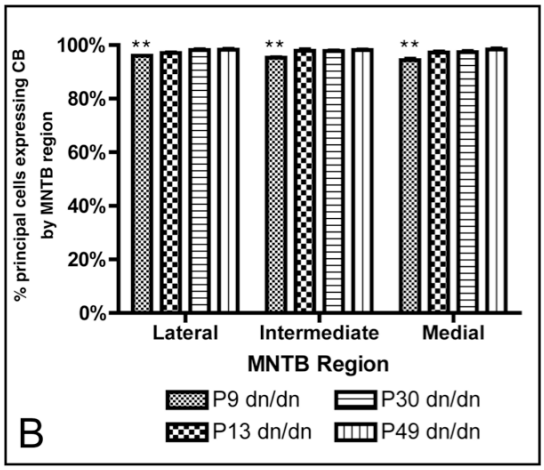

MNTB Region	Age	% principal cells expressing CB by region*	
		CBA/J	*dn/dn*
Lateral	P9	96.1 ± 0.3	96.0 ± 0.3
	P13	98.0 ± 0.6	97.6 ± 0.5
	P30	97.9 ± 0.5	98.1 ± 0.6
	P49	98.3 ± 0.4	98.3 ± 0.6
Intermediate	P9	95.1 ± 0.5	95.3 ± 0.4
	P13	97.4 ± 0.5	97.9 ± 0.8
	P30	98.0 ± 0.7	97.8 ± 0.5
	P49	97.8 ± 0.4	98.1 ± 0.5
Medial	P9	95.2 ± 0.6	94.4 ± 0.8
	P13	96.8 ± 0.8	97.2 ± 0.7
	P30	98.3 ± 0.5	97.4 ± 0.6
	P49	97.5 ± 0.6	98.4 ± 0.6

*Mean ± SEM

Figure 24. Calbindin D-28k expression in the MNTB of normal hearing wistar rats. Double immunofluorescence images with primary antibodies against Nissl (FITC) and CB (CY-3) are shown in a 14μm thick section of brainstem from the level of the MNTB. Boxed sections in A,B, & C are shown in D, E, and F. In **D**, arrow indicates the emergence of dendrite, visible with anti-CB antibodies, from a CB-IR principal cell. CB is expressed in nearly every principal cell. A, B, & C: Scale Bar = 100μm. D, E, &F: Scale Bar = 10μm.

P49 Wild-Type Wistar Rat MNTB
Calbindin-IR
Calbindin-IR + VGluT1-IR
VGluT1-IR
A
B
C
D
E
F
D
M

Figure 25. Calbindin D-28k in MNTB cell processes.
Calbindin D-28k antibodies label cell processes in P49 normal hearing mice (CBA/J), congenitally deaf mice (*dn/dn*), and wistar rats. Double immunofluorescence images stained for Nissl (FITC) and with primary antibodies against VGluT1 (FITC), gephyrin (FITC), and CB (CY-3) are shown. **A&B:** CB labeling reveals a dendrite emerging from a CB-IR principal cell. In B, VGluT1-IR calyx of Held is visible surrounding the principal cell as well as possible VGluT1-IR presynaptic terminal contacting the dendrite (arrowheads). **C&D:** CB labeling reveals dendrites extending from CB-IR principal cells. In D, gephryn immunoreactivity shown inhibitory presynaptic terminals contacting the principal cell somata as well as possible inhibitory contacts on the principal cell dendrites (arrowheads). **E:** Like CB staining in mice, CB reveals large dendrites extending from CB-IR principal cells. In this image, several dendrites (arrows) are seen extending ventrally outside the MNTB and into the trapezoid body. Scale Bars = 10μm.

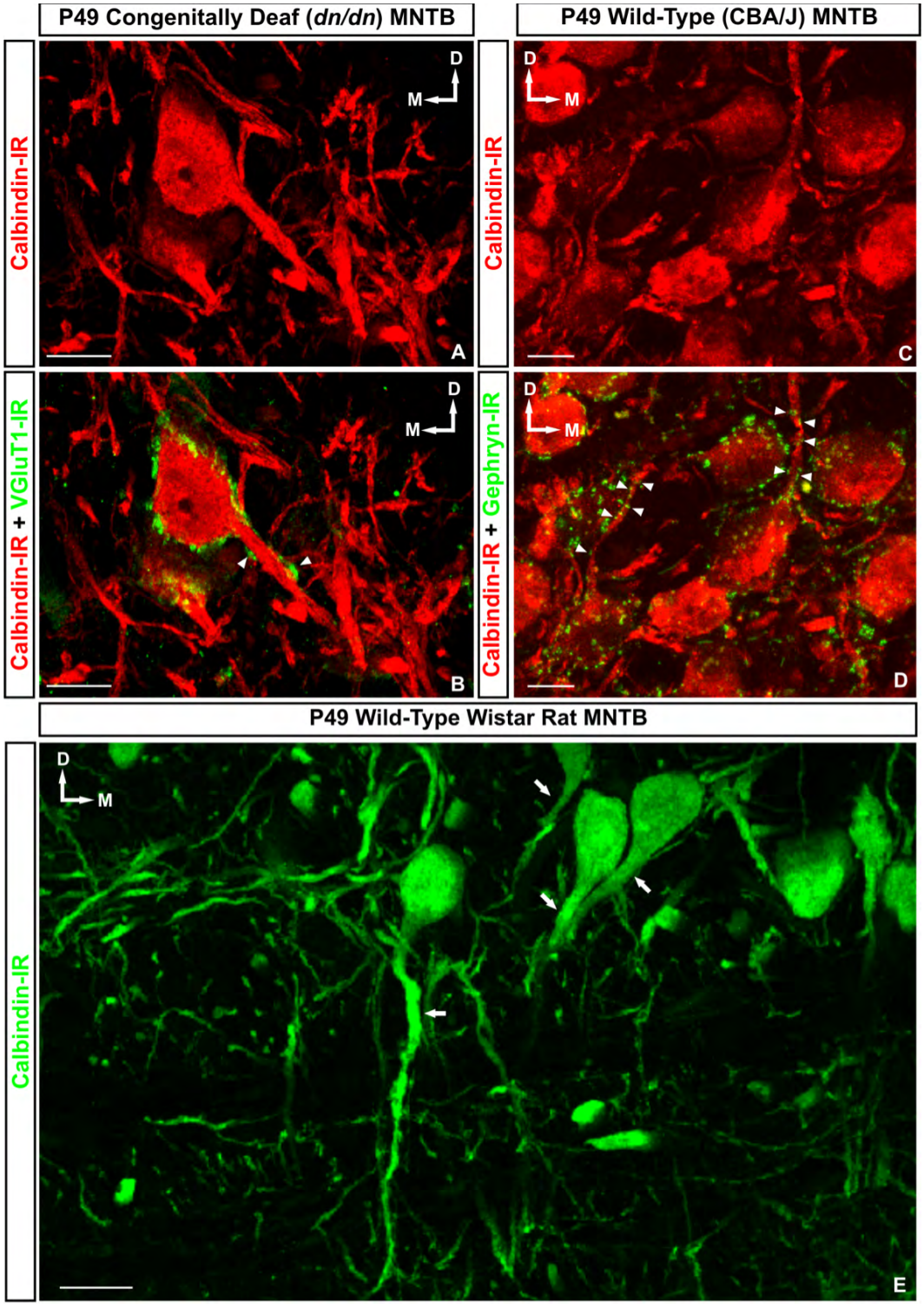
P49 Congenitally Deaf (dn/dn) MNTB
P49 Wild-Type (CBA/J) MNTB
Calbindin-IR
Calbindin-IR
Calbindin-IR + VGluT1-IR
Calbindin-IR + Gephryn-IR
P49 Wild-Type Wistar Rat MNTB
Calbindin-IR
D
M
A
B
C
D
E

Figure 26. Calbindin D-28k and MAP2 in MNTB principal cells.
Calbindin D-28k co-localizes with MAP2 in cell processes of CB-IR principal cells. Triple immunofluorescence images with primary antibodies against VGluT1-IR (FITC), CB (CY-3), and MAP2 (CY-5) are shown in a 14μm thick section of brainstem from the level of the MNTB in P49 CBA/J and *dn/dn* mice. Co-localization of CB and MAP2 within cell processes provides evidence that such processes are dendrites. (Arrows indicate primary dendrites. Arrowheads indicate secondary braches from the primary dendrite.) In A-C, the calyx of Held can be seen makes contact with a proximal dendrite. Because MAP2 heavily labels neuropil, CB may be a more useful stain for labeling the cell processes of principal cells. (Compare image D with image F.) Scale Bar = 20μm.

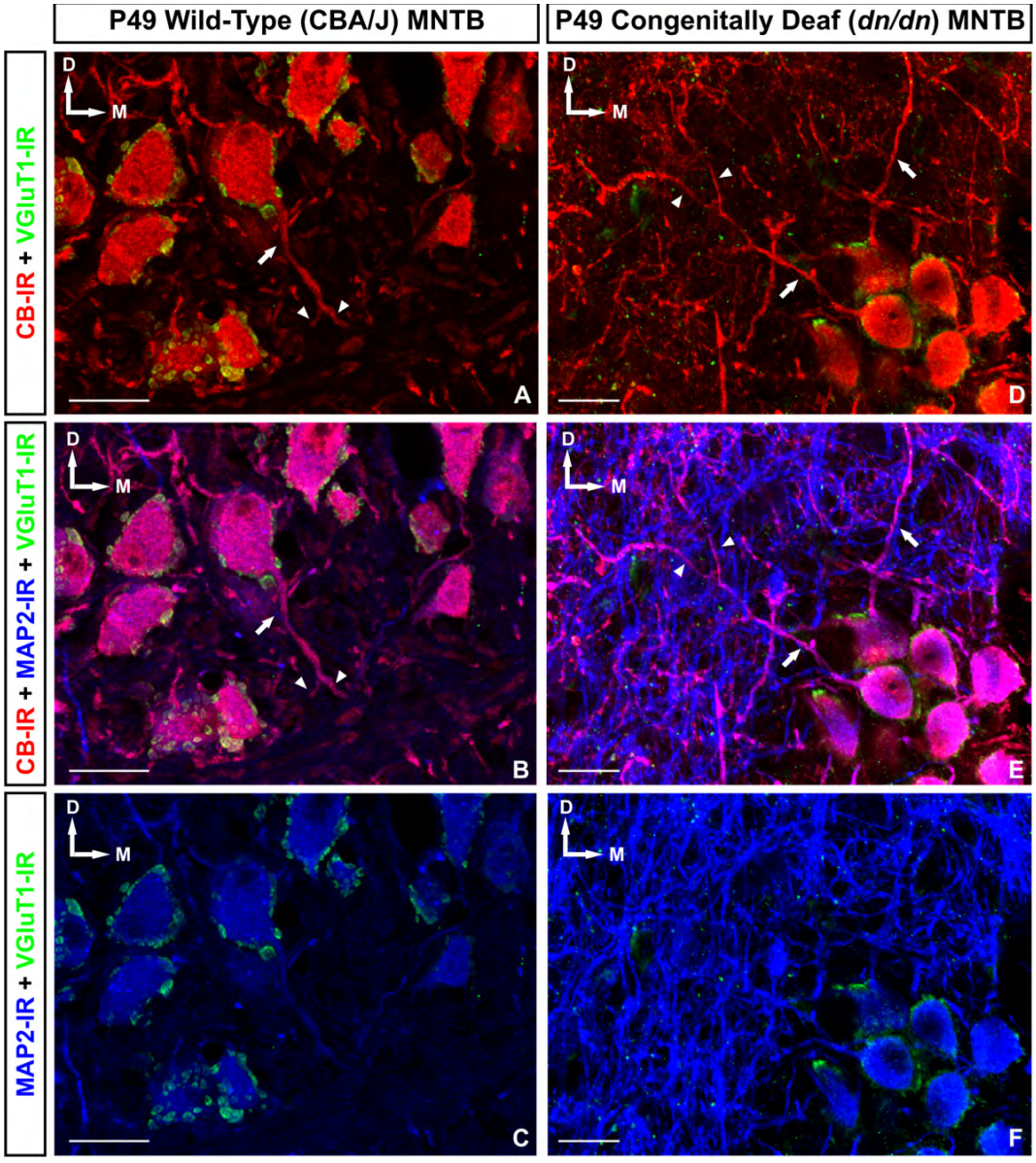
P49 Wild-Type (CBA/J) MNTB
P49 Congenitally Deaf (dn/dn) MNTB
CB-IR + VGluT1-IR
CB-IR + MAP2-IR + VGluT1-IR
MAP2-IR + VGluT1-IR
D
M
A
B
C
D
E
F

Figure 27. Calbindin D-28k labeling in cell processes of P49 principal cells in normal hearing (CBA/J) mice. Triple immunofluorescence images with primary antibodies against GAD65 or Kv3.4 (FITC), CB (CY-3), and VGluT1 or GAD65 (CY-5), as indicated, are shown. In B&E, GAD65 immunoreactivity shows inhibitory presynaptic terminals contacting the principal cell somata as well as possible inhibitory contacts on the principal cell dendrites (arrowheads). In H, GAD65 immunoreactivity shows inhibitory presynaptic terminals contacting the principal cell somata as well as possible inhibitory contacts on the principal cell dendrites (arrows). Additionally, Kv3.4 channels are shown on the surface of principal cell somata and dendrites (arrowheads). Asterisk indicates the close apposition of a GAD65-IR presynaptic terminal and Kv3.4 channel cluster. Scale Bars = 10μm.

P49 Wild-Type (CBA/J) MNTB
Calbindin-IR
CB-IR + VGluT1-IR + GAD65-IR
CB-IR + GAD65-IR
Calbindin-IR
CB-IR + GAD65-IR + Kv3.4-IR
CB-IR + Kv3.4-IR
A
B
C
D
E
F
G
H
I
D
M

Figure 28. Calbindin D-28k labeling in cell processes of P49 principal cells in congenitally deaf (*dn/dn*) mice. Triple immunofluorescence images with primary antibodies against GAD65 (FITC), CB (CY-3), and VGluT1 (CY-5) are shown. Boxed sections in A-C are shown in D-I. **D-I:** CB labeling reveals dendrites emerging from CB-IR principal cells. In D&H, VGluT1-IR calyces of Held are visible surrounding the principal cells. GAD65 immunoreactivity shows inhibitory presynaptic terminals contacting the principal cell somata as well as possible inhibitory contacts on the principal cell dendrites (arrowheads). Note in H, several of these possible dendritic contacts occur at distances greater than 50μm from the dendrite's origin at the principal cell. A-C: Scale Bar = 100μm. D-I: Scale Bar = 10μm.

P49 Congeintally Deaf (dn/dn) MNTB
Calbindin-IR
CB-IR + VGluT1-IR + GAD65-IR
CB-IR + GAD65-IR
D
M
A
B
C
D
E
F
G
H
I

Figure 29. Calbindin D-28k is not present in every principal cell.
Double immunofluorescence images with primary antibodies against VGluT1 (FITC) and CB (CY-3) are shown in a P49 CBA/J mouse. While CB is expressed in a vast majority of principal cells, occasional VGluT1-IR calyces of Held were observed surrounding CB (-) principal cells (asterisk). Scale Bar = 10μm.

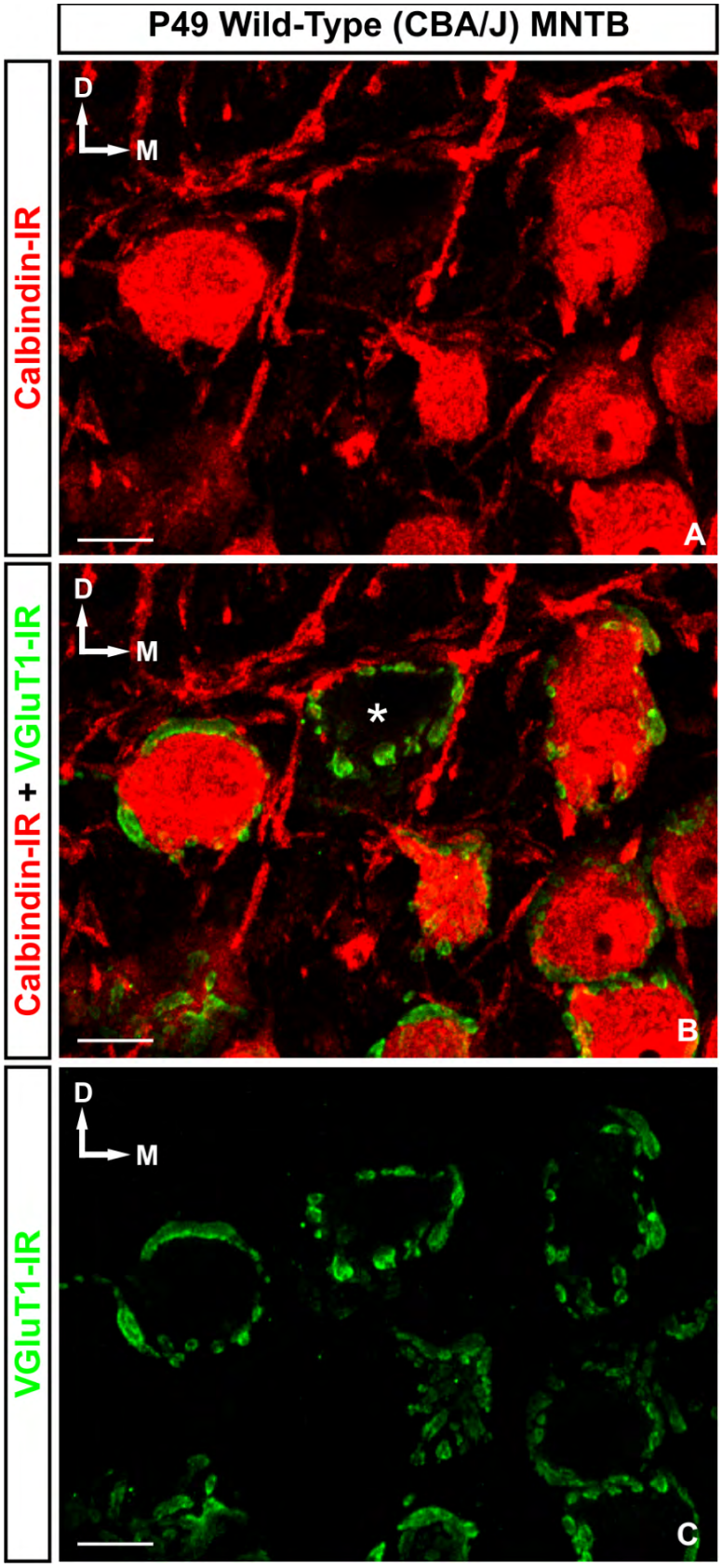
P49 Wild-Type (CBA/J) MNTB
Calbindin-IR
D
M
A
Calbindin-IR + VGluT1-IR
D
M
*
B
VGluT1-IR
D
M
C

IX. RESULTS

CALRETININ IN THE MNTB

Calretinin immunoreactivity (CR-IR) was compared in the MNTB of normal hearing (CBA/J) and congenitally deaf (dn/dn) mice. A number of postnatal time points were analyzed [9 days (P9), 13 days (P13), 30 days (P30), and 49 days (P49)] to obtain the normal time course of CR expression and possible alterations from its normal developmental expression in the absence of spontaneous and acoustically evoked afferent activity in the cochlear nerve. For analysis, tissue was co-labeled with VGluT1 antibodies and Nissl stain. When analyzing sections dual labeled with anit-VGluT1 and anti-CR, somatic CR-IR qualified as a CR-IR principal cell only if it met the criteria of displaying an oval somata 10-20μm in diameter across its long axis surrounded by a VGluT1-IR calyx. 6–8 sections of MNTB per animal were analyzed (n = 6 – 8) from 2–4 animals per age per strain (N = 2-4). The same sections of MNTB were used to analyze somatic CR expression in the whole MNTB as well as in subdivisions corresponding to different characteristic frequencies (broadly defined as high, medium, and low frequencies) of the tonotopic gradient. No statistical differences were found between sections from different animals of the same age and strain ($p>0.05$ One Way ANOVA). Therefore all data from sections of the same age and strain were pooled together.

Calretinin (CR) Expression is Heterogeneous in the MNTB of CBA/J and *dn/dn* Mice

Confocal analysis of CR-IR in the MNTB of CBA/J mice in low magnification (20X, 1.5 zoom) and high magnification (60x, 2.0 zoom) revealed that CR is heterogeneously expressed in only a minority of calyces of Held and principal cell somata throughout development (Figure 30). Similar findings were obtained in *dn/dn* mice (Figure 31). It should be noted that when principal cells are brightly stained for CR, it is possible to see primary as well as secondary dendrites as well as possible VGluT1-IR presynaptic terminals contacting them. This is striking as principal cells dendrites are rarely imaged receiving synaptic contacts.

A stepwise gradient of CR expression was observed in CBA/J and *dn/dn* mice throughout development, with CR-IR calyces preferentially located in the lateral portion of the nucleus and CR-IR principle cells preferentially located in the medial part of the nucleus. It may be that the differential expression of CR along the medial-lateral axis of the MNTB coincides with the tonotopic gradient of the MNTB. Developmental differences in this topographic gradient of CR expression are discussed in the following sections.

Developmental Expression of Calretinin in presynaptic calyces of Held in the MNTB of normal hearing (CBA/J) mice and congenitally deaf (*dn/dn*) mice

Low magnification (20X, 1.5 zoom) confocal analysis of calyceal CR-IR in the MNTB of CBA/J and *dn/dn* mice was performed by counting CR+ calyces

of Held through stacks of 2μm optical sections from 14μm thick coronal section of MNTB. An average of 1539 VGluT1-IR calyces of Held or principal cells were analyzed for CR expression per age group for CBA/J animals (range: 1375 – 1752) and 1434 per age group for *dn/dn* animal (range 963 – 1870). No statistically significant differences in the number of VGluT1-IR calyces of Held or principal cells per section were found between CBA/J and *dn/dn* mice (CBA/J: 112.0 ± 15.5, *dn/dn*: 100.8 ± 10.0; mean ± SEM; p = 0.56 *t-test*).

Percentages of VGlut1-IR calyces of Held which were also CR-IR were obtained for the whole of the MNTB. While CR is expressed in only a minority of calyces throughout development, the percent of VGluT1-IR calyces of Held expressing CR increased significantly at all time points analyzed in CBA/J mice (P9: 4.5 ± 0.2%, P13: 10.9 ± 0.5%, P30: 16.9 ± 1.2%, P49: 27.5 ± 2.4%; mean ± SEM; $p<0.001$ One Way ANOVA) (Figure 32, 34, 35, 39). In contrast, in *dn/dn* mice, the percent of VGluT1-IR calyces of Held expressing calretinin increased significantly from P9 to P13 but not after P13 (P9: 3.9 ± 0.3%; P13: 11.7 ± 0.7%; P30 12.2 ± 1.2%; P49: 9.7 ± 1.3%; $p<0.001$ One Way ANOVA) (Figure 33, 36, 37, 39). *Post hoc* test indicate that %VG-IR calyces expressing CR at P9 is significantly different than all other ages analyzed ($p<0.05$ *post hoc* Tukey's test), while the percentage of VGlut1-IR calyces expressing CR was not significantly different between P13, P30, and P49 (p = 0.318 One Way ANOVA). When comparing deaf mice to wild-types, no significant differences in the percentage of VGluT1-IR calyces that express CR were detected at P9 (CBA/J: 4.5 ± 0.2%, *dn/dn*: 3.9 ± 0.3; mean ± SEM; p = 0.363 t-test) and P13 (P13 CBA/J:

10.9 ± 0.5%; P13 *dn/dn*: 11.7 ± 0.7; mean ± SEM; p = 0.1308 t-test). However, at P30 and P49 control animals displayed significantly more CR-IR calyces (P30 CBA/J: 16.9 ± 1.2%, P30 *dn/dn*: P30 12.2 ± 1.2; mean ± SEM; p<0.001 t-test; P49 CBA/J: 27.5 ± 2.4%, P49 *dn/dn*: 9.7 ± 1.3; mean ± SEM; p<0.0001 t-test), suggesting that after the onset of hearing, CR immunoreactivity is upregulated in the Calyx of Held during normal development of CBA/J mice but not *dn/dn* mice.

In the following section, the expression of CR was separately analyzed in calyces of Held located in each of the lateral, intermediate, and medial thirds of the nucleus. These data indicate that, while CR-IR calyces remain preferentially located in the lateral portion of the MNTB in both wild-type and deaf mice, the developmental increase of CR which occurs in CBA/J mice can be detected throughout the nucleus.

Tonotopic Expression of Calretinin in Calyces of Held During Postnatal Development in Normal Hearing (CBA/J) and Congenitally Deaf (*dn/dn*) Mice

To assess the developmental distribution of CR-IR calyces along the tonotopic axis, the same confocal images used in the previous section were analyzed. The MNTB in each image was subdivided into lateral, intermediate, and medial thirds. Counts of VGluT1-IR and CR-IR calyces of Held were made for each of the 3 subdivisions so that percentages of VGlut1-IR calyces that co-express CR could be obtained for each third of the nucleus. In the lateral third of the MNTB of CBA/J mice, the frequency of VGluT1-IR calyces of Held which

co-express CR increased significantly from P9 to P13 and from P13 to P49 (P9: 10.7 ± 0.5%, P13: 25.6 ± 0.7%, P49: 40.2 ± 3.2%; mean ± SEM; $p<0.001$ One Way ANOVA; $p<0.05$ *post hoc* Tukey's test) (Figure 32, 34, 35, 40A). In contrast, in the lateral third of the MNTB in *dn/dn* mice the frequency of calyces expressing CR increased significantly from P9 to P13, but not after P13 (P9: 8.6 ± 0.9%, P13: 25.6 ± 0.9%; mean ± SEM; $p<0.001$ One Way ANOVA; $p<0.05$ *post hoc* Tukey's test) (Figure 33, 36, 37, 40B).

Additionally, in CBA/J mice, the frequency of VGluT1-IR calyces of Held which co-express CR increased significantly from P9 to P30 and from P30 to P49 in the intermediate (P9: 1.1 ± 0.4%, P30: 8.3 ± 0.9%, P49: 20.8 ± 2.6%, mean ± SEM; $p<0.001$ One Way ANOVA; $p<0.05$ *post hoc* Tukey's test) and medial (P9: 0.5 ± 0.3%, P30: 7.2 ± 1.0%, P49: 19.8 ± 2.5%, mean ± SEM; $p<0.001$ One Way ANOVA; $p<0.05$ *post hoc* Tukey's test) thirds of the MNTB (Figure 32, 34, 35, 40A). However, in *dn/dn* mice, the frequency of CR-IR calyces among VGluT1-IR calyces did not increase after P9 in intermediate ($p = 0.176$ One Way ANOVA) and medial ($p = 0.178$ One Way ANOVA) thirds of the MNTB (Figure 33, 36, 37, 40B). Figure 38 illustrates these differences in CR staining within the medial portion of the MNTB between P49 CBA/J and *dn/dn* mice. In the image, several CR-IR calyces of Held are visible in the medial portion of the MNTB in CBA/J mice, but none are visible in the medial portion of the MNTB in *dn/dn* mice.

These data indicate that, after P13, the significant differences seen in developmental calyceal CR expression between CBA/J and *dn/dn* mice (see

previous section) correspond to increases in calyceal CR expression detected in each region of the MNTB in CBA/J mice. Consequently, at P49, a significantly greater proportion of calyces of Held expressing CR were detected in CBA/J mice compared to *dn/dn* mice in each third of the MNTB (lateral: $p<0.001$ t test; intermediate and medial: $p<0.0001$ t test), (Figure 43A).

Additionally, percentages of VGluT1-IR calyces of Held co-expressing CR in each third of the MNTB were compared against the other two MNTB subdivisions in age matched mice. At all ages analyzed, a significant difference was detected in calyceal CR expression in the lateral third of the MNTB compared to the intermediate ($p<0.0001$ One Way ANOVA, $p<0.001$ *post hoc* Tukey's test) and medial ($p<0.0001$ One Way ANOVA, $p<0.001$ *post hoc* Tukey's test) thirds in both CBA/J and *dn/dn* mice (Figure 40A, B). No significant differences were seen between medial and intermediate thirds ($p>0.05$ *post hoc* Tukey's test) in either strain (Figure 40A, B). These data indicate that in both strains at all age points analyzed, and despite the increases in calyceal CR expression seen in the intermediate and medial regions of the MNTB in wild-type mice, calyceal CR expression is preferentially located in the lateral third of the MNTB.

To bolster this result, the percentage of all CR-IR calyces of Held found in each third of the MNTB was obtained from counts total CR-IR calyces within the MNTB as a whole. In CBA/J mice, a significant majority of all CR-IR calyces found in the MNTB are located in the lateral third of the MNTB at all ages analyzed (P9: 88.8 ± 3.2%, P13: 87.5 ± 3.0%, P30: 71.6 ± 2.5%, P49: 58.9 ±

2.4%; mean ± SEM; $p<0.0001$ One Way ANOVA) (Figure 40C). A significant decrease was detected in the proportion of CR-IR calyces located in the lateral third of the nucleus from P13 to P49 ($p<0.001$ One Way ANOVA; $p<0.001$ *post hoc* Tukey's test), corresponding to a significant increase detected from P13 to P49 in intermediate ($p<0.001$ One Way ANOVA; $p<0.001$ *post hoc* Tukey's test) and medial ($p<0.001$ One Way ANOVA; $p<0.001$ *post hoc* Tukey's test) thirds (Figure 40D). Similarly, in deaf mice, a significant majority of all CR-IR calyces found in the MNTB are located in the lateral third of the MNTB at all ages analyzed (P9: 86.2 ± 3.6, P13: 86.6 ± 2.8%, P30 85.2 ± 3.0%, P49: 90.2 4.2%) (Figure 40D). No significant differences were detected in the proportion of CR-IR calyces found in the lateral third at any age analyzed ($p = 0.825$ One Way ANOVA). Thus, throughout development in both CBA/J and *dn/dn* mice, CR-IR calyces of Held are preferentially located in the lateral third of the MNTB, corresponding to neurons of low characteristic firing frequency within the tonotopic gradient of the MNTB.

Developmental Expression of Calretinin in postsynaptic principal cells in the MNTB of normal hearing CBA/J mice and congenitally deaf (*dn/dn*) mice

The same confocal images used to analyze calyces of Held for CR expression were analyzed for somatic expression of CR in principal cells of the MNTB. Analysis was performed by counting CR+ principal cells through stacks of 2μm optical sections from 14μm thick coronal section of MNTB. When analyzing sections dual stained with anti-VGluT1 and anti-CR, somatic CR-IR

qualified as a CR+ principal cell only if it met the criteria of displaying an oval shaped somata that was 10-20μm in diameter surrounded by a VGluT1-IR calyx of Held.

Percentages of principal cells which were CR-IR were obtained for the whole of the MNTB. CR is expressed in only a minority of principal cells throughout development, and the percent of principal cells expressing CR significantly decreases from P13 to P49 (P9: 8.2 ± 0.6% P13: 10.5 ± 0.5%, P30: 10.9 ± 0.6%, P49: 6.2 ± 0.8%; mean ± SEM; $p<0.001$ Two Way ANOVA) (Figure 32, 34, 35, 41). *Post hoc* test indicated no significant change in somatic CR expression between P9 and P13 ($p>0.05$ *post hoc* Bonferroni's test). In contrast, in *dn/dn* mice, the percent of principal cell somata expressing calretinin significantly increased after P13 (P9: 9.2 ± 0.7%; P13: 10.7 ± 0.8%; P30 13.2 ± 0.7%; P49: 14.6 ± 1.7%; $p<0.001$ Two Way ANOVA) (Figure 33, 36, 37, 41). *Post hoc* test indicated no significant change in somatic CR expression between P9 and P13 ($p>0.05$ *post hoc* Bonferroni's test). When comparing deaf mice to wild-types, no significant differences in the percentage of principal cells that express CR were detected at P9, P13, or P30 ($p>0.05$ *post hoc* Bonferroni's test). However, significant differences were detected at P49 ($p>0.05$ *post hoc* Bonferroni's test). At these age points, deaf animals displayed significantly more CR-IR principal cells. These data suggest that after the onset of hearing, CR immunoreactivity in principal cell somata is downregulated during normal development of wild-type mice and upregulated in the absence of auditory nerve activity of congenitally deaf mice.

In the following section, the expression of CR was separately analyzed in principal cells located in each of the lateral, intermediate, and medial thirds of the nucleus. These data indicate that, while CR-IR principal remain preferentially located in the medial portion of the MNTB in both wild-type and deaf mice, the developmental increase of CR which occurs in *dn/dn* mice can be detected in the intermediate region as well.

Tonotopic Expression of Calretinin in principal cell somata During Postnatal Development in Normal Hearing (CBA/J) and Congenitally Deaf (*dn/dn*) Mice

To assess the developmental distribution of CR-IR calyces along the tonotopic axis, the same confocal images used in the previous section were analyzed. The MNTB in each image was subdivided into lateral, intermediate, and medial thirds. Counts of Nissl stained and CR-IR principal cells were made for each of the 3 subdivisions so that percentages of principal that express CR could be obtained for each third of the nucleus. In the medial third of the MNTB of CBA/J mice, the frequency of CR-IR principal cells decreased significantly from P13 to P49 (P9: 29.9 ± 1.7%, P13 34.2 ± 1.3 %, P30 33.4 ± 2.4%, P49 22.7 ± 3.0%; mean ± SEM, $p = 0.004$ One Way ANOVA) (Figure 32, 34, 35, 42A). *Post hoc* test indicates the percent of CR-IR principal cells in the medial third of P49 mice is significantly less than at P30 ($p<0.001$ *post hoc* Tukey's test) and P13 ($p<0.05$ *post hoc* Tukey's test). The percentage of CR-IR principal cells in the medial region of the MNTB expressing CR increases from P9 to P13, but not to a

significant degree ($p>0.05$ *post hoc* Tukey's test). In contrast, in the medial third of the MNTB in *dn/dn* mice, the frequency of principal cells which express CR increases significantly form P9 to P49 (P9: 28.8 ± 1.2%, P13: 36.4 ± 2.0%, P30: 39.5 ± 2.9%; mean ± SEM, $p = 0.015$ One Way ANOVA) (Figure 33, 36, 37, 42B). *Post hoc* tests indicate that the percent of CR-IR principal cells in the medial third of the MNTB of P9 mice is significantly less than at P30 ($p<0.05$ *post hoc* Tukey's test) and P40 ($p<0.05$ *post hoc* Tukey's test). Similar to CBA/J mice, the frequency of CR-IR principal cells in the medial region of the MNTB expressing CR increases from P9 to P13, but not to a significant degree ($p>0.05$ *post hoc* Tukey's test). These differences in somatic CR staining within the medial portion of the MNTB between P49 CBA/J and *dn/dn* mice are illustrated in Figure 38, as more CR-IR principal cells are visible in the medial portion of the MNTB of *dn/dn* mice than CBA/J mice. It should be noted that several cell processes can be seen emerging from CR-IR principal cells, and that these cell processes may receive contacts from VGluT1-IR synaptic terminals.

Additionally, in CBA/J mice, the frequency of principal cells expressing CR did not significantly change during development after P9 in intermediate ($p = 0.406$ One Way ANOVA) and lateral ($p = 0.804$ One Way ANOVA) thirds of the MNTB (Figure 42A). However, in *dn/dn* mice, the frequency of CR-IR principal cells also increased in the intermediate third of the MNTB (P9: 0.7 ± 0.3%, P13: 1.6 ± 0.5%, P30: 3.9 ± 0.8%, P49: 5.7 ± 0.9%; mean ± SEM; $p<0.0001$) (Figure 42B). *Post hoc* test indicates that the percent of CR-IR principal cells in the intermediate third of the MNTB is significantly less in P9 mice than in P30

($p<0.01$ *post hoc* Tukey's test) and P49 mice ($p<0.001$ *post hoc* Tukey's test). However, in *dn/dn* mice, no developmental increase was detected in the lateral of the MNTB at age points analyzed ($p = 0.448$ One Way ANOVA).

These data indicate that, during development, the significant differences detected between CBA/J and *dn/dn* mice in somatic CR expression (see previous section) correspond to increases in somatic CR expression detected in medial and intermediate thirds of the MNTB in *dn/dn* mice as well as a decrease in somatic CR expression seen in the medial third of the MNTB in CBA/J mice. Consequently, at P49, a significantly greater proportion of CR-IR principal cells were detected in the medial ($p<0.0001$ t test) and intermediate ($p<0.0001$ t test) thirds of the MNTB in *dn/dn* mice than CBA/J mice, comparatively (Figure 43B).

Additionally, percentages of Nissl stained principal cells expressing CR in each third of the MNTB were compared against the other two MNTB subdivisions in age matched mice. At all ages analyzed, a significantly greater proportion of CR expression among principal cells was detected in the medial third of the MNTB compared to intermediate ($p<0.0001$ One Way ANOVA, $p<0.001$ *post hoc* Tukey's test) and lateral ($p<0.0001$ One Way ANOVA, $p<0.001$ *post hoc* Tukey's test) thirds in CBA/J and *dn/dn* mice (Figure 42A, B). In *dn/dn* mice, a significantly greater proportion of CR expression was detected in intermediate compared to lateral thirds of the MNTB at P30 ($p<0.05$ *post hoc* Tukey's test) and P49 ($p<0.05$ *post hoc* Tukey's test) as well. No significant differences were seen between intermediate and lateral regions ($p>0.05$ *post hoc* Tukey's test) in CBA/J mice. These data indicate that in both age strains at all

age points analyzed, somatic calyceal expression is preferentially located in the medial third of the MNTB, although in *dn/dn* mice, there is an increase in CR expression in principal cells located in the intermediate third.

To bolster this result, the percentage of CR-IR principal cells found in each region of the MNTB was obtained from counts of total CR-IR principal cells within the MNTB as a whole. In CBA/J mice, a significant majority of all CR-IR principal cells are located in the medial third of the MNTB at all ages analyzed (P9: 97.9 ± 1.7%, P13: 94.4 ± 1.4%, P30: 94.8 ± 2.2, P49: 97.9 ± 1.3; mean ± SEM; $p<0.0001$ One Way ANOVA) (Figure 42C). No significant differences were detected at any age point analyzed in the percentage of CR-IR principal cells found within the medial third of the MNTB ($p = 0.690$ One Way ANOVA). Similarly, in *dn/dn* mice, a significant majority of all CR-IR principal cells located in the medial third of the MNTB at all ages analyzed (P9: 98.0 ± 0.9%, P13: 94.9 ± 5.3%, P30: 90.7 ± 2.0, P49: 85.0 ± 2.2; mean ± SEM; $p<0.0001$ One Way ANOVA (Figure 42D). In contrast to CBA/J mice, a significant decrease in the proportion of CR-IR principal cell located in the medial third of the MNTB was detected in *dn/dn* mice from P9 to P49 ($p<0.001$ One Way ANOVA, $p<0.05$ *post hoc* Tukey's test), corresponding to a significant increase detected from P9 to P49 in the intermediate region ($p<0.001$ One Way ANOVA, $p<0.01$ *post hoc* Tukey's test). No significant differences were detected in the medial third of *dn/dn* mice at any age analyzed ($p = 0.69$ One Way ANOVA). Thus, throughout development in both CBA/J and *dn/dn* mice, CR-IR principal cells are preferentially located in the medial third of the MNTB (although in *dn/dn* mice

there is an increase in the frequency of CR-IR cells located in the intermediate region), corresponding to neurons of high characteristic firing frequency within the tonotopic gradient of the MNTB.

Expression of Calretinin (CR) in the MNTB of adult Wistar Rats

It should be noted that the developmental expression of CR reported in this study, stands in contrast to the expression of CR observed in experiments conducted on adult wild-type Wistar rats. Images generated during this study indicate that adult Wistar rats express CR in a clear majority of both calyces of Held and MNTB principal cells (Figure 44, 45). (Although, the intensity of staining in calyces of Held was often much greater in calyces of Held.) Similar to CBA/J and *dn/dn* mice, CR-IR cell process, which appear to receive contacts from VGluT1-IR presynaptic terminals, are visible extending from rat MNTB principal cells (Figure 44, 45).

X. DISCUSSION

CALRETININ IN THE MNTB

Developmental regulation of Calretinin (CR) expression in the MNTB of normal hearing (CBA/J) mice

We investigated the cellular localization of CR in the MNTB during postnatal development of CBA/J mice. In normal hearing mice, the pattern of CR expression appears to be developmentally regulated. At postnatal day 9, VGluT1 reliably labeled calyces of Held in CBA/J mice. At this age, calyces appear less fenestrated as the VGluT1 immunoreactivity takes the shape of a smooth circle. At this age, CR staining is diffuse, and even under optimal imaging conditions, only faint calyceal immunoreactivity is detected in the lateral portion of the nucleus. At P9, only 4.5 ± 0.2% of all calyces within the MNTB contain CR, and 88.8 ± 3.2% of these are actually located in the lateral third of the nucleus. This means that even in the lateral part, only 10.7 ± 0.5% of all VG-IR calyces express CR. Similarly, CBA/J mice at 9 days postnatal express CR in principle cell somata in the medial third of the MNTB. On average, at P9, only 8.23 ± 0.6% of principle cells in the MNTB express CR, and 97.9 ± 1.7% of these were localized in the medial third of the nucleus. This means that even in the medial third of the MNTB, only 29.9 ± 1.7% of principle cells express CR.

At postnatal day 13, CBA/J mice express VGluT1 in the calyces of Held, which begin to acquire a more fenestrated appearance. At this age point we see

an increase in calyceal CR immunofluorescence which is preferentially located in the lateral portion of the MNTB. At this age, 10.9% ± 0.6% of calyces within the MNTB express CR. Of these, 87.5 ± 3.0% are located in the lateral third of the nucleus, meaning that even in this part of the MNTB still only 25.6 ± 0.7% of all VG-IR calyces express CR. Additionally, at P13, a distinct subset MNTB principal cells still predominantly located in the medial third of the nucleus express CR. At this age point, 11.3 ± 0.7% of all principal cells express CR, 94.8 ± 2.2% of which are located in the medial third of the nucleus. This means only 35.6 ± 1.3% of principle cells express CR within this portion of the nucleus.

By postnatal day 30, calyceal CR immunofluorescence in CBA/J mice increased to include a larger proportion of these presynaptic terminals but still represent only a fraction of calyces stained by VGluT1 antibodies. Additionally the intensity of calyceal staining has increased and the diffuse immunofluorescence observed in the neuropil has decreased enough to make calyceal staining readily apparent. At P30, CR is still predominantly located in the lateral portion of the MNTB, however occasional CR-IR calyces were seen in the intermediate and medial portions of the nucleus as well. Thus, there appears to be a progressive expansion of CR-IR calyces into the intermediate and medial thirds. Interestingly, while calyceal CR expression increased in P30 mice compared to earlier time points, CR expression in the principle cell somata remained relatively constant. Again, at this age point CR-IR principle cells were preferentially located in the medial third of the MNTB.

With further maturation, calyces of Held appear to have achieved the adult fenestration pattern. At postnatal day 49 in CBA/J mice, the CR expression in calyces continued to increase, and, while being predominantly located in the lateral third of the nucleus, were often found in the intermediate and medial third as well. On average, at P49, 27.5 ± 2.4% of calyces in the MNTB express CR. Of these, only 58.9 ± 2.4% are now located in the lateral third of the nucleus. However, even though a smaller percentage of CR-IR calyces found in the MNTB are now located in the lateral third of the nucleus, 40.2 ± 3.2% of all VG-IR calyces in the lateral third of the MNTB express CR.

While CR expression continued to increase in calyces of Held during maturation, CR expression in principle cell somata appeared to decrease in P49 CBA/J mice when compared to earlier time points. Only 6.2 ± 0.8% of principle cells at this age point express CR. Again, these CR-IR cells were preferentially located in the medial third of the nucleus. Of all CR-IR principle cells, an average of 97.9 ± 0.3% are found in the medial third of the nucleus, comprising 22.7 ± 3% of principal cells in that portion of the nucleus.

Several studies on endogenous calcium buffering capacity in the rat support the conclusion that, while CR increases during postnatal maturation, it is heterogeneously expressed in only a minority of calyces of Held. Before the onset of hearing, that less than 5% of calyces of Held in CBA/J mice express CR corresponds with the low endogenous calcium buffering capacity ($\kappa_s \sim 30$; Helmchen, et al., 1997) reported in rat calyces of Held at P8-P10. This value is among the lowest calcium buffering capacity seen in neuronal cells (Lips and

Keller, 1998). As the rats mature, Chuhma et al. (2002) report that the endogenous calcium buffering capacity of rat calyces of Held is higher at P11 than at P6, which could result from an increase in presynaptic calcium buffering capacity. Interestingly, Felmy and Schneggenburger (2004) reported an increase in CR expression in rat calyces of Held over a similar time period, indicating that the increase in CR expression in rat calyces of Held contributes to an increase in presynaptic calcium buffering capacity. Furthermore, the decay kinetics of $[Ca^{2+}]_i$ in calyces of Held was found to be variable between calyces, indicating a possible heterogeneity in the Ca^{2+} extrusion rate or in the expression of endogenous calcium buffers, such as CR (Felmy, et al., 2003).

The localization and developmental patterns of expression of CR in the MNTB of C57/BL6 mice was studied previously by Felmy and Schneggenburger (2004). They reported that CR was present in many, but not all calyces of Held, and that the number of CR(+) calyces increased from P6 to P31. In addition, they reported that calyces in the lateral region of the MNTB preferentially express CR. The results of the present experiment not only verify these findings, but also extend them by systematically quantifying CR expression along the tonotopic gradient.

The results of these experiments show that, with maturation, CR is expressed in progressively more calyces of Held and progressively fewer principle cells such that by P49 CR is expressed in only a few medially located principal cells and very many calyces of Held preferentially, but not exclusively, found in the lateral portion. Thus a stepwise topographic gradient of CR

expression was observed along the medial-lateral axis of the MNTB throughout development. Along this same gradient, neurons of the MNTB are topographically organized according to a tonotopic map present throughout the auditory system. Cells responding best to high frequency stimulation are located medially within the nucleus, while cells responding best to low frequency stimulation are located laterally. A variety of response mechanisms underlie MNTB synaptic response properties in accordance with the tonotopic map. One such mechanism is likely to be intracellular Ca^{2+} buffering. CR, which exhibits rapid binding kinetics, can reduce intracellular Ca^{2+} levels on the order of milliseconds and, when present at high concentrations, can buffer incoming Ca^{2+} before the ions reach their intracellular target. Such mechanisms are important both pre- and post-synaptically to modulate neurotransmitter release and high frequency firing. It may be, then, that the specific pattern of CR expression in the MNTB is important maintaining high fidelity synaptic communication across the range of characteristic firing frequencies in the MNTB.

It should be noted that the divergent CR expression in *dn/dn* mice discussed in the next section occurs despite apparently "normal" appearance of both calyces of Held and principal cells. Throughout development in *dn/dn* mice, VGLuT-1 reliably labels calyces of Held, which appear less fenestrated early in postnatal development, but attain typical adult-like appearance by P49 (Figure 33, 36, 37). Furthermore, there does not appear to be a significant change in total number of VGluT1-IR calyces of Held in *dn/dn* mice compared to CBA/J, nor is there a significant change in the number of Nissl stained principal cells.

Developmental regulation of Calretinin (CR) expression in the MNTB of congenitally deaf (*dn/dn*) mice vs. normal hearing (CBA/J) mice

Throughout development, VGluT1 reliably labeled calyces of Held within the MNTB of *dn/dn* mice. Early in postnatal development, the calyces appear less fenestrated, attaining their adult like appearance in P49 mice. Furthermore, there does not appear to be a significant change in total number of VG-IR calyces of Held in *dn/dn* mice compared to CBA/J, nor is there a significant change in the number of principles cells stained for Nissl.

The pattern of CR expression in the MNTB of *dn/dn* mice appears identical to age matched CBA/J mice at the first two developmental stages investigated. It is not until P30 that we begin to see a divergence CR expression between these two strains.

By postnatal day 30 in *dn/dn* mice, calyceal CR immunofluorescence has increased to include a larger proportion of presynaptic terminals but to a lesser degree than P30 CBA/J. In P30 CBA/J mice, while CR-IR calyces are still predominantly located in the lateral portion of the MNTB, there was also an increase in the expression of CR in calyces located in the intermediate and medial portions of the MNTB. The increase in calyceal CR expression in *dn/dn* mice is similar to that of CBA/J mice within the lateral third of the MNTB. However, *dn/dn* mice show no increase in calyceal CR immunofluorescence outside the lateral third of the nucleus. This difference accounts for the smaller increase in total calyceal CR expression seen in P30 *dn/dn* mice when compared to CBA/J

mice and represents the first developmental time point at which a divergence in the pattern of CR expression in the MNTB was observed between these two strains.

Additionally, in the P30 *dn/dn* mouse, the percentage of principle cells expressing CR increased slightly from P13 values. This increase in somatic CR expression represents a second divergence in the pattern of CR expression in the MNTB between these two strains of mice. In CBA/J mice, somatic CR expression remained relatively constant as the mice matured from P13 to P30 (in fact, somatic CR expression decreased slightly in these animals). Thus, the increase in total somatic CR staining seen in P30 *dn/dn* mice compared to CBA/J mice can be attributed to an increase in the proportion of principle cells expressing CR in the medial third of the nucleus in *dn/dn* mice.

The divergence in the pattern of MNTB CR expression between CBA/J and dn/dn mice which became apparent at postnatal day 30 progresses by postnatal day 49. With further maturation, the percentage of CR-IR calyces in CBA/J mice at postnatal day 49 continued to increase, and, while being predominantly located in the lateral third of the nucleus, were often found in the intermediate and medial thirds as well. In contrast, the percentage of CR-IR calyces in the lateral portion of the MNTB of P49 *dn/dn* mice declined from levels seen in P30 mice. No change was detected in the percentage of CR-IR calyces in the intermediate and medial regions of P49 *dn/dn* mice compare to those at P30. Thus, compared to P49 CBA/J mice, a smaller percentage of calyces in the whole of the MNTB express CR in the P49 *dn/dn* mice. This

decrease in CR immunoreactivity appears to be the result of the progressive decline of CR expression in lateral calyces as well as no increase in CR expression in non-lateral calyces.

There is also a divergence of CR expression in MNTB principal cells expression between *dn/dn* and CBA/J mice. In *dn/dn* animals, total somatic CR expression increased from P30 to P49, corresponding to an increased proportion of principle cells found in the medial and intermediate thirds of the nucleus. This is in contrast to CBA/J mice which show a decrease in somatic CR expression from P30 to P49. Thus, the larger proportion of CR-IR principle cells seen in the whole of the MNTB in P49 *dn/dn* mice compared to P49 CBA/J is a due to a decrease in somatic CR expression in the medial portion of the MNTB in CBA/J mice and in increase in somatic CR expression in the medial and intermediate thirds of the MNTB that occurs in *dn/dn* mice.

Like CBA/J mice, a stepwise topographic gradient of CR expression was observed in the MNTB of *dn/dn* mice throughout development. CR-IR calyces were preferentially located in the lateral portion of the nucleus and CR-IR principle cells were preferentially located in the medial part of the nucleus. After P13, the pattern of CR expression in dn/dn mice was only minimally altered, exhibiting a slight decrease in calyceal CR expression and a slight increase in somatic CR expression. Additionally, those calyces that were immunopositive for CR were rarely located outside the lateral third of the nucleus. CR-IR somata were typically found in the medial most region of the MNTB but, by P49, were occasionally found in the middle third of the nucleus.

It should be noted that the general topographic pattern of CR expression is quite similar in CBA/J and *dn/dn* mice. Both preferentially express CR in calyces located laterally within the nucleus and in principal cells located medially within the nucleus. (This developmental distribution corresponds to the topographic organized tonotopic map present in the MNTB. Cells responding best to high frequency stimulation are located medially within the nucleus, while cells responding best to low frequency stimulation are located laterally.) However, by P49 developmental divergences between these two strains create subtle differences between their patterns of CR expression. In the end, P49 CBA/J mice express CR primarily in calyces of Held which may be found throughout the nucleus, but are more likely to be found in the lateral portion. They express very little somatic CR, but those principal cells that do are preferentially located in the medial part of the nucleus. P49 *dn/dn* mice express CR mainly in principal cell somata, which may be located anywhere in the nucleus, but the vast majority of which are located in the medial portion. Occasionally, one may be found in the intermediate portion. These mice express calyceal CR as well, but far less than age matched CBA/J mice and rarely located outside the lateral third of the nucleus.

Figure 38 illustrates these differences in CR expression. High magnification images of the medial portion of the MNTB in CBA/J and *dn/dn* mice are compared. More CR-IR principal cells are visible in the image of the *dn/dn* MNTB. Additionally many cell processes are visible with anti-CR stain in the *dn/dn* image. Presumably, the lack of cell processes visible in the CBA/J

image is due to the lowered expression of somatic CR and its consequent inability to enter cell processes with a high enough concentration to produce a visible florescent signal. In support of this presumption, Figure 30 shows a brightly stained CR-IR principal cell from which a dendrite visible with anti-CR antibodies emerges. Furthermore, several CR-IR calyces of Held are visible in the medial portion of the MNTB in CBA/J mice, while none are visible in the *dn/dn* MNTB. It is interesting that throughout these experiments, in neither strain was CR observed both a postsynaptic principal cells and the presynaptic calyx of Held that contacted it. However, this was the norm in adult Wistar rats (Figure 45).

Because nearly 100% of MNTB principal cells coexpress CB and PV, those principal cells which are CR-IR represent cells which coexpress all three calcium buffering proteins. Additionally, because nearly 100% of calyces of Held express PV, there is a subpopulation of calyces which co-express PV and CR. These findings suggest the possibility for differential roles for each protein in pre- and postsynaptic calcium signaling. It is easy to speculate, AS STATED IN AIM 2, that such differential roles could arise from the differences in Ca^{2+} binding kinetics between slow (PV) and fast (CB, CR) calcium buffers. However, subtler are the different roles, if any, which two CaBPs with rapid Ca^{2+} binding kinetics like CB and CR might play in postsynaptic Ca^{2+} signaling.

Implications of calyceal Calretinin (CR) on synaptic transmission in the MNTB

Previous studies have shown that certain normal developmental changes in the calyx of Held synapse are abnormal or absent in animals with impaired auditory nerve activity (see Chapter III). It may be, therefore, that the divergence in calyceal CR expression between CBA/J and *dn/dn* mice observed in the present experiments is a result of the achievement of functional maturation during normal development of CBA/J mice but not in *dn/dn* mice.

Before the onset of hearing, as auditory circuitry is being established and labeled lines of different characteristic frequency are ascending in parallel from the cochlea to higher order brainstem nuclei, pre- and post-synaptic elements within the MNTB begin to express CR along a stepwise gradient which occurs in accordance with the tonotopic gradient of the MNTB. That calyceal and somatic CR is preferentially located in the lateral and medial portions of the nucleus, respectively, may subserve a specific role for CR in the temporally precise synaptic transmission necessary for the localization of low vs. high frequency sounds. That rats have a range of hearing which is lower than mice and images obtained in this study of the rat MNTB indicate CR is expressed in a majority of calyces of Held, a finding corroborated by Felmy and Schneggenburger (2004), further implicate distinct roles of pre- and postsynaptic CR in low vs. high frequency auditory processing. While such roles have yet to be determined, it would appear that, at least before the onset of hearing, critical factors other than auditory nerve activity predispose certain pre- and post-synaptic elements within the murine MNTB to express CR in accordance with the MNTB tonotopic gradient.

Stated in chapter VI, previous studies indicate that Ca^{2+} buffer saturation could cause a supralinearity in the summation of Ca^{2+} signals necessary to account for the observed transmitter release facilitation at the calyx of Held (Felmy et al., 2003). As CR is a high affinity Ca^{2+} buffer with rapid binding kinetics, it satisfies the requirements necessary for facilitation of transmitter release via the "Ca^{2+} buffer saturation" mechanism (Neher, 1998; Matveev et al., 2004; Muller et al., 2007). Fast binding kinetics allow CR, when present at high concentration, to intercept and bind Ca^{2+} ions in the vicinity of readily releasable vesicles before the ions reach intracellular Ca^{2+} sensors for vesicle release, thereby reducing initial release probability and preventing synaptic depression. Further, the partial saturation of CR, which occurs during a high frequency train of action potentials, would progressively reduce its buffering power, causing an increase in the effectiveness of residual Ca^{2+} ions in inducing synaptic facilitation. CR, thus, may serve a postulated role (Felmy et al., 2003) for a high affinity Ca^{2+} buffer present in calyces of Held capable of influencing transmitter release facilitation for temporally precise, high frequency synaptic transmission.

At around the onset of hearing, synaptic transmission at the calyx of Held undergoes characteristic developmental changes, among which are a reduction in transmitter release probability and an increase in the size of readily releasable vesicle pools (Taschenberger and von Gersdoff, 2000; Iwasaki and Takahashi, 2001; Taschenberger et al, 2002). Together, these changes "equalize" the first EPSC with subsequent EPSCs and reduce the synaptic depression that may occur in response to a train of presynaptic action potentials (Felmy and

Schneggenburger, 2004). Because of its possible effect on transmitter release facilitation and initial release probability, the developmental increase in calyceal CR may further counter the effects of synaptic depression and, thus, supplement these other presynaptic developmental changes. It is tempting, therefore, to speculate that the increase in CBA/J calyceal CR expression represents an additional stage in the acquisition of functional maturity which maintains high fidelity synaptic transmission and precise timing at the calyx of Held synapse, and that the developmental divergence in the pattern of CR expression which occurs between CBA/J and *dn/dn* mice, is evidence that acoustically evoked auditory nerve activity is necessary for synaptic maturation to be occur. Nevertheless, such a role for a CR as a saturable Ca^{2+} buffer in calyces of Held still needs to be established (Felmy and Schneggenburger, 2004).

Figure 30. Calretinin expression in the MNTB is heterogeneous in normal hearing (CBA/J). A-C: 60x double immunofluorescence images with stained for Nissl (FITC) and with primary antibodies against CR (CY-3) are shown in a 14μm thick section of brainstem from the lateral portion of the MNTB in a P49 CBA/J mouse. Two brightly stained CR-IR calyces of Held are shown. Nissl stained principal cells which lack CR-IR calyces of Held are visible in the same field of view. In **B**, asterisks indicate several Nissl stained principal cells lacking CR-IR calyces of Held. **D-F:** 60x double immunofluorescence images with primary antibodies against VGluT1 (FITC) and CR (CY-3) are shown in a 14μm thick section of brainstem from the medial portion of the MNTB in a P49 CBA/J mouse. A brightly stained CR-IR principal cell surrounded by calyceal VGluT1-IR presynaptic contacts is shown. It appears that a single primary dendrite, emerging from the principal cell and visible with anti-CR stain, receives several VGluT1-IR presynaptic contacts of unknown origin (arrowheads, in **E**). Several less intensely stained CR-IR principal cells as well as CR (-) principal cells (asterisk, in **E**) are visible in the same field of view. In **F**, the arrow indicates possible VGluT1-IR presynaptic terminals that appear to extend form the calyx of Held and correlate to arrowheads in **E** . Scale bar = 10μm. D = dorsal. M = medial.

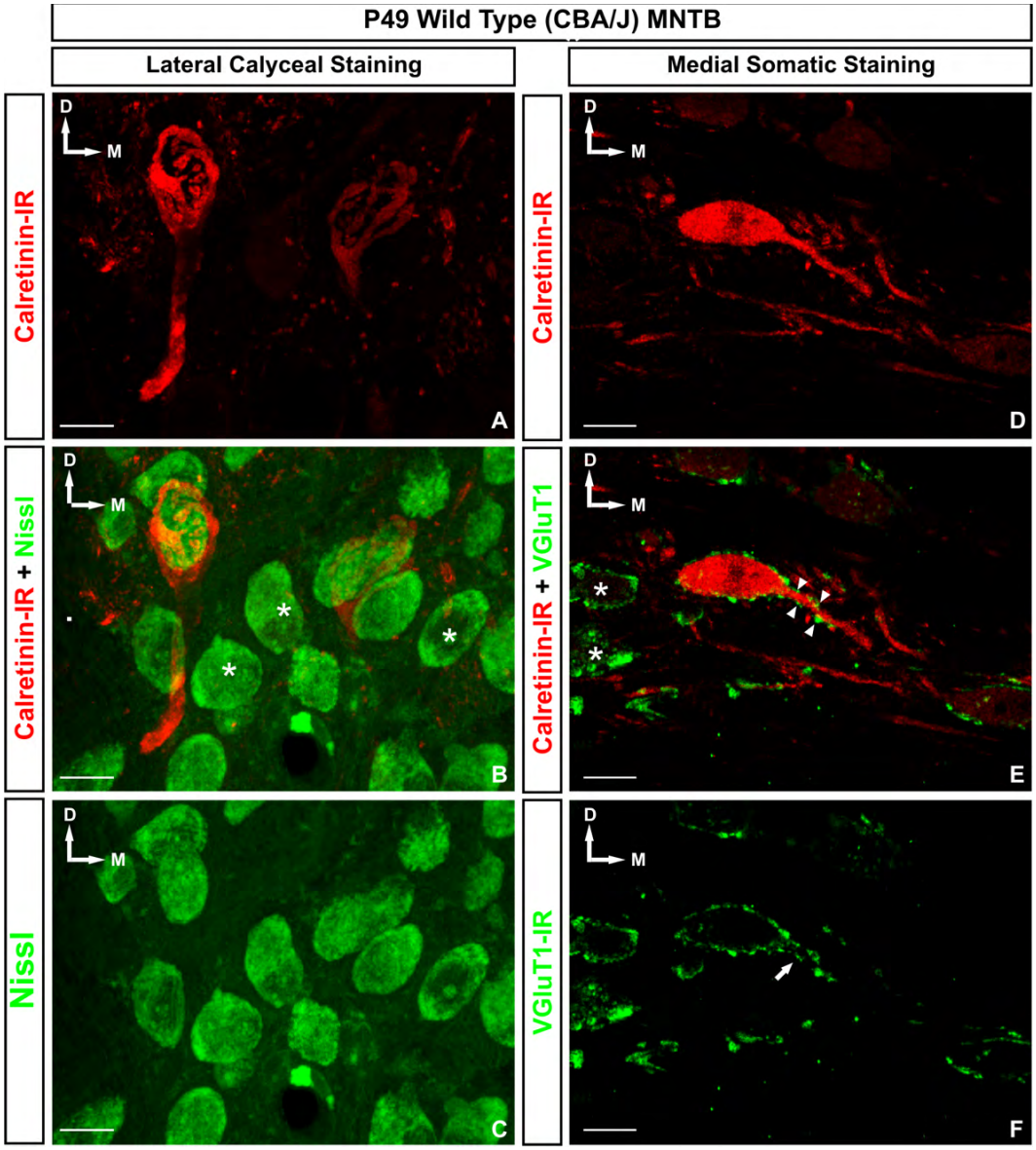
P49 Wild Type (CBA/J) MNTB
Lateral Calyceal Staining
Medial Somatic Staining
Calretinin-IR
Calretinin-IR + Nissl
Nissl
Calretinin-IR
Calretinin-IR + VGluT1
VGluT1-IR
D
M
A
B
C
D
E
F

Figure 31. Calretinin expression in the MNTB is heterogeneous in congenitally deaf mice (*dn/dn*). 60x double immunofluorescence images stained with primary antibodies against VGluT1 (FITC) and CR (CY-3) are shown in a 14μm thick section of brainstem from the lateral and medial portions of the MNTB in a P49 *dn/dn* mouse. **A-C:** A single, brightly stained CR-IR calyx of Held from the lateral third of the MNTB is visible among several calretinin negative calyces of Held. In **B**, asterisks indicate 2 VGluT1-IR calyces of Held which do not express CR. **D-F:** Several brightly stained CR-IR principal cells are shown surrounded by VGluT1-IR calyces of Held. Primary and secondary dendrites are visible extending from the principal cells when stained with anti-CR antibody. In **E**, these dendrites appear to receive VGluT1-IR presynaptic contacts of unknown origin (arrowhead). CR (-) calyces of Held are indicated visible and indicated by asterisks. In **F**, the arrow indicates possible VGluT1-IR presynaptic terminals that appear to extend form the calyx of Held and correlate to arrowheads in **E**. Scale bar = 10μm. D = dorsal. M = medial.

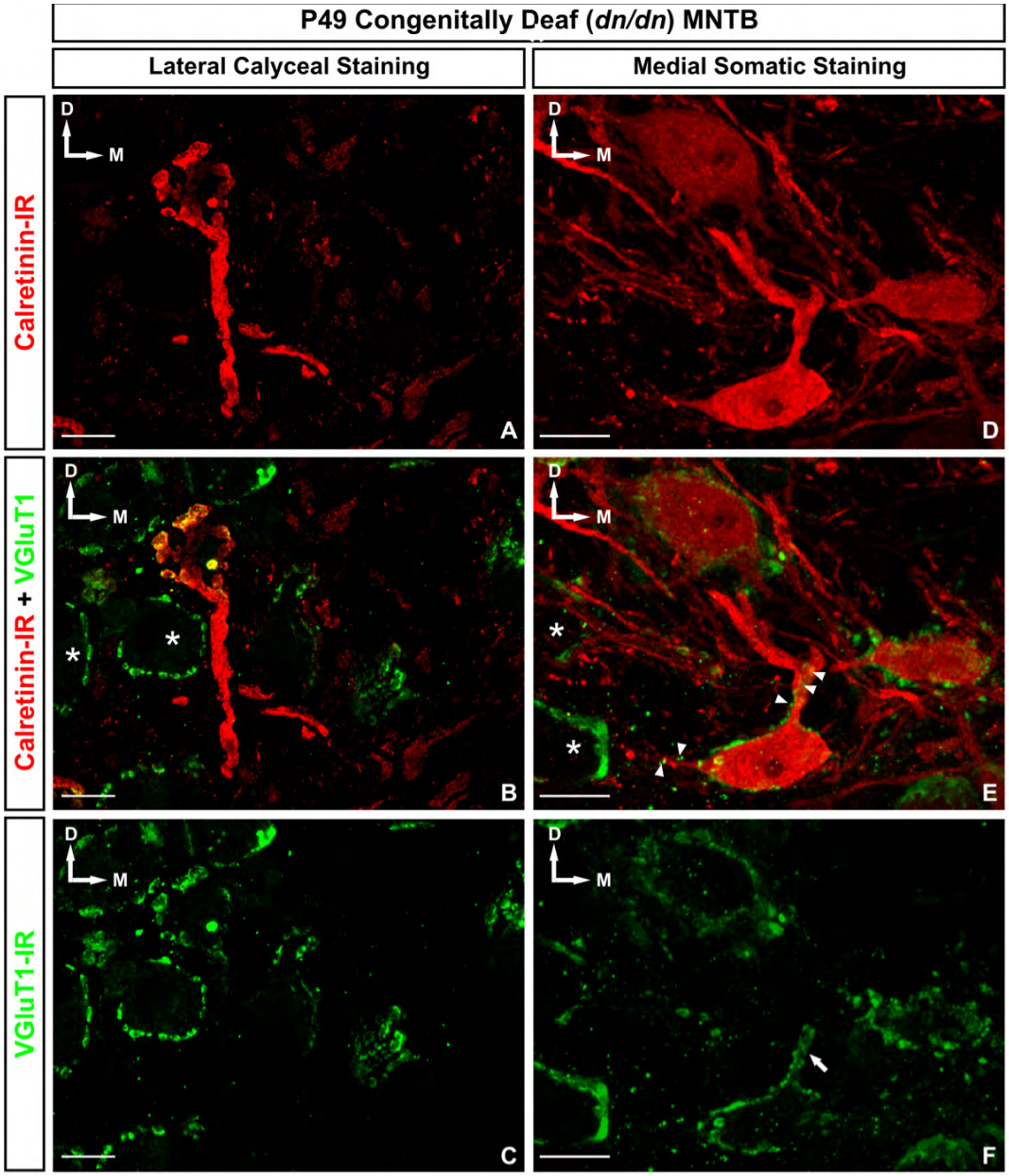
P49 Congenitally Deaf (dn/dn) MNTB
Lateral Calyceal Staining
Medial Somatic Staining
Calretinin-IR
Calretinin-IR + VGluT1
VGluT1-IR
D
M
A
B
C
D
E
F

Figure 32. Calretinin expression in the MNTB of normal hearing (CBA/J) mice at 9 days postnatal. Low magnification double immunofluorescence images with primary antibodies against VGluT1 (FITC) and CR (CY-3) are shown in a 14μm thick section of brainstem from the level of the MNTB in a P9 CBA/J mouse. At this age a subset of medially located principal cells express CR. Additionally, an occasional calyx of Held very faintly expressed CR in the lateral region of the nucleus (asterisk). High magnification of dashed boxes A,B,C, and D depicted to illustrate the stepwise differential expression of CR along the medial-lateral axis of the MNTB. Scale bar = 100μm. D = dorsal. M = medial. **High magnification** of dashed boxes A,B,C, and D depicted to illustrate the stepwise differential expression of CR along the medial-lateral axis of the MNTB. Scale bar = 20μm.

P9 Wild-Type (CBA/J) MNTB
VGluT1-IR
Calretinin-IR
VGluT1-IR + Calretinin-IR
VGluT1-IR + Calretinin-IR
D
M
A
B
C
D
*
*

Figure 33. Calretinin expression in the MNTB of congenitally deaf (*dn/dn*) mice at 9 days postnatal. Low magnification double immunofluorescence images with primary antibodies against VGluT1 (FITC) and CR (CY-3) are shown in a 14μm thick section of brainstem from the level of the MNTB in a P9 CBA/J mouse. At this age, no detectable differences exist between CBA/J and *dn/dn* strains. A subset of medially located principal cells expresses CR. Additionally, an occasional calyx of Held very faintly expressed CR in the lateral region of the nucleus. Scale bar = 100μm. D = dorsal. M = medial. **High magnification** of dashed boxes A,B,C, and D depicted to illustrate the stepwise differential expression of CR along the medial-lateral axis of the MNTB. Scale bar = 20μm.

P9 Congenitally Deaf (dn/dn) MNTB
VGluT1-IR
Calretinin-IR
VGluT1-IR + Calretinin-IR
VGluT1-IR + Calretinin-IR
D
M
A
B
C
D
*
*

Figure 34. **Calretinin expression in the MNTB of normal hearing (CBA/J) mice at 49 days postnatal. Low magnification** double immunofluorescence images with primary antibodies against VGluT1 (FITC) and CR (CY-3) are shown in a 14μm thick section of brainstem from the level of the MNTB in a P49 CBA/J mouse. CR expression is heterogeneous. CR immunofluorescence is colocalized with VGluT1 immunofluorescence in many calyces of Held located throughout the nucleus, but primarily found in the lateral region. An occasional CR-IR principal cell is detected in the medial region of the nucleus, surrounded by a single VGluT1-IR calyx of Held (see Figure 35 for CR colocalization with Nissl stained principal cells in a P49 CBA/J mouse). Scale bar = 100μm. D = dorsal. M = medial. **High magnification** of dashed boxes A,B,C, and D depicted to illustrate the stepwise differential expression of CR along the medial-lateral axis of the MNTB. Scale bar = 20μm.

P49 Wild-Type (CBA/J) MNTB
VGluT1-IR
Calretinin-IR
VGluT1-IR + Calretinin-IR
VGluT1-IR + Calretinin-IR
D
M
A
B
C
D

Figure 35. **Calretinin expression in the MNTB of normal hearing (CBA/J) mice at 49 days postnatal. Low magnification** double immunofluorescence images for Nissl (FITC) and with primary antibodies against CR (CY-3) are shown in a 14μm thick section of brainstem from the level of the MNTB in a P49 CBA/J mouse. CR expression is heterogeneous. CR immunofluorescence is colocalized with very few Nissl stained principal cells restricted to the medial third of the MNTB. Many CR-IR calyces surrounding Nissl stained principal cells, while primarily located in the lateral region of the nucleus, can be seen throughout the MNTB (see Figure 34 for CR colocalization with VGLuT1-IR calyces of Held in a P49 CBA/J mouse)**.** Scale bar = 100μm. D = dorsal. M = medial. **High magnification** of dashed boxes A,B,C, and D depicted to illustrate the stepwise differential expression of CR along the medial-lateral axis of the MNTB. Scale bar = 20μm.

P49 Wild-Type (CBA/J) MNTB
Calretinin-IR
Nissl-IR + Calretinin-IR
Nissl-IR
Nissl-IR + Calretinin-IR
A
B
C
D
M
D

Figure 36. Calretinin expression in the MNTB of congenitally deaf (*dn/dn*) mice at 49 days postnatal. Low magnification double immunofluorescence images with primary antibodies against VGluT1 (FITC) and CR (CY-3) are shown in a 14μm thick section of brainstem from the level of the MNTB in a P49 CBA/J mouse. CR expression is heterogeneous. CR immunofluorescence is colocalized with very few VGluT1-IR calyces of Held located only in the lateral third of the MNTB. Many CR-IR principal cells, each surrounded by a single VGluT1-IR calyx of Held, are detected in the medial and intermediate regions of the nucleus (see Figure 37 for CR colocalization with Nissl stained principal cells in a P49 *dn/dn* mouse). Far fewer calyces of Held and far more principal cells express CR in P49 congenitally deaf animals compared to age matched wild-type (compare with Figures 34, 35). Scale bar = 100μm. D = dorsal. M = medial. **High magnification** of dashed boxes A,B,C, and D depicted to illustrate the stepwise differential expression of CR along the medial-lateral axis of the MNTB. Scale bar = 20μm.

P49 Congenitally Deaf (dn/dn) MNTB
VGluT1-IR
Calretinin-IR
VGluT1-IR + Calretinin-IR
VGluT1-IR + Calretinin-IR
D
M
A
B
C
D

Figure 37. Calretinin expression in the MNTB of congenitally deaf (*dn/dn*) mice at 49 days postnatal. Low magnification double immunofluorescence images for Nissl (FITC) and with primary antibodies against CR (CY-3) are shown in a 14μm thick section of brainstem from the level of the MNTB in a P49 CBA/J mouse. CR expression is heterogeneous. CR immunofluorescence is colocalized with many Nissl stained principal cells primarily located in the medial and intermediate regions of the MNTB. Very few CR-IR calyces, restricted to the lateral third of the nucleus, can be seen surrounding Nissl stained principal cells (see Figure 36 for CR colocalization with VGLuT1-IR calyces of Held in a P49 *dn/dn* mouse). Far fewer calyces of Held and far more principal cells express CR in P49 congenitally deaf animals compared to age matched wild-type (compare with Figures 34, 35). Scale bar = 100μm. D = dorsal. M = medial. **High magnification** of dashed boxes A,B,C, and D depicted to illustrate the stepwise differential expression of CR along the medial-lateral axis of the MNTB. Scale bar = 20μm.

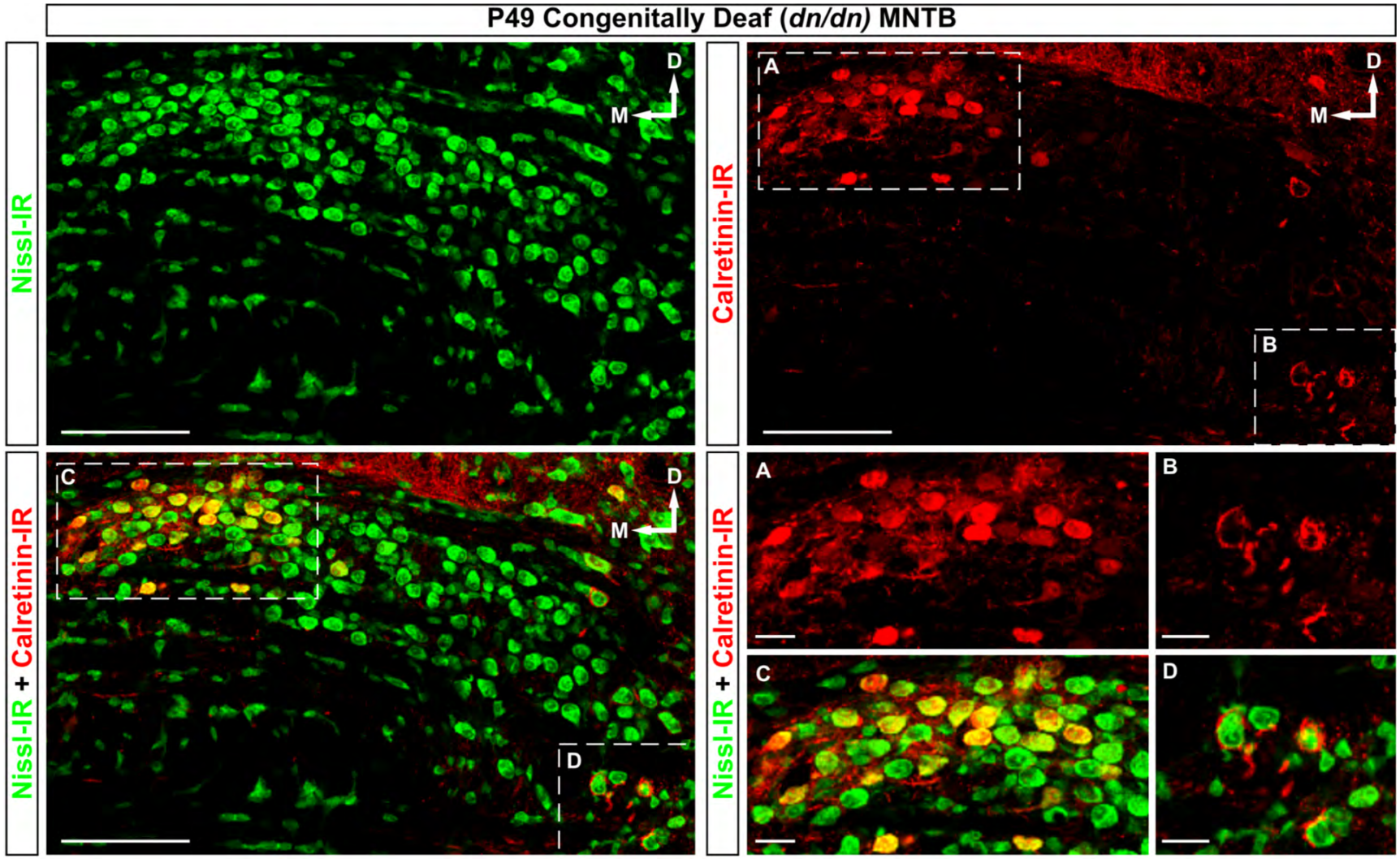
P49 Congenitally Deaf (dn/dn) MNTB
Nissl-IR
Calretinin-IR
Nissl-IR + Calretinin-IR
Nissl-IR + Calretinin-IR
A
B
C
D
D
M

Figure 38. Calretinin expression in the medial portion of the MNTB differs in normal hearing (CBA/J) and congenitally deaf (*dn/dn*) mice. A & B: CR is expressed in both calyces of Held (arrows) and principal cell somata. However, CR is not ubiquitous. CR (-) calyces of Held (asterisks) as well as CR (+) calyces are visible surrounding (presumably) CR (-) principal cells. Interestingly, no CR-IR calyces of Held were observed surrounding CR-IR principal cells were observed in this study. **C & D:** CR is expressed more principal cell in *dn/dn* animals than CBA/J animals. Further, more cell processes are visible than in CBA/J mice. Arrowhead indicates a possible VGluT1-IR presynaptic terminal contacting a primary dendrite. No calyces of Held are CR (+). Two VGluT1-IR calyces of Held (asterisks) are shown presumably surrounding CR (-) principal cells. Scale bar = 10μm. D = dorsal. M = medial.

P49 Wild-Type (CBA/J) MNTB
P49 Congenitally Deaf (dn/dn) MNTB
Calretinin-IR
Calretinin-IR + VGluT1
A
B
C
D
D
M

Figure 39: Calretinin expression in calyces of Held.
Top shows the percent of VGluT1-IR calyces found throughout the medial lateral axis of the MNTB which also express CR. A significant increase in the expression of CR was found throughout the first 49 days of postnatal development in CBA/J mice. In contrast, a significant increase in the expression of CR was detected during development from postnatal day 9 to postnatal day 13 only in *dn/dn* mice. No further developmental increases were detected after postnatal day 13 in *dn/dn* mice. Also, significantly more VGLuT1-IR calyces expressed CR at postnatal days 30 and 49 in CBA/J mice that *dn/dn* mice. Asterisk indicates $p < 0.001$. **Bottom:** Chart of data used in graph (above).

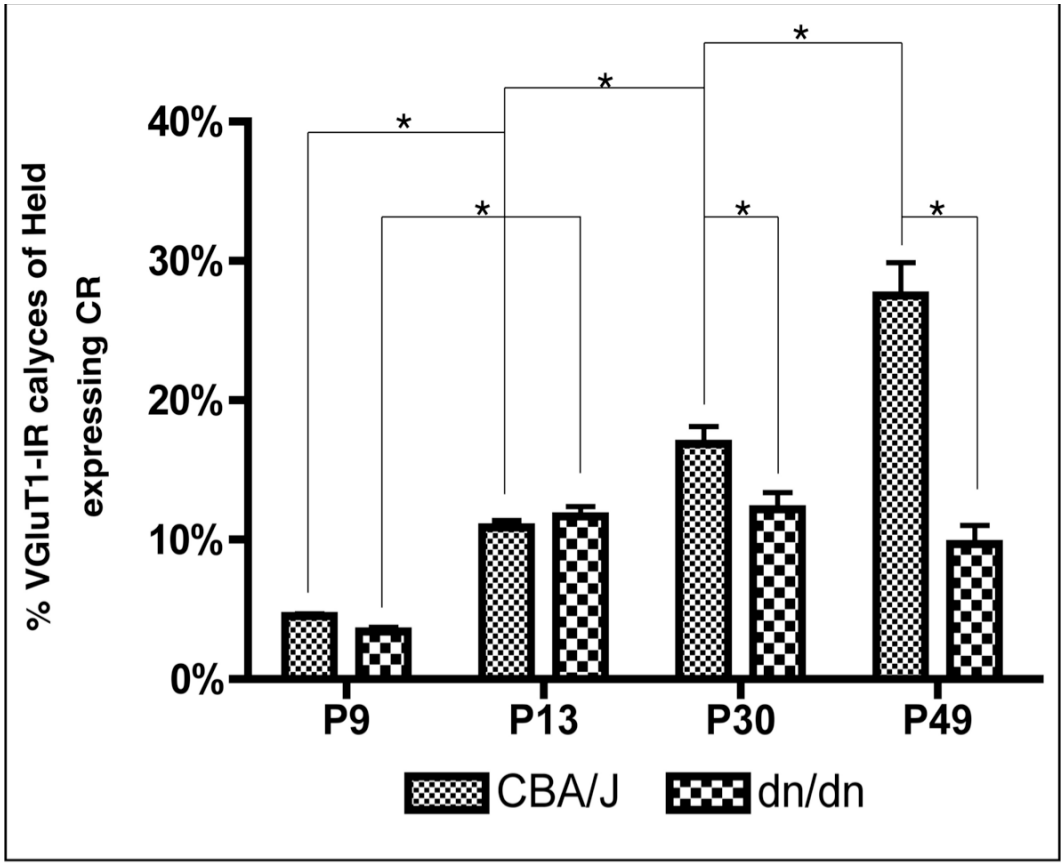

Age	% VGluT1-IR calyces of Held expressing CR*	
	CBA/J	*dn/dn*
P9	4.5 ± 0.2	3.9 ± 0.3
P13	10.5 ± 0.5	11.7 ± 0.7
P30	16.9 ± 1.2	12.2 ± 1.2
P49	27.5 ± 2.4	9.7 ± 1.3

*Mean ± SEM

Figure 40. Regional calretinin expression in calyces of Held

Above: In **A & B**, the percent of VGLuT1-IR calyces of Held located in each region of the MNTB which also express CR are shown for each age point analyzed in CBA/J and *dn/dn* mice, respectfully. In contrast, in **C & D**, the regional distribution of CR-IR calyces of Held found in the MNTB is expressed as a percentage of the total CR-IR calyces of Held found throughout the medial lateral extent of the MNTB for CBA/J and *dn/dn* mice, respectively. An average of 1539 VGluT1-IR calyces of Held or principal cells were analyzed for CR expression per age group for CBA/J animals (range: 1375 – 1752) and 1434 per age group for *dn/dn* animal (range 963 – 1870). **A)** At each age point analyzed, CR expression in the lateral region of the MNTB is significantly higher than the intermediate and medial regions (double asterisk: $p<0.001$). However, in each region there is a significant increase in calyceal CR expression in each region of the MNTB (single asterisk: $p<0.001$). ($n = 1375 – 1752$ cells per age group). **B)** Like CBA/J mice, at each age point, CR expression in the lateral region of the MNTB is significantly higher than intermediate and medial regions (double asterisk: $p<0.001$). Unlike CBA/J mice, there was a significant increase in CR expression in the lateral region of the MNTB only as the mice developed from P9 to P13 (single asterisk: $p<0.001$). No significant changes were detected after P13 in the lateral region or after P9 in intermediate and media regions. (963 – 1870 cells per age group) **C)** At all age points analyzed in CBA/J mice, a majority of CR-IR calyces are located in the lateral region of the MNTB. Corresponding with the increase in calyceal CR expression after P13 in intermediate and medial regions of the MNTB (in A), a significantly greater percentage of CR-IR calyces are detected intermediate and medial regions. **D)** At all age points analyzed in *dn/dn* mice, a majority of CR-IR calyces of Held are found in the lateral region of the MNTB. **Below:** Data used in compiling the above graphs. The fist data column corresponds with graph A, the second with graph B, the third with graph C, and the fourth with graph D.

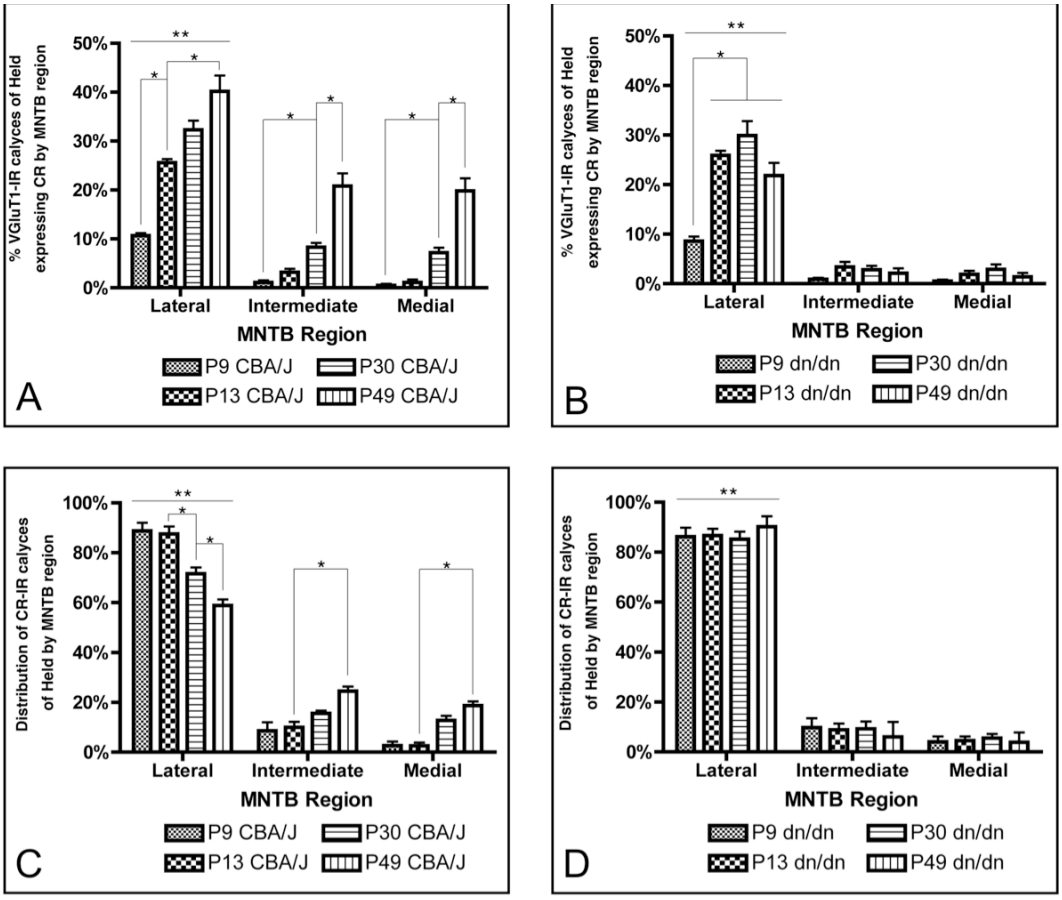

MNTB Region	Age	% VGluT1-IR calyces of Held expressing CR by region*		% Distribution of CR-IR calyces of Held by region*	
		CBA/J	dn/dn	CBA/J	dn/dn
Lateral	P9	10.7 ± 0.5	8.6 ± 0.9	88.8 ± 3.2	86.2 ± 3.6
	P13	25.6 ± 0.7	25.9 ± 0.9	87.5 ± 3.0	86.6 ± 2.8
	P30	32.3 ± 1.9	29.9 ± 2.9	71.6 ± 2.5	85.2 ± 3.0
	P49	40.2 ± 3.2	21.8 ± 2.6	58.9 ± 2.4	90.2 ± 4.2
Intermediate	P9	1.1 ± 0.4	0.9 ± 0.3	8.6 ± 2.6	9.8 ± 3.7
	P13	3.2 ± 0.7	3.4 ± 1.0	10.0 ± 2.2	8.9 ± 2.5
	P30	8.3 ± 0.9	2.8 ± 0.8	15.6 ± 2.5	9.3 ± 2.9
	P49	20.8 ± 2.6	2.1 ± 1.0	24.5 ± 1.9	6.0 ± 2.3
Medial	P9	0.5 ± 0.3	0.5 ± 0.3	2.6 ± 1.7	4.0 ± 2.2
	P13	1.1 ± 0.6	1.9 ± 0.7	2.5 ± 1.4	4.5 ± 1.7
	P30	7.2 ± 1.0	2.9 ± 1.0	12.8 ± 1.8	5.5 ± 1.7
	P49	19.8 ± 2.5	2.4 ± 0.8	18.7 ± 1.7	3.9 ± 1.3

*Mean ± SEM

Figure 41: Calretinin expression in MNTB principal cells.
Top shows the percent of principal cells found throughout the medial lateral axis of the MNTB which express CR. A significant decrease in the expression of CR was found in CBA/J mice after the onset of hearing from 13 days postnatal to 49 days postnatal. In contrast, a significant increase in the expression of CR was detected during development from postnatal day 13 to postnatal day 49 only in *dn/dn* mice. No further developmental increases were detected after postnatal day 13 in *dn/dn* mice. Also, significantly less principal cells expressed CR at postnatal day 49 in CBA/J mice than *dn/dn* mice. Asterisk indicates $p < 0.05$.
Bottom: Chart of data used in graph (above).

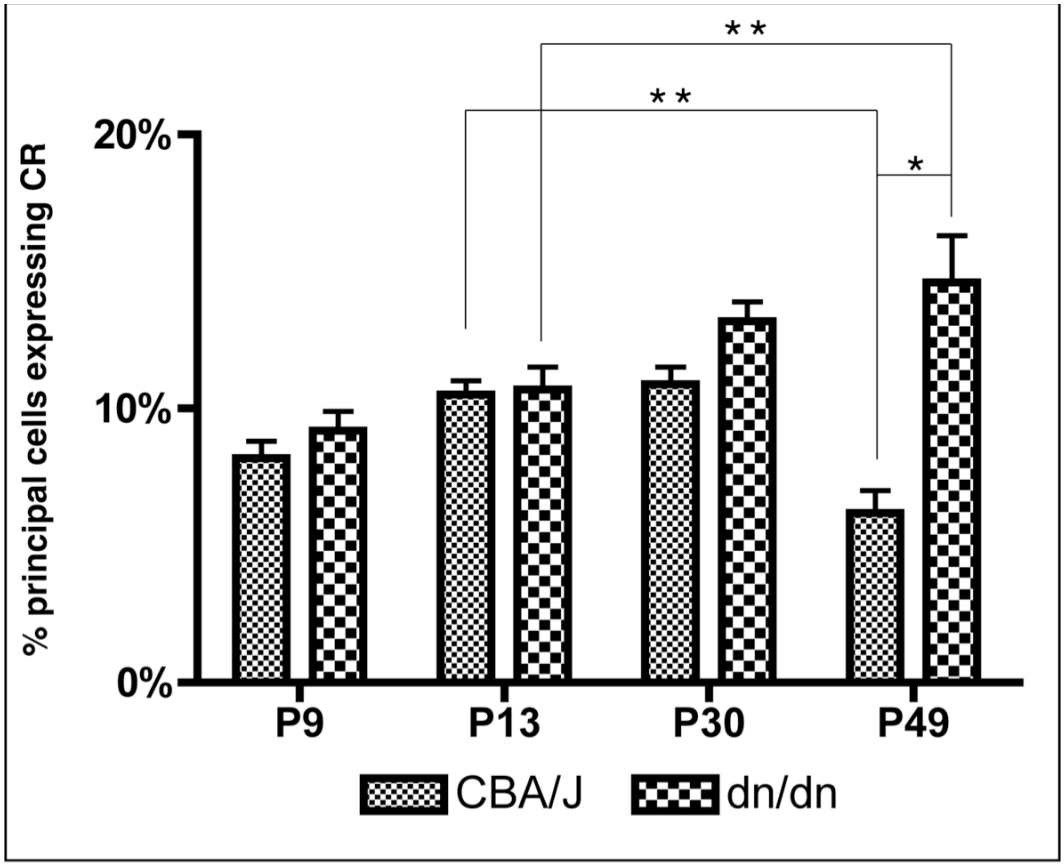

Age	% principal cells expressing CR*	
	CBA/J	*dn/dn*
P9	8.2 ± 0.6	9.2 ± 0.7
P13	10.5 ± 0.5	10.7 ± 0.8
P30	10.9 ± 0.6	13.2 ± 0.7
P49	6.2 ± 0.8	14.6 ± 1.7

*Mean ± SEM

Figure 42. Regional calretinin expression in MNTB principal cells.
Above: In **A & B**, the percent of principal cells located in each region of the MNTB which also express CR are shown for each age point analyzed in CBA/J and *dn/dn* mice, respectively. In contrast, in **C & D**, the regional distribution of CR-IR principal cells found in the MNTB is expressed as a percentage of the total CR-IR calyces of Held found throughout the medial lateral extent of the MNTB for CBA/J and *dn/dn* mice, respectively. An average of 1539 VGluT1-IR calyces of Held or principal cells were analyzed for CR expression per age group for CBA/J animals (range: 1375 – 1752) and 1434 per age group for *dn/dn* animal (range 963 – 1870). **A)** At each age point analyzed, CR expression in principal cells in the medial region of the MNTB is significantly higher than the intermediate and medial regions (triple asterisk: $p<0.001$). However, as the mice develop from P13 to P49 there is a significant decrease in CR expression within principal cells of the medial region (single asterisk: $p<0.01$). ($n = 1375 – 1752$ cells per age group). **B)** Like CBA/J mice, at each age point, somatic CR expression in the medial region of the MNTB is significantly higher than intermediate and medial regions at all age points analyzed (triple asterisk: $p<0.001$). Unlike CBA/J mice, there was a significant increase in somatic CR expression in the medial and intermediate regions of the MNTB only as the mice developed from P9 to P49 (single asterisk: $p<0.001$). No significant changes in somatic CR expression were detected after P9 in the lateral region. Further, significantly higher somatic CR expression was detected in the intermediate region compared to the medial region at P30 and P49 (double asterisk: $p<0.001$). (963 – 1870 cells per age group). **C)** At all age points analyzed in CBA/J mice, a majority of CR-IR principal cells are found in the medial region of the MNTB. **D)** At all age points analyzed in *dn/dn* mice, a majority of CR-IR principal cells are located in the medial region of the MNTB. Corresponding with the increase in somatic CR expression after from P9 to P49 in intermediate and medial regions of the MNTB (in A), a significantly greater percentage of CR-IR principal cells are detected in intermediate and medial regions. **Below:** Data used in compiling the above graphs. The fist data column corresponds with graph A, the second with graph B, the third with graph C, and the fourth with graph D.

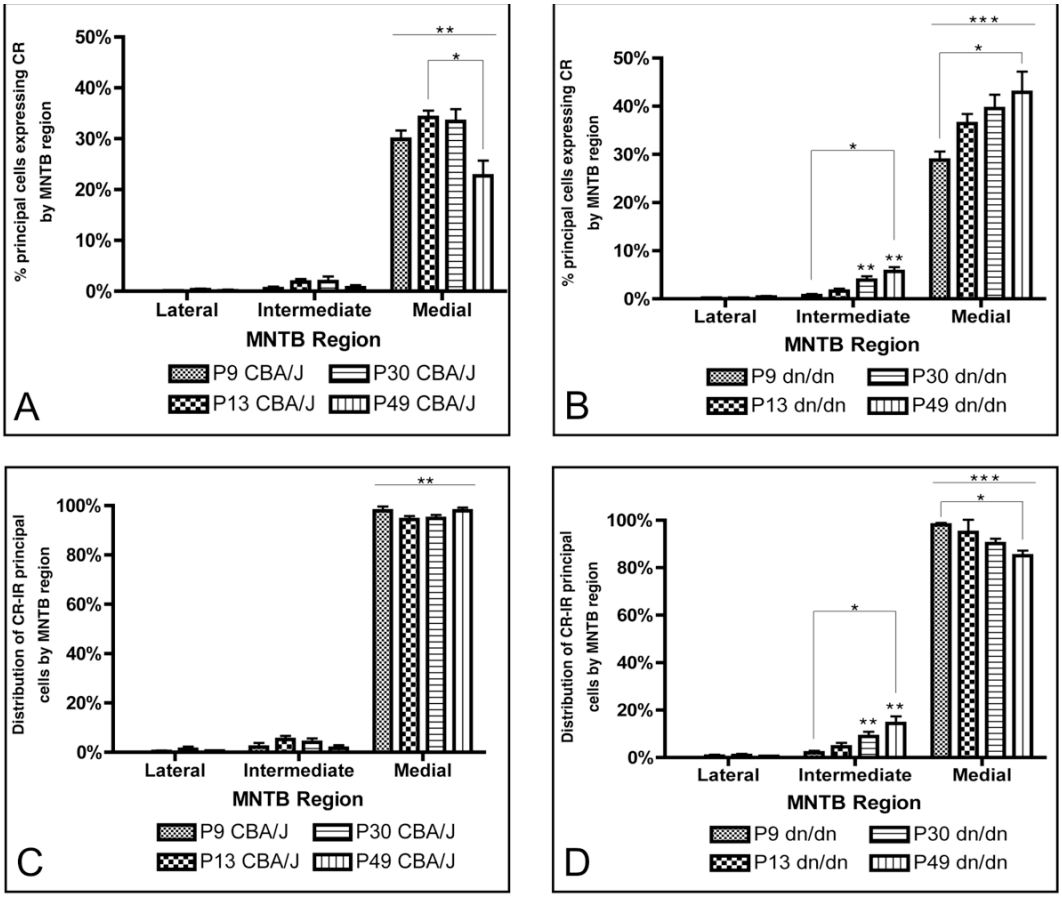

MNTB Region	Age	% principal cells expressing CR by region*		% Distribution of CR-IR principal cells by region*	
		CBA/J	dn/dn	CBA/J	dn/dn
Lateral	P9	0.0 ± 0.0	0.0 ± 0.0	0.0 ± 0.0	0.0 ± 0.0
	P13	0.1 ± 0.1	0.2 ± 0.1	0.4 ± 0.4	0.6 ± 0.6
	P30	0.3 ± 0.2	0.2 ± 0.1	1.2 ± 1.1	0.9 ± 0.6
	P49	0.1 ± 0.2	0.4 ± 0.2	0.5 ± 0.2	0.5 ± 0.3
Intermediate	P9	0.5 ± 0.4	0.7 ± 0.3	2.1 ± 1.7	2.9 ± 0.9
	P13	1.8 ± 0.6	1.6 ± 0.5	5.2 ± 1.4	4.5 ± 1.7
	P30	1.9 ± 1.0	3.9 ± 0.8	4.0 ± 1.6	8.9 ± 2.0
	P49	0.7 ± 0.5	5.7 ± 0.9	1.6 ± 1.3	14.4 ± 3.0
Medial	P9	29.9 ± 1.7	28.8 ± 1.8	97.9 ± 1.7	98.0 ± 0.9
	P13	34.2 ± 1.3	36.4 ± 2.0	94.4 ± 1.4	94.9 ± 5.3
	P30	33.4 ± 2.4	39.5 ± 2.9	94.8 ± 2.2	90.7 ± 2.0
	P49	22.7 ± 3.0	42.9 ± 4.3	97.9 ± 1.3	85.0 ± 2.2

*Mean ± SEM

Figure 43: Regional expression of calretinin in the MNTB at 49 days postnatal. Top The percent of VGLuT1-IR calyces of Held located in each region of the MNTB which also express CR are shown for postnatal day 49 in CBA/J and *dn/dn* mice. In each region of the MNTB, a significantly larger percentage of VGluT1-IR calyces of Held express CR in CBA/J mice compared to *dn/dn* mice. Asterisk indicates $p < 0.001$. **Bottom:** The percent of principal cells in each region of the MNTB which express CR are shown for postnatal day 49 in CBA/J and *dn/dn* mice. In each intermediate and medial regions of the MNTB, a significantly smaller percentage of principal cells express CR in CBA/J mice compared to *dn/dn* mice. Asterisk indicates $p < 0.001$.

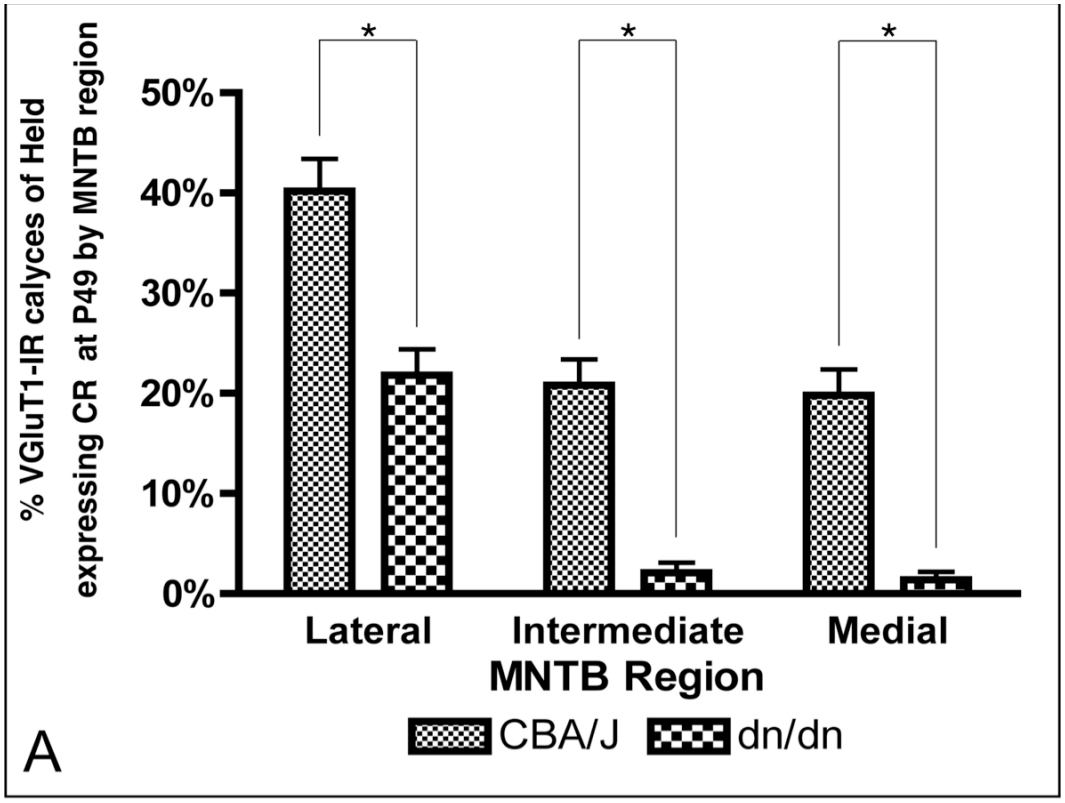
% VGluT1-IR calyces of Held expressing CR at P49 by MNTB region
50%
40%
30%
20%
10%
0%
*
*
*
Lateral
Intermediate
Medial
MNTB Region
CBA/J
dn/dn
A

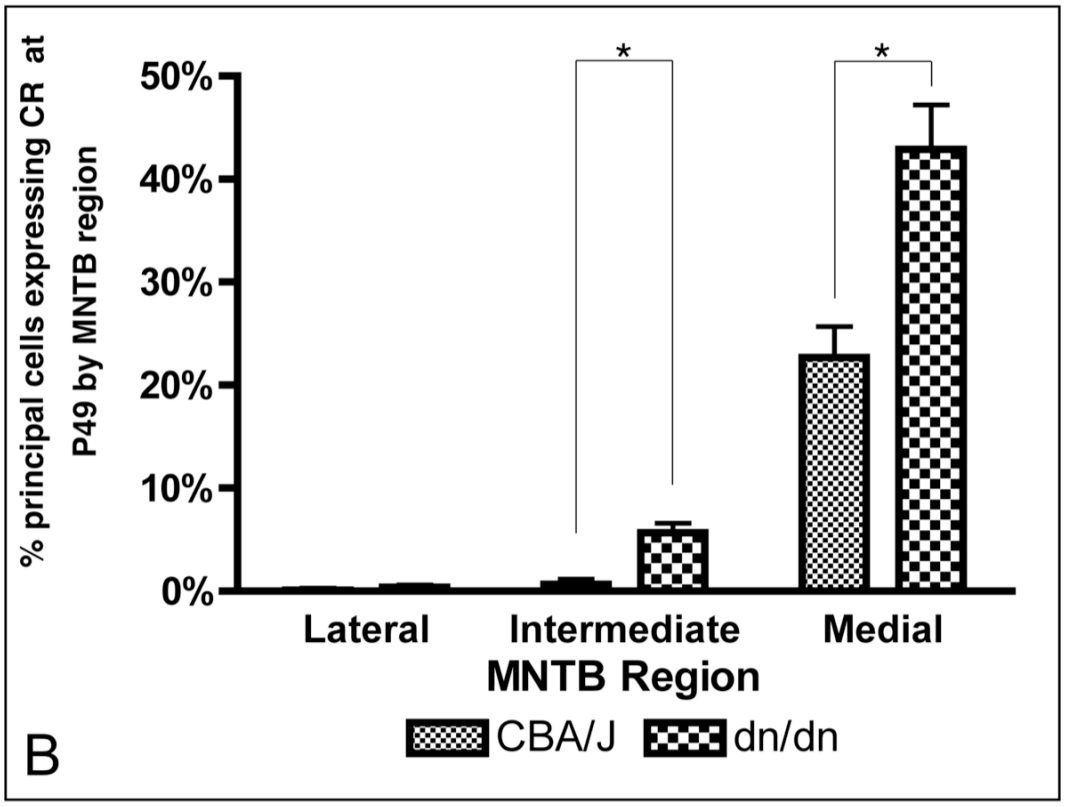
% principal cells expressing CR at P49 by MNTB region
50%
40%
30%
20%
10%
0%
*
*
Lateral
Intermediate
Medial
MNTB Region
CBA/J
dn/dn
B

Figure 44. Calretinin expression in normal hearing wistar rats.
CR is expressed in the majority of principal cells as well as calyces of Held with no apparent gradient along the medial lateral axis of the MNTB. **A & B:** 20X double immunofluorescence images with primary antibodies against VGluT1 (FITC) and CR (CY-3) are shown in a 20μm thick section of brainstem from the level of the MNTB in an adult Wistar rat. **C & D:** 20X double immunofluorescence images stained for Nissl (FITC) and primary antibodies against CR (CY-3) are shown in a 20μm this section of the MNTB in an adult Wistar rat. Scale bar = 100μm. D = dorsal. M = medial.

P49 Wild-Type Wistar Rat MNTB
Calretinin-IR
Calretinin-IR
VGluT1-IR + Calretinin-IR
Nissl + Calretinin-IR
A
B
C
D
D
M

Figure 45. Calretinin expression normal hearing wistar rats.
A-C: 60x double immunofluorescence images stained for Nissl and with primary antibodies against CR (CY-3) are shown in a 20μm thick section of brainstem from the level of the MNTB in an adult Wistar rat. Several CR-IR principal cells surrounded by more intensely stained CR-IR calyces of held are visible. Arrow indicates CR-IR presynaptic terminals that appear to extend from calyx of Held onto the principal cell's primary dendrite, which is devoid of Nissl stain. **D-F:** 60x double immunofluorescence stained with primary antibodies against VGluT1-IR (FITC) and CR (CY-3) from the MNTB in an adult Wistar rat. A CR-IR principal cell surrounded by a more intensely stained CR-IR calyx of Held is shown. In **E**, yellow indicates colocalization of the CR with VGluT1 in the calyx. Arrowhead indicates a possible presynaptic terminal of unknown origin coexpressing VGluT1 and CR contacting a dendrite extending from the CR-IR principal cell. Arrow indicates the final portion of the CR-IR axon before it differentiates into the calyx of Held presynaptic terminal. In **F**, the subcellular distribution of VGluT1 in this portion of the axon appears to be localized to its periphery (arrow). Scale bar = 10μm. D = dorsal. M = medial.

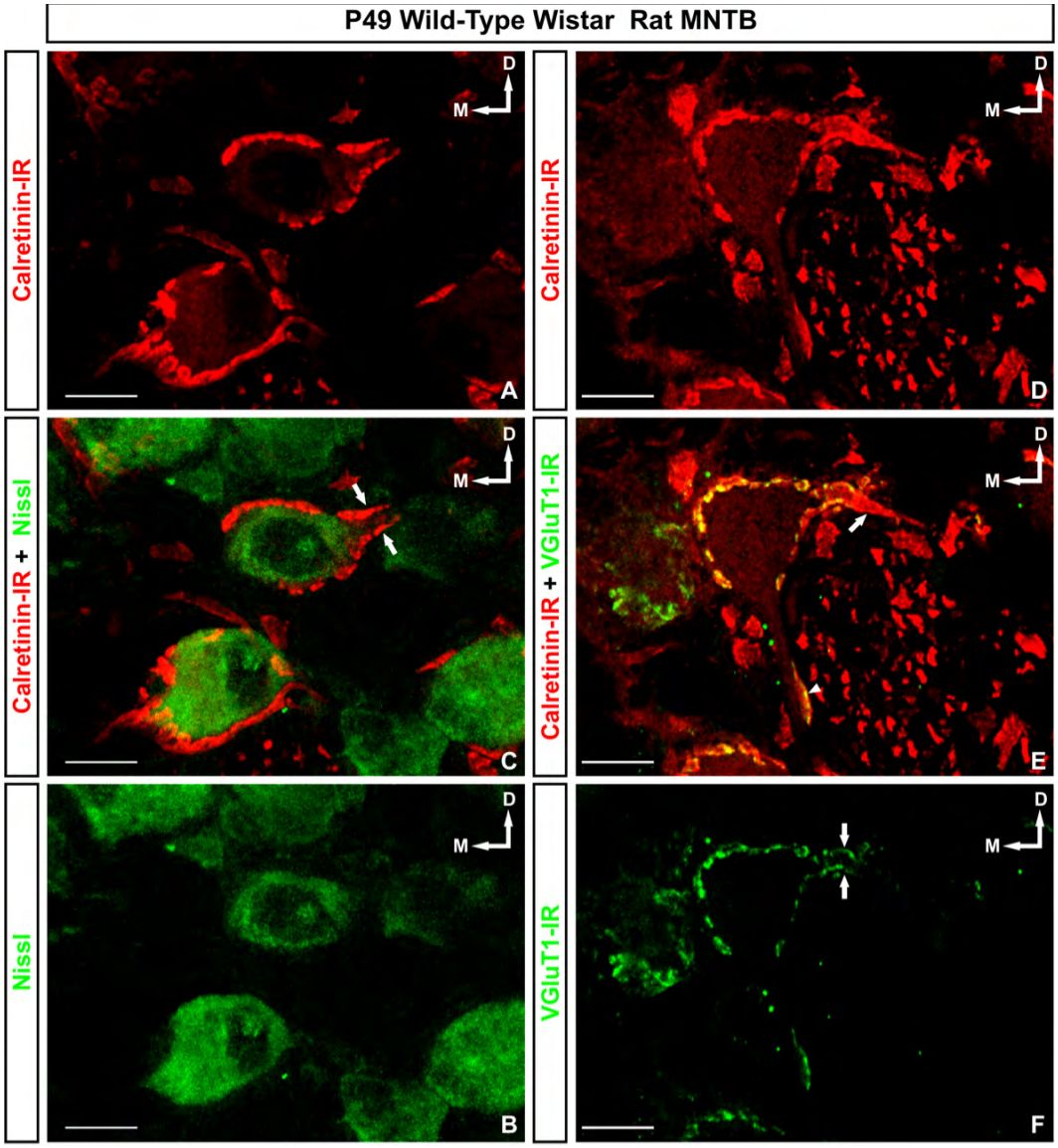
P49 Wild-Type Wistar Rat MNTB
Calretinin-IR
Calretinin-IR + Nissl
Nissl
Calretinin-IR
Calretinin-IR + VGluT1-IR
VGluT1-IR
D
M
A
B
C
D
E
F

XI. RESULTS

COEXPRESSION OF CALCIUM BUFFERING PROTEINS IN THE MNTB

MNTB Principal Cells and Calyces of Held Co-Express Different Calcium Buffering Proteins (CaBPs)

Because nearly 100% of calyces of Held express PV, there exists a subpopulation of predominantly laterally located calyces within the MNTB of both normal hearing (CBA/J) and congenitally deaf (*dn/dn*) mice that coexpress PV and CR. Additionally, nearly 100% of principal cells coexpress PV and CB (Figure 46), while a subpopulation of predominantly medially located principal cells also express CR (Figure 47). These data suggest the possibility that different CaBPs are capable of performing unique roles in both pre- and postsynaptic calcium signaling.

XII. DISCUSSION

COEXPRESSION OF CALCIUM BUFFERING PROTEINS IN THE MNTB

Parvalbumin (PV) and calretinin (CR) may have distinct roles in presynaptic calcium signaling

Calyces of Held exhibit a low endogenous Ca^{2+} buffering capacity ($\kappa_s \sim 30$) and a high Ca^{2+} extrusion rate (Helmchen et al., 2007). In such a presynaptic terminal, the presence of PV, a high affinity CaBP with slow binding kinetics, causes a faster decay of spatially averaged presynaptic $[Ca^{2+}]_I$ transient, without effecting its amplitude (Muller et al., 2007). In this way, PV will limit the accumulation of residual Ca^{2+} during high frequency trains of action potentials, enhancing the decay of presynaptic facilitation. Conversely, a high affinity CaBP with rapid binding kinetics, such as CR, when present within calyces of Held can decrease the amplitude of the peak $[Ca^{2+}]_I$ by binding incoming Ca^{2+} ions before they reach their intracellular target (Nagerl et al., 2000, Felmy and Schneggenburger, 2004). In doing so, CR reduces initial transmitter release probability and, particularly when high frequency trains of action potentials saturate the buffering capacity of CR, enhances presynaptic facilitation. It may be that these two seemingly opposing effects of PV and CR are uniquely suited and work together to preserve high fidelity synaptic transmission at the calyx of Held, particularly in those calyces processing lower frequency afferent auditory stimulation.

Parvalbumin (PV), calbindin D-28K (CB), and calretinin (CR) may have distinct roles in postsynaptic calcium signaling

When introduced into DRG cells, CB, a high affinity CaBP with rapid binding kinetics, caused an 8-fold decrease in the rate of rise of $[Ca^{2+}]_I$ and altered the decay kinetics of $[Ca^{2+}]_I$ to a single slow component (Chard, et al., 1993). PV, however, only minimally slowed the rate of rise $[Ca^{2+}]_I$ and selectively increased the fast component of the decay of $[Ca^{2+}]_I$ signal (Chard, et al., 1993). Like the differential effects of PV and CR, these effects on $[Ca^{2+}]_I$ in DRG cells arise from differential binding kinetics. Although the precise role of postsynaptic calcium buffers in the MNTB remains elusive, the expression of both PV and CB within nearly 100% of principal suggests that these proteins may serve different roles in postsynaptic calcium signaling. CB decreases the amplitude of the peak $[Ca^{2+}]_I$ and PV blocks the accumulation of residual Ca^{2+} ions.

A subpopulation of principal cells express all three CaBPs addressed in this study. While the possibility of unique signaling roles for CaBPs with slow (PV) versus rapid (CB, CR) binding kinetics is an easy speculation, it is less clear why principal cells would coexpress CR and CB, two different high affinity CaBPs with rapid binding kinetics. The structural similarity of CR and CB has led most researchers to traditionally believe these proteins function and similar physiological roles. However, that only a minority of principal cells expresses both CR and CB indicates the possibility that subtle differences exist in the effect each protein could have on the Ca^{2+} signal. Further, that the subpopulation of principal cells coexpressing PV, CB, and CR are predominately medially located

suggests that postsynaptic CR may subserve specific functional requirements for the temporally precise signal transduction necessary for the localization of high frequency sounds.

Recent studies have shown that CR contains 5, not 4 (like CB), functionally active Ca^{2+} binding domains, of which two pairs (sites I-II and III-IV) exhibit cooperative binding (Schwaller et al., 1997). The cooperative binding of Ca^{2+} to CR results in accelerated binding as free $[Ca^{2+}]_I$ increases from cytoplasmic resting conditions (Faas et al., 2007). As a consequence, the Ca^{2+} buffering speed of CR is largely dependent on the free $[Ca^{2+}]_I$, which may fluctuate more rapidly in medially located principal cells processing high frequency afferent stimulation of the auditory nerve. In these cells, the cooperative binding of Ca^{2+} to CR, may allow CR to respond more rapidly than CB to perturbations in the Ca^{2+} signal. However, that rats have a have a range of hearing which is lower than mice and nearly 100% of rat principal cells express PV, CB, and CR indicates that such a postulated role for CR in high frequency synaptic transmission may be species specific and requires further study.

Figure 46. Calbindin D-28k and parvalbumin expression in the MNTB of normal hearing (CBA/J) mice at 30 days postnatal. Triple immunofluorescence images with primary antibodies against Nissl (FITC), CB (CY-3), and PV (CY-5) are shown in a 14μm thick section of brainstem from the level of the MNTB. CB and PV are coexpressed in nearly every principal cell of the MNTB. Scale Bar = 100μm.

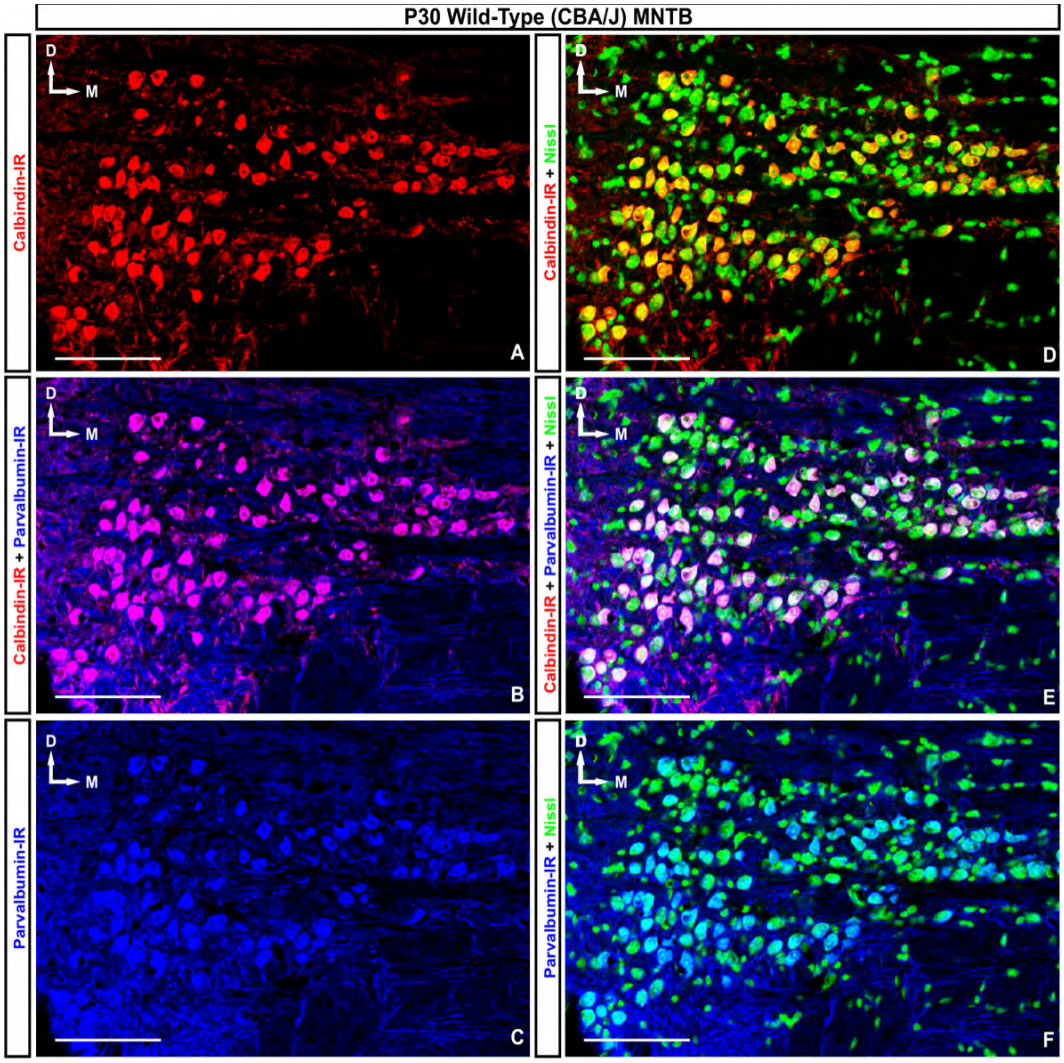
P30 Wild-Type (CBA/J) MNTB
Calbindin-IR
Calbindin-IR + Nissl
Calbindin-IR + Parvalbumin-IR
Calbindin-IR + Parvalbumin-IR + Nissl
Parvalbumin-IR
Parvalbumin-IR + Nissl
D
M
A
B
C
D
E
F

Figure 47. Calbindin D-28k and calretinin expression in the MNTB of normal hearing (CBA/J) mice at 30 days postnatal. Triple immunofluorescence images with primary antibodies against VGluT1 (FITC), CR (CY-3), and CB (CY-5) are shown in a 14μm thick section of brainstem from the level of the MNTB. CB and CR are coexpressed in a subpopulation of principal cells predominantly located in the medial of the MNTB. CR is also expressed in a subpopulation of calyces of Held predominantly located in the lateral region of the MNTB Scale Bar = 100μm.

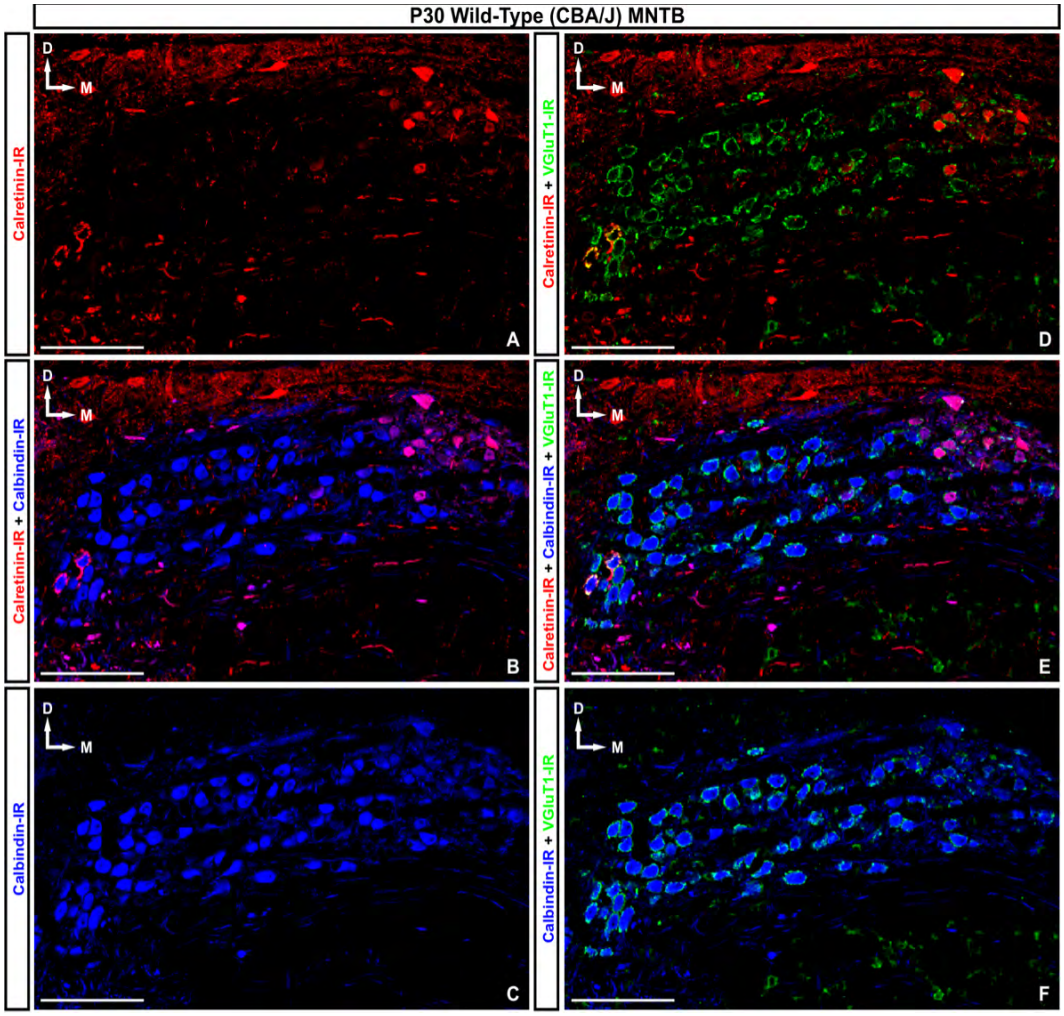
P30 Wild-Type (CBA/J) MNTB
Calretinin-IR
Calretinin-IR + VGluT1-IR
Calretinin-IR + Calbindin-IR
Calretinin-IR + Calbindin-IR + VGluT1-IR
Calbindin-IR
Calbindin-IR + VGluT1-IR
D
M
A
B
C
D
E
F

XIII. RESULTS

EXPRESSION OF CALCIUM BUFFERING PROTEINS IN THE AVCN

The cochlear nucleus was analyzed in the region just rostral to and including the entrance and bifurcation of the cochlear nerve root, which is composed primarily of globular bushy cells (GBCs) and stellate along the entire dorso-ventral axis. Globular bushy cells were identified based on the morphologic criteria of a an ovoid cell body, 10-20μm across its long axis, with one or two primary dendrites, and a characteristically eccentric nucleus, which often appeared as if it were bulging from the surface of the cell (Osen, 1969) and differentiated from stellate cells, which have a rectangular body and multiple primary dendrites giving them a multipolar appearance (Figure 48). At the level of the eighth nerve bifurcation, globular bushy cells span the entire dorso-ventral axis of the cochlear nerve. Just rostral to the bifurcation, GBCs can be found in the region ventral to the small cell cap (Figure 48).

CaBP immunoreactivity (CaBP-IR) was compared in the AVCN of normal hearing (CBA/J) and congenitally deaf (dn/dn) mice at a number of postnatal time points [9 days (P9), 13 days (P13), and 30 days (P30] to obtain the normal time course of CR, CB, and PV expression in GBCs and possible alterations from its normal developmental expression in the absence of spontaneous and acoustically evoked afferent activity in the cochlear nerve. 6–8 sections of MNTB per animal were analyzed (n = 6 – 8) from 2–4 animals per age per strain (N = 2-4). For analysis, tissue stained with CR, CB, or PV antibodies

was co-labeled with VGluT1 antibodies or Nissl stain. CaBP-IR GBCs were identified by the above characteristics as well as co-labeling with Nissl stain or being surrounded by VGuT1-IR endbulbs of Held. CaBP-IR presynaptic endbulbs of Held were identified by apposition to identified Nissl stained GBCs or by co-localization with anti-VGluT1 antibodies in a region of the AVCN confirmed to contain GBCs by Nissl stain.

Calretinin (CR) is expressed in a majority of AVCN endbulbs of Held cells and a minority of globular bushy cell somata in CBA/J and *dn/dn* mice

Confocal analysis of CR-IR in the AVCN of CBA/J and *dn/dn* mice in low magnification (20X, 1.5 zoom) and high magnification (60x, 2.0 zoom) was performed by counting CR+ GBCs as well as GBCs surrounded by CR+ endbulbs of Held through stacks of 2μm optical sections from 14μm thick coronal section of MNTB. Image analysis revealed that throughout development CR is expressed in a majority of presynaptic nerve fibers and endbulb of Held terminals, but only rarely in postsynaptic bushy cell somata (Figure 49). Similar findings were obtained in dn/dn mice.

Percentages of GBCs receiving presynaptic contacts from VGlut1-IR endbulbs of Held which co-express CR were obtained. While CR is expressed in a majority of endbulbs throughout development, the percent of GBCs receiving VGluT1-IR endbulbs of Held co-expressing CR increased significantly at all time points analyzed in CBA/J mice (P9: 81.1 ± 0.6%, P13: 91.7 ± 0.4%, P30: 97.0 ± 0.9%; mean ± SEM; $p<0.001$ One Way ANOVA) and *dn/dn* mice (P9: 82.4 ±

0.9%; P13: 91.3 ± 0.7%; P30: 98.0 ± 1.2%; $p<0.001$ One Way ANOVA) (Figure 50, 52, 53, 54, 55, 56). *Post hoc* tests indicate that, within each strain, significant differences exist between all age points in the percentage of GBCs receiving VG-IR endbulbs co-expressing CR ($p<0.05$ *post hoc* Tukey's test). These data indicate that as development progresses, an increasing percentage of GBCs are contacted by endbulbs of Held that express CR. When comparing deaf mice to wild-types, no significant differences in the percentage of GBCs receiving VGluT1-IR calyces that co-express CR were detected at P9 (CBA/J: 81.1 ± 0.6%, *dn/dn*: 82.4 ± 0.9%; mean ± SEM; $p = 0.238$ t-test), P13 (CBA/J: 91.7 ± 0.4%, *dn/dn*: 91.3 ± 0.7%; mean ± SEM; $p = 0.598$ t-test) and P30 (CBA/J: 97.0 ± 0.9%, *dn/dn*: 12.2 ± 1.2; mean ± SEM; $p=0.386$ t-test), suggesting that the developmental increase in CR immunoreactivity in the endbulbs of Held that occurs in CBA/J occurs to a similar, if not equal extent, in *dn/dn* mice (Figure 56). Interestingly, at 9 days postnatal, CR is visible in many eighth nerve fibers ascending through the cochlear nerve nucleus (Figure 51) as development proceeds and more endbulbs of held express CR, the intensity of staining of CR staining in the nerve fibers decreases.

Additionally, analysis of the percentage of GBCs expressing calretinin revealed that, in both strains and at all time points analyzed, only a minority of cells expresses this calcium buffering protein, but that the percentage of CR-IR GBCs does significantly increase throughout development in both CBA/J (P9: 3.5 ± 0.4%, P13: 10.8 ± 0.2%, P30: 11.6 ± 0.6%; mean ± SEM; $p<0.001$ One Way ANOVA) and *dn/dn* mice (P9: 2.7 ± 0.2%; P13: 11.1 ± 0.4%; P30: 12.0 ± 0.6%;

p<0.001 One Way ANOVA) (Figure 50, 52, 53, 54, 55, 57). Within each strain analyzed, *post hoc* test indicate that percentage of GBCs expressing CR at P9 is significantly different than all other ages analyzed (p<0.05 *post hoc* Tukey's test), while the percentage of GBCs expressing CR was not significantly different between P13 and P30 (p>0.05 *post hoc* Tukey's test). When comparing deaf mice to wild-types, no significant differences in the percentage of GBCs expressing CR were detected at P9 (CBA/J: 3.5 ± 0.4%, *dn/dn*: 2.7 ± 0.2%; mean ± SEM; p = 0.075 t-test), P13 (CBA/J: 10.8 ± 0.2%, *dn/dn*: 11.1 ± 0.4%; mean ± SEM; p = 0.504 t-test) and P30 (CBA/J: 11.6 ± 0.6%; *dn/dn*: 12.0 ± 0.6%; mean ± SEM; p=0.571 t-test). These data indicate that in both CBA/J and *dn/dn*, mice there is a similar developmental increase in CR immunoreactivity in globular bushy cells, however, those CR-IR globular bushy cells still represent only a minority of the entire GBC population (Figure 57).

Calbindin D-28k (CB) is expressed in a minority of AVCN globular bushy cells in CBA/J and *dn/dn* mice

Confocal analysis of CB-IR in the AVCN of CBA/J and *dn/dn* mice in low magnification (20X, 1.5 zoom) and high magnification (60x, 2.0 zoom) was performed as described above. Image analysis revealed that throughout development CB markedly absent from presynaptic fibers and nerve terminals, but is expressed in a small percentage of globular bushy cell somata. Similar findings were obtained in dn/dn mice.

Percentages of GBCs staining positive for CB were obtained. No presynaptic fibers or endbulbs of Held expressed any CB immunoreactivity. In both strains and at all time points analyzed, only a minority of cells expresses this CB, but the percentage of CB-IR GBCs does significantly increase throughout development in both CBA/J (P9: 7.7 ± 2.5%, P13: 17.6 ± 3.4%, P30: 22.2 ± 2.8%; mean ± SEM; p=0.0128 One Way ANOVA) (Figure 58, 60) and *dn/dn* mice (P9: 8.3 ± 2.7%; P13: 20.9 ± 3.8%; P30: 23.8 ± 3.1%; p=0.011 One Way ANOVA) (Figure 59, 60). Within each strain analyzed, *post hoc* test indicate that percentage of GBCs expressing CB at P9 is significantly different than at P13 and P30 ($p<0.05$ *post hoc* Tukey's test), while the percentage of GBCs expressing CB was not significantly different between P13 and P30 ($p>0.05$ *post hoc* Tukey's test). When comparing deaf mice to wild-types, no significant differences in the percentage of GBCs expressing CB were detected at P9 (CBA/J: 7.7 ± 2.5%, *dn/dn*: 8.3 ± 2.7%; mean ± SEM; p = 0.855 t-test), P13 (CBA/J: 17.6 ± 3.4%, *dn/dn*: 20.9 ± 3.8%; mean ± SEM; p = 0.529 t-test) and P30 (CBA/J: 22.2 ± 2.8%; *dn/dn*: 23.8 ± 3.1%; mean ± SEM; p=0.704 t-test). These data indicate that there is a similar increase in CB GBC expression in both CBA/J and *dn/dn* mice age, but that CB-IR GBCs only represent a minority of the total GBC population (Figure 60).

Parvalbumin (PV) is expressed in a majority of AVCN endbulbs of Held cells and globular bushy cell somata in CBA/J and *dn/dn* mice

Confocal analysis of PV-IR in the AVCN of CBA/J and *dn/dn* mice in low magnification (20X, 1.5 zoom) and high magnification (60x, 2.0 zoom) was performed as described above. Image analysis revealed that throughout development CR is expressed in a majority of presynaptic nerve fibers and endbulb of Held terminals, but only rarely in postsynaptic bushy cell somata. Similar findings were obtained in dn/dn mice.

Percentages of GBCs receiving presynaptic contacts from VGlut1-IR endbulbs of Held which co-express PV were obtained. A clear majority of GBCs receive VGluT1-IR endbulbs coexpressing PV, with only a slight increase in the proportion of such GBCs age the mice age from P9 to P13 in both the CBA/J (P9: 93.7 ± 0.5%, P13: 95.9 ± 0.2%, P30: 95.5 ± 0.4%; mean ± SEM; $p<0.001$ One Way ANOVA) and *dn/dn* strain (P9: 92.5 ± 0.4%; P13: 95.6 ± 0.5%; P30: 96.4 ± 0.5%; $p<0.001$ One Way ANOVA) (Figure 61, 62, 63, & 64). *Post hoc* tests indicate that, within each strain, significant differences exist in the percentage of GBCs receiving VG-IR endbulbs co-expressing CR between P9 and all other age points analyzed ($p<0.05$ *post hoc* Tukey's test), indicating that no significant difference exists in the percentage of GBCs contacted by PV-IR endbulbs of Held between P13 and P30. Further, no significant differences in the percentage of GBCs receiving VGluT1-IR calyces that co-express CR were detected between CBA/J and *dn/dn* mice at P9 (CBA/J: 93.7 ± 0.5%, *dn/dn*: 92.5 ± 0.4%; mean ± SEM; $p = 0.087$ t-test), P13 (CBA/J: 95.9 ± 0.2%, *dn/dn*: 95.6 ± 0.5%; mean ± SEM; $p = 0.545$ t-test) and P30 (CBA/J: 95.5 ± 0.4%, *dn/dn*: 96.4 ± 0.5%; mean ± SEM; $p=0.141$ t-test), suggesting that the developmental expression of CR

immunoreactivity in the endbulbs of Held occurs similarly in CBA/J and *dn/dn* mice (Figure 64).

Additionally, analysis of GBCs expressing calretinin revealed that, in both strains and at all time points analyzed, a clear majority of cells expresses PV. However, a significant increase is observed between the percentages of PV-IR GBCs after P9 in both CBA/J (P9: 81.0 ± 3.7%, P13: 95.5 ± 2.4%, P30: 97.2 ± 1.8%; mean ± SEM; $p<0.001$ One Way ANOVA and *dn/dn* mice (P9: 80.5 ± 1.0%; P13: 93.4 ± 2.5%; P30: 96.4 ± 2.8%; $p<0.001$ One Way ANOVA) (Figure 61, 62, 63, 65)). Within each strain analyzed, *post hoc* test indicate that percentage of GBCs expressing CR at P9 is significantly different than all other ages analyzed ($p<0.05$ *post hoc* Tukey's test), while the percentage of GBCs expressing CR was not significantly different between P13 and P30 ($p>0.05$ *post hoc* Tukey's test). When comparing deaf mice to wild-types, no significant differences in the percentage of GBCs expressing PV were detected at P9 (CBA/J: 81.0 ± 3.7%, *dn/dn*: 80.5 ± 1.0%; mean ± SEM; $p = 0.631$ t-test), P13 (CBA/J: 95.5 ± 2.4%, *dn/dn*: 93.4 ± 2.5%; mean ± SEM; $p = 0.733$ t-test) and P30 (CBA/J: 97.2 ± 1.8%; *dn/dn:* 96.4 ± 2.8%; mean ± SEM; $p=0.973$ t-test). These data indicate that in both CBA/J and *dn/dn*, mice there is a similar developmental expression of PV immunoreactivity in globular bushy cells (Figure 65).

XIV. DISCUSSION

EXPRESSION OF CALCIUM BUFFERING PROTEINS IN THE AVCN

Developmental regulation of calretinin (CR) expression in the AVCN of normal hearing (CBA/J) and congenitally deaf (*dn/dn*) mice

Very little differences were observed regarding the developmental expression of CR in AVCN globular bushy cells between normal hearing and congenitally deaf mice. In both strains, CR is expressed in a majority of presynaptic nerve fibers and endbulb of Held terminals, but only rarely in postsynaptic bushy cell somata.

At 9 days postnatal, CR is expressed in a majority of nerve fibers and endbulbs of Held. After 9 days postnatal, CR is progressively expressed in fewer nerve fibers and in more endbulbs of Held and globular bushy cell somata. Hence, the overall pattern of the developmental expression in CBA/J and *dn/dn* mice is for young mice to express CR in many nerve fibers and few endbulbs of Held, and for more mature mice to express CR in progressively fewer nerve fibers and progressively more endbulbs of Held and globular bushy cells (Figure 50, 52, 53, 54, 55, 56, 57). It should be noted that while significant differences were not seen in the percentage of globular bushy cells expressing CR in this study, an upward trend was observed and it is likely that significance would be achieved if later time points were analyzed.

Calretinin (CR) expression is heterogeneous in the cochlear nucleus complex of mice

Interestingly, while CR is expressed in only a minority of cell somata in the AVCN, this pattern of expression is not consistent throughout the cochlear nuclear complex of mice. In this study, brightly immunofluorescent somatic CR staining was observed in the cochlear nucleus octopus cell area.

The octopus cell area is located in the central division of the posteroventral cochlear nucleus (PVCN). These cells, which do not appear in clusters, but rather as solitary cells amidst a sea of neuropil, intermingle with globular bushy cells in the border between the globular bushy cell area and the octopus cell area. They are easily identified by their long straight primary dendrites that arise from the cell body like tentacles from an octopus (Figure 66).

While CR Immunoreactivity is evident in the small VGluT1-IR presynaptic terminals covering the soma and primary dendrites of the P9 octopus cell, it does not appear to be expressed postsynaptically within the cell body of any octopus cells. However, by P30, somatic CR expression increases, as nearly every octopus cell is brightly Immunofluorescent for CR (Figure 67, 68). This stands in stark contrast to the globular cell area, where only a minority of somata express calretinin.

Globular bushy cells, which preserve and encode the precise temporal characteristics of an acoustic stimulus, fire action potentials in a “primary-like with notch” pattern that closely mimics the of the primary afferent input via the cochlear nerve. Indeed, globular bushy cells fire at a near 1:1 ratio with action

potentials. Octopus cells, however, fire one or few action potentials at the onset of an acoustic stimulus, regardless of its duration. The differential expression of calretinin in these two cell populations may confer the unique firing properties seen in each cell population, and may, perhaps, further elucidate the precise role of calretinin in auditory pathways.

Developmental regulation of calbindin D-28k (CB) expression in the AVCN of normal hearing (CBA/J) and congenitally deaf (*dn/dn*) mice

Very little differences were observed regarding the developmental expression of CB in AVCN globular bushy cells between normal hearing and congenitally deaf mice. In both strains, CB is only expressed in globular bushy cell somata. Further, the amount of CB expression in the AVCN is far less than observed for CR and PV. These results applied to both the normal hearing and congenitally deaf mice.

At 9 days postnatal, CB appeared to be expressed weakly in just a few bushy cell somata. After 9 days postnatal, CB is progressively expressed in more globular bushy cell somata (Figure 58, 59, 60). Hence, the overall pattern of the developmental expression in CBA/J and *dn/dn* mice is for young mice to express CB in a minority of bushy cell somata and for more mature mice to express CB in a greater percentage of GBCs. However, throughout development, only a minority of GBCs expresses CB.

Developmental regulation of parvalbumin (PV) expression in the AVCN of normal hearing (CBA/J) and congenitally deaf (*dn/dn*) mice

In the AVCN of both CBA/J and *dn/dn* mice, PV was expressed both presynaptically, in endbulbs of Held, and postsynaptically, in globular bushy cell somata. Very few differences were observed in the expression of PV in the globular bushy cell area of CBA/J and *dn/dn* mice.

At 9 days postnatal, PV is expressed in a majority of nerve fibers, endbulbs of Held, and globular bushy cell somata. At this stage of development, the intensity of PV staining in the endbulbs of Held was far greater than the staining intensity in the bushy cell somata. After 9 days postnatal, CR is progressively expressed in more endbulbs of Held and globular bushy cell somata.). By 30 days postnatal, the strength of PV intensity was so strong postsynaptically that it was difficult to distinguish PV staining in the bushy cells from that in the endbulbs of Held, mainly because of the close opposition of the endbulbs with the bushy cell somata (Figure 61, 62, 63, 64, 65). Hence, the overall pattern of the developmental expression in CBA/J and *dn/dn* mice is for young mice to express CR in many nerve fibers and few endbulbs of Held, and for more mature mice to express CR in progressively fewer nerve fibers and progressively more endbulbs of Held and globular bushy cells. A similar pattern was observed for CR expression in globular bushy cell somata. However, it should be noted that at early time points, because the intensity of staining within bushy cell somata is less than that presynaptically, it is possible that the PV(-)

globular bushy cells observed at this age are in fact expressing PV, albeit at a level too low to detect adjacent to the intensely immunofluorescent endbulbs.

Figure 48. **Nissl stained sections of the AVCN in normal hearing mice.**
A: 20x immunofluorescence image of the AVCN with stained for Nissl (FITC) are shown in a 14μm thick section of brainstem at the level of the bifurcation of cochlear nerve root in the AVCN in a P9 CBA/J mouse. The arrow indicated the cochlear nerve root, characterized by GBCs organized in columns aligned between intervening fibers of the cochlear nerve. **B:** 20x immunofluorescence image of the AVCN with stained for Nissl (FITC) are shown in a 14μm thick section of brainstem at the level rostral to the bifurcation of cochlear nerve root in the AVCN in a P30 CBA/J mouse. GBC can be found arranged in clusters in the region ventral to the small cell cap, indicated by the arrow. **C-E:** 60x immunofluorescence images of globular bushy cells stained for Nissl (FITC). The characteristic morphological criteria used in this study to distinguish GBCs are an eccentric nucleus in an ovoid cell body. In **C**, note the emergence of a primary dendrite from the cell soma (arrow). **F:** For comparison, the multipolar appearance of a stellate cell is shown. In **A&B:** scale bar = 100μm, D = dorsal, M = medial. In **C-F:** scale bar = 10μm.

P9 Wild-Type (CBA/J) AVCN
P30 Wild-Type (CBA/J) AVCN
High Magnification
A
B
C
D
E
F
D
M
D
M

Figure 49. Calretinin expression in the globular cell area of the AVCN in normal hearing mice. 60x double immunofluorescence images stained with primary antibodies against VGluT1 (FITC) and CR (CY-3) are shown in a 14μm thick section of brainstem from the AVCN in a P13 CBA/J mouse. **A:** Brightly stained CR-IR endbulbs of Held are visible surrounding calretinin negative globular bushy cells. In **B**, asterisks indicate the calretinin immunoreactivity shown in A co-localizes with anti-VGluT1 (shown in yellow), confirming the presence of CR in presynaptic endbulbs of held, but not in postsynaptic globular bushy cells. **C:** VGlut1 immunoreactivity in endbulbs of held. Scale bar = 10μm. D = dorsal. M = medial.

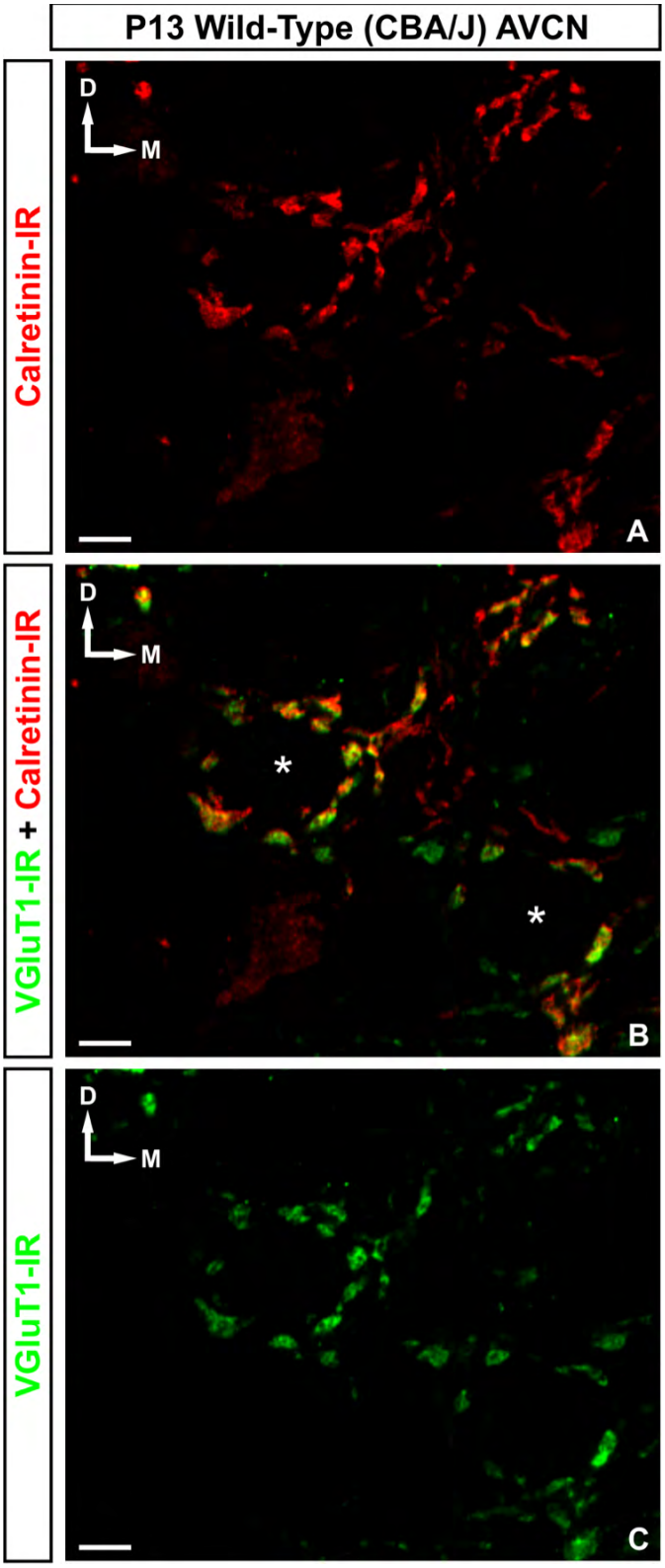
P13 Wild-Type (CBA/J) AVCN
Calretinin-IR
VGluT1-IR + Calretinin-IR
VGluT1-IR
D
M
A
B
C
*
*

Figure 50. Calretinin expression in the globular cell area of the AVCN of normal hearing (CBA/J) mice at 9 days postnatal CR is expressed in a majority of cochlear nerve fibers and presynaptic endbulb of Held terminal, but very few globular bushy cell somata. No difference in CR expression seen between normal hearing (CBA/J) and congenitally deaf (*dn/dn*) mice at this age. **A-C:** 20x double immunofluorescence images with Nissl stain (FITC) and primary antibodies against CR (CY-3) are shown in a 14μm thick section of AVCN in a P9 CBA/J mouse. **D-F:** 20x double immunofluorescence images with primary antibodies against VGluT1 (FITC) and CR (CY-3) are shown in a 14μm thick section of AVCN in a P9 CBA/J mouse. Scale bar = 100μm. D = dorsal. M = medial.

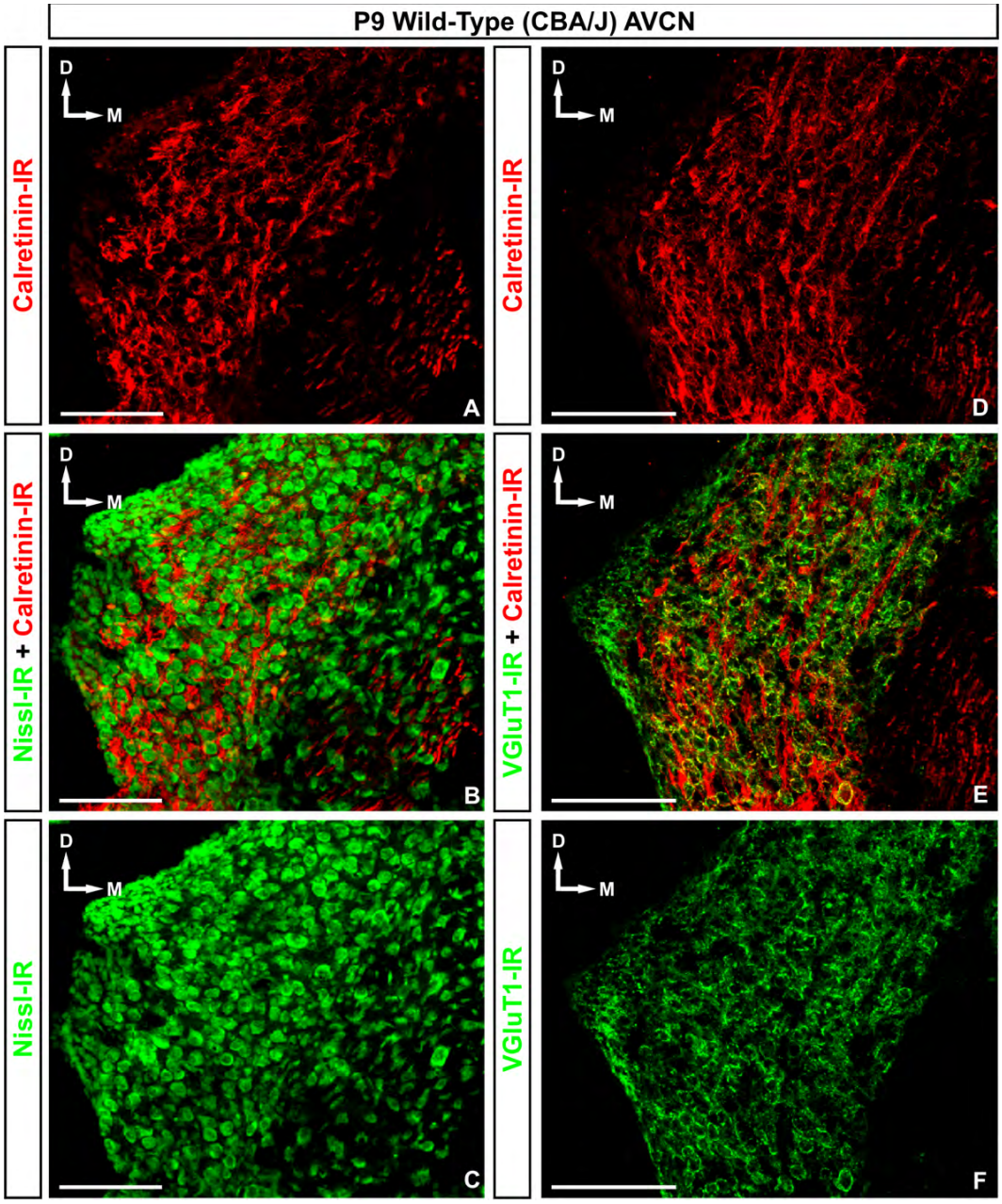
P9 Wild-Type (CBA/J) AVCN
Calretinin-IR
Calretinin-IR
Nissl-IR + Calretinin-IR
VGluT1-IR + Calretinin-IR
Nissl-IR
VGluT1-IR
D
M
A
B
C
D
E
F

Figure 51. Calretinin expression in the globular cell area of the AVCN of normal hearing (CBA/J) mice at 9 days postnatal. CR is expressed in a majority of cochlear nerve fibers and presynaptic endbulb of Held terminal, and only a minority of globular bushy cell somata. No difference in CR expression seen between normal hearing (CBA/J) and congenitally deaf (*dn/dn*) mice at this age. **A-C:** 20x double immunofluorescence images with Nissl stain (FITC) and primary antibodies against CR (CY-3) are shown in a 14μm thick section of AVCN in a P9 CBA/J mouse. **B-D:** 60x double immunofluorescence images with primary antibodies against VGluT1 (FITC) and CR (CY-3) are shown. Arrows indicate CR immunoreactivity in cochlear nerve fibers as they ascend in the nucleus. Scale bar = 100μm. D = dorsal. M = medial.

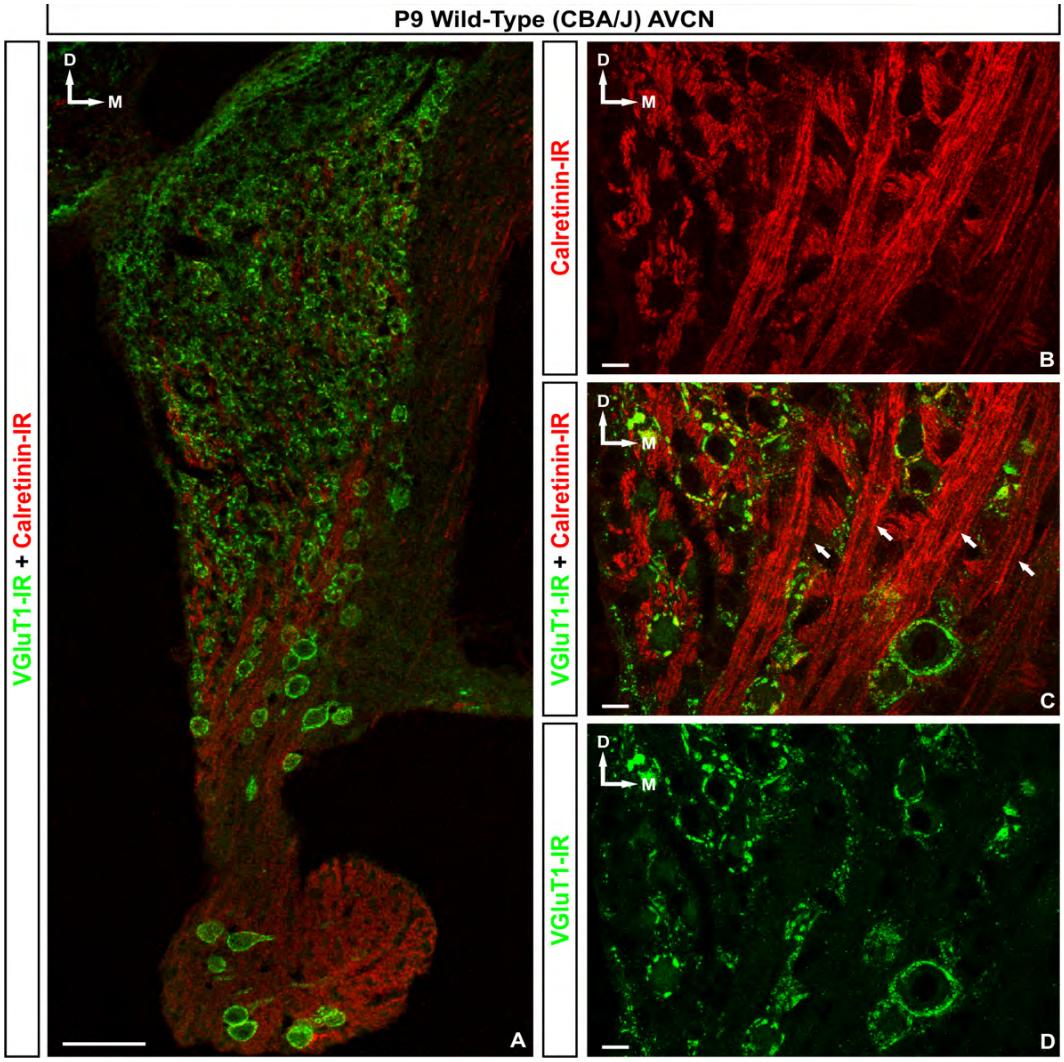
P9 Wild-Type (CBA/J) AVCN
VGluT1-IR + Calretinin-IR
Calretinin-IR
VGluT1-IR + Calretinin-IR
VGluT1-IR
D
M
A
B
C
D

Figure 52. Calretinin expression in the globular cell area of the AVCN of normal hearing (CBA/J) mice at 13 days postnatal. CR is expressed in a majority of cochlear nerve fibers and presynaptic endbulb of Held terminal, and only a minority of globular bushy cell somata. No difference in CR expression seen between normal hearing (CBA/J) and congenitally deaf (*dn/dn*) mice at this age. **A-C:** 20x double immunofluorescence images with Nissl stain (FITC) and primary antibodies against CR (CY-3) are shown in a 14μm thick section of AVCN in a P9 CBA/J mouse. **D-F:** 20x double immunofluorescence images with primary antibodies against VGluT1 (FITC) and CR (CY-3) are shown in a 14μm thick section of AVCN in a P9 CBA/J mouse. Scale bar = 100μm. D = dorsal. M = medial.

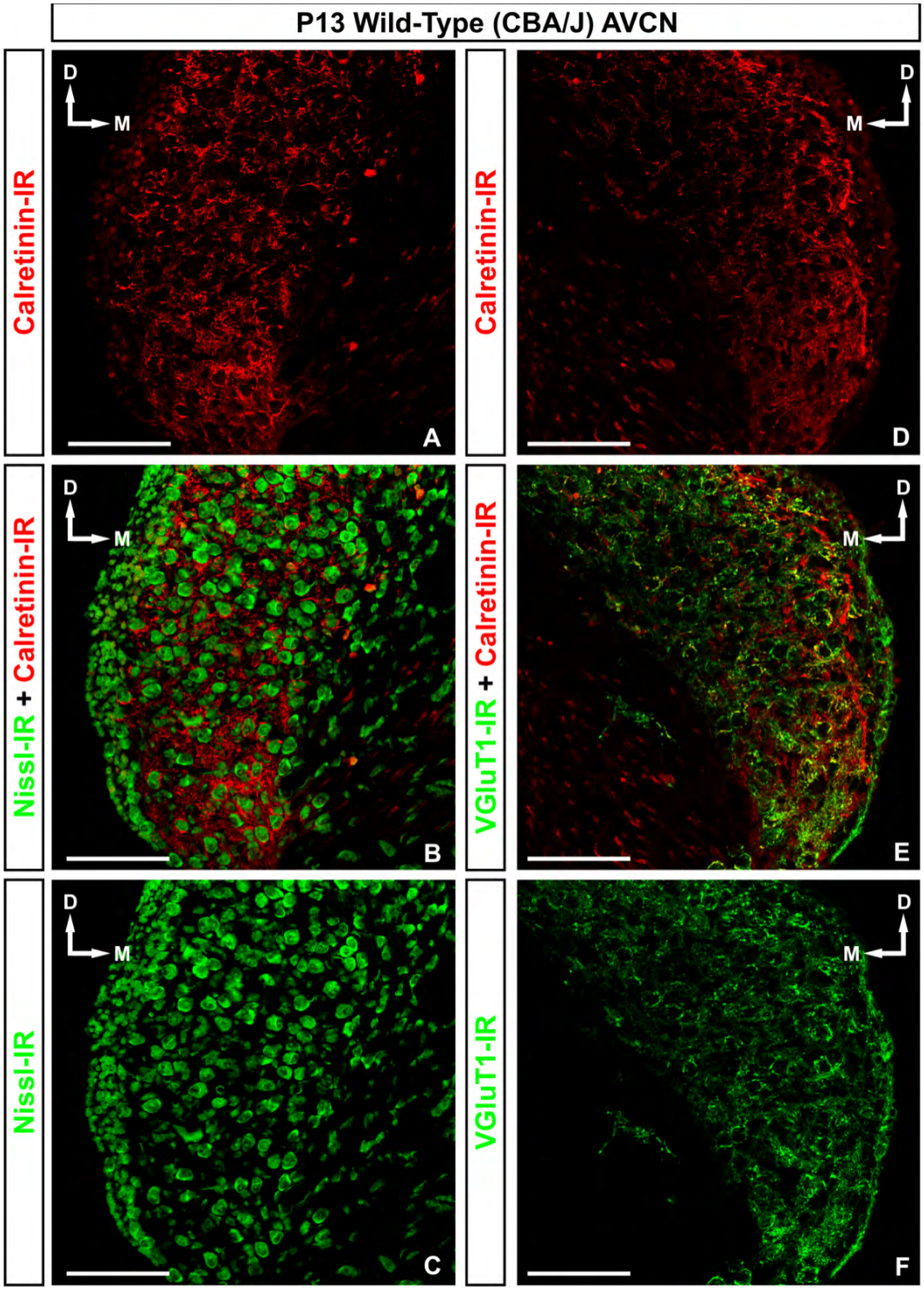
P13 Wild-Type (CBA/J) AVCN
Calretinin-IR
Calretinin-IR
Nissl-IR + Calretinin-IR
VGluT1-IR + Calretinin-IR
Nissl-IR
VGluT1-IR
D
M
A
B
C
D
E
F

Figure 53. Calretinin expression in the globular cell area of the AVCN of normal hearing (CBA/J) mice at 13 days postnatal CR is expressed in a majority of cochlear nerve fibers and presynaptic endbulb of Held terminal, and only a minority of globular bushy cell somata. No difference in CR expression seen between normal hearing (CBA/J) and congenitally deaf (*dn/dn*) mice at this age. **A-C:** 60x double immunofluorescence images with Nissl stain (FITC) and primary antibodies against CR (CY-3) are shown. Double asterisk indicates a CR negative GBC receiving CR-positive endbulbs of Held. Single asterisk indicates a CR negative GBC that does not receive CR-positive endbulb of Held. **D-F:** 60x double immunofluorescence images with primary antibodies against VGluT1 (FITC) and CR (CY-3) are shown. Double asterisk indicates a CR-positive GBC receiving CR-positive endbulbs of Held. Single asterisks indicate CR-negative GBCs receiving CR-positive endbulbs of held. Scale bar = 100μm. D = dorsal. M = medial.

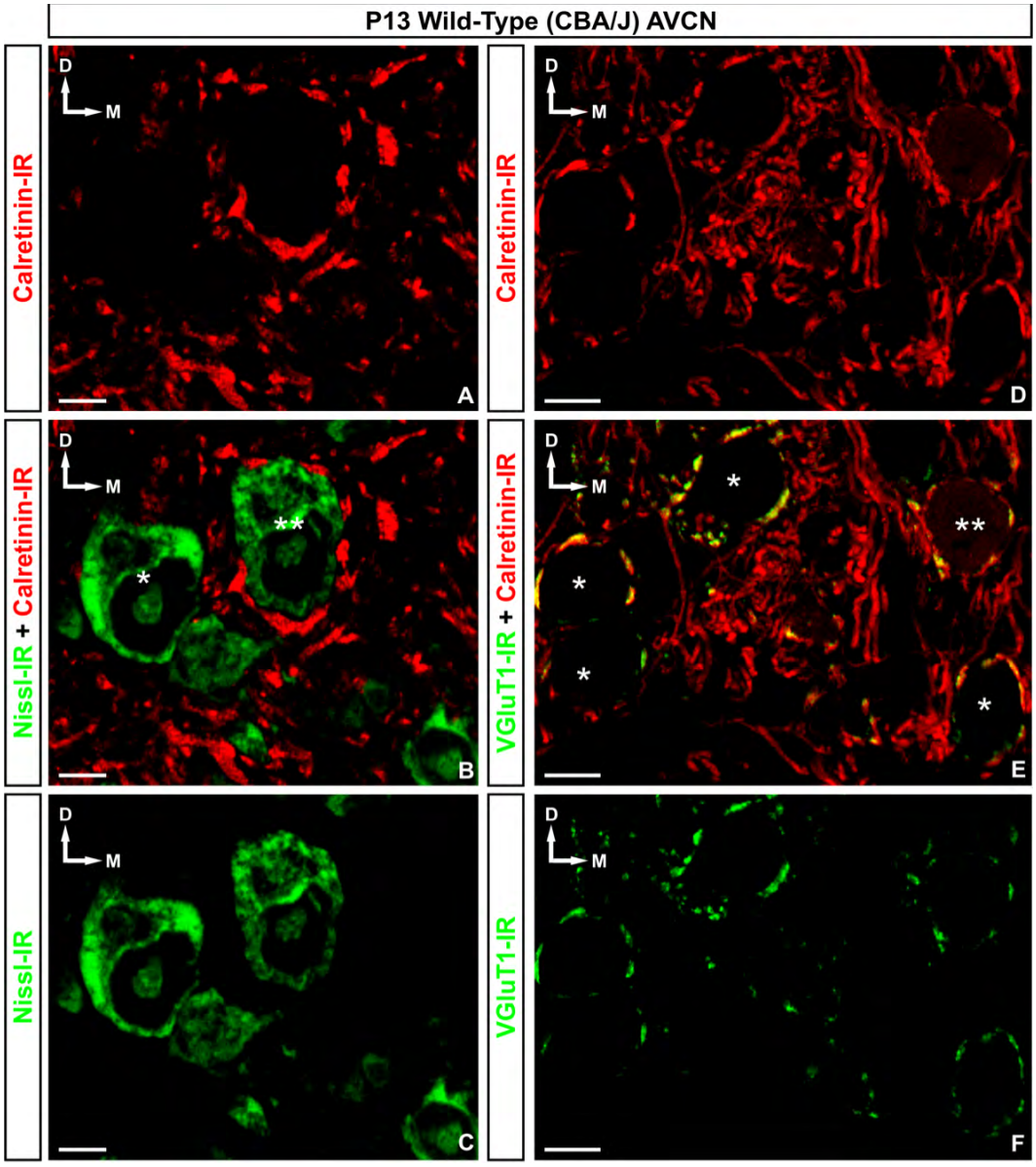
P13 Wild-Type (CBA/J) AVCN
Calretinin-IR
Calretinin-IR
Nissl-IR + Calretinin-IR
VGluT1-IR + Calretinin-IR
Nissl-IR
VGluT1-IR
D
M
A
B
C
D
E
F
*
**

Figure 54. Calretinin expression in the globular cell area of the AVCN of normal hearing (CBA/J) mice at 30 days postnatal. CR is expressed in a majority of cochlear nerve fibers and presynaptic endbulb of Held terminal, and only a minority of globular bushy cell somata. No difference in CR expression seen between normal hearing (CBA/J) and congenitally deaf (*dn/dn*) mice at this age. **A-C:** 20x double immunofluorescence images with Nissl stain (FITC) and primary antibodies against CR (CY-3) are shown in a 14μm thick section of AVCN in a P30 CBA/J mouse. **D-F:** 60x double immunofluorescence images with Nissl stain (FITC) and primary antibodies against CR (CY-3) are shown in a 14μm thick section of AVCN in a P30 CBA/J mouse. Asterisk indicates a CR-positive GBC. 20x Scale bar = 100μm. 60x scale bar = 10μm. D = dorsal. M = medial.

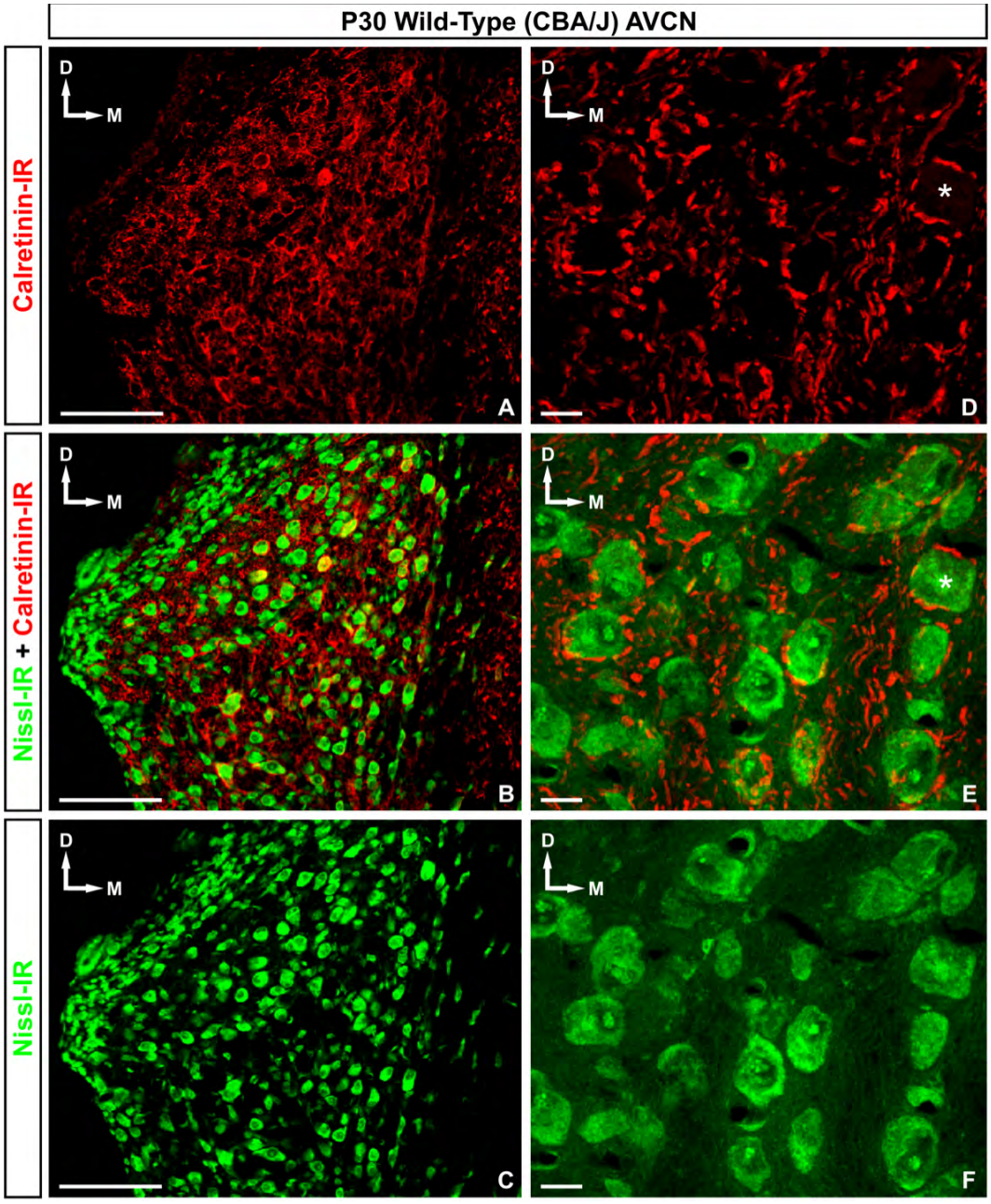
P30 Wild-Type (CBA/J) AVCN
Calretinin-IR
Nissl-IR + Calretinin-IR
Nissl-IR
D
M
A
B
C
D
E
F
*
*

Figure 55. Calretinin expression in the globular cell area of the AVCN of congenitally deaf (*dn/dn*) mice at 30 days postnatal. CR is expressed in a majority of cochlear nerve fibers and presynaptic endbulb of Held terminal, and only a minority of globular bushy cell somata. No difference in CR expression seen between normal hearing (CBA/J) and congenitally deaf (*dn/dn*) mice at this age. **A-C:** 20x double immunofluorescence images with Nissl stain (FITC) and primary antibodies against CR (CY-3) are shown in a 14µm thick section of AVCN in a P30 *dn/dn* mouse. **D-F:** 60x double immunofluorescence images with Nissl stain (FITC) and primary antibodies against CR (CY-3) are shown in a 14µm thick section of AVCN in a P30 *dn/dn* mouse. Asterisk indicates a CR-positive GBC. 20x Scale bar = 100µm. 60x scale bar = 10µm. D = dorsal. M = medial.

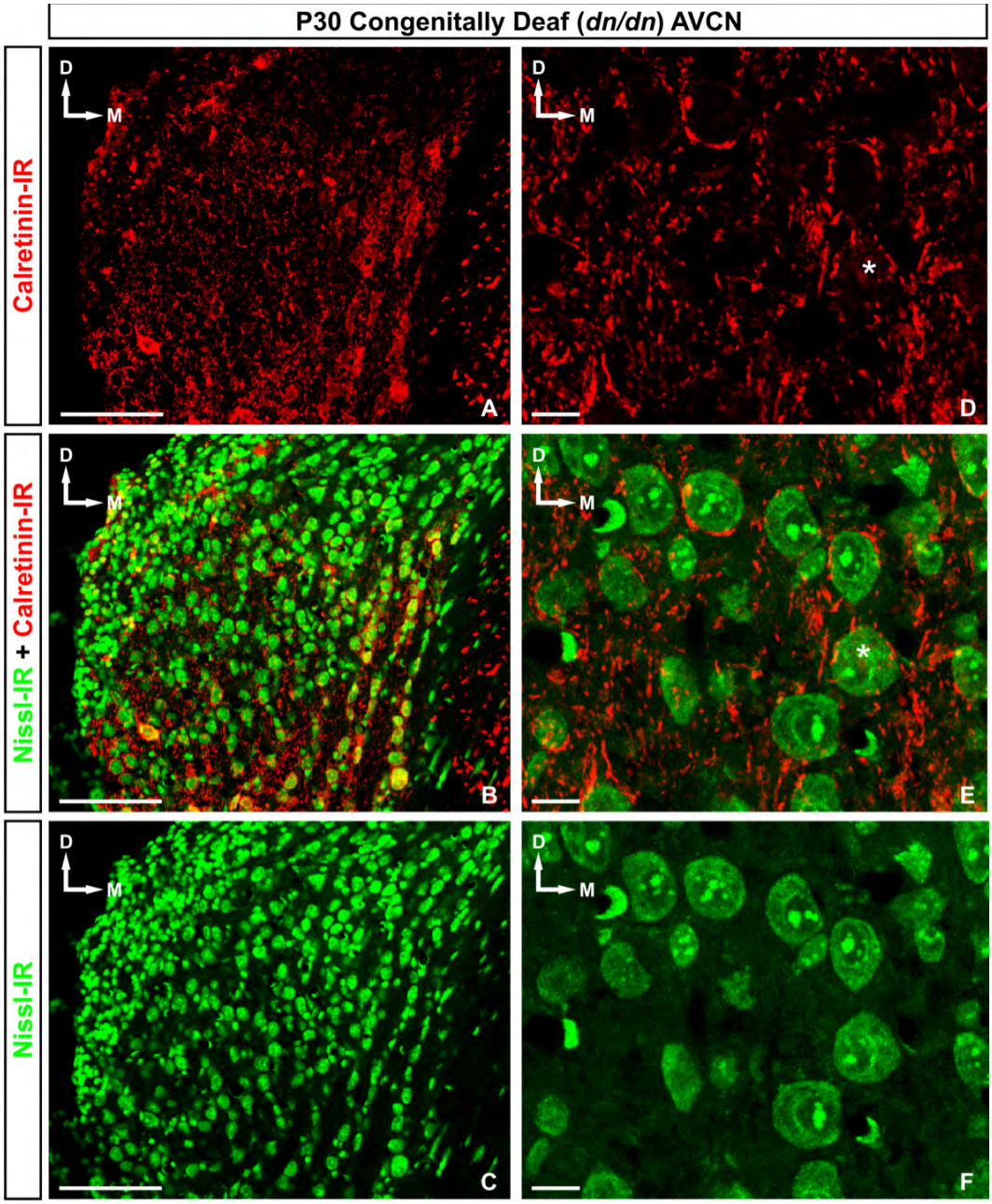
P30 Congenitally Deaf (dn/dn) AVCN
Calretinin-IR
Nissl-IR + Calretinin-IR
Nissl-IR
D
M
A
B
C
D
E
F
*

Figure 56: Calretinin expression in endbulbs of Held.
Top shows the percent of globular bushy cells found throughout in the AVCN which are contacted by endbulbs of Held expressing CR. A significant increase in the expression of CR was found in CBA/J as well as *dn/dn* mice from 9 days postnatal to 13 days to 30 days postnatal. No significant differences were detected in the proportion of globular bushy cells contacted by endbulbs expressing CR between age matched CBA/J and *dn/dn* animals. Single, double, and triple asterisk indicates $p<0.001$. **Bottom:** Chart of data used in graph (above).

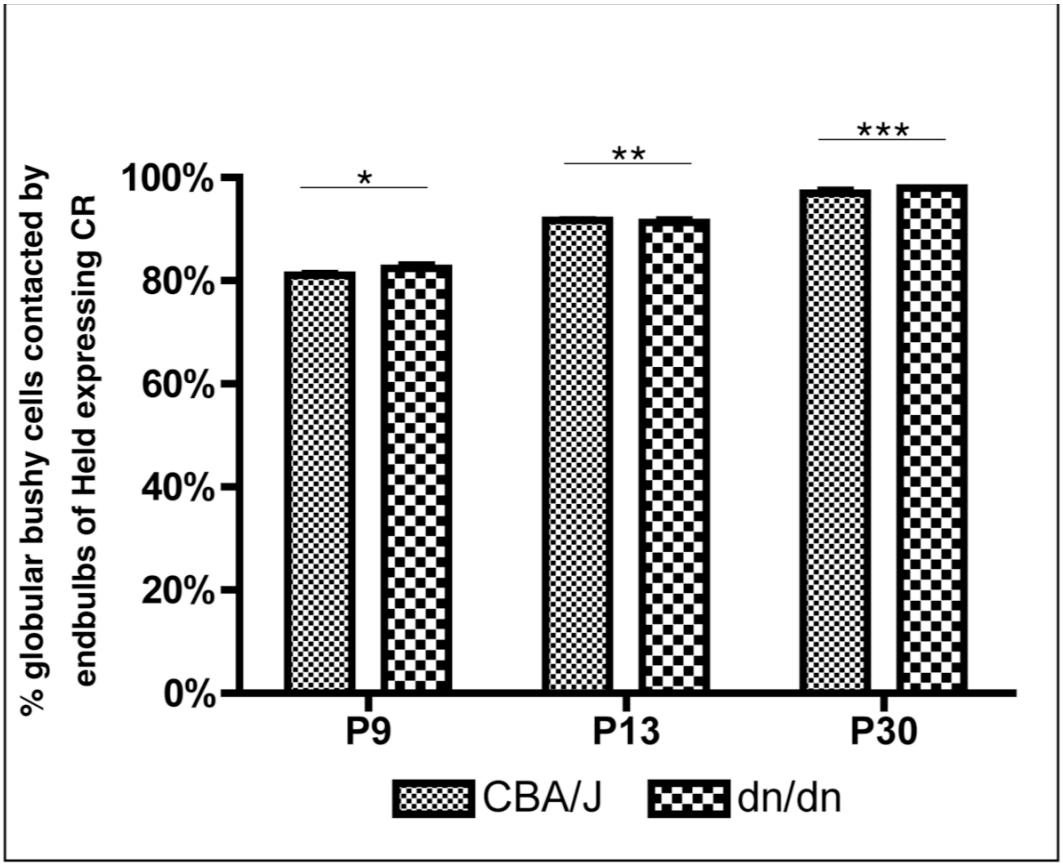

Age	% globular bushy cells contacted by endbulbs of Held expressing CR*	
	CBA/J	dn/dn
P9	81.1 ± 0.6	82.4 ± 0.9
P13	91.7 ± 0.4	91.3 ± 0.7
P30	97.0 ± 0.9	98.0 ± 1.2

*Mean ± SEM

Figure 57: Calretinin expression in AVCN globular bushy cells.
Top shows the percent of globular bushy cells found throughout in the AVCN which express CR. A significant increase in the expression of CR was found in CBA/J as well as *dn/dn* mice from 9 days postnatal to 13 days postnatal. In neither strain were further developmental increases were detected after postnatal day 13. No significant differences were detected in the proportion of principal cells expressing CR between age matched CBA/J and *dn/dn* animals. Double asterisk indicates $p<0.001$. **Bottom:** Chart of data used in graph (above).

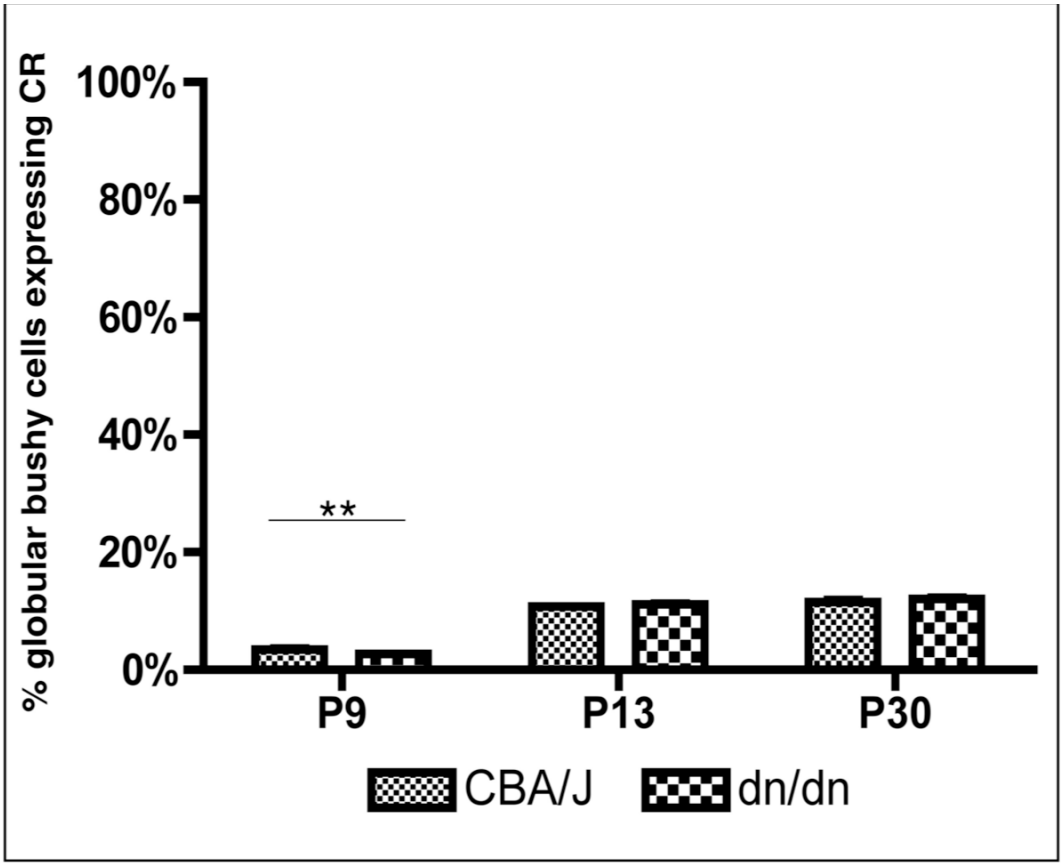

Age	% globular bushy cells expressing CR*	
	CBA/J	dn/dn
P9	3.5 ± 0.4	2.7 ± 0.2
P13	10.8 ± 0.2	11.1 ± 0.4
P30	11.6 ± 0.6	12.0 ± 0.6

*Mean ± SEM

Figure 58. Calbindin D-28k expression in the globular cell area of the AVCN of normal hearing (CBA/J) mice at 30 days postnatal. CB-IR is absent from cochlear nerve fibers and presynaptic endbulb of Held terminals, and expressed in only a minority of globular bushy cell somata. No difference in CR expression seen between normal hearing (CBA/J) and congenitally deaf (*dn/dn*) mice at this age. **A-C:** 20x double immunofluorescence images with Nissl stain (FITC) and primary antibodies against CB (CY-3) are shown in a 14μm thick section of AVCN in a P30 CBA/J mouse. **D-F:** 60x double immunofluorescence images with Nissl stain (FITC) and primary antibodies against CB (CY-3) are shown in a 14μm thick section of AVCN in a P30 CBA/J mouse. Asterisks indicate CB-positive GBCs. 20x Scale bar = 100μm. 60x scale bar = 10μm. D = dorsal. M = medial.

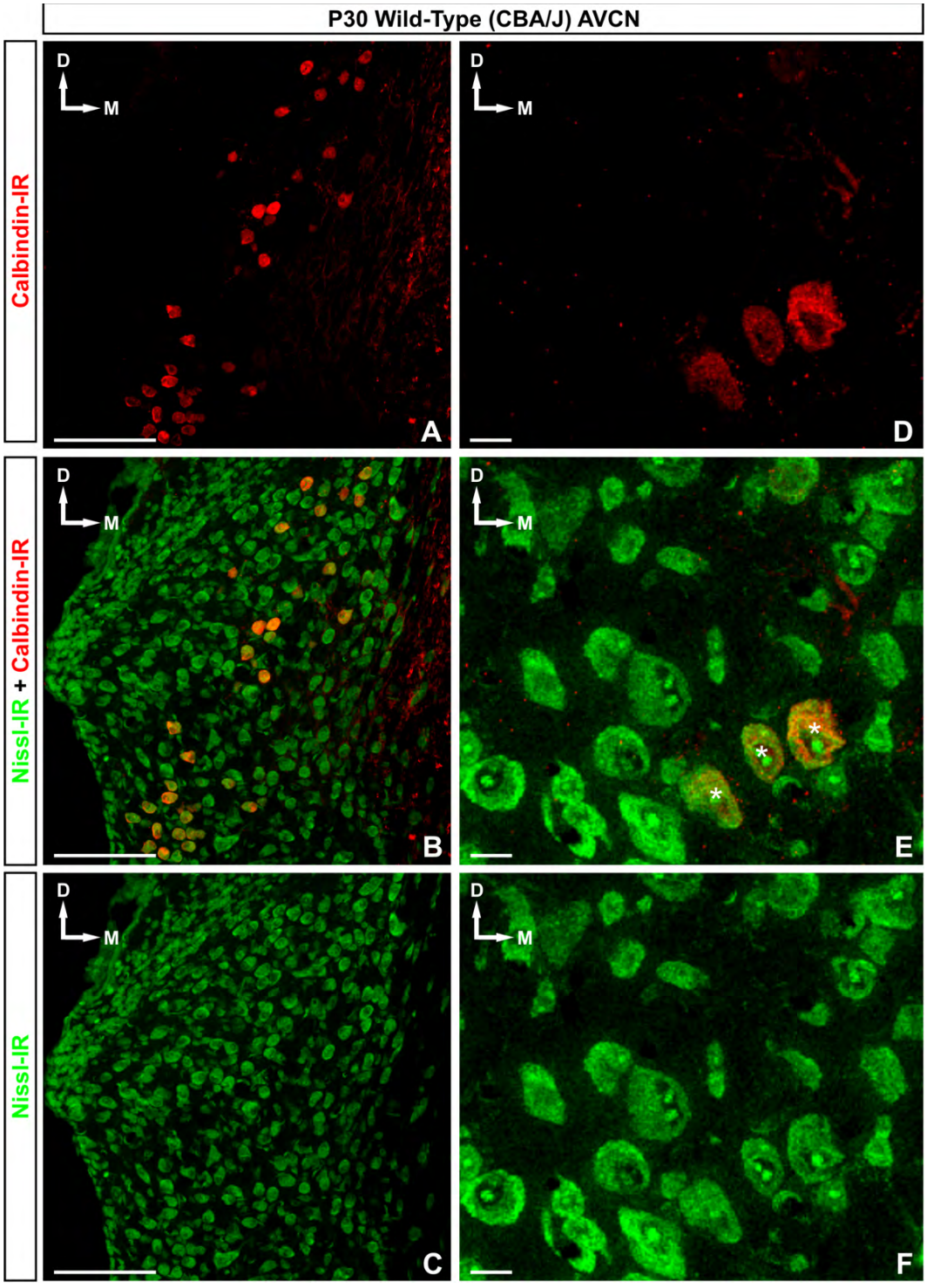
P30 Wild-Type (CBA/J) AVCN
Calbindin-IR
Nissl-IR + Calbindin-IR
Nissl-IR
D
M
A
B
C
D
E
F
*
*
*

Figure 59. Calbindin D-28k expression in the globular cell area of the AVCN of congenitally deaf (*dn/dn*) mice at 30 days postnatal. CB-IR is absent from cochlear nerve fibers and presynaptic endbulb of Held terminals, and expressed in only a minority of globular bushy cell somata. No difference in CR expression seen between normal hearing (CBA/J) and congenitally deaf (*dn/dn*) mice at this age. **A-C:** 20x double immunofluorescence images with Nissl stain (FITC) and primary antibodies against CB (CY-3) are shown in a 14μm thick section of AVCN in a P30 *dn/dn* mouse. **D-F:** 60x double immunofluorescence images with Nissl stain (FITC) and primary antibodies against CB (CY-3) are shown in a 14μm thick section of AVCN in a P30 *dn/dn* mouse. Asterisks indicates CB-positive GBCs. 20x Scale bar = 100μm. 60x scale bar = 10μm. D = dorsal. M = medial.

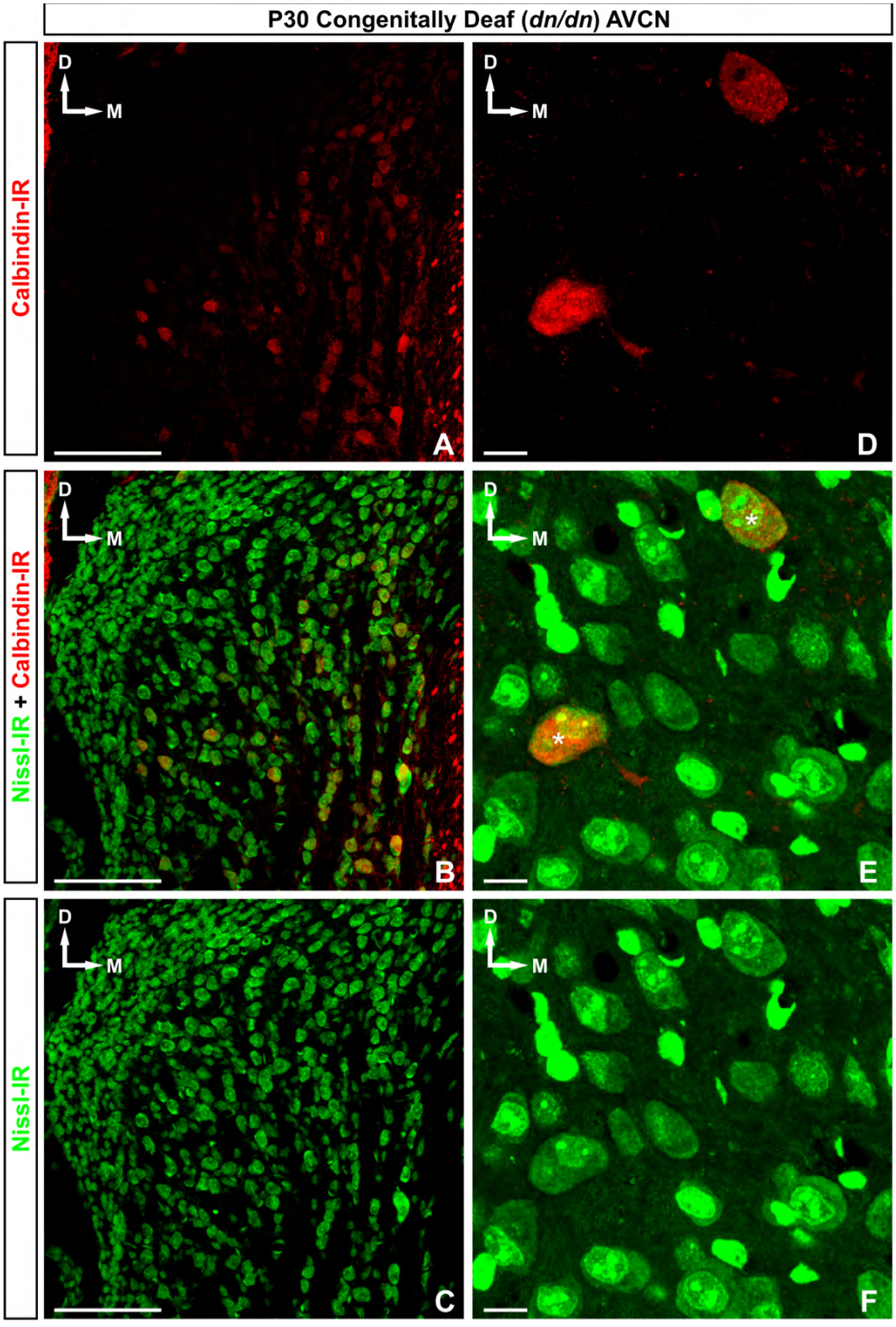
P30 Congenitally Deaf (dn/dn) AVCN
Calbindin-IR
Nissl-IR + Calbindin-IR
Nissl-IR
D
M
A
B
C
D
E
F
*
*

Figure 60: Calbindin D-28k expression in AVCN globular bushy cells.
Top shows the percent of globular bushy cells found throughout in the AVCN which express CB. A significant increase in the expression of CB was found in CBA/J as well as *dn/dn* mice from 9 days postnatal to 13 days postnatal. In neither strain were further developmental increases were detected after postnatal day 13. No significant differences were detected in the proportion of globular bushy cells expressing CB between age matched CBA/J and *dn/dn* animals. Double asterisk indicates $p<0.001$. **Bottom:** Chart of data used in graph (above).

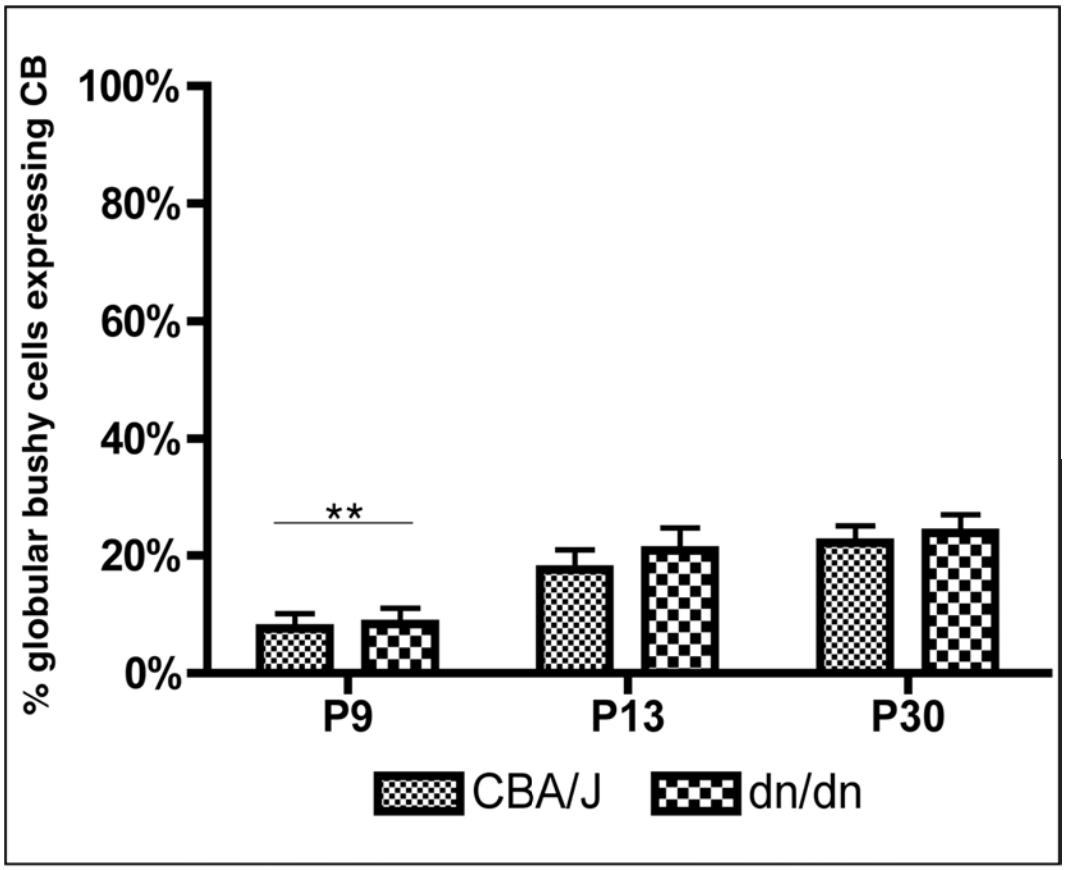

Age	% globular bushy cells expressing CB*	
	CBA/J	dn/dn
P9	7.7 ± 2.5	8.3 ± 2.7
P13	18.6 ± 3.4	20.9 ± 3.8
P30	22.3 ± 2.8	23.8 ± 3.1

*Mean ± SEM

Figure 61. Parvalbumin expression in the globular cell area of the AVCN of normal hearing (CBA/J) and congenitally deaf (*dn/dn*) mice at 9 days postnatal. 20x double immunofluorescence images with Nissl stain (FITC) and primary antibodies against PV (CY-3) are shown in a 14μm thick section of AVCN in a P9 CBA/J (**A-C**) and *dn/dn* (**D-F**) mouse. In both strains, PV is expressed in a majority of cochlear nerve fibers, presynaptic endbulb of Held terminals, and globular bushy cell somata. Intensity of PV staining is brighter presynaptically than postsynaptically. No difference in PV expression seen between normal hearing (CBA/J) and congenitally deaf (*dn/dn*) mice at this age. Scale bar = 100μm. D = dorsal. M = medial.

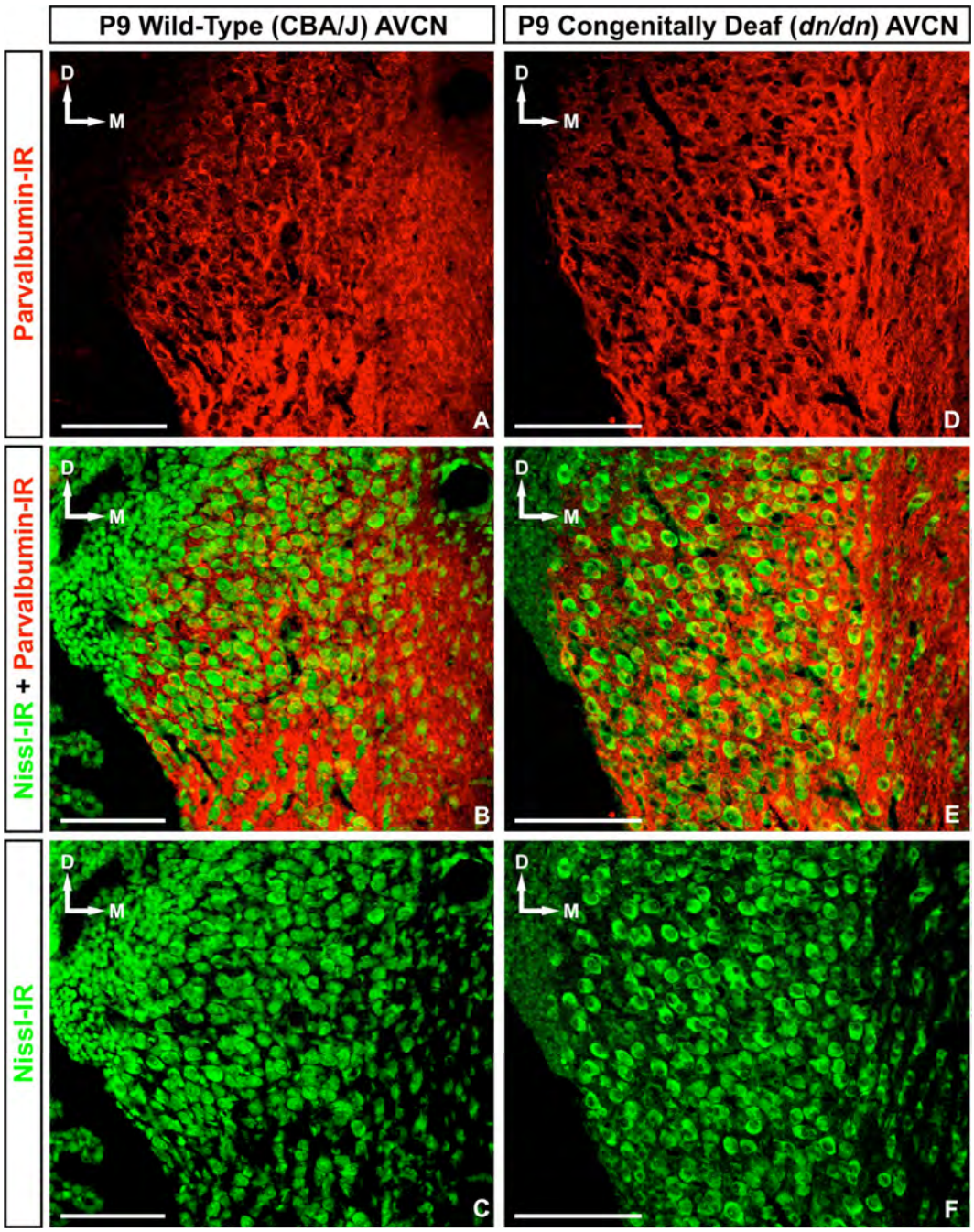
P9 Wild-Type (CBA/J) AVCN
P9 Congenitally Deaf (dn/dn) AVCN
Parvalbumin-IR
Nissl-IR + Parvalbumin-IR
Nissl-IR
D
M
A
B
C
D
E
F

Figure 62. Parvalbumin expression in the globular cell area of the AVCN of normal hearing (CBA/J) and congenitally deaf (*dn/dn*) mice at 13 days postnatal. 20x double immunofluorescence images with Nissl stain (FITC) and primary antibodies against PV (CY-3) are shown in a 14μm thick section of AVCN in a P9 CBA/J (**A-C**) and *dn/dn* (**D-F**) mouse. In both strains, PV is expressed in a majority of cochlear nerve fibers, presynaptic endbulb of Held terminals, and globular bushy cell somata. No difference in PV expression seen between normal hearing (CBA/J) and congenitally deaf (*dn/dn*) mice at this age. Scale bar = 100μm. D = dorsal. M = medial.

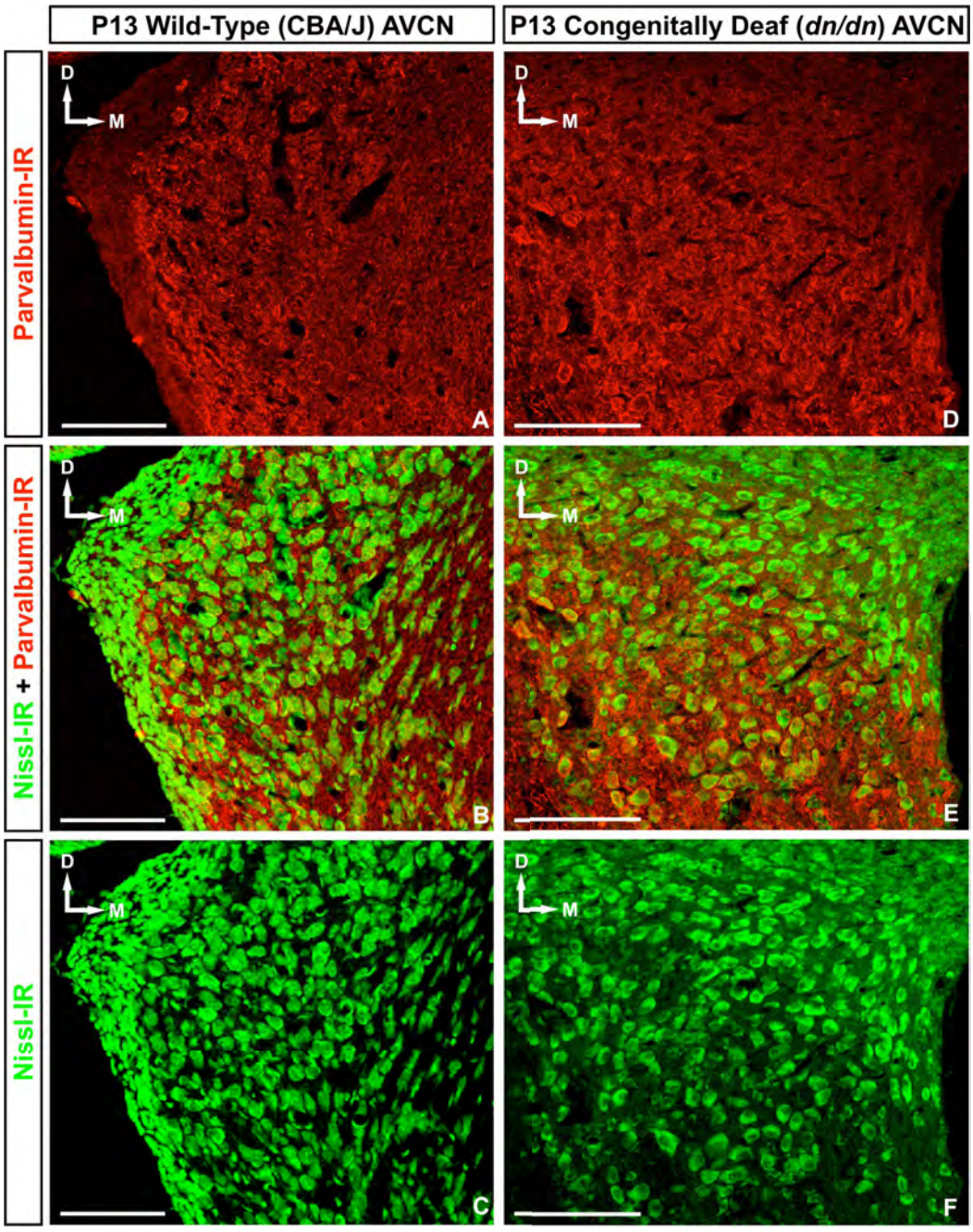
P13 Wild-Type (CBA/J) AVCN
P13 Congenitally Deaf (dn/dn) AVCN
Parvalbumin-IR
Nissl-IR + Parvalbumin-IR
Nissl-IR
D
M
A
B
C
D
E
F

Figure 63. Parvalbumin expression in the globular cell area of the AVCN of normal hearing (CBA/J) and congenitally deaf (*dn/dn*) mice at 30 days postnatal. 20x double immunofluorescence images with Nissl stain (FITC) and primary antibodies against PV (CY-3) are shown in a 14μm thick section of AVCN in a P9 CBA/J (**A-C**) and *dn/dn* (**D-F**) mouse. In both strains, PV is expressed in a majority of cochlear nerve fibers, presynaptic endbulb of Held terminals, and globular bushy cell somata. No difference in PV expression seen between normal hearing (CBA/J) and congenitally deaf (*dn/dn*) mice at this age. Scale bar = 100μm. D = dorsal. M = medial.

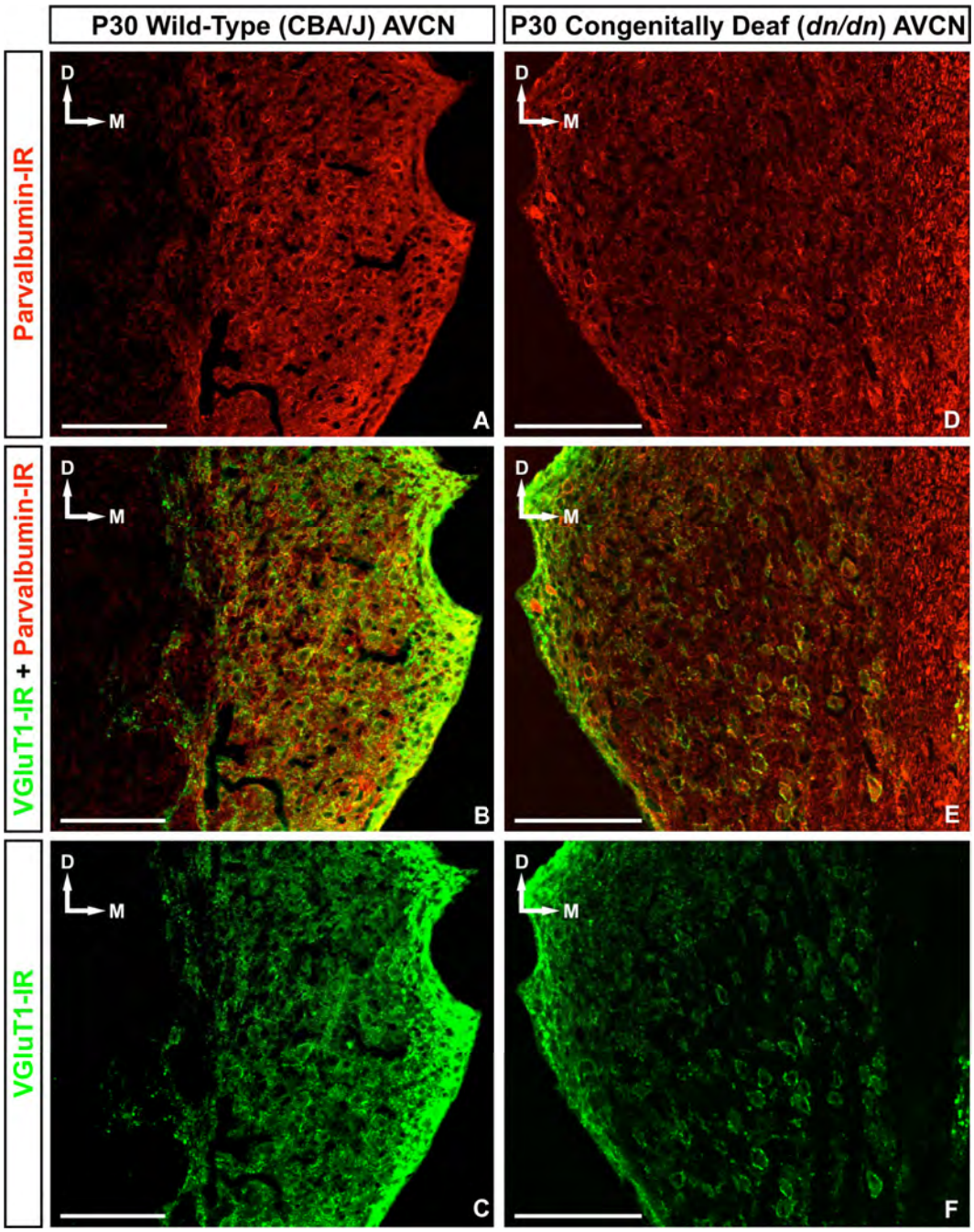
P30 Wild-Type (CBA/J) AVCN
P30 Congenitally Deaf (dn/dn) AVCN
Parvalbumin-IR
VGluT1-IR + Parvalbumin-IR
VGluT1-IR
D
M
A
B
C
D
E
F

Figure 64: Parvalbumin expression in endbulbs of Held.
Top shows the percent of globular bushy cells found throughout in the AVCN which are contacted by endbulbs of Held expressing PV. A significant increase in the expression of PV was found in CBA/J as well as *dn/dn* mice from 9 days postnatal to 13 days postnatal. In neither strain were further developmental increases were detected after postnatal day 13. No significant differences were detected in the proportion of globular bushy cells contacted by endbulbs expressing PV between age matched CBA/J and *dn/dn* animals. Single, double, and triple asterisk indicates $p<0.001$. **Bottom:** Chart of data used in graph (above).

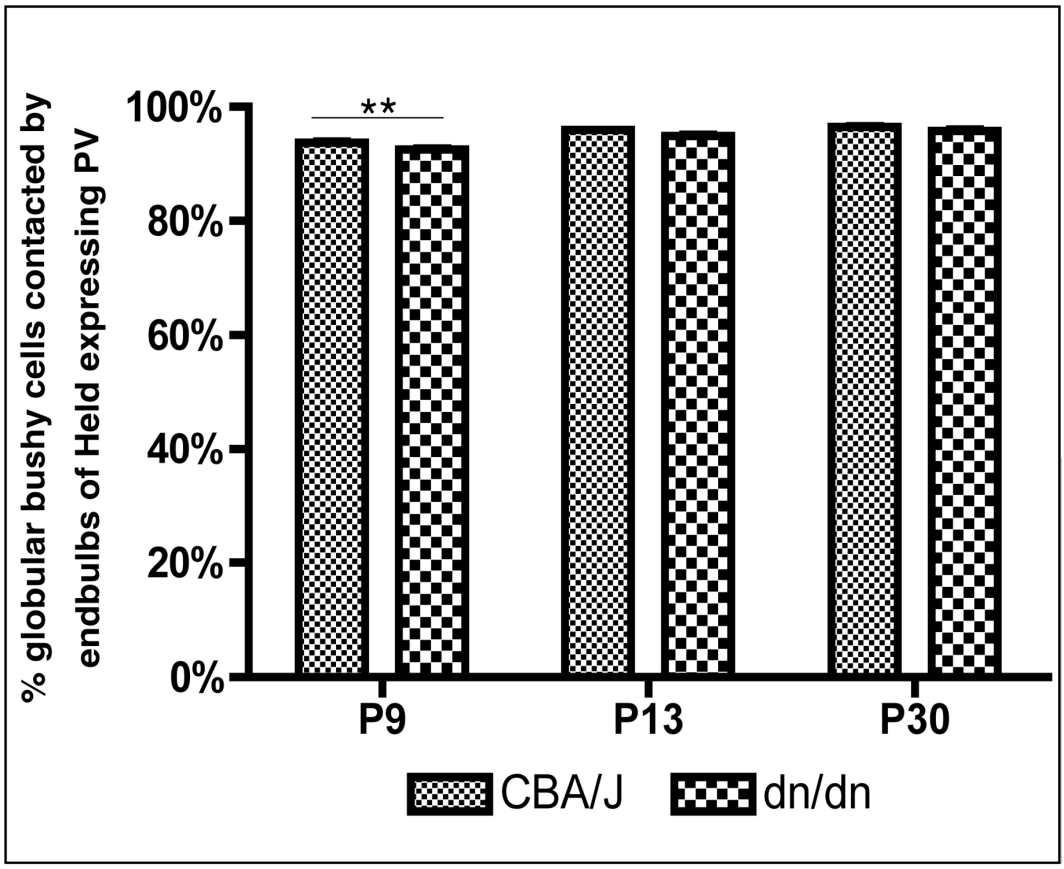

Age	% globular bushy cells contacted by endbulbs of Held expressing PV*	
	CBA/J	dn/dn
P9	93.7 ± 0.5	92.5 ± 0.4
P13	95.9 ± 0.2	95.6 ± 0.5
P30	95.5 ± 0.4	96.4 ± 0.5

*Mean ± SEM

Figure 65: Parvalbumin expression in AVCN globular bushy cells.
Top shows the percent of globular bushy cells found throughout in the AVCN which express PV. A significant increase in the expression of PV was found in CBA/J as well as *dn/dn* mice from 9 days postnatal to 13 days postnatal. In neither strain were further developmental increases were detected after postnatal day 13. No significant differences were detected in the proportion of principal cells expressing PV between age matched CBA/J and *dn/dn* animals. Double asterisk indicates $p<0.001$. **Bottom:** Chart of data used in graph (above).

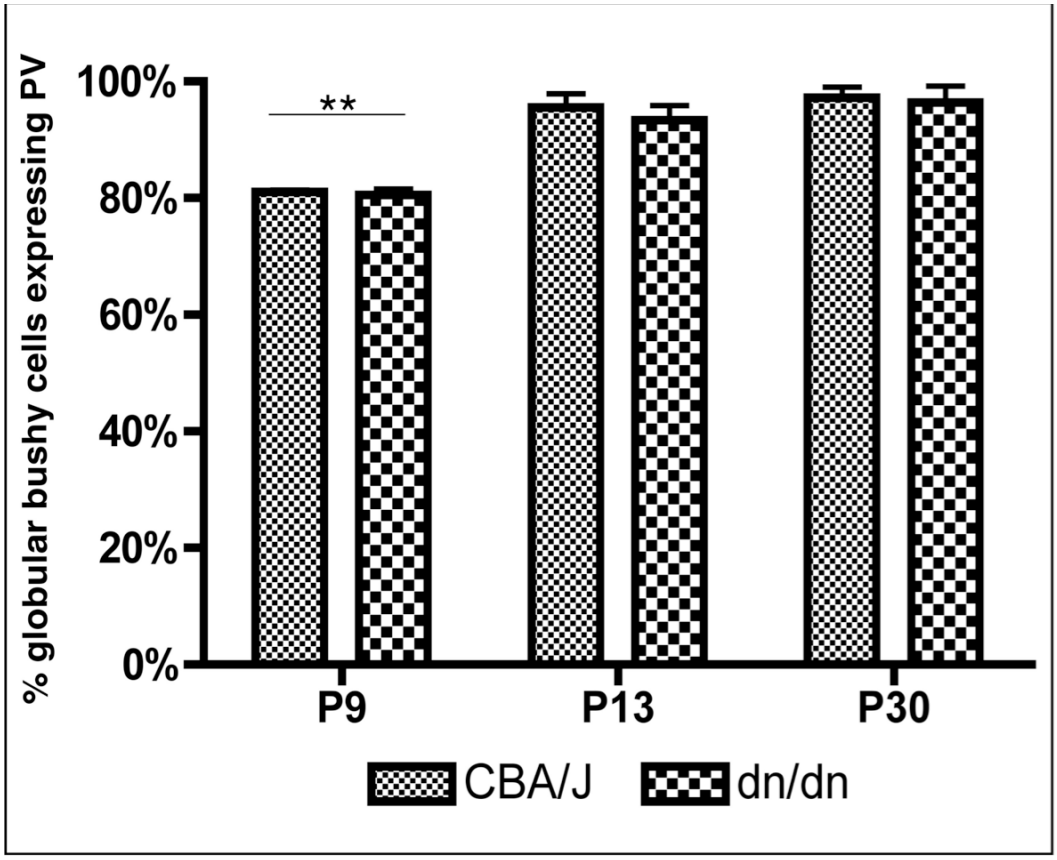

Age	% globular bushy cells expressing PV*	
	CBA/J	dn/dn
P9	81.0 ± 3.7	80.5 ± 1.0
P13	95.5± 2.4	93.4 ± 2.5
P30	97.2 ± 1.8	96.4 ± 2.8

*Mean ± SEM

Figure 66: The octopus cell area in normal hearing mice (CBA/J) at 9 days postnatal. The octopus cell is identified by its long primary dendrites extending from the cell body like tentacles of an octopus. **A-C:** 60x double immunofluorescence images with primary antibodies against VGluT1 (FITC) and CR (CY-3) are shown in a 14μm thick confocal stack of an octopus cell in a P9 CBA/J mouse. Arrows indicate long primary dendrites extend from the octopus cell soma, indicated by the asterisk. Note the cell soma and primary branches receive numerous small VGluT-IR synaptic contacts from cochlear nerve fibers. Double asterisk indicates a second octopus cell soma visible in the plane of section. **D-F:** Single optical section of the octopus cell shown in A-C. Asterisk indicates the cell body. Arrows indicate primary dendrites. Note the absence of CR immunoreactivity in the octopus cell, but the presence if CR immunoreactivity in its small VGluT1-IR presynaptic contacts. **G-I:** Same as D-F but in different optical plane. Scale bar = 10μm. D = dorsal. M = medial.

P9 Wild-Type (CBA/J) AVCN
Confocal Image Stack
Single Optical Plane
Single Optical Plane
Calretinin-IR
VGluT1-IR + Calretinin-IR
VGluT1-IR
A
B
C
D
E
F
G
H
I
D
M

Figure 67: The octopus cell area in normal hearing mice (CBA/J) at 9 and 30 days postnatal. **A-C:** 20x double immunofluorescence images with primary antibodies against VGluT1 (FITC) and CR (CY-3) are shown in a 14μm thick confocal stack of an octopus cell in a P9 CBA/J mouse. Circled area indicates a group of octopus cells devoid of CR immunoreactivity. At P9, neuropil is scant, ad octopus cells appear very close together in tissue section. Note the cell soma and primary branches receive numerous small VGluT-IR synaptic contacts from cochlear nerve fibers. **D-F:** 20x double immunofluorescence images with primary antibodies against VGluT1 (FITC) and CR (CY-3) are shown in a 14μm thick confocal stack of an octopus cell in a P30 CBA/J mouse. Arrows indicate several octopus cells. At P30, individual octopus cells are separated by neuropil and correspond to the classic description of individual cells scattered in a sea of neuropil. Nearly all octopus cells at this age are brightly CR immunoreactive. Scale bar = 100μm. D = dorsal. M = medial.

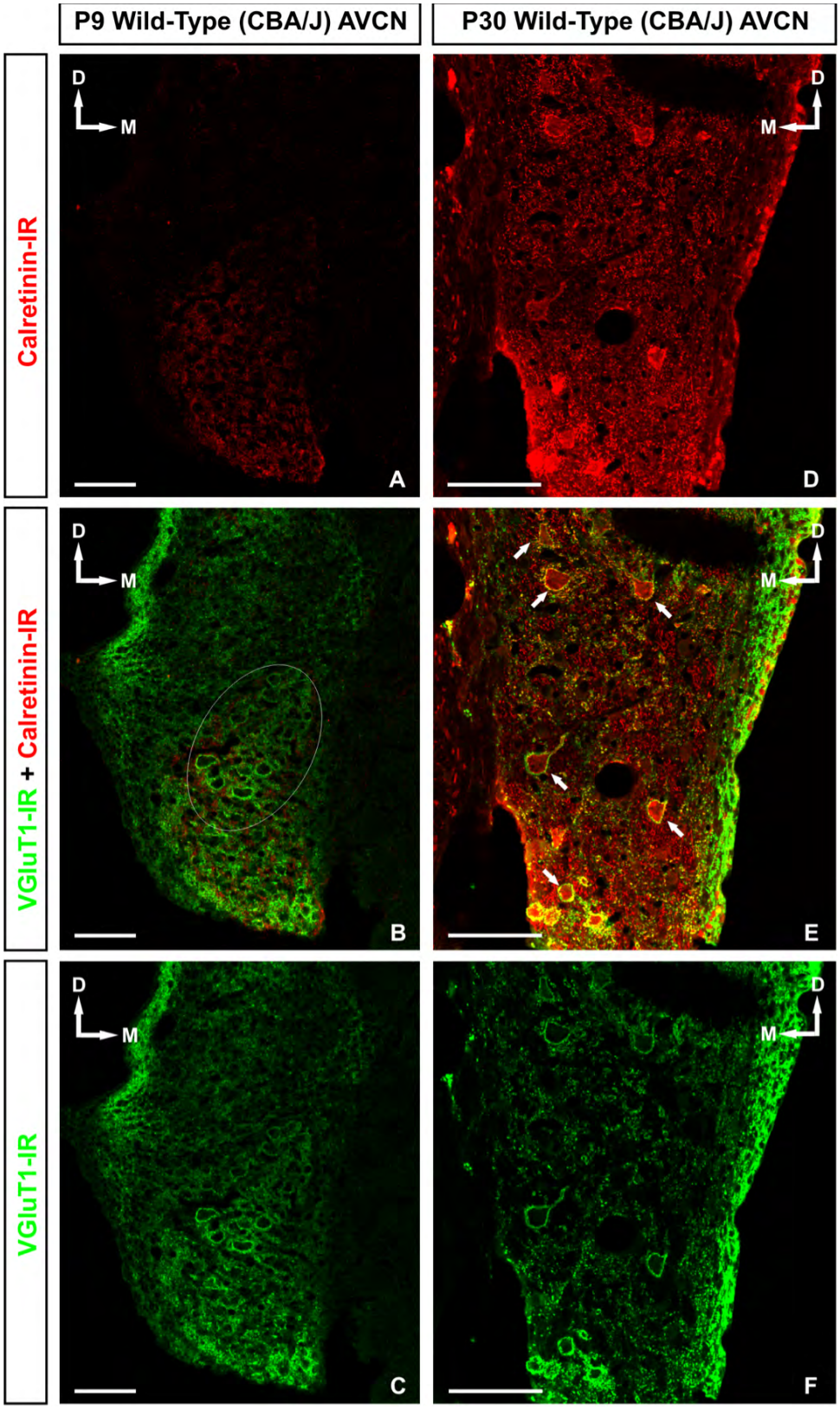
P9 Wild-Type (CBA/J) AVCN
P30 Wild-Type (CBA/J) AVCN
Calretinin-IR
VGluT1-IR + Calretinin-IR
VGluT1-IR
D
M
A
B
C
D
E
F

Figure 68: The octopus cell in normal hearing mice (CBA/J) at 9 and 30 days postnatal. **A-C:** 60x double immunofluorescence images with primary antibodies against VGluT1 (FITC) and CR (CY-3) are shown in a P9 CBA/J mouse. Asterisks indicate several octopus cell somata devoid of CR immunoreactivity. At P9, neuropil is scant, ad octopus cells appear very close together in tissue section. Note the cell soma and primary branches receive numerous small VGluT-IR synaptic contacts from cochlear nerve fibers. These synaptic contacts co-express CR. **D-F:** 60x double immunofluorescence images with primary antibodies against VGluT1 (FITC) and CR (CY-3) are shown in a P30 CBA/J mouse. At P30, the cell body and primary dendrites (arrow) are brightly immunoreactive for CR. Numerous small VGluT1-IR synaptic contacts which co-express CR are visible terminating on the cell body and primary dendrite of the octopus cell. Scale bar = 10μm. D = dorsal. M = medial.

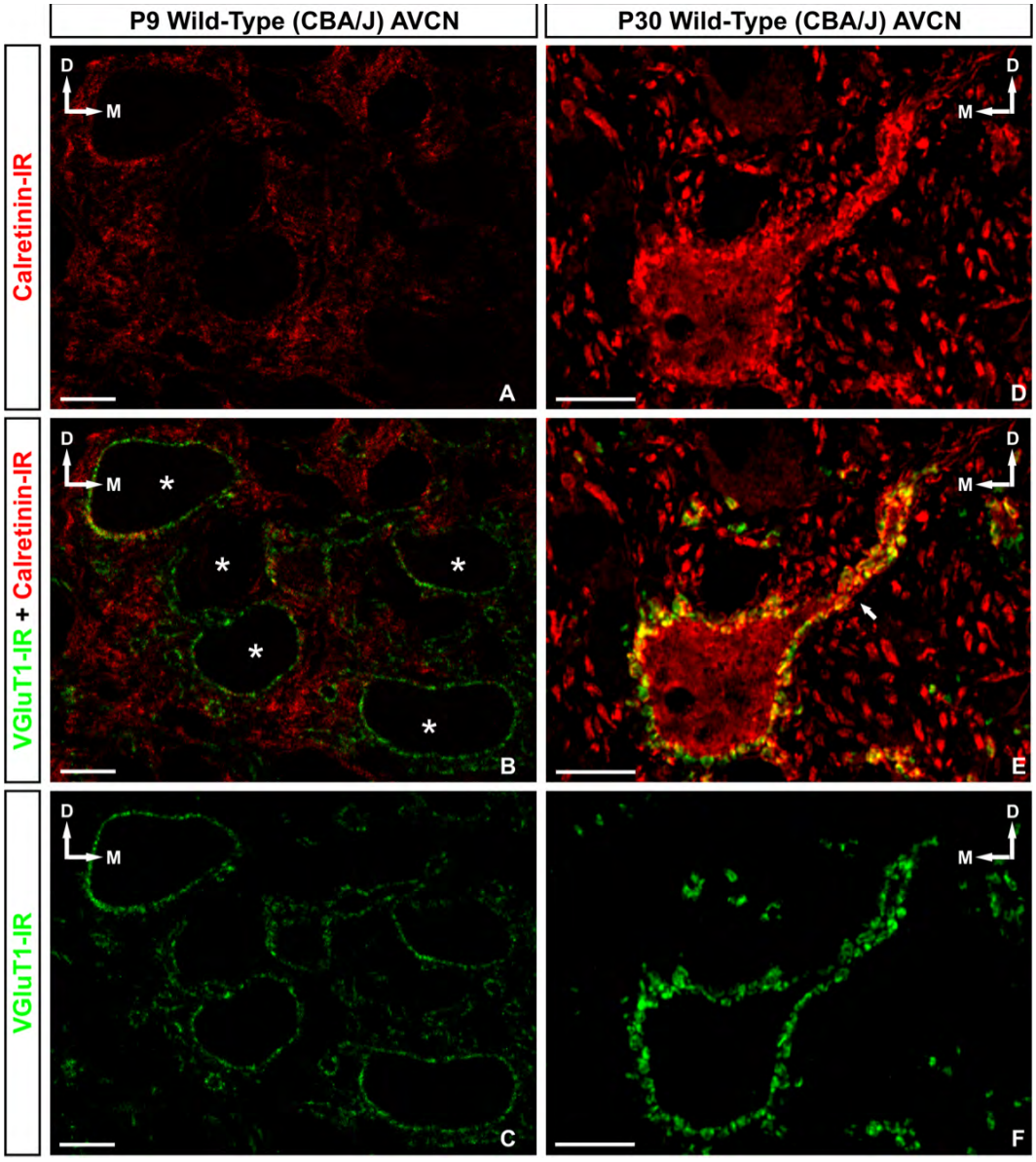
P9 Wild-Type (CBA/J) AVCN
P30 Wild-Type (CBA/J) AVCN
Calretinin-IR
VGluT1-IR + Calretinin-IR
VGluT1-IR
D
M
A
B
C
D
E
F

XV. CONCLUSIONS

The pattern of expression for the calcium buffering proteins calretinin (CR), calbindin D-28k (CB), and parvalbumin (PV) in the medial nucleus of the trapezoid body (MNTB) and anteroventral cochlear nucleus (AVCN) is unique for each calcium buffering protein.

Within the MNTB, nearly every principal cell expresses CB and PV and a subset of predominantly of medially located principal cells also express CR. Additionally, nearly every calyx of Held expresses PV and a subset of predominantly laterally located calyces also expresses CR. This pattern of CR expression within the MNTB, which corresponds with the MNTB tonotopic map, may implicate distinct roles of pre- and postsynaptic CR in low vs. high frequency auditory processing. There is no indication from these experiments that CB or PV is differentially expressed along the tonotopic map, however, detailed analysis of immunofluorescence intensity needs to be performed to quantify the relative amount of expression of each calcium buffering protein within each principal cell and calyx of Held.

Within the AVCN, early every globular bushy cell expresses PV while only a minority also express either CB or CR. A globular bushy cell which simultaneously expresses all three calcium buffering proteins was not observed in this study. These data indicate the possibility for unique functional roles for CR and CB within globular bushy cells, although a detailed analysis of the frequency map of the AVCN globular bushy cell area needs to be performed before specific

functions can be postulated. Further, these experiments suggest that nearly every endbulb of Held expresses both CR and PV. Given that CR and PV have rapid and slow calcium binding kinetics, respectively, it is possible that within endbulbs PV may serve to accelerate the decay of $[Ca^{2+}]_I$ while CR decreases the amplitude of the Ca^{2+} signal.

Interestingly, very few differences are seen in the developmental pattern of PV, CB, and CR expression between normal hearing (CBA/J) and congenitally deaf (*dn/dn*) mice. The most striking alteration in protein expression in response to an absence of afferent stimulation observed in these experiments is in CR expression in the MNTB. While the general

topographic pattern of CR expression is quite similar in CBA/J and *dn/dn* mice, by P49 developmental divergences between these two strains create subtle differences between their patterns of CR expression. In the end, P49 CBA/J mice express CR primarily in calyces of Held which may be found throughout the nucleus, but are more likely to be found in the lateral portion. They express very little somatic CR, but those principal cells that do are preferentially located in the medial part of the nucleus. P49 *dn/dn* mice express CR mainly in principal cell somata, which may be located anywhere in the nucleus, but the vast majority of which are located in the medial portion. These mice express calyceal CR as well, but far less than age matched CBA/J mice and rarely located outside the lateral third of the nucleus.

In conclusion, it appears that the specific pattern of calcium buffering proteins expression is necessary to ensure precise fidelity of high frequency

synaptic transmission, and that numerous variables, some activity-driven and some not, control this expression. In order to develop a more accurate quantitative analysis of calcium buffering protein expression, DAB experiments followed by optical density analysis need to be performed. By doing so, researchers may be able to ascertain more subtle differences in protein expression, indicating an even greater role in afferent auditory nerve activity in synaptic maturation.

XVI. APPENDIX 1

THE AUDITORY CODE

The mammalian auditory system represents a marvelous achievement in the biological optimization of neuronal signaling. The human internal ear can detect acoustic information over an intensity range spanning twelve orders of magnitude (120 dB) and a frequency range of 20 Hz to 20 kHz, while bats and whales can detect frequencies as high as 100 kHz (Robles and Ruggero, 2001). Trained musicians can distinguish tones that differ in pitch by only 0.1%, and when localizing sounds in space, the average human can compare differences as small as 10 μs in the time the signal reaches each ear. Such performance requires a neural code exhibiting a temporal responsiveness that far exceeds that of vision (Hudspeth, 1997).

The auditory temporal code exists in different forms, yet the timing of action potentials remains the common denominator of auditory processing (Trussell, 1999). From cochlea to cortex, it is the lingua franca used to transmit information regarding the envelope, frequency, and intensity of sound. Inner hair cells encode the periodicity and temporal features of an acoustic waveform with remarkable precision, and central pathways serve as parallel processing arrays that sharpen and preserve the timing of action potentials through sequential synaptic levels.

The rate at which synaptic activation can follow the periodicity of sound depends on the temporal resolution of neurotransmitter release from inner hair cells as well as peripheral response properties of the spiral ganglion cells on which the neurotransmitter acts. As acoustic information traverses peripheral and central structures, and signals are continually and necessarily passed from synapse to axon to synapse, conduction and synaptic delays will inevitably accumulate. It is crucial, therefore, for the precise processing temporal information, that these delays be highly uniform.

The series of events underlying action potential propagation and synaptic communication provides a framework for understanding the source of these delays and the manner in which they can accumulate. After its initiation, an action potential propagates down the axon and eventually reaches the presynaptic bouton, where it provides the depolarizing stimulus necessary to open voltage gated calcium channels. The delay, called the conduction delay, between action potential initiation and the moment it reaches the bouton depends on the length of the axon and the velocity of the action potential. Coupling the presynaptic calcium current to the release of neurotransmitter also presents several sources of delay, among which is the interaction between the depolarizing presynaptic action potential waveform and the kinetics of voltage gated calcium channels, the diffusion of Ca^{2+} from the Ca_v channel to appropriate Ca^{2+} sensors, fusion of the synaptic vesicle to the cell membrane, and diffusion of neurotransmitter across the synaptic cleft and subsequent binding to postsynaptic receptors. Finally, the shape of the excitatory postsynaptic potential (EPSP), which can be modulated by

Ca^{2+}, is fundamental to precise processing of temporal cues since narrow EPSPs help to minimize temporal summation. Since Ca^{2+} is so closely tied to these delays, it is important to have an understanding of the expression of calcium binding proteins within the auditory system.

Mechano-electrical transduction at the inner hair cell

The general mechanisms whereby higher vertebrates hear seem to have evolved with the ancient reptiles (Oertel, 1999). Of the inner ear, A.J Hudspeth (1997) said "[it] is an evolutionary triumph of miniaturization, a three-dimensional inertial guidance system and an acoustical amplifier and frequency analyzer compacted into the volume of a child's marble. That we are ordinarily oblivious to what goes on within the [bony] labyrinth reflects the ear's reliable performance: our bipedal stance, our capacity for locomotion on foot and in vehicles, and our ability to communicate vocally all stem from the ear's incessant activity [which]… in turn owes its success to its complement of hair cells." That receptors similar in structure and function exist in the inner ears of nearly all vertebrates is testimony to the evolutionary success of this remarkable cell.

Sound localization is one of the most important roles of hearing. Information regarding the location of sound is extracted from interaural timing differences (ITD) and interaural intensity differences (IID). These differences are a functional consequence of the separation of peripheral auditory receptors about the head. Because of this anatomical specialization, sound originating from any point in space not equidistant from the two ears will differ in arrival time,

intensity levels and/or phase characteristics at each ear. In other words, the separation of the ears about the head creates differences in arrival time and intensity levels that are represented by patterns of activity in central neuronal structures encoding the source of the sound. While temporally precise network computation by central auditory circuits is required to extract timing and intensity differences from neuronal code (Joris et al. 1994), the inner hair cell – the site of original encryption of the acoustic stimulus - remains the pivotal lynchpin of the system. In transducing sound waves to neural signals, the inner hair cell must encode the onset, duration, amplitude, and phase of the sound with the highest possible temporal acuity so that central auditory nuclei can compare essential timing information from each ear to localize the sound.

The hair bundle

The defining feature (the feature for which they are, in fact, named) of a hair cell is the hair bundle, a complex mechano-electrical conduction apparatus comprised of a V-shaped array of dozens to hundreds of specialized microvilli, called stereocilia, that protrude form the apical surface of the cell (Hudspeth and Jacobs, 1979). Each process is a tubular, isodiamteric evagination of plasmalemma stiffened by a cytoskeleton of actin filaments extensively cross-linked by fimbrin (Hudspeth, 1997). Approximately one micrometer above their base, the diameters of stereocilia drastically attenuate from between 100 – 900 nm to below 100 nm, corresponding to a decrease in actin filaments from as many 3000 to about 20 (Hudspeth, 1989).

Each hair bundle is interconnected by various linking molecules, such that a single microvillus is incapable of independent movement. Scanning and transmission electron microscopy has revealed a specific type of cadherin-like, inter-stereociliary connection known as tip links, which are 150 – 200 nm long helical filaments that extend from the tip of each stereocilium to its next tallest neighbor (Jaramillo, 1995, Kachar, et al., 2000). Tip links are essentially asymmetric adhesion complexes composed of cadherin 23 (CDH23) and protocadherin 15 (PCDH15) which interact at their N-termini to form the upper and lower parts of the tip link, respectively (Kazmierczak, et al., 2007).[1] Experimental evidence gathered from current sink experiments in which extracellular potentials were measured from various points around a stimulated hair cell in the frog sacculus has suggested that these tip links are coupled to mechanically gated cation channels (Hudspeth, 1982).

The stereocilia vary in length from one end of the hair bundle to the other, such that the V-shaped array has the appearance of a beveled needle. Tip links take advantage of this asymmetry in height. Incoming sound waves deflect the bundle by applying a mechanical force at a right angle to its long axis, causing the stereocilia to pivot at their attenuated base (Hudspeth,1989). When deflection occurs in the positive direction (toward its tallest edge), the height differential creates a shearing motion between adjacent stereocilia that stretches each tip link (Hudspeth,1997). At rest, about 15% of the mechanosensitive cation channels are

[1]Interestingly, adhesion between cadherins is typically optimal at concentrations ≥1 mM Ca^{2+}. However, interactions between CDH23 and PCDH15 are maximal at ≥0.1 mM Ca^{2+}, which is well within the range of Ca^{2+} concentration of the endolymph. This may be due to a lack of Trp residues, which are found on the extracellular cadherin (EC) domain EC1 of typical cadherins, but are distinctly absent from CDH23 and sparse in PCDH15 (Kazmierczak, et al., 2007).

open, sustaining high rates of spontaneous transmitter release. However, as tip links stretch, the increased tension exerts a force to mechanosensitive transduction channels, instantaneously increasing their open probability and creating an inward K^+ current that depolarizes the cell (Fettiplace and Ricci, 2003; Kennedy et al., 2003)[1]. Upon depolarization, open probability of somatic voltage gated Ca^{2+} channels ($Ca_v1.3$) rises, increasing the release of neurotransmitter and activating large conductance Ca^{2+}-activated K^+ channels (BK) that repolarize the cell (Roberts, et al. 1990; Fuchs, et al., 2003)[2]. Conversely, deflecting the hair bundle in the negative direction decreases the open probability of the cation channels, reduces baseline K^+ current and hyperpolarizes the cell.

Acoustic stimulus transduction

Sound, by definition, is a mechanical disturbance which propagates itself through a conductive medium. (Because of its physiological significance, the conductive medium used for purposes of the current discussion shall be air but may be any gas, liquid, or solid capable of transmitting vibrations of a certain frequency and intensity to be within an organism's audible range. In fact, sound energy reaching the inner hair cell is conveyed through endolymph, a liquid!) Most of the sounds in which we are interested, especially speech and music,

[1] Typically, K^+ conductance causes K^+ efflux and hyperpolarization, reflecting an equilibrium potential for K^+ below resting membrane potential. However, hair cell stereocilia are bathed in endolymph which has a high $[K^+]$ altering the equilibrium potential for K^+ to about 0mv. Ca^{2+} has also been proposed to carry receptor current, but its concentration is quite low in mammalian endolymph. Because the transduction channel is nonspecific, the current *in vivo* will be carried by cations approximately in proportion to their endolymphatic concentration (Corey and Hudspeth, 1979).

[2] Unlike the hair bundle, inner hair cell somata is bathed in perilymph, which has a $[K^+]$ roughly equal to that of extracellular fluid. Somatic K^+ conductance, therefore, is outwardly directed and will repolarize the cell.

involve sinusoidal oscillations in air pressure at one or several frequencies. A nearly infinite number of oscillators (ie: a falling book, vibrating guitar strings, or an organism's vocal cords) are capable of producing mechanical energy that results in audible sound. Such energy exerts a force which outwardly displaces air molecules from the region of space immediately adjacent to its source. When the force is removed, the molecules recoil. Conservation of energy dictates this mechanical disturbance propagate through air as a longitudinal pressure wave, a series of compressions and rarefactions of air molecules that spread through adjacent areas of space like ripples from a thrown pebble spreading out on the surface of a pond. Upon reaching the inner ear, the effect of these waves is to alternately displace stereocilia in the positive and negative direction such that the ensuing electrical response is sigmoidal in every instance.

The effectiveness of this system is quite extraordinary. Hair cells, like the photoreceptor and bipolar cells of the retina, tonically release neurotransmitter. This sustained release can evoke spontaneous action potentials in auditory nerve fibers at rates as high as 100 Hz. Since environmental noise is continuously varying (much like environmental light), hair cells respond to graded receptor potentials by modulating the tonic release of neurotransmitter as a function of stimulus intensity (Glowatzki and Fuchs 2002). Although hair cell displacement – response relationships vary across species, a high intensity acoustic stimulus capable of eliciting an electrical response of about 90% maximum occurs by deflecting stereocilia through an angle of about 1º, corresponding to a total displacement less than the diameter of the stereocilia itself (Fettiplace and Ricci,

2003). At the opposite extreme, a 3 kHz tone (the frequency at which human hearing is most sensitive) at threshold intensity moves the tympanic membrane approximately 0.3 nm, slightly less than the diameter of a single hydrogen atom. A movement that small is capable of bending the stereocilia through an angle of only 0.003 degree. Bending the Eiffel Tower through an angle of 0.003 degree would move its pinnacle by only a thumb's breadth, yet deflecting the stereocilia on this small scale will modulate transmitter release (Hudspeth, 1989).

It is worth noting, however, that given the narrow stimulus limits of stereocilia displacement and subsequent hair cell transduction, mechanoelectrical transduction is not static, and, reflecting an ability for dynamic adaptation, each end of the structurally distinct tip link is also functionally distinct (Kazmierczak, et al., 2007). The mechanical input must be tightly regulated by Ca^{2+}-controlled mechanisms of adaptation to preserve their high sensitivity for external stimuli, as well as generate resonance and confer tuning on transduction (see section on tonotopic map) (Fettiplace and Ricci, 2003). A non-muscle myosin, myosin-1c (Myo1c) has been shown to be associated with CDH23 in hair cell stereocilia and is absent in the CDH23-deficient *waltzer* mice, suggesting that it interacts with the upper end of tip links (Siemens et al., 2004; Kazmierczak, et al., 2007). Myo1c has been suggested to be an adaptation motor for mechanoelectrical transduction at the inner hair cell, capable of adjusting the insertion point of the upper end of the tip link and, thereby, altering the tension placed on the mechanosensitive transduction channel (Fettiplace and Ricci, 2003). This, in turn, suggests that the exerted tension applies a force to the stereocilia attached to the

lower end of the tip link, raising the possibility that the mechanosensitive gating spring may localize close with PCDH15 (Kazmierczak, et al., 2007).

The afferent synapse of the inner hair cell

In order to faithfully encode acoustic frequencies in the kilohertz range, the afferent synapse of the inner hair cell must respond with submillisecond precision. Direct transduction of the mechanical stimulus, in which a force directly displaces the gate from a channel's ion-passing pore without the intervention of a second messenger is an adaptation employed by hair cells to ensure rapid electrical transduction. However, as is the case with all peripheral synapses, this electrical signal must be again transduced into the chemical signal that is neurotransmission. In encoding the acoustic waveform, it is necessary that synaptic machinery controlling neurotransmission at the inner hair cell afferent synapse ensure that transmitter release is tightly bound to fluctuations in membrane potential.

Synaptic transmission occurs at the basolateral pole of the inner hair cell. In contrast to a typical presynaptic terminal, in which exocytosis is mediated through Ca^{2+} influx linked to P/Q-, N-, and/or R-type Ca^{2+} channels (Doughty, et al., 1998; Westenbroek et al, 1998; Catterall, W.A., 2000), roughly 92% of Ca^{2+} channels at inner hair cell active zones of the inner hair cell are L-type $Ca_v1.3$ channels that employ nanodomain control of transmitter release (Zidanich and Fuchs, 1995; Husdpeth, 1997; Brandt, et al. 2003; Brandt, et al., 2005; Moser, et al., 2006; Goutman and Glowatzki, 2007). The paucity of peripheral and central

synapses relegating transmitter release to $Ca_v1.3$ channels gives testament to their adaptive significance in the inner hair cell, where their distribution and kinetics ensure minimal delay in the coupling of the presynaptic Ca^{2+} current to the release of neurotransmitter.

L-type $Ca_v1.3$ channels activate at voltages close to resting potential (-65 mV to -77mV obtained by *in vitro* patch clamp studies) and do not inactivate to any significant degree, allowing the afferent synapse to modulate transmitter release in response to small deviations in membrane potential and prolonged stimulation (Lewis and Hudspeth, 1983, Brandt et al., 2003). This would seem ideally suited to the inner hair cell, which is responds to continued mechanical perturbations of the basilar membrane with graded changes in membrane potential rather than action potentials. However, when considering the coding of temporal structure, an important source of synaptic delay is the time between stimulus onset and the first channel opening. $Ca_v1.3$ channels activate close to resting potential, but at such low stimulus strength, the time constant for activation may be as high as several milliseconds (Moser et. al., 2006). It remains unclear how, at threshold intensity, a stimulus can elicit neuronal response that is phase locked to the auditory waveform in the face of such delays, but the answer may lie in the large number and distribution of the channels.

Each inner hair cell makes synaptic connections consisting of only one active zone on approximately ten to thirty auditory nerve fibers (Fuchs, 2005; Goutman, and Glowatzki, 2007). This connection represents the entire afferent signal for an auditory nerve fiber. At the active zone, 125 – 200 small clear

synaptic vesicles containing glutamate are tethered to a submicrometer, electron-dense structure called a synaptic ribbon (Khimich et al., 2005). Of the approximately 1700 $Ca_v1.3$ channels present in each inner hair cell, roughly 80 are located within an active zone. Ultrastructural and physiological studies of hair cell synaptic ribbons estimate a readily releasable pool of 50 – 60 vesicles, 5 – 30 of which are docked (Khimich et al, 2005; Fuchs, 2005). Although the actual channel-release sight topography is unknown, simply distributing the channels among sufficiently separated docked vesicles would yield 3-5 $Ca_v1.3$ channels surrounding each docked vesicle (Brandt et al., 2005).

But how many channels open during a normal physiological response? Brandt et al. (2005) determined a maximum open probability of each channel ~0.4, which when applied to a pool of 80 $Ca_v1.3$ channels would allow for 30 simultaneously open channels during maximal *in vitro* depolarization. Alternatively, dividing the Ca^{2+} current at -20 mV (130 to 170 pA) by the single channel current reported for L-type channels (0.3 pA at -20 mV, 10mM $[Ca^{2+}]_e$) yields an upper limit of 20 open channels (Chruch and Stanley, 1996; Brandt et al., 2005; Goutman and Glowatzki, 2007).

In vivo, an upper limit of 20 or 30 open channels per active zone may never be reached. However, the conclusion that very few of the available channels contribute to transmitter release at maximal stimulation remains and, in fact, poses a new question regarding the number of channels necessary to drive exocytosis of a single vesicle. It has been shown that, like the neuromuscular junction, the intrinsic Ca^{2+} dependence of exocytosis at the inner hair cell synapse

shows a supralinear relation with a power of 3 to 4, presumably resulting from the cooperative binding of 3 to 4 Ca^{2+} ions necessary to trigger vesicular release (Dodge and Rahamimoff, 1967; Brandt, et al., 2005; Goutman and Glowatzi, 2007). Interestingly, despite showing a supralinear relation at the Ca^{2+} sensor, the same studies found a near linear relation, with a power of 1.1 to 1.4, between exocytosis of the readily releasable vesicle pool and Ca^{2+} influx during inhibitory / augmenting DHP or voltage modulation of the Ca^{2+} current (Brandt, et a., 2005; Goutman and Glowatzi, 2007).

The opening of Ca^{2+} channels elicits a Ca^{2+} signal of very complicated spatial and temporal distribution (Neher, 1998). According to the microdomain model of vesicular release, several open Ca^{2+} channels cooperate to impose a local rise in $[Ca^{2+}]_i$ in the vicinity of a synaptic vesicle's release sight. In this scenario, single channel gating averages out, such that changes in either the number of open channels or current through a single channel would similarly change the $[Ca^{2+}]$ contributing to the microdomain and, thus, have indistinguishable effects on exocytosis kinetics (Moser et al., 2006). This sort of stimulus-secretion coupling should reduce the jitter created by stochastic channel gating in the Ca^{2+} signal "seen" at the synaptic vesicle.

If exocytosis at the inner hair cell is governed by Ca^{2+} microdomains, then the high intrinsic Ca^{2+} cooperativity of transmitter release should be mirrored by the dependence of release on Ca^{2+} influx when changing single current, which would simply change the amplitude of the Ca^{2+} signal seen at the Ca^{2+} sensor.

However, this is not the case, and a much lower power dependency was observed upon changing the number of open Ca^{2+} channels.

The linear dependence of transmitter release on Ca^{2+} influx in light of high Ca^{2+} cooperativity of exocytosis at the Ca^{2+} sensor supports a tighter, nanodomain model of coupling between Ca^{2+} channels and synaptic vesicles (Brandt et al., 2005; Goutman and Glowatzi, 2007). In such a model, the Ca^{2+} influx through a single channel is sufficient to activate release of a vesicle located within a radius of 10 to 20 nm. The Ca^{2+} signal can elevate $[Ca^{2+}]_i$ to 100 μM or more in the vicinity of a channel (more than enough to saturate a tightly coupled Ca^{2+} sensor) in less than 100 μs (Neher, 1998). The brevity of this signal reduces the delay inherent in the diffusion of Ca^{2+} from the channel to the sensor to negligible levels. As membrane potential rises, so does Ca^{2+} channel open probability, and assuming that the Ca^{2+} sensor is saturated, the postsynaptic response grows in a linear proportion to the presynaptic Ca^{2+} current because each newly recruited open Ca^{2+} channel brings its own "unit" of vesicular release (Goutman and Glowatzki, 2007).

Unlike the microdomain model, stochastic channel gating in the nanodomain model does not average out. The time constants for $Ca_v1.3$ channel activation vary between a few milliseconds and hundreds of microseconds and, in the nanodomain model, are a substantial source in the variance of synaptic delay (Zidanich and Fuchs, 1995). If the time for activation reaches several milliseconds, the precision of auditory coding could substantially deteriorate. However, with the approximately 80 $Ca_v1.3$ channels present at each synapse

distributed such that 3-5 $Ca_v1.3$ channels surround each vesicle and a single $Ca_v1.3$ channels can elicit, via its Ca^{2+} nanodomain, the release of a nearby vesicle, it might just be a matter of statistics that always some channels open within a few hundred microseconds of stimulus onset (Moser et a., 2006).

In this manner the distribution and kinetics of L-type $Ca_v1.3$ channels reflects an adaptation at the inner hair cell which counters two very distinct sources of presynaptic delay that could hinder temporal acuity during sound coding: 1) the interaction between a presynaptic waveform of variable amplitude and the kinetics of voltage gated calcium channels, and 2) the diffusion of Ca^{2+} from the Ca_v channel to appropriate Ca^{2+} sensors. These adaptations enable the hair cell to be involved in sound coding with high temporal precision even at low sound intensities.

Timing and intensity coding at the inner hair cell synapse

Within these neuronal processes lies the encryption of the auditory code, and the manner in which envelope, frequency, and intensity of environmental noise are conveyed to auditory nerve fibers. The encoding can be done in a number of ways and exist in a number of forms, but the timing of action potentials remains critical. Intensity can be coded as a function of impulse frequency as well as the number of axons carrying the signal. Frequency can be coded by labeled lines - selectively exciting axons of different spiral ganglion cells so that each represents a different frequency - as well as through phase locked timing of action potentials. Thus, each synaptic ribbon fulfills a demanding signaling task.

It must encode, as a function of afferent action potential firing rate, both timing and intensity information necessary for sound localization.

Phase-locking occurs when acoustic information is fed by inner hair cells to the auditory nerve cycle by cycle, such that the onset of an action potential appears reproducibly at a particular point in the sinusoid of the stimulating sound wave. Post-synaptic cells are thus endowed with a temporal code directly corresponding to sound frequency. Phase locking declines with decreasing sound intensity and increasing sound frequency. However, even at sound levels too low to elicit a significant increase in auditory nerve firing from the spontaneous rate, the discharge patterns still cluster at a preferred phase of the stimulus cycle (Rose et al., 1966; Rose et al., 1967; Moser et al., 2006). At higher frequencies, the biophysical specializations necessary for inner hair cells and auditory nerves to transmit sinusoidal information (firing within 250 μs to 50 μs for frequencies between 4 kHz and 9 kHz) can no longer entrain neuronal firing directly to sound frequency. In reptiles, this sort of phase-locked transmission reaches about 1 kHz and in mammals about 4 kHz (humans about 2 kHz) before breaking down. It is interesting to note, however, that species specially adapted for echolocation, such as barn owls, can phase lock to frequencies as high as 9 kHz.

Above these frequencies, neuronal properties still allow cells to fire action potentials and transmit / receive synaptic communication with the precision necessary to encode, with great temporal resolution, the envelope of the incoming sound. This code often includes an alternative form of phase-locking that entrains

neuronal firing to the cycle of the amplitude modulation of the sound (Cooper et al, 1993).

During a phase locked response, the relative timing of action potentials remains constant throughout much of the auditory nerve's intensity range (Fuchs, 2005). In other words, the response phase at a fiber's characteristic frequency does not vary with intensity. This poses a conundrum in the encryption of the auditory code since varying stimulus intensity would be expected, at a conventional synapse, to increase Ca^{2+} influx, thereby reducing synaptic delay and causing a phase advance. At the inner hair cell synapse, the coding of timing and intensity must somehow be uncoupled.

An important observation was made by Glowatzki and Fuchs (2002) who, when measuring EPSCs in cochlear afferents, determined not only that the amplitude of spontaneous EPSC is highly variable but also that the distribution of EPSC amplitudes does not vary during increasing levels of depolarization, despite an increase in release frequency. To account for these variable responses, the authors propose that Ca^{2+} influx raised the probability of a "controlling step" in the release process that then affected the coordinate release of varying number of vesicles by the ribbon synapse. On average 3 – 6 vesicles but occasionally 20 contribute to a single EPSC. Although the method of multivesicular release is still undefined, the presynaptic ribbon's ability to tether and stabilize hundreds of synaptic vesicles to the active zone while concentrating docked vesicles near $Ca_v1.3$ channels have implicated it as a critical component (Fuchs et al., 2003).

The nanodomain and multivesicular release hypotheses may help to understand the coding of timing and intensity at the hair cell ribbon synapse (Fuchs, 2005). In a typical synapse, increasing depolarization should cause a larger presynaptic Ca^{2+} influx that will drive the process of transmitter release at a higher rate. Subsequently, if increasing vesicular release rate also raised quantal content, then increasingly larger EPSPs would bring the postsynaptic cell to threshold more quickly, eliciting a phase advance. However, the phenomenon of phase locking precludes this as a response to increasing sound intensity at the hair cell synapse where the interdependencies of time and intensity must be avoided.

At the inner hair cell, varying sound intensities will result in varying degrees of membrane depolarization. As expected, an increase in depolarization will increase the open probability of $Ca_v1.3$ channels. However, it will also decrease the driving force moving Ca^{2+} across the membrane, reducing the current through a single $Ca_v1.3$ channel (Brandt, et al., 2005; Moser et al., 2006).

According to the nanodomain hypothesis of exocytosis, a change in open channel number will dominate over the reduction of single channel current. Since a Ca^{2+} signal large enough to saturate the Ca^{2+} sensor rises and falls within microseconds, varying levels of depolarization will only minimally affect the rate of transmitter release. Once the Ca^{2+} sensor is saturated, vesicle fusion, not Ca^{2+} binding, is rate limiting (Moser et al., 2006). This allows for the precise timing at low intensity stimulation necessary for the phase locking of synaptic output to weak sounds (Rose, et al., 1967), but may also ensure that the delay between the

presynaptic waveform and [Ca^{2+}] seen at a Ca^{2+} sensor stays constant as depolarization varies.

The significance of the nanodomain hypothesis, in terms of sound coding, is that stimulus intensity varies the number of active Ca^{2+} channel-release sight units and not the release probability for a given synaptic vesicle. This is indeed the case, as Brandt et al. (2005) shows more exocytosis at a stronger depolarization than at a weak one for the same Ca^{2+} influx. (In a Ca^{2+} microdomain scenario the same Ca^{2+} influx should be equally potent at both potentials.) In this manner, nanodomain control of vesicular release counters the phase advance with increasing Ca^{2+} influx seen in a typical synapse.

Postsynaptically, the invariant distribution of EPSC amplitudes shown by Glowatzki and Fuchs (2002) demonstrates that an increase in quantal content due to larger presynaptic depolarization may not occur at the inner hair cell synapse. Since release is multivesicular and EPSC amplitude is essentially randomized with respect to depolarization / release probability, there is no correlation between postsynaptic time to threshold and presynaptic stimulus intensity.

Instead, increasing presynaptic stimulus intensity opens more Ca^{2+} channel-release sight units, which in turn, increases the number of axons carrying the signal. Since $Ca_v1.3$ channels exhibit activation times ranging from 100 μs to a few ms (Zidanic and Fuchs, 1995; Moser, et al., 2006), multivesicular release could serve to reduce the collective jitter among several cochlear afferents during an auditory stimulus. In other words, although a single vesicle may be enough to trigger a postsynaptic action potential, temporally precise coding across a range of

intensities requires multivesicular release (Moser, et al, 2006). In a study using ribbon-deficient mouse mutants, Khimich, et al. (2005) show that, although the mice have a similar Ca^{2+} sensitivity of release, there is a vast reduction in fast exocytosis per unit of Ca^{2+} influx corresponding to a substantially smaller readily releasable vesicle pool. Additionally the mutant mice fail to synchronously activate cochlear afferents. The authors suggest that synchronous auditory nerve firing relies on precisely timed release of several synaptic vesicles, which in turn requires the synaptic ribbon.

The functional significance of nanodomain control of multivesicular release could be to decouple timing and intensity during auditory coding, a necessity for cochlear afferents to fire synchronously as well as phase lock over a range of intensity levels. By selectively activating axons of different spiral ganglion cells, and phase locking to the auditory waveform, inner hair cells are able to encode information regarding the frequency in the incoming sound. Intensity, which would be expected to cause a phase advance, does not alter this process. At higher intensity levels, more and more Ca^{2+} channel-release sight units are activated, causing multivesicular release induced by an auditory stimulus. As previously mentioned, a given inner hair cell active zone can spontaneously release transmitter at frequencies as high as several hundred hertz. By increasing the amplitude of stereocilia deflection, high intensity auditory stimuli ensure that mechanically gated K^+ channels are only open during the proper phase of the auditory stimulus. This, in turn, decreases the temporal jitter arising from spontaneous transmitter release at the upward of 30 active zones

present at an inner hair cell, causing a larger proportion of action potentials in synchronously activated cochlear afferents to become entrained to the phase of the auditory stimulus (Rose et al., 1967). (This is why, as mentioned earlier, phase locking breaks down at low intensities. An auditory stimulus below threshold is masked by spontaneous activity.) It is in this manner that timing and intensity can be decoupled, yet information regarding both aspects of a sound's envelope can be transmitted to central structures via an auditory code based upon the timing of action potentials.

XVII. APPENDIX II

ANATOMY OF SOUND LOCALIZATION

The mouse, like all vertebrates, is capable of critically examining the auditory code to reveal where events arise in the environment and what they represent. A goal fundamental to understanding the auditory system concerns identifying the critical features of sound necessary for the detection, localization, and interpretation of acoustic events and the manner in which these features are represented within the central nervous system.

The previous appendix necessarily was concerned with the cochlear encryption of an auditory signal into precisely timed action potentials conveying information regarding both the frequency and intensity of a sound. From the cochlea, auditory information, which is contained in both the spatial activation of auditory nerve fibers as well as their temporally precise firing patterns, is sent to the cochlear nucleus. It is the job of the cochlear nucleus, the obligate terminal for auditory nerve fibers, to begin deciphering this spatial and temporal code, rebuilding its elements into a coherent image of the outside world (Ferragamo and Oertel, 2002). Here, I will discuss the manner in which divergent central pathways faithfully propagate this information through several synapses before extracting information regarding the location of sound from temporally precise binaural comparisons of time and intensity.

The cochlear nucleus and the origin of divergent auditory pathways

Upon entering the cochlear nucleus, the fibers of the auditory nerve bifurcate into ascending branches that innervate the anteroventral part of the cochlear nucleus (AVCN) and descending branches that innervate the posteroventral and dorsal parts of the cochlear nucleus (PVCN and DCN, respectively). Each auditory nerve fiber establishes contact with a large number of cells in various subdivisions of the cochlear nucleus (Osen, 1969), from which several parallel, ascending pathways emerge. Each pathway can be described by the manner in which it is contacted by the incoming auditory nerve fibers, by its central projections, and by specialized anatomical and biophysical specializations that customize it to perform a specific function (Ferragamo and Oertel, 2002). This is a crucial point in the processing of the auditory signal because it represents the first location where messages carried by the auditory nerve are recoded and a potential source of synaptic delay.

The complexity of the mammalian cochlear nucleus far exceeds the aforementioned divisions into dorsal and ventral components. Numerous anatomical studies have divided this complex collection of neurons into various subnuclei distinguished from one another by the morphological characteristics of their constituent cells as well as the arrangement and types of synaptic endings. Concurrent electrophysiological studies have shown that associated with each morphological cell type is a characteristic response pattern designed to either preserve or transform the features of the cochlear nerve input (Kiang, et al, 1965; Feng et al., 1994; Ostapoff, et al., 1994).

Response patterns of cochlear nuclei

Response patterns of cochlear nucleus neurons are typically grouped into three broad categories based on their responses to both auditory stimuli as well as current injections: primary-like, chopper, and onset (Pfeiffer, 1966; Kiang et al., 1965, Feng, et al, 1994; Ostapoff et al., 1994; Joris et al, 1994). Within these broad categories are many subdivisions of response type (one of which, primary-like with notch, will be discussed below). Based on different stimulation protocols, a neuron may exhibit response properties which vary across several categories. These findings may very well prove that rather than distinct subsets of response types, there exists a continuum of response properties within the cochlear nucleus. However, we can still say that there are several distinct ways in which the cochlear nucleus responds to auditory stimulation.

Primary-like neuronal responses are described as resembling the responses of auditory fibers. They respond to tones with a vigorous onset component, followed by an exponential decay to a stable discharge level characterized by irregularly spaced action potentials capable of phase locking to the stimulus. Injection of depolarizing current into the neurons produces a single action potential at stimulus onset, which is occasionally followed by a few irregularly spaced action potentials. The response rate typically does not vary with current level. Chopper neuronal responses are described as regularly spaced action potentials occurring at intervals unrelated to stimulus frequency. These neurons respond in this manner whether presented with tones or depolarizing current injections. As opposed to primary-like neurons, their response rate increases with

increased levels of current injection to a maximum level from which no further increase in firing rate was seen and which was comparable to the rate evoked by suprathreshold tones. Onset neuronal responses are described as one or few action potentials occurring at the onset of a tone or depolarizing current injection despite sustained depolarization throughout the stimulus.

There is direct evidence that different response patterns are associated morphologically distinct cell types (Wu and Oertel, 1984; Oertel et al., 1990; Smith et al., 1991, 1993). For example, in the ventral cochlear nucleus (VCN), primary-like discharge patterns are associated with bushy cells, whereas chopper and onset responses are associated with stellate and octopus cells, respectively. Each morphological type of neuron has a distinctive synaptic organization, which can be defined in terms of the cytology of the synaptic endings, the pattern of synapse distribution on the surface of the cell, the transmitters used, and the connections with other central auditory neurons. Thus, the different response patterns may be the result of both specific patterns of synaptic organization as well as intrinsic postsynaptic membrane properties that allow cells to integrate their synaptic inputs in different ways (Feng, et al, 1994; Ostapoff et al., 1994).

The functional consequence of differential processing is that the cochlear nucleus is able to process the relatively homogeneous input it receives from the cochlea into a divergent and heterogeneous output (Pfeiffer, 1966). At the level of the cochlear nucleus, the auditory nerve can be thought of as a single tonotopic pathway. (To illustrate, consider two auditory nerves with low characteristic frequencies exhibiting a phase locked response. Between two such fibers, there is

little variation in the encoded information being sent to the cochlear nucleus.) Within the VCN, each auditory nerve fiber contacts several different types of cell, each with their own unique efferent projections into the brainstem. The presence of a variety of auditory nerve terminations suggests that individual fibers are not limited to a single aspect of audition, but contribute to the range of signal processing necessary for organisms to interpret all aspects of acoustic stimuli.

In this manner, the auditory pathway is split into several parallel, ascending pathways, with each morphologically distinct group of cells (bushy, stellate, and octopus) forming one or several ascending pathways. Such an arrangement allows the auditory code to be simultaneously processed in several different ways, allowing for ongoing, fluctuating environmental sounds to be rapidly localized and understood. Two such parallel processing arrays arising from globular and spherical bushy cells of the AVCN extract information regarding the location of sound using precisely timed binaural timing and intensity cues.

Morphology, physiology, and connectivity of the bushy cells of the AVCN

The timing ability and relatively simple morphology of AVCN bushy cells have made them the subject of many structure function studies. They are anatomically distinctive from the rest of the cochlear nucleus in that they receive large axosomatic calyceal type endings, known as endbulbs of Held, from one to several auditory nerve fibers (Feldman and Harrison, 1969; Liberman, 1991; Joris, et al., 1994a&b). The endbulbs present multiple release sights directly onto

the bushy cell somata, allowing them to dominate bushy cell output, avoid the temporal complications of dendritic filtering, and preserve the temporal features of their auditory nerve inputs (Feldman and Harrison, 1969; Smith, et al., 1991, 1993; Nicol and Walmsley, 2002). Additionally, the convergence of auditory nerve fibers enhances the temporal precision of bushy cell firing, increasing their synchronization and phase locking ability to a level that exceeds that of their auditory nerve inputs (Smith, et al., 1993; Joris, et al. 1994a&b).

In all mammals, bushy cells are characterized by one or few primary dendrites that branch profusely but are only sparsely innervated (Harrison and Irving, 1965; Brawer, et al., 1974; Cant and Morest; 1979; Tolbert and Morest, 1982; Wu and Oertel, 1984; Isaacson and Walmsley, 1995). However, three types of bushy cells can be distinguished from one another based on their morphology, patterns of connectivity with the superior olivary complex, and to a lesser extent physiologically (Kiang, et al., 1965; Osen, 1969; Harrison and Warr, 1962; Harrison and Irving, 1965a&b; Kuwbara and Zook, 1991; Smith et al., 1991, 1993). The pattern of distribution of these bushy cells is relatively constant among mammalian species.

Large spherical bushy cells are present in the anterior portion of the anterior division of the anteroventral cochlear nucleus (Brawer et al, 1974). Although interspecies differences do exist, these cells are tightly packed, have spherical to ovoid somata containing abundant cytoplasm and a centrally placed nucleus, and one to two dendritic processes (Osen, 1969, Harrison and Irving, 1965; Martin, 1981; Webster and Trune, 1982). These cells form prominent

bilateral connections with the medial superior olive (MSO) as well as to the contralateral ventral nucleus of the lateral leminiscus (VNLL) and, occasionally, small collateral projections to the ventral and lateral nuclei of the trapezoid body (VNTB and LNTB, respectively) (Warr, 1966; Smith, et al, 1993). Physiologically, these cells respond to an auditory stimulus with a primary-like response and have characteristic frequencies that are skewed to the low end of the auditory spectrum (Spirou, et al., 1990; Smith, et al., 1993). This frequency distribution corresponds with the projection to the MSO and the preponderance of low frequencies represented there (Yin and Chan, 1990) and the anatomical observations that these cells do not receive innervation from the basal portion of the cochlea (Feldman and Harrison, 1969; Osen, 1969).

Small spherical bushy cells are found just caudal to the large spherical cell area, in the posterodorsal and posterior portions of the anterior division of the anteroventral cochlear nucleus (Brawer, et al., 1974). These cells appear morphologically similar to the large spherical bushy cells, and can be distinguished primarily by their smaller size (Osen, 1969). Their somata are spherical to ovoid, have a centrally placed nucleus, and less abundant cytoplasm than large spherical bushy cells (Osen, 1969, Webster and Trune, 1982). These cells form prominent connections with the ipsilateral lateral superior olive (LSO) (Cant and Casseday, 1986; Smith, et al., 1993). In keeping with their similarity to large spherical bushy cells, these cells preserve the firing pattern of their auditory nerve inputs by responding to tones with a primary-like response pattern (Kiang, et al., 1965; Smith et al., 1993). However, the cells are predominantly skewed to

high frequencies (Ferregamo and Oertel, 2002). This frequency distribution corresponds with the projection to the LSO and the preponderance of high frequencies represented there (Joris, 1996; Batra, et al., 1997) as well to the tonotopic arrangement of high characteristic frequency auditory nerve fibers located within the dorsal regions of the ventral cochlear nucleus (Feldman and Harrison, 1969). However, the anatomical findings that some of these cells project to the low frequency region of the LSO (Smith, et al., 1993) and that the region of small spherical bushy cells is topographically related to the entire frequency spectrum of ascending auditory nerve fibers suggests that lower characteristic frequencies are also represented by this cell type (Osen, 1969).

Globular bushy cells are found caudal to the small spherical cell area, in the ventral and dorsal portions of the posterior division of the anteroventral cochlear nucleus (Brawer, et al., 1974). This region is located rostral to and consisting of the entry and primary bifurcation of the eighth cranial nerve into ascending and descending branches and includes the interstitial nucleus of Lorente de No' (1933) (Harrison and Irving, 1965a&b, 1966; Feldman and Harrison, 1969). In many mammalian species, these cells are also found just caudal to the region of the cochlear nerve root (Harrison and Irving, 1965a&b, 1966; Tolbert and Morest, 1982a&b; Webster and Trune, 1982). These cells are characterized by their oval somata which contain abundant cytoplasm and an eccentric nucleus, which often bulges on the cell surface as if partly extruded from the cell (Harrison and Irving, 1965; Osen, 1969; Tolbert and Morest, 1982a&b; Webster and Trune, 1982.) Occasionally, one to two dendrites

(Harrison and Irving, 1965) or a remarkable thick axon can be seen emanating from the cell (Osen 1969). In the region of the cochlear nerve root, these cells are organized in columns oriented along a dorsoventral axis and separated by large, heavily myelinated fascicles of the auditory nerve (Webster and Trune, 1982a&b). Axons from globular bushy cells form a single (although occasionally two) large, axosomatic calyceal-type presynaptic terminal, known as the calyx of Held, on principle cells of the contralateral medial nucleus of the trapezoid body (MNTB), which, in turn, provide inhibitory input to the homolateral LSO (Harrison and Irving, 1964, 1965a&b, 1966; Morest, 1968; Kuwabara and Zook, 1991; Smith, et al., 1991, 1993; Bergsman, et al., 2004). Ipsilaterally, globular bushy cell axons form several collaterals which may contact various periolivary nuclei, most notably the lateral nucleus of the trapezoid body (LNTB), and, rarely, the LSO (Smith, et al., 1991, 1993). Contralaterally, collateral projections were also seen to terminate the ventral nucleus of the trapezoid body (VNTB), amongst other periolivary nuclei, and the ventral nucleus of the lateral leminiscus (VNLL) (Smith, et al., 1991, 1993). Physiologically, these cells respond to an auditory stimulus with a primary-like with notch response pattern (Kiang, et al., 1965, Feng, et al., 1994; Ostapoff et al., 1994). This response is characterized by an abrupt, precisely timed onset, followed by a brief 1 to 2 ms pause, then a resumption of a sustained pattern of activity similar to its auditory nerve input (Smith, et al., 1991, 1993; Joris, et al., 1994a&b). Like the small spherical bushy cell, the characteristic frequencies of globular bush cells are skewed toward high

frequencies but encompass the frequency range of the entire auditory spectrum (Smith et al., 1991).

It is worth noting that it was the evolution of the mammalian middle and inner ear that made possible the extension of hearing to the higher frequency range (Fettiplace and Fuchs, 1999). Because non-mammalian species lack structures homologous to globular bushy cells, while maintaining cells homologous in structure and function to large spherical bushy and their targets in the SOC, pathways through small spherical and globular bushy cells can be viewed as specializations associated with high frequency hearing (Oertel, 1999). As I will discuss below, this is indeed the case. Pathways arising from these cells are uniquely suited for high frequency sound localization.

The trapezoid body

Axons arising from the principle neurons of the ventral cochlear nucleus enter the midbrain though the trapezoid body (TB), or ventral acoustic stria, one of three major routes for fibers to exit the cochlear nucleus (Smith et al., 1991). In most mammalian species, after emerging from the ventral portion of the cochlear nucleus, the TB passes around the spinal root of the fifth cranial nerve to run medial-laterally along the ventral aspect of the medulla (Harrison and Warr, 1962). As the TB crosses the midline, it curves along the dorsal aspect of the medullary pyramids (Smith, et al., 1993). In the midsagittal plane, the TB displays a stratified appearance, with axons segregated on the basis of fiber diameter and the cell type from which the originate (Harrison and Warr, 1962;

Warr, 1966, 1969, 1972; Spirou, et al., 1990; Smith et al., 1991, 1993; Joris et al., 1994a&b). Anatomical and physiological characterization of these fibers has shown that the dorsal component contains primarily medium diameter fibers thought to originate from large and small spherical bushy cells in the AVCN. The middle component, which comprises most of the ventral half of the TB, contains large diameter fibers from the globular bushy cell region of the AVCN. The ventral component is composed of small diameter fibers running in the rostral and ventral-most aspects of the TB which are thought to arise from stellate cells of the AVCN and PVCN (Smith, et al., 1991). There are several neuronal groups clustered within the TB, including the medial, lateral, and ventral nuclei of the trapezoid body (MNTB, LNTB, and VNTB).

Nuclei of the trapezoid body: medial nucleus

The MNTB is the most easily visualized nucleus within the trapezoid body. It consists of a prominent cluster of globular shaped cells located lateral to the abducens nerve root, medial to the superior paraolivary nucleus (SPN and MSO, and dorsolateral to the medullary pyramids (Harrison and Warr, 1962; Morest, 1968a). The boundaries of this nucleus are often loosely defined as the otherwise densely packed cells may be separated by large, myelinated fascicles of the trapezoid body and abducens nerve which contort its shape. Three types of neurons, distinguished by their respective morphology, can be seen within the MNTB: the elongate cell, the stellate cell, and the principle cell. Despite the presence of elongate and stellate cells, the principle cell is the most apparent

component of this relatively homogeneous nucleus. As such, its cytoarchitecture is far simpler than that of the cochlear nucleus.

Principle cells are morphologically similar to their primary input, the globular bushy cells of the AVCN. They are characterized by an oval somata, eccentric nucleus, and one to three short, tufted dendrites (Harrison and Warr, 1962; Morest, 1968a&b, 1973; Spangler, et al., 1985; Smith et al., 1998). Elongate cells are sparse in number and characterized by a centrally placed nucleus within an oval perikaryon from which four to five primary dendrites extend in the dorsoventral direction, occasionally spanning the entire length of the nucleus (Morest, 1968b; Frisina and Walton, 2001). Stellate cells have large, elongate somata, radially oriented dendrites, and a centrally located nucleus (Morest, 1968b).

The largest presynaptic terminal in the mammalian central nervous system is the glutamatergic calyx of Held, which forms an excitatory, axosomatic synapse on the principle cells of the MNTB, which, in turn, provide inhibitory input to the homolateral LSO (Harrison and Irving, 1964, 1965, 1966; Morest, 1968a&b; Kuwabara and Zook, 1991; Smith, et al., 1991, 1993, 1998; Bergsman, et al., 2003). Each postsynaptic cell receives only one calyx, which arises from a singular globular bushy cell of the contralateral AVCN (Harrison and Warr, 1962; Harrison and Irving, 1964, 1965, 1966; Morest, 1968; Kuwabara, et al., 1991; Smith, et al., 1991, 1993; Bergsman, et al., 2003). Additionally, smaller synaptic boutons have been observed to contact the principle cell somata as well as its primary dendrites. Most of these small contacts are thought to be GABAergic or

glycinergic inhibitory terminals as well as "calycine collaterals," boutons extending from calyciferous axons (Morest, 1968a; Harrison and Irving, 1964, 1965; Kuwabara, et al., 1991; Smith, et al., 1998).

Like the endbulb-bushy cell synapse, the calyx of Held provides multiple release sites directly onto the MNTB principle cell somata and is capable of dominating the response of the principle cell (Smith et al., 1998). Thus, postsynaptic response patterns mirror those of their globular bushy cell inputs. In response to pure tones, principle cells exhibit primary-like with notch response patterns. However, while they show a well timed, sharp onset component, it was not as well timed as their busy cell inputs (Smith, et al., 1998). Additionally, while principle cells show enhanced phase locking to both the waveform of low frequency sound and the envelope of high frequency sound compared to auditory nerve fibers, their timing is not quite as precise as that of globular bushy cells (Smith et al., 1998).

Functionally, the MNTB serves as a sign-inverting relay center. Because of the high release probability of the glutamatergic calyx of Held directly onto the glycinergic principle cell somata, the synapse avoids the temporal complications of dendritic filtering and precisely converts the temporal features of the auditory code from the contralateral ear to an inhibitory signal. The primary sites of inhibitory innervation from MNTB principle cells is the homolateral LSO and VNLL, however collaterals frequently innervate the homolateral MSO, SPN, LNTB, and VNTB (Spangler et al., 1985, Kuwabara and Zook, 1991; Smith et al., 1998).

Nuclei of the trapezoid body: ventral and lateral nuclei

Aside from the MNTB, several other groups of neurons have been described within the fibers of the TB, namely the VNTB and LNTB. The VNTB is located ventral to the MNTB and the LNTB is located ventral to the LSO. Descriptions of the connections and functions of these nuclei remain sparse in the literature, although it is known that they receive collateral projections from AVCN bushy cells as well as MNTB principle cells (Kuwabara and Zook, 1991; Smith et al., 1991, 1993). LNTB axons project bilaterally to the inferior colliculus (IC), whereas VNTB axons to the ipsilateral IC (Willard and Ryugo, 1983). Additionally, LNTB axons have been shown send inhibitory projections to the ipsilateral LSO and MSO.

The role of timing in a pathway for localizing low frequency sound: the medial superior olive and interaural time differences

The human auditory system is capable of detecting interaural time differences (ITDs) of less the 10 μs and uses this binaural cue to localize low frequency sound. Jeffress (1948) proposed a model using ITD to extract the azimuthal location of sound. This model requires that cells in a nucleus receiving binaural input act as coincidence detectors. They must be maximally excited when convergent input from each ear simultaneously stimulates a cell. Thus, synaptic inputs must arise from afferent axonal lines with systematic differences

in timing. The large spherical bushy cell – medial superior olive pathway satisfies the assumptions of this model.

The MSO is a narrow strip of cells composed of unicellular of multicellular, isofrequency sheets of cells tonotopically arranged such that cells of lower characteristic frequencies are located dorsally and higher characteristic frequencies are located ventrally (Smith, et al., 1993). The left and right sides of these cellular sheets receive input from right and left large spherical bushy cells, respectively (Oertel, 1999).

Yin and Chan (1990) determined that MSO cells respond maximally when input from each ear arrives in coincidence and that these cells are arranged topographically with respect to ITDs. This topographic arrangement runs from 0 μs at the rostral pole to 400 μs at the caudal pole, with the positive ITDs corresponding to delays of the ipsilateral stimulus.

Axons of large spherical bushy cells cross the midline at a level rostral to the MSO on their way to the VNLL (Warr, 1966). Smith et al. (1993) determined these axons send collaterals caudally to innervate isofrequecy bands in the contralateral MSO with a "ladder-like" branching pattern. Thus, for large spherical bushy fibers innervating the contralateral MSO there is a clear spread in the terminal aborization pattern such that caudally directed processes have a greater total axonal length than rostrally directed processes. In contrast, axons from large spherical bushy cells terminate in isofrequency bands in the ipsilateral MSO with collaterals that are of roughly equal length.

The initial arrival of the contralateral axon at more rostral location and subsequent innervation caudally is appropriate given the finding of Yin and Chan (1990) that the MSO has a topographical map along an isofrequency axis that has small ITDs rostrally and large ITDs caudally, corresponding to longer delays of the ipsilateral stimulus. Thus, cells in caudal portion of the MSO respond optimally when the ipsilateral stimulus is delayed just enough to compensate for the delay in arrival in the contralateral response along the delay line (Smith, et al., 1993).

The neurons of the MSO fit with the model proposed by Jeffress (1948). However the view that neurons of the MSO serve as simple binaural coincidence detectors of excitatory inputs for sound localization is overly simplistic. The cells can respond to monaural stimulation, indicating that binaural coincidence is not required for firing (Oertel, 1999). Also, neurons of the MSO receive inhibitory inputs from the medial and lateral nuclei of the trapezoid body (MNTB and LNTB), which may sharpen the temporal resolution of coincidence detection (Spangler, et al., 1985; Yin and Chan 1990, Kuwabara and Zook, 1992; Smith, et al., 1998).

Thus, the proper maintenance of synaptic and conductive delays is crucial for proper sound localization using ITDs contained within the binaural auditory code. Large spherical bushy cells receive axosomatic input from one to three auditory nerve fibers through large, endbulb of Held synaptic terminals (Brawer and Morest, 1975; Liberman, 1991). These endbulbs present multiple release sights capable of dominating the response of their postsynaptic bushy cell, such

that their response to auditory stimuli mirrors their auditory nerve input and have, thus, been termed primary-like (Pfeiffer, 1966; Kiang, et al., 1965; Nicol and Walmsley, 2002). Endbulb-bushy cell connections are designed to sharpen the temporal nature of the auditory code, preserving both timing and intensity information, and just as these features are ubiquitous among bushy cells of higher vertebrates, so is the ability of MSO neurons to compare the timing information contained in bushy cell firing patterns.

Phase locking is a necessary requirement for using ITDs to localize sound. If altering intensity created a phase advance, the ability of the MSO to compare the time difference in an auditory signal reaching each ear would dramatically deteriorate. The pathway requires consistency and surety of action potential timing, particularly at the endbulb-bushy cell synaptic connection. It is inevitable that synaptic delays will accumulate, but it is a functional necessity that these delays be minimal as well as consistent among a large population of neurons. The manner in which endbulb-bushy cell synaptic connections maintain timing and intensity information encoded by the inner hair cell will be discussed in the following section.

The role timing in a pathway for localizing high frequency sound: the lateral superior olive and interaural intensity differences

Measurements for the upper frequency limit of high resolution phase locking vary widely among mammals. In order to extract the location of a sound from ITDs, the MSO requires the precisely timed action potential trains inherent

in a phase locked response. Correspondingly, the size of the MSO is directly related to the upper frequency limit of phase locking and temporal resolution of interaural phase differences. The manner in which temporal resolution of ITDs relates to spatial resolution of a sound source depends on the size of the animal's head. Humans can resolve ITDs as small as 10μs, enough to pinpoint the location of a sound to within a single degree. However, for equivalent spatial resolution, animals with small heads need far greater temporal resolving capabilities to use ITDs for sound localization. In many instances, the neuronal processing speed necessary to resolve ITDs on a microsecond time scale exceeds neuronal firing capacity. Thus, the size of the MSO is reduced in "small-headed" mammals, such as mice, which are deficient in low frequency hearing and relatively incapable of using ITDs to localize sound.

In addition to large spherical bushy cells, mammals have globular and small spherical bushy cells, which target the MNTB and LSO. The LSO has generally been considered to be the site where interaural intensity comparisons are made for azimuthal localization. Interaural intensity differences (IIDs) of high frequency sounds are important cues for localizing sounds in animals that hear frequencies high enough to produce head shadowing. Head shadowing is an effect which occurs when the wavelength of a high frequency acoustic waveform is too small to "bend" around the animal's head. As a result, the head casts an acoustic shadow on the ear farther from the source of the sound, creating an intensity disparity between the two ears.

Despite the use of intensity in this pathway, timing still plays a critical role. LSO neurons receive precisely timed excitation from small spherical bushy cells of the ipsilateral AVCN and precisely timed inhibition, via the MNTB, from globular bushy cells of the contralateral AVCN (Joris, 1996; Batra et al., 1997). The integrity of the AVCN-MNTB-LSO pathway appears to be critical for proper sound localization (Kuwabara and Zook, 1991). It is the ability of LSO neurons to be excited by the ipsilateral ear and inhibited by the contralateral ear that allows them to extract the location of a sound from IIDs.

In order to utilize binaural intensity cues to localize sound, the timing of excitatory and inhibitory inputs must be roughly equal. As a result of the longer conduction distance and the intervening synapse, inhibitory input originating in the contralateral AVCN must overcome several sources of delay. One such source of delay is inherent in the large distance axons of globular bushy cells from the contralateral cochlear nucleus must travel compared to the axons of small spherical bushy cells, which provide ipsilateral excitation to the LSO. To overcome this delay, globular bushy cell axons are significantly thicker that those of small spherical bushy cells allowing for action potentials to propagate along their length at a faster rate. Furthermore, inhibitory inputs from MNTB principle cells are located mainly on the proximal dendrites of LSO neurons, whereas excitatory inputs are located more distally, a feature which increases the efficacy of IPSPs. Finally, the calyx of Held-principal cell synapse must be able to tightly regulate calcium signals in order to maintain precise timing of high frequency synaptic transmission. One such mechanism is likely to be intracellular calcium

buffers. It is the aim of the experiments outlined in this document to describe the developmental pattern of expression of intracellular calcium buffering proteins, to understand the role of synaptic activity in protein expression and, ultimately, in sound localization.

XVIII. REFERENCES

Batra R, Kuwada S, Fitzpatrick DC (1997) Sensitivity to interaural temporal disparities of low- and high-frequency neurons in the superior olivary complex. I. Heterogeneity of responses. *J Neurophysiol.* 78(3): 1222-36.

Barnes-Davies M, Forsythe ID (1995) Pre- and postsynaptic glutamate receptors at a giant excitatory synapse in rat auditory brainstem slices. *J Physiol.* 488(2): 387-406.

Bergsman JB, De Camilli P, McCormick DA (2004) Multiple large inputs to principal cells in the mouse medial nucleus of the trapezoid body. *J Neurophysiol.* 92(1): 545-52.

Bock GR, Frank MP, Steel KP (1982) Preservation of central auditory function in the deafness mouse. *Brain Res.* 239(2): 608-12.

Borst JG, Sakmann B (1996) Calcium influx and transmitter release in a fast CNS synapse. *Nature.* 383(6599): 431-4.

Brandt A, Striessnig J, Moser T (2003) CaV1.3 channels are essential for development and presynaptic activity of cochlear inner hair cells. *J Neurosci.* 23(34): 10832-40.

Brandt A, Khimich D, Moser T (2005) Few CaV1.3 channels regulate the exocytosis of a synaptic vesicle at the hair cell ribbon synapse. *J Neurosci.* 25(50): 11577-85.

Brawer JR, Morest DK, Kane EC (1974) The neuronal architecture of the cochlear nucleus of the cat. *J Comp Neurol.* 155(3): 251-300.

Brawer JR, Morest DK (1975) Relations between auditory nerve endings and cell types in the cat's anteroventral cochlear nucleus seen with the Golgi method and Nomarski optics. *J Comp Neurol.* 160(4): 491-506.

Brew HM, Forsythe ID (1995) Two voltage-dependent K+ conductances with complementary functions in postsynaptic integration at a central auditory synapse. *J Neurosci*. 1995 Dec;15(12):8011-22.

Brew HM, Hallows JL, Tempel BL (2003) Hyperexcitability and reduced low threshold potassium currents in auditory neurons of mice lacking the channel subunit Kv1.1. *J Physiol.* 2003 548(1): 1-20.

Caillard O , Moreno H, Schwaller B, Llano I, Celio MR, Marty A (2000) Role of the calcium-binding protein parvalbumin in short-term synaptic plasticity. Proc. Natl. Acad. Sci. USA 97, 13372 – 13377.

Cant NB, Morest DK (1979) The bushy cells in the anteroventral cochlear nucleus of the cat. A study with the electron microscope. *Neuroscience*. 4(12): 1925-45.

Cant NB, Casseday JH (1986) Projections from the anteroventral cochlear nucleus to the lateral and medial superior olivary nuclei. *J Comp Neurol.* 247(4): 457-76.

Catterall WA (2000) Structure and regulation of voltage-gated Ca2+ channels. *Annu Rev Cell Dev Biol*. 16:521-55.

Carafoli E, Santella L, Branca D, Brini M (2001) Generation, control, and processing of cellular calcium signals. *Crit Rev Biochem Mol Biol*. 36(2): 107-260.

Celio MR (1990) Calbindin D-28k and parvalbumin in the rat nervous system. *Neuroscience*. 35(2): 375-475.

Center for Disease Control and Prevention (2009) National Center for Birth Defects and Developmental Disabilities, Early Hearing Detection and Intervention Program. http://www.cdc.gov/ncbddd/ehdi/default.htm

Chard PS, Bleakman D, Christakos S, Fullmer CS, Miller RJ (1993) Calcium buffering properties of calbindin D28k and parvalbumin in rat sensory neurones. *J Physiol*. 472: 341-57.

Church PJ, Stanley EF (1996) Single L-type calcium channel conductance with physiological levels of calcium in chick ciliary ganglion neurons. *J Physiol.* 496 (1): 59-68.

Collin T, Chat M, Lucas MG, Moreno H, Racay P, Schwaller B, Marty A, Llano I (2005) Developmental changes in parvalbumin regulate presynaptic Ca^{2+} signaling. *J Neurosci* 25:96 –107.

Cooper NP, Robertson D, Yates GK (1993) Cochlear nerve fiber responses to amplitude-modulated stimuli: variations with spontaneous rate and other response characteristics. *J Neurophysiol*. 70(1): 370-86.

Corey DP, Hudspeth AJ (1979) Ionic basis of the receptor potential in a vertebrate hair cell. *Nature*.281(5733): 675-7.

Chuhma N, Ohmori H (2002) Role of Ca(2+) in the synchronization of transmitter release at calyceal synapses in the auditory system of rat. *J Neurophysiol.* 87(1): 222-8.

Desai NS, Rutherford LC, Turrigiano GG (1999) Plasticity in the intrinsic excitability of cortical pyramidal neurons. *Nat Neurosci.* 2(6): 489-91.

Dodge FA Jr, Rahamimoff R (1967) Co-operative action a calcium ions in transmitter release at the neuromuscular junction. *J Physiol.* 193(2): 419-32.

Doughty JM, Barnes-Davies M, Rusznák Z, Harasztosi C, Forsythe ID (1998) Contrasting Ca2+ channel subtypes at cell bodies and synaptic terminals of rat anteroventral cochlear bushy neurones. *J Physiol.* 512(2): 365-76.

Elssmann SF Maki JE (1987) Speech spectrographic display: use of visual feedback by hearing-impaired adults during independent articulation practice. *Am Ann Deaf.* 132(4): 276-9.

Faas GC, Schwaller B, Vergara JL, Mody I (2007) Resolving the fast kinetics of cooperative binding: Ca2+ buffering by calretinin. *PLoS Biol.* 5(11): e311.

Ferragamo MJ, Oertel D. (2002) Octopus cells of the mammalian ventral cochlear nucleus sense the rate of depolarization. *J Neuorphysiol.* 87(5): 2262-70.

Feldman ML, Harrison JM (1969) The projection of the acoustic nerve to the ventral cochlear nucleus of the rat. A Golgi study. *J Comp Neurol.* 137(3): 267-94.

Felmy F, Neher E & Schneggenburger R (2003) The timing of phasic transmitter release is Ca^{2+}-dependent and lacks a direct influence of presynaptic membrane potential. *Proceedings of the National Academy of Sciences of the United States of America.* 100(25): 15200-5.

Felmy F, Schneggenburger R (2004) Developmental expression of the Ca2+-binding proteins calretinin and parvalbumin at the calyx of held of rats and mice. *Eur J Neurosci.* 20(6): 1473-82.

Feng JJ, Kuwada S, Ostapoff EM, Batra R, Morest DK (1994) A physiological and structural study of neuron types in the cochlear nucleus. I. Intracellular responses to acoustic stimulation and current injection. *J Comp Neurol.* 346(1): 1-18.

Fettiplace R, Fuchs PA (1999) Mechanisms of hair cell tuning. *Annu Rev Physiol.* 61: 809-34

Fettiplace R, Ricci AJ (2003) Adaptation in auditory hair cells. *Curr Opin Neurobiol.* 13(4): 446-51

Forsythe, ID (1994) Direct patch recording from identified presynaptic terminals mediating glutamatergic EPSCs in the rat CNS, in vitro. *J Physiol.* 479(3): 381-7.

Friauf E, Lohmann C (1999) Development of auditory brainstem circuitry. Activity-dependent and activity-independent processes. *Cell Tissue Res*. 297(2): 187-95.

Frisina RD, Walton JP (2001) Aging of the Mouse Central Auditory System. In: Handbook of Mouse Auditory Research. (ed., J.F. Wilott), CRC Press, Boca Raton, FL, pp. 339–378.

Fuchs PA, Glowatzki E, Moser T (2003) The afferent synapse of cochlear hair cells. *Curr Opin Neurobiol*. 13(4): 452-8.

Fuchs PA (2005) Time and intensity coding at the hair cell's ribbon synapse. *J Physiol.* 566(1): 7-12.

Garcia ML, Strehler EE (1999) Plasma membrane calcium ATPases as critical regulators of calcium homeostasis during neuronal cell function. *Front Biosci.* 4: D869-82.

Glowatzki E, Fuchs PA (2002) Transmitter release at the hair cell ribbon synapse. *Nat Neurosci.* 5(2): 147-54.

Goutman JD, Glowatzki E (2007) Time course and calcium dependence of transmitter release at a single ribbon synapse**.** *Proc Natl Acad Sci U S A.* 104(41): 16341-6.

Gross SJ, Mettelman BB, Dye TD, Slagle TA (2001) Impact of family structure and stability on academic outcome in preterm children at 10 years of age. *J Pediatr.* 138(2): 169-75.

Grosse S. (2001) Cost Comparison of screening newborns for hearing impairment and biochemical disorders. Center for Disease Control and Prevention. Presented at the Newborn Screening and Genetics Conference.

Harrison JM, Warr WB (1962) A study of the cochlear nuclei and ascending auditory pathways of the medulla. *J Comp Neurol.* 119: 341-79.

Harrison JM, Warr WB, Irving RE (1962) Second order neurons in the acoustic nerve. *Science*. 138: 893-5.

Harrison JM, Irving RE (1964) Nucleus of the Trapezoid Body: Dual Afferent Innervation. *Science*. 143: 473-4.

Harrison JM, Irving RE (1965a) The Anterior Ventral Cochlear Nucleus. *J Comp Neurol*. 124: 15-41.

Harrison JM, Irving RE (1965b) Ascending connections of the anterior ventral cochlear nucleus in the rat. *J Comp Neurol.* 126(1): 51-63.

Harrison JM, Irving RE (1966) The organization of the posterior ventral cochlear nucleus in the rat**.** *J Comp Neurol.* 126(3): 391-401.

Heizmann CW, Hunziker W (1991) Intracellular calcium-binding proteins: more sites than insights. *Trends Biochem Sci.* 16(3): 98-103.

Helmchen F, Borst JG, Sakmann B (1997) Calcium dynamics associated with a single action potential in a CNS presynaptic terminal. *Biophys J.* 72(3): 1458-71.

Hudspeth AJ, Jacobs R (1979) Stereocilia mediate transduction in vertebrate hair cells (auditory system/cilium/vestibular system). *Proc Natl Acad Sci U S A*. 76(3): 1506-9.

Hudspeth AJ (1982) Extracellular current flow and the site of transduction by vertebrate hair cells. *J Neurosci.* 2(1): 1-10.

Hudspeth AJ (1989) How the ear's works work**.** *Nature*. 341(6241): 397-404

Hudspeth AJ (1997) How hearing happens. *Neuron.* 19(5): 947-50.

Isaacson JS, Walmsley B (1995) Receptors underlying excitatory synaptic transmission in slices of the rat anteroventral cochlear nucleus. *J Neurophysiol.* 73(3): 964-73.

Ishikawa T, Nakamura Y, Saitoh N, Li WB, Iwasaki S, Takahashi T (2003) Distinct roles of Kv1 and Kv3 potassium channels at the calyx of Held presynaptic terminal. *J Neurosci.* 23(32): 10445-53.

Iwasaki S, Takahashi T (2001) Developmental regulation of transmitter release at the calyx of Held in rat auditory brainstem. *J Physiol.* 534(3): 861-71.

Jaramillo F (1995) Signal transduction in hair cells and its regulation by calcium. *Neuron*. 15(6): 1227-30.

Jeffress LA (1948) A place theory of sound localization. *J Comp Physiol Psychol.* 41(1): 35-9.

Joint Committee on Infant Hearing (2000) Year 2000 position statement: principles and guidelines for early hearing detection and intervention programs. Joint Committee on Infant Hearing, American Academy of Audiology, American Academy of Pediatrics, American Speech-Language-Hearing Association, and Directors of Speech and Hearing Programs in State Health and Welfare Agencies. *Pediatrics*. 106(4): 798-817.

Joris PX, Carney LH, Smith PH, Yin TC (1994a) Enhancement of neural synchronization in the anteroventral cochlear nucleus. I. Responses to tones at the characteristic frequency. *J Neurophysiol.* 71(3): 1022-36.

Joris PX, Smith PH, Yin TC (1994b) Enhancement of neural synchronization in the anteroventral cochlear nucleus. II. Responses in the tuning curve tail. *J Neurophysiol.* 71(3): 1037-51.

Joris PX (1996) Envelope coding in the lateral superior olive. II. Characteristic delays and comparison with responses in the medial superior olive. *J Neurophysiol.* 76(4): 2137-56.

Kachar B, Parakkal M, Kurc M, Zhao Y, Gillespie PG (2000) High-resolution structure of hair-cell tip links. *Proc Natl Acad Sci U S A*. 97(24): 13336-41.

Kaczmarek LK, Bhattacharjee A, Desai R, Gan L, Song P, von Hehn CA, Whim MD, Yang B (2005) Regulation of the timing of MNTB neurons by short-term and long-term modulation of potassium channels. *Hear Res.* 206(1-2): 133-45.

Kazmierczak P, Sakaguchi H, Tokita J, Wilson-Kubalek EM, Milligan RA, Müller U, Kachar B (2007) Cadherin 23 and protocadherin 15 interact to form tip-link filaments in sensory hair cells. *Nature*. 449(7158): 87-91.

Kandler K, Friauf E (1993) Pre- and postnatal development of efferent connections of the cochlear nucleus in the rat. *J Comp Neurol.* 328(2): 161-84.

Katz B & Miledi R (1965) The effect of Calcium on Acetylcholine release from motor nerve terminals. *Proceedings of the Royal Society of London. Series B, Containing Papers of a Biological Character* 161: 496-503.

Katz B & Miledi R (1967) The timing of calcium action during neuromuscular transmission. *J Physiol.* 189(3): 535-544.
101

Katz B & Miledi R (1968) The role of calcium in neuromuscular facilitation. *J Physiol.* 195(2): 481-492.

Katz B & Miledi R (1970) Further study of the role of calcium in synaptic transmission. *J Physiol.* 207(3): 789-801

Keats BJ, **Berlin CI** (1999) Genomics and hearing impairment. *Genome Res.* 9(1): 7-16

Kennedy HJ, Evans MG, Crawford AC, Fettiplace R (2003) Fast adaptation of mechanoelectrical transducer channels in mammalian cochlear hair cells. *Nat Neurosci.* 6(8): 832-6.

Khimich D, Nouvian R, Pujol R, Tom Dieck S, Egner A, Gundelfinger ED, Moser T (2005) Hair cell synaptic ribbons are essential for synchronous auditory signaling. *Nature*. 434(7035) :889-94.

Kiang NY, Pfeiffer RR, Warr WB, Backus AS (1965) Stimulus coding in the cochlear nucleus. *Trans Am Otol Soc.* 53: 35-58.

Kotak VC, **Fujisawa S**, **Lee FA**, **Karthikeyan O**, **Aoki C**, **Sanes DH**. (2005) Hearing loss raises excitability in the auditory cortex. *J Neurosci.* 25(15): 3908-18.

Kurima K, Peters LM, Yang Y, Riazuddin S, Ahmed ZM, Naz S, Arnaud D, Drury S, Mo J, Makishima T, Ghosh M, Menon PS, Deshmukh D, Oddoux C, Ostrer H, Khan S, Riazuddin S, Deininger PL, Hampton LL, Sullivan SL, Battey JF Jr, Keats BJ, Wilcox ER, Friedman TB, Griffith AJ (2002) Dominant and recessive deafness caused by mutations of a novel gene, TMC1, required for cochlear hair-cell function. *Nat Genet.* 30(3): 277-84.

Kuwabara N, Zook JM (1991) Classification of the principal cells of the medial nucleus of the trapezoid body. *J Comp Neurol*. 314(4): 707-20.

Kuwabara N, DiCaprio RA, Zook JM (1991) Afferents to the medial nucleus of the trapezoid body and their collateral projections. *J Comp Neurol*. 314(4): 684-706.

Kuwabara N, Zook JM (1992) Projections to the medial superior olive from the medial and lateral nuclei of the trapezoid body in rodents and bats. *J Comp Neurol.* 324(4): 522-38.

Kurima K, Yang Y, Sorber K, Griffith AJ (2003) Characterization of the transmembrane channel-like (TMC) gene family: functional clues from hearing loss and epidermodysplasia verruciformis. *Genomics*. 82(3):300-8.

Lewis RS, Hudspeth AJ (1983) Voltage- and ion-dependent conductances in solitary vertebrate hair cells. *Nature*. 304(5926): 538-41.

Leao RN, Berntston A, Forsythe ID & Walmsley B (2004a) Reduced low-voltage activated K+ conductances and enhanced central excitability in a congenitally deaf (dn/dn) mouse. *J Physiol.* 559(1): 25-33.

Leao RN, Oleskevich S, Sun H, Bautista M, Fyffe RE & Walmsley B (2004b) Differences in glycinergic mIPSCs in the auditory brain stem of normal and congenitally deaf neonatal mice. *J Neurophysiol.* 91(2): 1006-12.

Leao RN, Svahn K, Berntson A, Walmsley B (2005) Hyperpolarization-activated (I) currents in auditory brainstem neurons of normal and congenitally deaf mice. *Eur. J. Neurosci.* 22(1): 147-57.

Leao RN, Sun H, Svahn K, Berntson A, Youssoufian M, Paolini AG, Fyffe RE & Walmsley B (2006) Topographic organization in the auditory brainstem of juvenile mice is disrupted in congenital deafness. *J Physiol.* 571(Pt 3): 563-78.

Leão RN, Leão RM, da Costa LF, Rock Levinson S, Walmsley B (2008) A novel role for MNTB neuron dendrites in regulating action potential amplitude and cell excitability during repetitive firing. *Eur J Neurosci*. 27(12): 3095-108.

Liberman MC (1991) Central projections of auditory-nerve fibers of differing spontaneous rate. I. Anteroventral cochlear nucleus. *J Comp Neurol.* 313(2): 240-58.

Lips MB, Keller BU (1998) Endogenous calcium buffering in motoneurones of the nucleus hypoglossus from mouse. *J Physiol.* 511(1): 105-17.

Lohmann C, Friauf E (1996) Distribution of the calcium-binding proteins parvalbumin and calretinin in the auditory brainstem of adult and developing rats. *J Comp Neurol.* 367(1): 90-109.

Lorente de No' (1933) Anatomy of the Eighth Nerve. III. General Plan of Structure of the Primary Cochlear Nuclei. *Laryngoscope.* 35:839-52.

Matveev V, Zucker RS, Sherman A (2004) Facilitation through buffer saturation: constraints on endogenous buffering properties. *Biophys J.* 86(5): 2691-709.

Martin MR (1981) Morphology of the cochlear nucleus of the normal and reeler mutant mouse. *J Comp Neurol.* 197(1): 141-52.

Morest DK (1968a) The growth of synaptic endings in the mammalian brain: a study of the calyces of the trapezoid body. *Z Anat Entwicklungsgesch.* 127(3): 201-20.

Morest DK (1968b) The collateral system of the medial nucleus of the trapezoid body of the cat, its neuronal architecture and relation to the olivo-cochlear bundle. *Brain Res*. 9(2): 288-311.

Morest DK (1973) Auditory neurons of the brain stem. *Adv Otorhinolaryngol*. 20: 337-56.

Moser T, Brandt A, Lysakowski A (2006) Hair cell ribbon synapses. *Cell Tissue Res.* (2): 347-59.

Müller M, Felmy F, Schwaller B, Schneggenburger R (2007) Parvalbumin is a mobile presynaptic Ca2+ buffer in the calyx of held that accelerates the decay of Ca2+ and short-term facilitation. *J Neurosci.* 27(9): 2261-71.

Nägerl UV, Novo D, Mody I, Vergara JL (2000) Binding kinetics of calbindin-D(28k) determined by flash photolysis of caged Ca(2+). *Biophys J.* 79(6): 3009-18.

Neher E, Augustine GJ (1992) Calcium gradients and buffers in bovine chromaffin cells. *J Physiol.* 450: 273-301.

Neher, E (1998) Vesicle pools and Ca2+ microdomains: new tools for understanding their roles in neurotransmitter release. *Neuron.* 20(3): 389-99.

Nicol MJ, Walmsley B (2002) Ultrastructural basis of synaptic transmission between endbulbs of Held and bushy cells in the rat cochlear nucleus. *J Physiol.* 539(3): 713-23.

Oertel D, Wu SH, Garb MW, Dizack C (1990) Morphology and physiology of cells in slice preparations of the posteroventral cochlear nucleus of mice. *J Comp Neurol.* 295(1): 136-54.

Oertel D (1999) The role of timing in the brain stem auditory nuclei of vertebrates. *Annu Rev Physiol.* 61: 497-519.

Oleskevich S & Walmsley B (2002) Synaptic transmission in the auditory brainstem of normal and congenitally deaf mice. *J Physiol.* 540(2): 447-55.

Oleskevich S, Youssoufian M, Walmsley B (2004) Presynaptic plasticity at two giant auditory synapses in normal and deaf mice. *J Physiol*. 560(3): 709-19.

Osen KK (1969) Cytoarchitecture of the cochlear nuclei in the cat. *J Comp Neurol.* 136(4): 453-84.

Ostapoff EM, Feng JJ, Morest DK (1994) A physiological and structural study of neuron types in the cochlear nucleus. II. Neuron types and their structural correlation with response properties. *J Comp Neurol.* 346(1): 19-42.

Pfeiffer RR (1966) Classification of response patterns of spike discharges for units in the cochlear nucleus: tone-burst stimulation. *Exp Brain Res.* 1(3): 220-35.
Roberts WM, Jacobs RA, Hudspeth AJ (1990) Colocalization of ion channels involved in frequency selectivity and synaptic transmission at presynaptic active zones of hair cells. *J Neurosci.* 10(11): 3664-84.

Robles L, Ruggero MA (2001) Mechanics of the mammalian cochlea. *Physiol Rev.* 81(3): 1305-52.

Rogers JH, Résibois A (1992) Calretinin and calbindin-D28k in rat brain: patterns of partial co-localization. *Neuroscience*. 51(4): 843-65.

Rogers JH, Résibois A (1992) Calretinin in rat brain: an immunohistochemical study. *Neuroscience*. 46(1): 101-34.

Rose JE, Brugge JF, Anderson DJ, Hind JE (1966) Some neural mechanisms in the inferior colliculus of the cat which may be relevant to localization of a sound source. *J Neurophysiol*. 30(4): 769-93.

Rose JE, Brugge JF, Anderson DJ, Hind JE (1967) Phase-locked response to low-frequency tones in single auditory nerve fibers of the squirrel monkey. *J Neurophysiol.* 1967 Jul;30(4):769-93.

Ryugo DK, Pongstaporn T, Huchton DM, Niparko JK (1997) Ultrastructural analysis of primary endings in deaf white cats: morphologic alterations in endbulbs of Held. *J Comp Neurol*. 385(2): 230-4.

Ryugo DK, Montey KL, Wright AL, Bennett ML, Pongstaporn T (2006) Postnatal development of a large auditory nerve terminal: the endbulb of Held in cats. *Hear Res.* 216-217: 100-15.

Saada AA, Niparko JK, Ryugo DK (1996) Morphological changes in the cochlear nucleus of congenitally deaf white cats. *Brain Res.* 736(1-2): 315-28.

Siemens J, Lillo C, Dumont RA, Reynolds A, Williams DS, Gillespie PG, Müller U (2004) Cadherin 23 is a component of the tip link in hair-cell stereocilia. *Nature*. 428(6986): 950-5.

Seldon HL, Clark GM (1991) Human cochlear nucleus: comparison of Nissl-stained neurons from deaf and hearing patients. *Brain Res.* 551(1-2): 185-94.

Schwaller B, Durussel I, Jermann D, Herrmann B, Cox JA (1997) Comparison of the Ca2+-binding properties of human recombinant calretinin-22k and calretinin. *J Biol Chem*. 272(47): 29663-71.

Shepherd RK, Hartmann R, Heid S, Hardie N, Klinke R (1997) The central auditory system and auditory deprivation: experience with cochlear implants in the congenitally deaf. *Acta Otolaryngol Suppl.* 532: 28-33.

Smith PH, Joris PX, Carney LH, Yin TC (1991) Projections of physiologically characterized globular bushy cell axons from the cochlear nucleus of the cat. *J Comp Neurol.* 304(3): 387-407.

Smith PH, Joris PX, Yin TC (1993) Projections of physiologically characterized spherical bushy cell axons from the cochlear nucleus of the cat: evidence for delay lines to the medial superior olive. *J Comp Neurol.* 331(2): 245-60.

Smith PH, Joris PX, Yin TC (1998) Anatomy and physiology of principal cells of the medial nucleus of the trapezoid body (MNTB) of the cat. *J Neurophysiol.* 79(6): 3127-42.

Spangler KM, Warr WB, Henkel CK (1985) The projections of principal cells of the medial nucleus of the trapezoid body in the cat. *J Comp Neurol.* 238(3): 249-62.

Spirou GA, Brownell WE, Zidanic M (1990) Recordings from cat trapezoid body and HRP labeling of globular bushy cell axons. *J Neurophysiol.* 63(5): 1169-90.

Steel KP, Bock GR (1980) The nature of inherited deafness in deafness mice. *Nature*. 288(5787): 159-61.

Taschenberger H, von Gersdorff H (2000) Fine-tuning an auditory synapse for speed and fidelity: developmental changes in presynaptic waveform, EPSC kinetics, and synaptic plasticity. *J Neurosci.* 20(24): 9162-73.

Taschenberger H, Leão RM, Rowland KC, Spirou GA, von Gersdorff H (2002) Optimizing synaptic architecture and efficiency for high-frequency transmission. *Neuron*. 36(6): 1127-43.

Tolbert LP, Morest DK (1982a) The neuronal architecture of the anteroventral cochlear nucleus of the cat in the region of the cochlear nerve root: electron microscopy. *Neuroscience*. 7(12): 3053-67.

Tolbert LP, Morest DK (1982b) The neuronal architecture of the anteroventral cochlear nucleus of the cat in the region of the cochlear nerve root: Golgi and Nissl methods. *Neuroscience*. 7(12):3013-30

Trussell LO (1999) Synaptic mechanisms for coding timing in auditory neurons. *Annu Rev Physiol.* 61: 477-96.

Turrigiano GG, Nelson SB (2004) Homeostatic plasticity in the developing nervous system. *Nat Rev Neurosci*. 5(2): 97-107.

von Gersdorff H, Borst JG (2002) Short-term plasticity at the calyx of held. *Nat Rev Neurosci.* 3(1): 53-64.

Walmsley B, Berntson A, Leao RN, Fyffe RE (2006) Activity-dependent regulation of synaptic strength and neuronal excitability in central auditory pathways. *J Physiol*. 572(2): 313-21.

Wang LY, Gan L, Forsythe ID, Kaczmarek LK (1998) Contribution of the Kv3.1 potassium channel to high-frequency firing in mouse auditory neurones. *J Physiol.* 509(1): 183-94.

Warr WB (1966) Fiber degeneration following lesions in the anterior ventral cochlear nucleus of the cat. *Exp Neurol.* 14(4): 453-74.

Warr WB (1969) Fiber degeneration following lesions in the posteroventral cochlear nucleus of the cat. *Exp Neurol.* 23(1): 140-55.

Warr WB (1972) Fiber degeneration following lesions in the multipolar and globular cell areas in the ventral cochlear nucleus of the cat. *Brain Res.* 40(2): 247-70.

Webster DB, Trune DR (1982) Cochlear nuclear complex of mice. *Am J Anat.* 163(2): 103-30.

Webster DB (1985) The spiral ganglion and cochlear nuclei of deafness mice**.** *Hear Res*. 18(1): 19-27.

Webster DB (1992) Degeneration followed by partial regeneration of the organ of Corti in deafness (dn/dn) mice. *Exp Neurol.* 1: 27-31.

Westenbroek RE, Hoskins L, Catterall WA (1998) Localization of Ca2+ channel subtypes on rat spinal motor neurons, interneurons, and nerve terminals. *J Neurosci.* 1998 18(16): 6319-30.

Willard, F.H., and D.K. Ryugo (1983) Anatomy of the central auditory system. In: The Auditory Psychobiology of the Mouse, (ed., J.F. Willott). Charles C Thomas Publisher, Springfield, IL, pp. 201-304.

World Health Organization. (2006) Deafness and Hearing Impairment Fact Sheet. http://www.who.int/mediacentre/factsheets/fs300/en/print.html

Wu SH, Oertel D (1984) Intracellular injection with horseradish peroxidase of physiologically characterized stellate and bushy cells in slices of mouse anteroventral cochlear nucleus. *J Neurosci.* 4(6): 1577-88.

Yin TC, Chan JC (1990) Interaural time sensitivity in medial superior olive of cat. *J Neurophysiol.* 64(2): 465-88.

Yoshinaga-Itano C, Apuzzo ML (1998) Identification of hearing loss after age 18 months is not early enough. *Am Ann Deaf.* 143(5): 380-7.

Youssoufian M, Couchman K, Shivdasani MN, Paolini AG, Walmsley B (2008) Maturation of auditory brainstem projections and calyces in the congenitally deaf (dn/dn) mouse. *J Comp Neurol.* 506(3): 442-51.

Zidanic M, Fuchs PA (1995) Kinetic analysis of barium currents in chick cochlear hair cells. *Biophys J.* 68(4): 1323-36.